

POINT-TO-AXIAL CHIRALITY TRANSFER:  
I. ABSOLUTE STEREOCHEMICAL DETERMINATION OF CHIRAL  
PHOSPHORUS COMPOUNDS  
II. DESIGN AND DEVELOPMENT OF A PROGRAMMABLE ORGANOCATALYST

By

Debarshi Chakraborty

A DISSERTATION

Submitted to  
Michigan State University  
in partial fulfillment of the requirements  
for the degree of

Chemistry – Doctor of Philosophy

2023

## ABSTRACT

This dissertation consists of two sections. The common thread between these two sections is the transfer of chirality (point to helical). In the first section, (Chapters I, II and III) the absolute stereochemical determination of chiral organic molecules using the principle of chirality transfer is described. The non-covalent interaction between the receptor and chiral analyte of interest leads to induction of helicity in the host-guest complex, and the helicity is measured by circular dichroism. In Chapter I, the design and development of the bis-porphyrin based hosts that perform as “reporters of chirality” has been discussed. Chapter II describes the development of a single chiroptical sensor for the absolute stereochemical determination of  $\alpha$ -aminophosphonates and  $\alpha$ -hydroxyphosphonates. In chapter III, a simple chiroptical solution for the determination of absolute configuration of P(V) chiral molecules has been discussed. The developed methodology has been successfully extended to determine the absolute stereochemistry at the P center of the antiviral Sofosbuvir.

In the second part of the thesis (Chapters IV), design and application of a programmable enantiodivergent organocatalyst is described. The newly developed catalyst eliminates the requirement of two enantiomeric catalysts to afford antipodal products. The asymmetry in the racemic catalyst is introduced through coordination with chiral ligands and therefore can be programmed at will. To understand the chirality transfer phenomenon (point-to-axial to point) in depth, the sterics and electronics of the catalyst and the ligands are also explored.

Dedicated to my 'Kaku'

## **ACKNOWLEDGEMENTS**

I would like to express my sincere gratitude to my advisor Professor Babak Borhan. I feel extremely lucky and privileged to be a part of his scientific family. He has been a great mentor and always encourages to think independently. He provided the freedom to work on our own ideas and that is something I would always cherish. He was there for me in my most vulnerable days during my stay in grad school. I would also like to thank him for letting me watch cricket, soccer, tennis in the lab, for those happy memories inside and outside the lab (camping and group parties) and for valuable career advice.

I am grateful to all my committee members, Professor James E. Jackson, Professor Robert E. Maleczka Jr., and Professor Heedeok Hong for their support and guidance over the past few years.

I would also like to thank Dr. Daniel Holmes (NMR), Dr. Richard Staples (Crystallography), Dr. Anthony Schillmiller (Mass spectrometry) for their time and help. I specially thank Dr. Ardeshir Azadnia for giving me the opportunity to teach organic labs at MSU.

I am grateful to all the members of the Borhan group with whom I had the pleasure to work. All of you have been supportive, friendly, and most importantly humorous that made my journey a memorable one. I would like to thank Dr. Chrysoula Vasileiou for always helping me since I joined this group. My special gratitude to Dr. Hadi and Dr. Yi for your guidance and support during my early days in the Borhan lab. I am thankful for the friendship and unnumbered memories I have with Dr. Saeedeh, Dr. Dan, Dr. Aliakbar,



Dr. Emily, Soham, Ankush, Mehdi and Aria. I thank James, Joban, and Channel for helping me in my research.

I would like to thank Dr. Li, Dr. Badru, Dr. Aziz, Shuang, and Swetha for making those early days of graduate school memorable.

I would like to express my sincere gratitude to my supportive family and friends. Without the support of my Amma, Maa and Dada I would have never made to graduate school. Thank you Maa for letting me dream and for motivating me to turn them into reality; thank you for showering me with light and hope. The guidance from my Dada has been instrumental in my academic journey since childhood. I would also like to thank Somnath, Swarup, Mrinmoy, Gora, Avishek and Prakash Da for their love, support, and suggestions.

Lastly, I want to thank Esita. No words are enough to express my gratitude to her. The only reason I am writing this page today is because of her unconditional love and unwavering support. Literally, she did everything to keep me sane during those nervous moments of my graduate school. Thank you for everything.

## TABLE OF CONTENTS

LIST OF SYMBOLS AND ABBREVIATIONS.....	vii
CHAPTER I: ABSOLUTE STEREOCHEMICAL DETERMINATION OF CHIRAL ORGANIC MOLECULES THROUGH INDUCTION OF HELICITY IN BIS- PORPHYRIN HOSTS.....	1
REFERENCES.....	23
CHAPTER II: ABSOLUTE STEREOCHEMICAL ASSIGNMENT OF $\alpha$ -AMINO AND $\alpha$ - HYDROXYPHOSPHONATES EMPLOYING A SINGLE CHIROPTICAL SENSOR.....	26
REFERENCES.....	49
CHAPTER III: A CHIROPTICAL APPROACH FOR THE ABSOLUTE STEREOCHEMICAL DETERMINATION OF P-STEREOGENIC CENTER.....	51
REFERENCES.....	126
CHAPTER IV: POINT-TO-AXIAL-TO-POINT CHIRALITY TRANSFER: DESIGN AND DEVELOPMENT OF A PROGRAMMABLE ORGANOCATALYST.....	129
REFERENCES.....	242

## LIST OF SYMBOLS AND ABBREVIATIONS

Å	angstrom
[α] <sub>D</sub>	specific rotation
A	ECCD amplitude
ABq	AB quartet
ACN	acetonitrile
AcOH	acetic acid
APCI	atmospheric pressure chemical ionization
Ar	aromatic
BINOL	1,1'-Bi-2-naphthol
Bn	benzyl
Boc	tert-butyloxycarbonyl
CD	circular dichroism
CE	Cotton effect
cm	centimeter
d	doublet
DBU	1,8-diazabicyclo(5.4.0)undec-7-ene
DCM	dichloromethane
DDQ	2,3-dichloro-5,6-dicyano-1,4-benzoquinone
DFT	density functional theory
DIBAL-H	diisobutylaluminium hydride
DMF	dimethylformamide

DMSO	dimethyl sulfoxide
DMI	1,3-dimethyl-2-imidazolidinone
dr	diastereomeric ratio
ECCD	exciton coupled circular dichroism
ECD	electronic circular dichroism
equiv	equivalents
ESI	electrospray ionization
EtOH	ethanol
<i>etdm</i>	electronic transition dipole moment
EtOAc	ethyl acetate
HBPIn	pinacolborane
HOMO	highest occupied molecular orbital
HPLC	high-performance liquid chromatography
HRMS	high resolution mass spectrometry
IR	infrared
$K_a$	association constant
lcp	left circularly polarized light
LUMO	lowest unoccupied molecular orbital
M	molar
<i>M</i>	minus
Me	methyl
MeOH	methanol

MHz	megahertz
mg	milligram
Mg-TPP	magnesium tetraphenylporphyrin
min	minute
mM	millimolar
mmol	millimole
MPA	methoxyphenyl acetic acid
MTPA	methoxy trifluoromethyl phenylacetic acid
MS	mass spectrometry
m/z	mass to charge ratio
NaOAc	sodium acetate
Bu	<i>n</i> -butyl
nBuLi	<i>n</i> -butyllithium
NBS	N-bromosuccinimide
NH <sub>2</sub> Boc	tert-butyl carbamate
nm	nanometer
NMR	nuclear magnetic resonance
NIS	N-iodosuccinimide
ORD	optical rotatory dispersion
<i>P</i>	plus
Ph	phenyl
PhB(OH) <sub>2</sub>	phenylboronic acid

PhLi	phenyllithium
PPh <sub>3</sub>	triphenylphosphine
q	quartet
rcp	right circularly polarized light
rt	room temperature
s	singlet
t	triplet
TFA	trifluoroacetic acid
THF	tetrahydrofuran
TLC	thin layer chromatography
TMSOTf	trimethylsilyl trifluoromethanesulfonate
tz	tweezer
μg	micro gram
μM	micro molar
UV-vis	ultraviolet-visible spectroscopy
VCD	vibrational circular dichroism
X	mole fraction
Zn-TPFP	zinc 5-(4-carboxyphenyl)-10,15,20-tri(pentafluorophenyl)porphyrin tweezer
Zn-TPP	zinc tetraphenylporphyrin
Zn-TPP-tz	zinc 5-(4-carboxyphenyl)-10,15,20- triphenylporphyrin tweezer
>	larger than
<	less than

CHAPTER I: ABSOLUTE STEREOCHEMICAL DETERMINATION OF CHIRAL  
ORGANIC MOLECULES THROUGH INDUCTION OF HELICITY IN BIS-  
PORPHYRIN HOSTS

## I-1 Introduction

Stereochemistry is a fundamental molecular property with important ramifications for structure, function, and activity of organic molecules. The basic building blocks of living organisms (amino acids and sugars) exhibit molecular handedness that has evolved over millions of years. The absolute stereochemistry of these building blocks is manifested in the structure and function of the cell machinery (*e.g.*, enzymes, proteins, etc.), which are essential components of life. Most biologically active molecules and pharmaceutical agents are stereochemically-rich structures. Examples of the latter are citalopram, an antidepressant, sold as a racemic mixture of both the enantiomers (Figure I-1). Only the (*S*)-enantiomer has the desired effect.<sup>1</sup> Thalidomide, the ‘morning sickness’ anti-nausea medicine for pregnant women, where the (*R*)-enantiomer was teratogenic, led to devastating malformities in embryonic development.<sup>2</sup> Important to point out, the active (*S*)- enantiomer can racemize due to the presence of the acidic hydrogen at the chiral

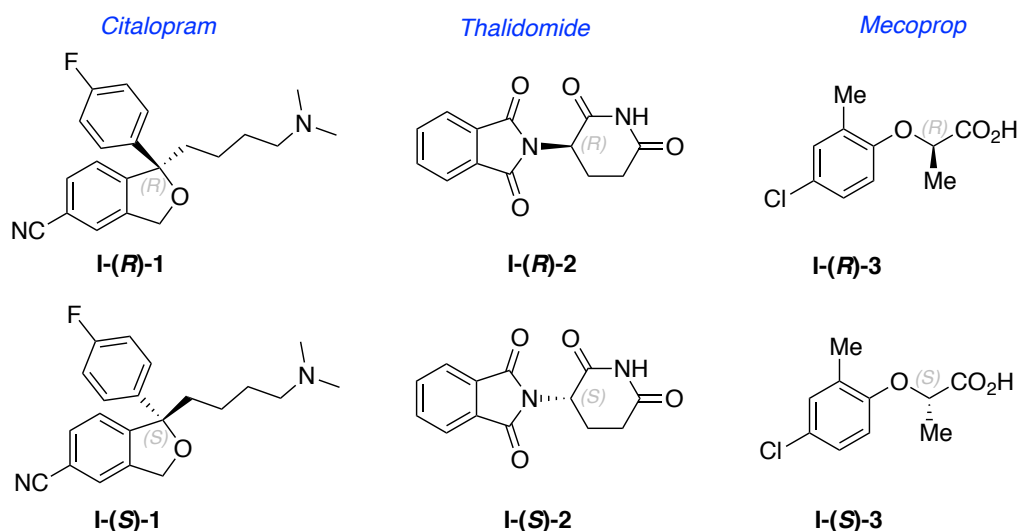


**Figure I-1.** Represented enantiomers with different activities.



center. In the 1960's almost 10,000 infants have been affected by this drug. Nearly 40% of them died and those that survived suffered from severe birth defects. Mecoprop, an herbicide, is used in many households as a weed killer. It is only the (*R*)-mecoprop that possesses the desired activity.<sup>3</sup> Organic chemists have, and certainly will continue to design and develop tools and techniques to install stereocenters with precise selectivity to access important chiral molecules. In parallel to the advancements in stereoselective synthesis, there has been a growing interest and need for creative solutions to the challenge of absolute stereochemical determination of molecules with asymmetric centers. Under the current scenario, it is often the difficulty of assigning absolute stereochemistry, as opposed to synthesis, which has become a non-trivial challenge, requiring the attention of the community. There will not be a general solution to this problem, as each system will have its own unique requirements and challenges. However, the need for rapid, routine, and microscale analysis is apparent. This is especially true with parallel and high-throughput arrays for screening conditions and catalysts, generating many samples that require analysis.

## **I-2 NMR based methods of determining absolute stereochemistry**

Direct detection of chirality, however, is not straightforward without the presence of a proper frame of reference. A reliable method is to compare the optical properties (*i.e.*, optical rotation) of a compound to that of a known sample. This approach is valid only if the data of an authentic sample with known configuration is present in the literature. Most of the time, synthetic organic chemists developed new methodologies through different disconnections within the molecule. Therefore, finding the exact molecule in literature with

the desired configuration is often not possible. X-ray crystallography can provide an unambiguous assignment of configuration for molecules with heavy atoms due to its ability to yield high atomic resolution.<sup>4</sup> Despite its remarkable success, this requires the molecule to be crystallizable in the first place. Often, obtaining a high-quality crystal is time consuming, laborious at times, and finding the right solvent or combination of solvents makes it even more tedious.

In the past few decades, the NMR based Mosher model has been a cornerstone in determining the absolute stereochemistry of chiral organic molecules. Pioneered by Mosher, and further modified by Dale and other researchers,<sup>5-7</sup> this approach has offered a practical method for the absolute stereochemical determination of chiral alcohols and

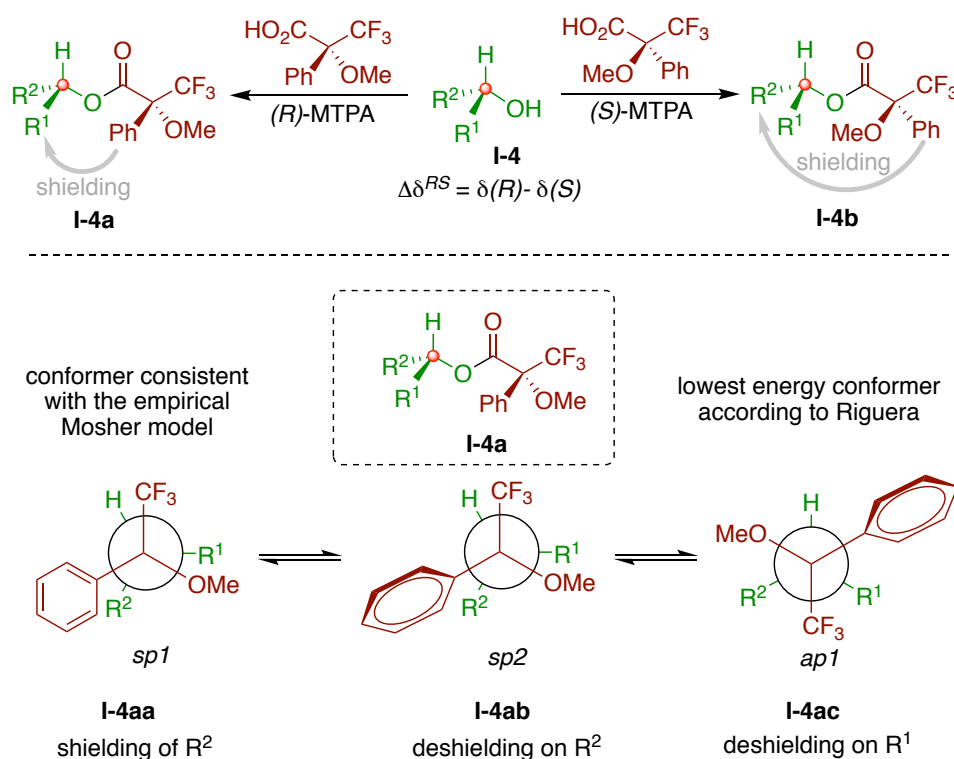


**Figure I-2.** Assignment of the absolute configuration of a secondary alcohol using Mosher ester protocol. The most representative conformers of MTPA esters.

amines. Derivatization of these functionalities with both enantiomers of a known chiral carboxylic acid or carboxylic acid chloride, and subsequent NMR analysis of the diastereomeric molecules (as esters or amides) can lead to the absolute stereochemical determination of the desired molecule (Figure I-2). Nonetheless, this technique is limited to only secondary chiral carbon center with a site for derivatization (*i.e.*, hydroxyl or amino group), and relies on subtle chemical shift changes that can potentially lead to ambiguous assignment of the absolute stereochemistry. Mosher first represented an empirical model to determine the absolute configuration of chiral alcohols via an MTPA ester (Figure I-2). However, there are examples of chiral alcohols in the literature that do not agree with this model, making it difficult to determine their absolute stereochemistry. Through rigorous theoretical calculations, NMR and CD studies Riguera et al.<sup>8</sup> found out that along with the conformer **I-4aa** predicted by Mosher, two other conformers **I-4ab** and **I-4ac** of the MTPA ester remain in equilibrium (Figure I-2). Due to the presence of three different but equally populated conformers the differences in their chemical shifts are either too small or inconsistent leading to the discrepancies in the assignments of their absolute configuration.

Another NMR based method that has been used widely for the determination of absolute configuration is the chiral solvating agent (CSA) based method.<sup>9-10</sup> This protocol eliminates the necessity of any chemical derivatization and therefore no synthesis or purification prior to analysis is required. Furthermore, the difference in chemical shift of the NMR originates mainly from the non-covalent interactions (hydrogen bonding and  $\pi$ -stacking) between the chiral solvating agent and chiral analyte of interest. Nonetheless,

the major limitation of this protocol is the challenge in predicting a conformational model that can relate to chirality of the organic molecule with the changes in the NMR chemical shift. Moreover, subtle chemical shift changes and exclusiveness of a particular chiral solvating agent towards a small set of target molecules, limit the application of this technique.

### **I-3 Absolute stereochemical determination of chiral organic molecules: chiroptical techniques**

An enabling alternative is to exploit the unique properties of chiroptical techniques, and optical rotatory dispersion (ORD) or circular dichroism (CD) to interrogate absolute stereochemistry. In these approaches, the stereochemical identity of a target molecule is translated into a detectable chiroptical response that ultimately leads to its absolute stereochemical determination. Fundamental to this tactic are the diastereomeric interactions of circularly polarized light, both left and right-handed components, with the chiral entities or complexes (Pfeiffer effect). Nonetheless, neither of these techniques can be independently utilized to assign the absolute configuration of a stereocenter since the sign of the resultant spectra in both instances is empirical in nature. A solution to this has entailed coupling of the results with theoretical spectra via computational methods. The computationally obtained spectrum provides the so-called frame of reference for the experimentally collected spectra. Nonetheless, the scope of these techniques is inadequate. The difficulties in predicting the lowest energy conformers in the solution phase stem from the flexibility (rotation around C-C bonds), complexity of the structures and their interactions with the solvent.

#### I-4 Exciton coupled circular dichroism: a non-empirical chiroptical approach

Within the realm of chiroptical techniques, Exciton Coupled Circular Dichroism (ECCD) provides a non-empirical alternative to the assignment of helicity. The fundamentals of the ECCD approach are based on the pioneering work by Nakanishi and Harada,<sup>11-13</sup> who showed that the through space exciton coupling between two or more helically oriented electric transition dipole moments (*etdm*) of independently conjugated chromophores leads to a bisignate Cotton effect, with a sign that is directly correlated to the helicity of the coupling chromophores. Their initial investigations exploited ECCD for the assignment of absolute configuration of conformationally rigid sterols **I-5** and **I-ent-5** (Figure I-3). The alcohol functionalities were derivatized as dibenzoates to introduce the required chromophoric entities. The solution to the absolute configuration was obtained

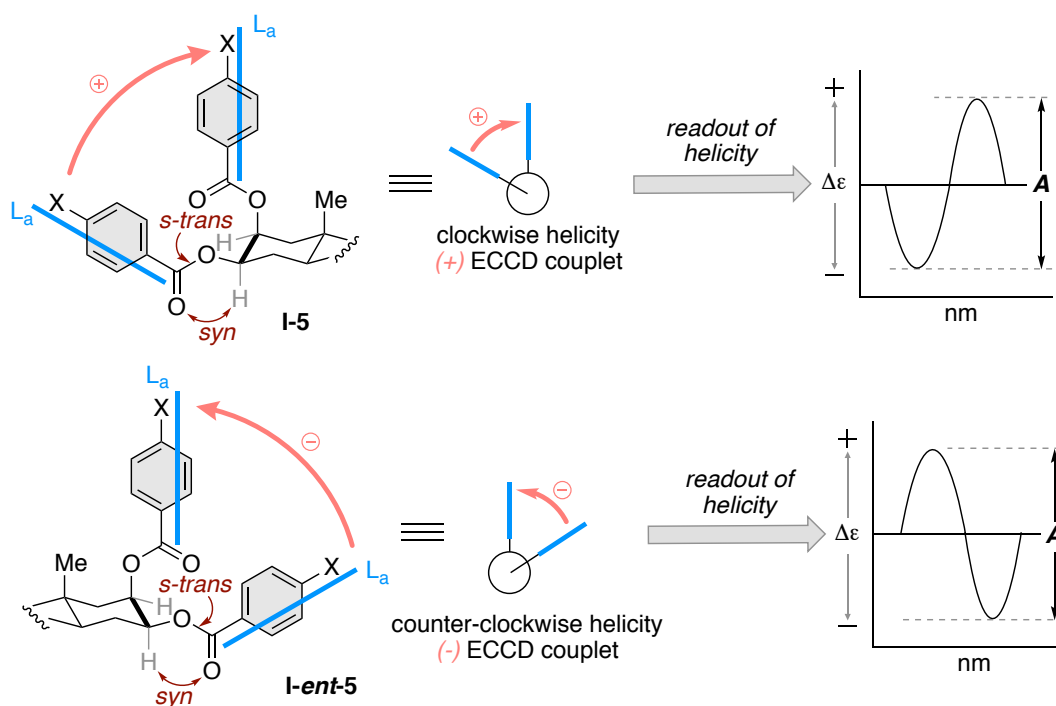


**Figure I-3.** Absolute stereochemical assignment of rigid sterols via non-empirical Exciton Coupled Circular Dichroism.

from the ECCD spectra, which originated from the through space coupling of the benzoate groups. The sign of the ECCD spectrum is directly correlated to the specific helical arrangement of the chromophores, which arises from the absolute configuration of the derivatized carbinol stereocenters (Figure I-3). Since either the positive or negative ECCD signal is directly correlated to the *clockwise* or *counterclockwise* arrangement of the chromophores (helicity) respectively, the method unambiguously assigns the absolute configuration of the carbinol centers in a non-empirical fashion. Several groups have engaged in exploring CD active complexes to elucidate the absolute stereochemistry of organic molecules.<sup>14-18</sup> The commonality in these approaches is the non-empirical readout of asymmetry via analysis of the resultant ECCD spectra.

#### **I-5    Porphyrin tweezer methodology: Absolute stereochemical determination of molecules with two sites of attachment**

One of the greatest successes of the ECCD method is that it can be applied to organic molecules that lack absorbing chromophores or a suitable site for derivatization. In this case, formation of a strong host-guest complex between the chiral analyte and an achiral host molecule containing two or more chromophores is highly desired. The chirality of the organic molecule of interest is transferred to the achiral host via noncovalent interactions. The observed chirality measured via circular dichroism is then correlated to the absolute stereochemistry of the guest molecule. The porphyrin tweezer methodology developed by Nakanishi and coworkers<sup>19</sup> (Figure I-4) is one of the most utilized protocols for this class of organic molecules. In this approach, two porphyrin subunits tethered via a flexible alkyl chain constitute a molecular tweezer that functions

as a sensor of asymmetry for bound chiral guest molecules.<sup>20-23</sup> The high extinction coefficient of porphyrin chromophores allows the determination of absolute configuration at a very low concentration. Chiral molecules containing two sites of attachments (*for example diamines*), form stable complexes with the **I-C<sub>5</sub>-Zn-TPPtz 6**, leading to the formation a complex with specific helicity of the porphyrin subunits with respect to each other. The key to absolute stereochemical determination lies in correlating the experimentally observed helical arrangement of the porphyrins with the chirality of the bound guest molecule. The porphyrin closest to the chiral center adopts an orientation to

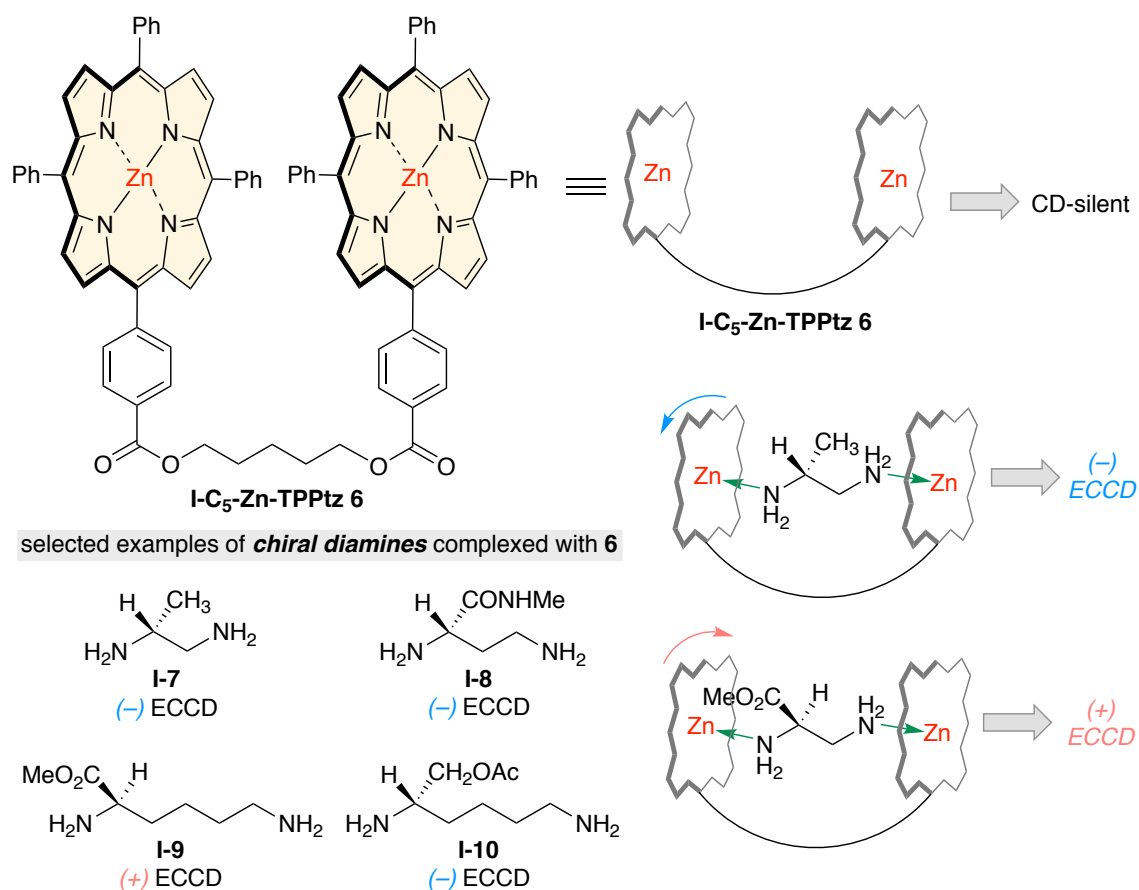


**Figure I-4.** Utilization of porphyrin tweezer methodology for the determination of absolute configuration of chiral diamines.

minimize steric repulsion with the larger group (**L**) on the chiral center. This event leads to a preponderance of either the *P* or *M* helical population, and thus a positive or negative ECCD signal is observed, respectively. This method has been utilized to report the absolute configuration of various molecules with two sites of attachment.

Initially, the porphyrin tweezer methodology was effective in determining the absolute configuration of chiral molecules containing *two* strongly coordinating groups that bound to the divalent zinc center (i.e; diamines). The interaction of the Lewis basic nitrogen atoms with the Lewis acidic divalent zinc atoms of the tweezer was central to the transfer of chirality. Extending this approach to chiral diols or amino alcohols was not trivial. Reduced binding ability of the electronegative oxygen atom as a coordinating functionality led to weak complexation with **I-C<sub>5</sub>-Zn-TPPtz 6**, yielding either no ECCD spectra or weak signals that could not be correlated to the absolute stereochemistry of the guest diol molecule.<sup>24</sup> This was demonstrated by measuring the binding affinity of 2-propanol with monomeric zinc porphyrin (Zn-TPP monoester **I-11**), exhibiting a substantially lower affinity as compared to *iso*-propylamine (Figure I-5, dashed box,  $K_{assoc}$  of 49 M<sup>-1</sup> versus 11,400 M<sup>-1</sup>, respectively). Li et al.<sup>24</sup> solved this problem by increasing the binding affinity for oxygen-based donors with the divalent zinc atoms embedded within the porphyrin by using electron deficient porphyrin rings. The polyfluorinated porphyrin analog (Zn-TPFP monoester **I-12**) was designed to enhance the Lewis acidity of the divalent zinc center, thus leading to stronger complexation with oxygen-based nucleophiles. Comparison of the HOMO and LUMO energies as well as the charge density on the zinc center in Zn-TPFP monoester **I-12** with the parent zinc porphyrin Zn-



TPP monoester **I-11** indicated a lower LUMO energy as well as a higher positive charge density on the zinc center (Figure I-5). These theoretically computed properties were further corroborated with experimentally obtained results. The association constants ( $K_{\text{assoc}}$ ) of 2-propylamine and 2-propanol complexed with Zn-TPFP monoester **I-12** showed much higher amine and alcohol affinities (~40x larger) in comparison to Zn-TPP monoester **I-11** (Figure I-5).

Based on the above understanding, **I-C<sub>5</sub>-Zn-TPFPtz 13** was prepared and complexed with chiral diols in hexane, leading to consistent ECCD signals (Figures I-6a and I-6b). The choice of solvent for ECCD analysis is critical. It is of utmost importance that the solvent does not compete or interfere with the complexation of the chiral guest

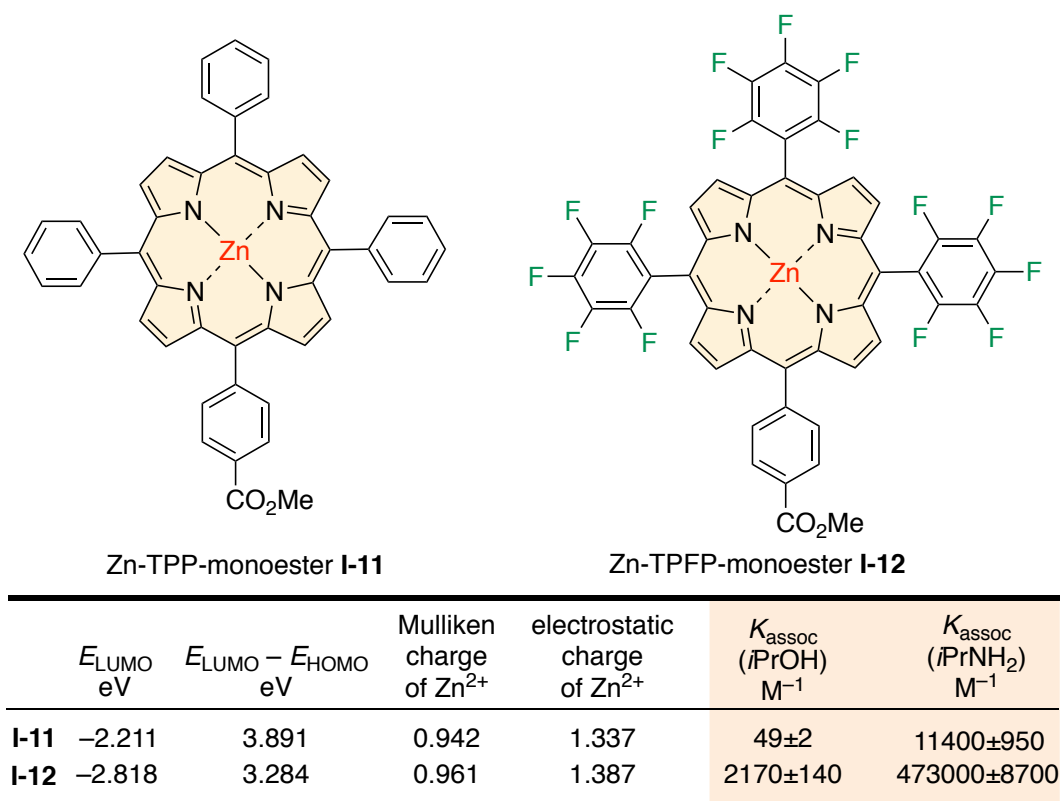


**Figure I-5.** Lowering of LUMO energy via electronic manipulation.

molecule with the zincated porphyrin host system. Notably, in the case of *erythro* and *threo* diols, and 1,2-amino alcohols, the porphyrin bound to each stereogenic functionality governs the induced helicity of the bound porphyrins. Analogous to the mnemonic described for **I-C<sub>5</sub>-Zn-TPPtz 6** with chiral diamines (Figure I-2), the sterics projected from the chiral centers of the guest molecules determine the respective arrangements of the bound porphyrins. As illustrated in Figure I-6c for *erythro* compounds (for instance **I-16**),

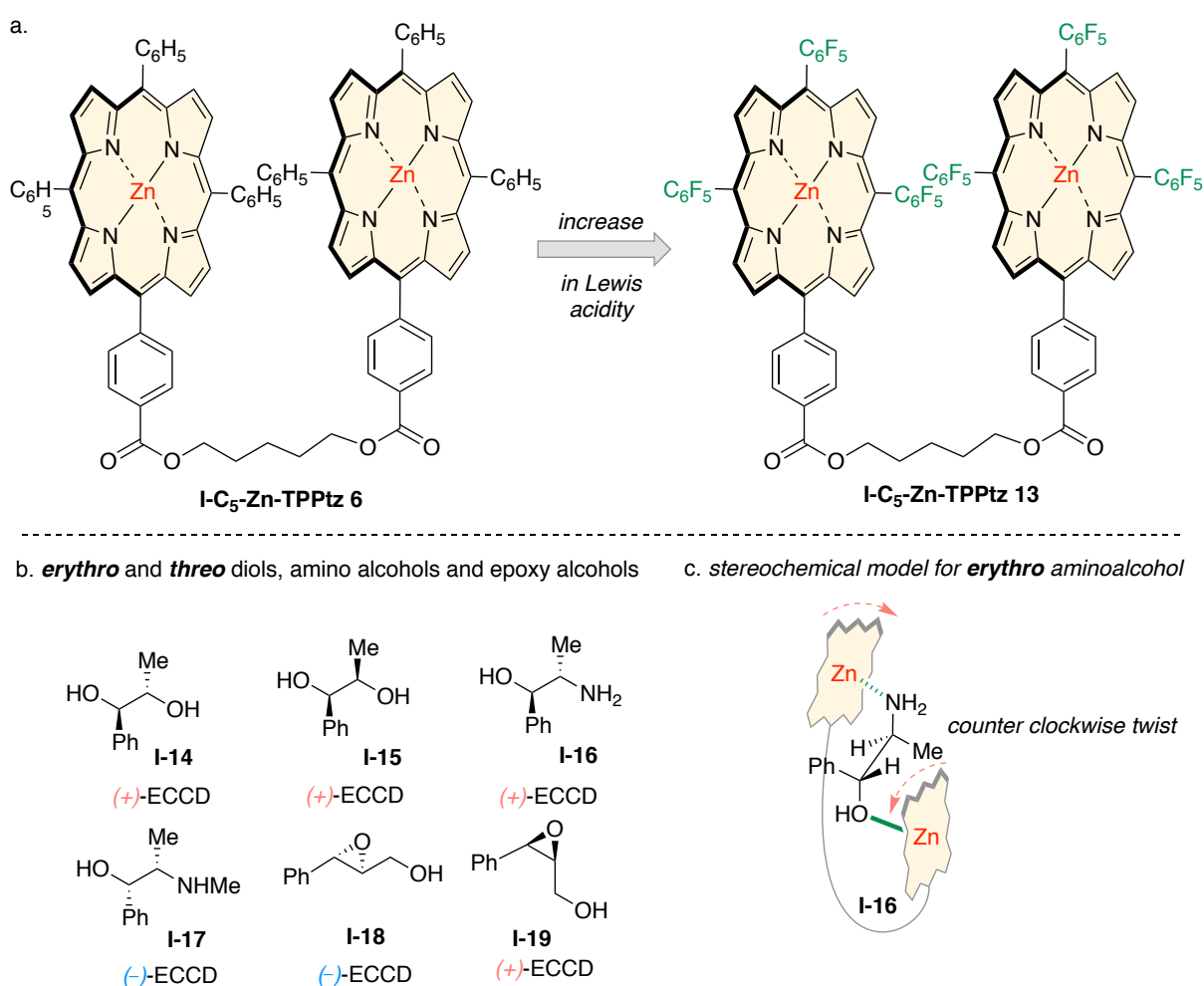


**Figure I-6.** a. Design of a highly Lewis acidic porphyrin tweezer host. b. Absolute stereochemical determination of *erythro*, *threo* diols, amino alcohols, and epoxy alcohols. c. Stereochemical model for *erythro* aminoalcohol.

the two coordinating sites prefer the *anti*-arrangement to alleviate steric repulsion of the substituents on vicinal stereocenters. Furthermore, the porphyrin rings coordinate to the binding sites (oxygen or nitrogen atoms) *anti* to the largest group on the chiral center (phenyl and methyl groups). The porphyrin rings would further adopt a twist towards the small group (hydrogen), which in the illustrated case leads to a clockwise twist, and thus a positive ECCD signal. Notably prior to this work, absolute stereochemical determination of *erythro* diols via the dibenzoate methodology was not possible since the highest populated rotamer places the benzoates *anti* to each other. This is an ECCD silent conformation since no coupling of the chromophore's electronic transition dipole moment

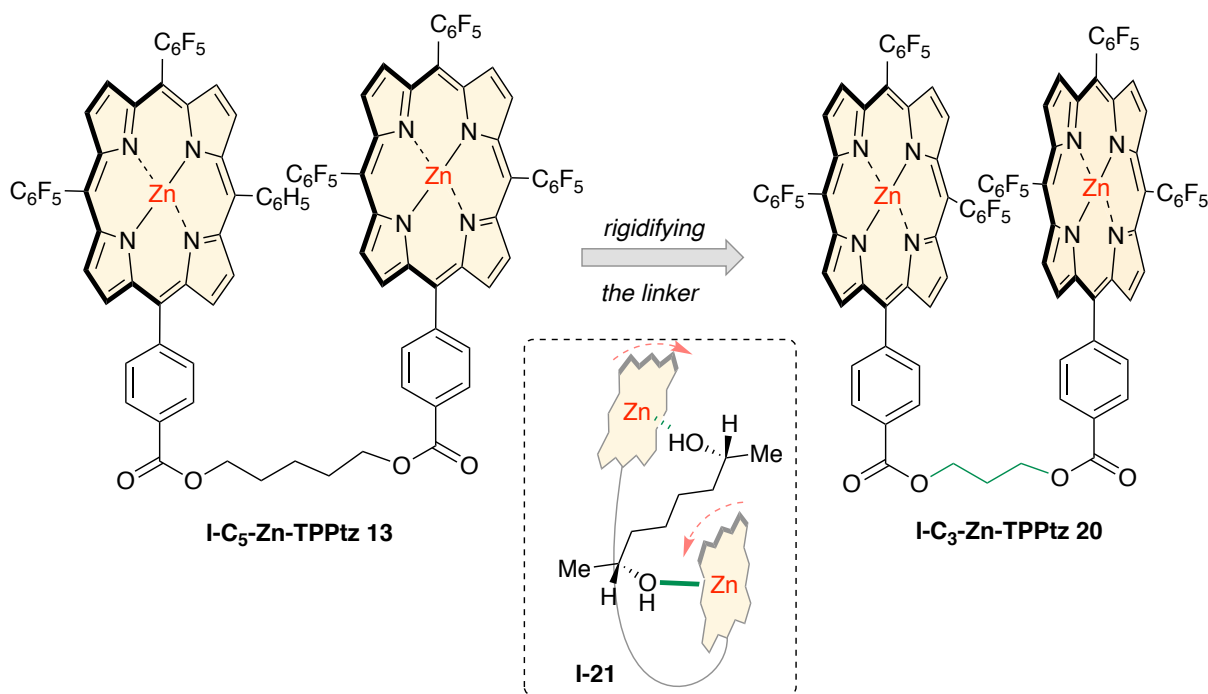


**Figure I-7.** Design of a new host via rigidification of the linker. Stereochemical model to predict the absolute configuration of 1,n diols. ‘Side-on’ coordination, a new mode of binding to accommodate the long diols inside the cavity.

is possible. The use of the fluorinated tweezer **I-C<sub>5</sub>-Zn-TPFPtz 13** was easily extended to these *threo* diols, as well as to epoxy alcohols (Figure I-6b).<sup>24 25</sup>

When a set of chiral *1,n*-diols ( $n \geq 3$ ) were complexed with **I-C<sub>5</sub>-Zn-TPFPtz 13**, the observed helicities were not predictable based on the binding mnemonic that was developed for 1,2-diols. The observed inconsistencies were attributed to the increased flexibility of the complex, resulting in multiple undesired conformations. These discrepancies were resolved by switching to a more rigid porphyrin tweezer that reduced the flexibility of the overall complex when bound with *1,n*-diols (Figure I-7).<sup>26</sup> Tweezer **I-C<sub>3</sub>-Zn-TPFPtz 20** with a shorter alkyl linker (C<sub>3</sub>) was complexed with chiral diols shown in Figure I-7 to provide ECCD signals in full agreement with the predicted helicities. The shorter linker forced the ‘side-on’ binding to accommodate the diols of different chain lengths inside the cavity. This newly predicted ‘side-on’ binding as opposed to the regular ‘head-on’ binding was confirmed based on UV-vis data, computational modeling studies and X-ray studies of long chain diols.

#### **I-6 Porphyrin tweezer methodology: absolute stereochemical determination of molecules with one site of attachment**

The tweezer methodology was initially confined to chiral molecules with *two* sites of attachment. This methodology was later amended to sense the absolute configuration of chiral molecules with *one* site of attachment through a derivatization step prior to complexation with porphyrin tweezers. The strategy entailed the use of a “*carrier*”, which was installed on the chiral molecule to provide an additional binding site for complexation with the chromophoric tweezers. The constraints for a suitable carrier were set as follows:

*a.* It should bear an appropriate functionality for derivatization, *b.* It should have functional groups, preferably nitrogen-based motifs, for strong coordination to the zincated porphyrins; *c.* A desirable carrier would have a rigid framework, so that it will not add new conformations that could complicate prediction of stereochemistry; *d.* A carrier should be

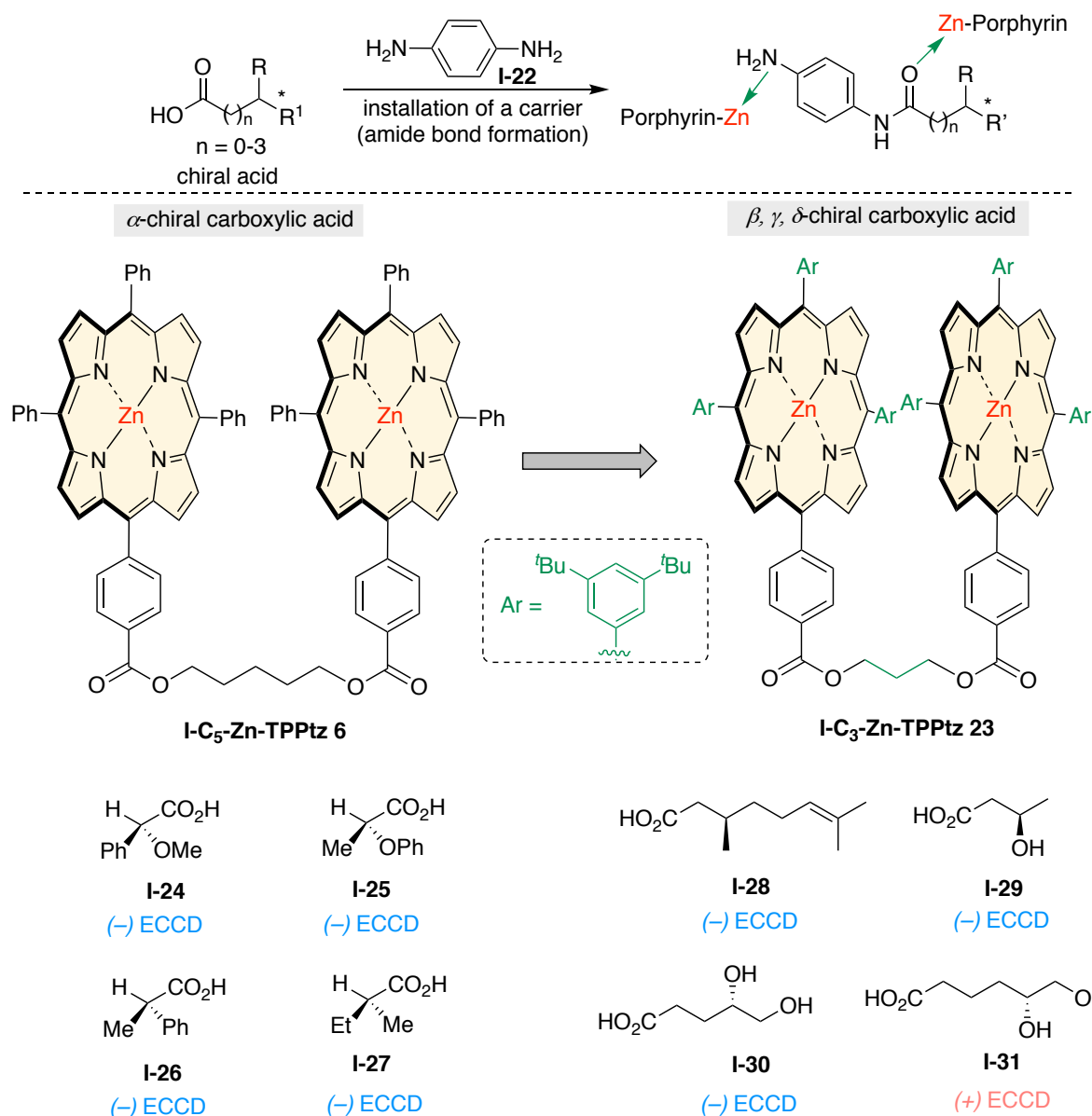


**Figure I-8.** Assignment of absolute stereochemistry for chiral carboxylic acids. Design of a rigidified and sterically encumbered host for sensing the asymmetry at the remote stereocenters.

achiral since the asymmetry of the unknown molecule should be the only chiral element that dictates the helicity of the bound porphyrin tweezer.

Inspired from Nakanishi's prior work,<sup>27-28</sup> Yang et al.<sup>29</sup> developed a rigid carrier 1,4-diamino benzene **I-22** for facile derivatization with chiral carboxylic acids (Figure I-8). The resultant amides complexed with **I-C<sub>5</sub>-Zn-TPPtz 6**, generated ECCD signals consistent with the asymmetry of the guest molecule.

Most of the methodologies discussed so far have the binding element next to the chiral carbon. Applying the same strategy to detect the absolute stereochemistry of chiral centers remote from the point of attachment is often fruitless. It was quickly realized that to sense the absolute configuration on remote stereocenters in chiral carboxylic acid, the sterics of the porphyrin substituents need to be revised. To achieve this goal, a new host with bulky 3,5 di-tertbutyl substituted phenyl rings was synthesized **I-C<sub>3</sub>-Zn-TPPtz 23** (Figure I-8) and complexed with derivatized chiral carboxylic acids bearing  $\beta$ ,  $\gamma$ ,  $\delta$  remote stereocenters.<sup>30</sup> The resultant ECCD signals were consistent with the chirality of the guest molecules.

## I-7 Determination of absolute configuration for molecules with one site of attachment without derivatization

One of the major drawbacks of the porphyrin tweezer methodology is that it requires two sites of attachment. For molecules with one site of attachment, one needs to attach a secondary binding element through derivatization. Based on Inoue's work on the determination of the absolute configuration of chiral monoamines,<sup>31</sup> Borhan and coworkers envisioned that further rigidification of the host tweezer system would be necessary such that a monodentate binder could exert its influence and force a preferred helicity of the host system.<sup>32</sup> Further inspiration came from the elegant work of Feringa

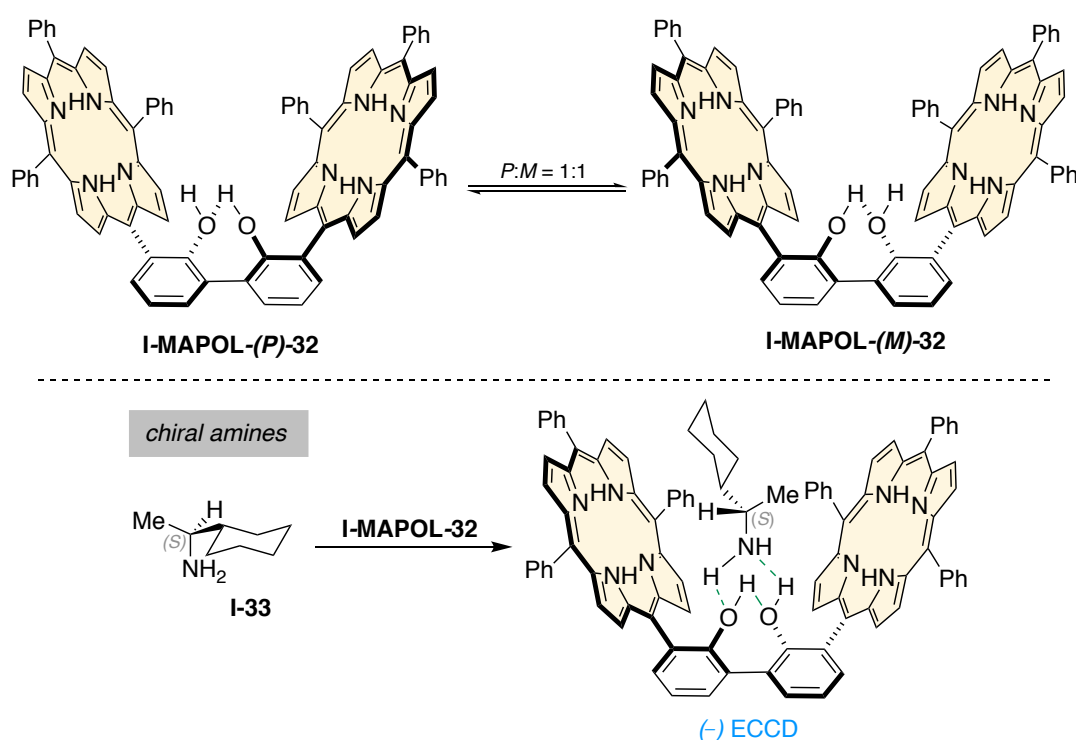


**Figure I-9. I-MAPOL 32**, a class of chiroptical reporter designed for chiral molecules with one binding site. Absolute stereochemical determination of chiral monoamine **I-33**, host-guest complexation via H-bonding.

and coworkers,<sup>33-34</sup> where they had utilized the biphenol core to induce atropisomerism through hydrogen bonding interaction with chiral amino alcohols.

The latter thoughts led to the design of a bis-porphyrin substituted biphenol **I-MAPOL-32** shown in Figure I-9.<sup>32</sup> Biphenol's relatively low barrier to rotation (8-13 kcal/mol) enables the system to equally populate *P* and *M* helicities at any given temperature. Additionally, the anticipated intramolecular hydrogen bonding of the 2,2'-hydroxyl groups favors a *syn* arrangement of the porphyrins, i.e., having the porphyrin rings on the same side as opposed to having them rotate away (*anti*) to each other. The racemic *P/M* equilibrium can be perturbed through the interaction of the chiral guest molecule with the host system.

As a proof of concept, chiral monoamines were complexed with **I-MAPOL 32**, noting that **I-MAPOL 32** is not zincated, and thus the only mode of interaction would be through intermolecular hydrogen binding with the biphenol hydroxyl groups. Based on NMR analyses of the complex, a mnemonic was developed to predict the absolute configuration of the bound monoamines as function of the observed ECCD spectra. As illustrated in Figure I-9, it was hypothesized that the hydrogen bonding of the amine with the 2,2'-biphenol hydroxyl groups would orient the chiral molecule such that the substituents on the asymmetric center are positioned between the porphyrin rings on a 3-fold rotamer (looking through the C-N bond). The free rotation about the C-N bond enables the molecule to adopt an energetically preferred rotamer. As such, the most demanding steric element (cyclohexyl group in the illustration, Figure I-9) would occupy the most open quadrant between the two porphyrins placing the medium methyl group



gauche to the opposite porphyrin. Such orientation would lead to the formation of *M*-helicity for compound **I-33**. Indeed, this was observed experimentally.

Extending this concept for chiral cyanohydrins was not fruitful. Surprisingly, no ECCD signal was observed. This was attributed to a weak hydrogen bonding interaction between **I-MAPOL 32** and the hydroxyl group of cyanohydrin **I-34**. To improve the binding interaction, **I-MAPOL 32** was zincated to potentially achieve a dual binding scenario. As

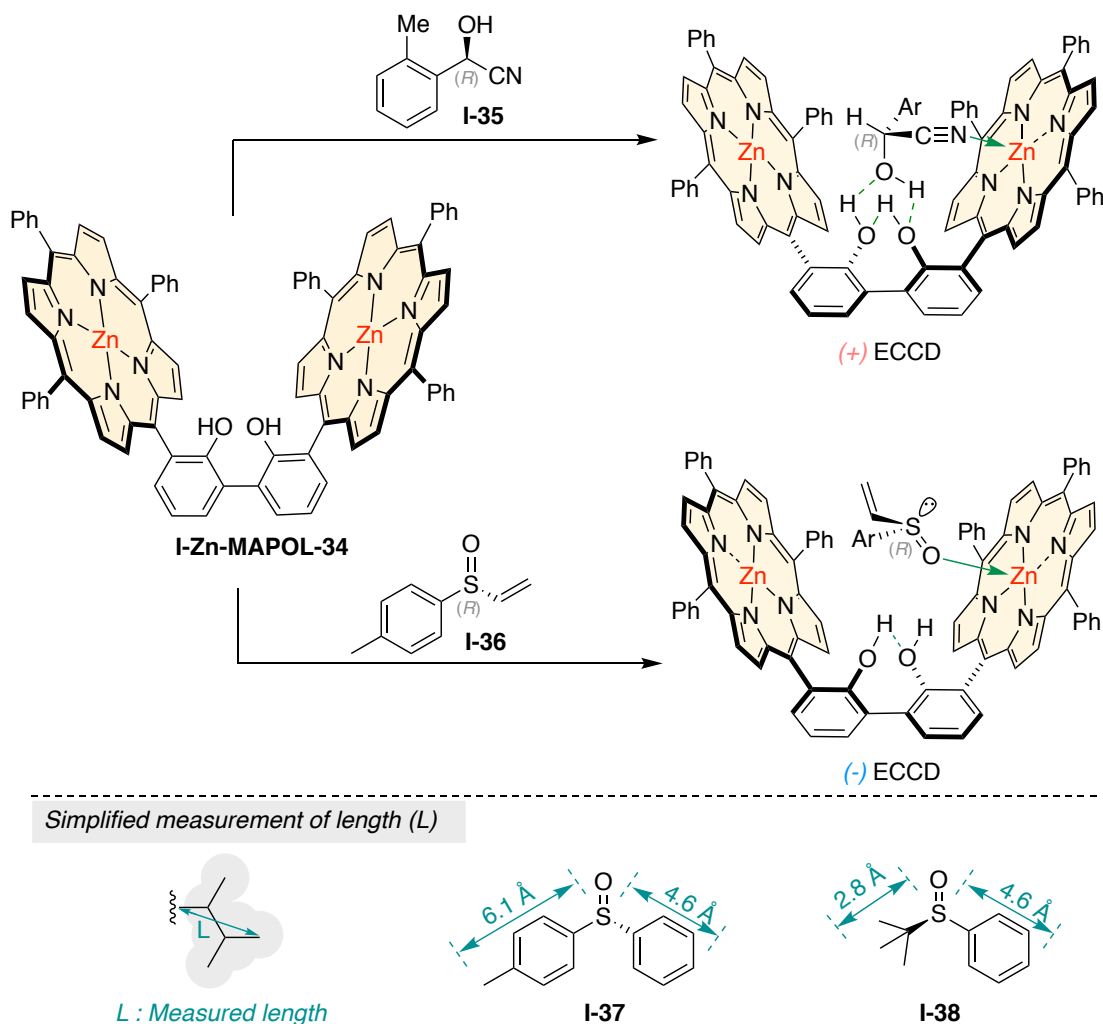


**Figure I-10.** Absolute stereochemical determination of chiral cyanohydrin and chiral sulfoxide molecule. L parameter defined to measure the relative length of the substituents.

discussed above, the porphyrin rings in **I-MAPOL 32** were originally chosen only because

of their chromophoric value and were not intended for complexation with chiral molecules. Nonetheless, their zincation could provide a second coordination site along with the hydrogen bonding that could entropically aid complexation. In fact, addition of **I-35** to **I-Zn-MAPOL 34** resulted in a positive ECCD signal (Figure I-10).<sup>35</sup> It was also found out that both the coordination to the divalent zinc atom, and hydrogen bonding with the biphenol core, were necessary to obtain a consistent ECCD signal. A binding mnemonic was proposed to correlate the sign of the ECCD signals to the stereochemical identity of the bound cyanohydrins. The hydroxyl group hydrogen bonds with the biphenol moiety of the host system whereas the nitrile group coordinates to the metal center. Such an arrangement directs the projection of the two remaining substituents towards the unbound porphyrin ring. As depicted in Figure I-10, placement of the larger tolyl group in the open quadrant is favored, leading to the preponderance of the P-helicity.

With the successful utilization of **I-Zn-MAPOL 34** for cyanohydrins, Borhan and coworkers turned their attention towards exploiting the binding ability of the Zn metal embedded in the porphyrin core. Sulfoxides contain a highly polarized sulfur oxygen bond that can potentially bind with  $\text{Zn}^{2+}$ . Stemming from the strong binding affinity of sulfoxides with **I-Zn-MAPOL 34** (*i.e.*,  $K_{\text{assoc}} = 14,500 \text{ M}^{-1}$ ),<sup>36</sup> strong ECCD signals were obtained with low detection limits and high sensitivities. In many cases, a clear ECCD signal was observed with small sample amounts (*i.e.*,  $<1 \text{ }\mu\text{g}$  of sample per analysis), rendering this methodology suitable for analyses of compounds with limited quantities. The crystal structure of DMSO bound to Zn-TPP confirmed the coordination of sulfoxide to  $\text{Zn}^{2+}$  through its oxygen lone pair, and not via the lone pair on sulfur. With these boundary

conditions, the proposed mnemonic featured coordination of the oxygen atom of sulfoxide **I-36** with the metallocenter, while orienting the lone pair of the sulfur atom towards the bound porphyrin (Figure I-10). This arrangement would project the remaining substituents towards the second porphyrin. Given the projected orientation of the substituents on **I-36** towards the porphyrin ring not bound to the sulfoxide (larger *p*-tolyl vs smaller vinyl group), the *M* complex should be more stable than the *P*, leading to a negative ECCD signal. This agrees with the experimental results.

The success for all methods discussed so far relies on the ability to correlate the relative size of the substituents on a chiral center, which is presumably dictating the helicity of the host-guest complex. Borhan and coworkers have mainly trusted A-strain values as a thermodynamic parameter to rank the substituents based on their relative size. Nonetheless, this analysis failed for chiral sulfoxides. Notably, sulfoxide **I-37**, the *p*-tolyl group would be considered “larger” than the phenyl group, although not by much based on A-strain values (the *p*-methyl substituent would not affect the A-strain value to any large degree), yet the host can discern their subtle steric differences. On the other hand, the lengths of these two substituents are substantially different. Length as a steric parameter is described best by the sterimol analysis, which considers “bulkiness” of a substituent in terms of its length and its width. Analogously, for sulfoxides the measured length *L* was considered as the distance from the sulfur atom to the furthest heavy atom. A representative example of such measurements is shown for the substituents on chiral sulfoxide **I-37** (Figure I-10). Thus, revisiting the observed ECCD with **I-37**, the *p*-tolyl substituent is substantially “longer” than the phenyl group (6.1 Å vs 4.8 Å) and as

projected towards the unbound porphyrin, dictates steric differentiation to yield the observed signal. The perfect example to validate this assumption was found in **I-38**. Based on their A strain values one would anticipate tert-butyl to be larger than phenyl and this would lead to a positive signal for this compound. Nonetheless, an opposite signal was observed. This scenario could be rationalized by taking into consideration of their L values. The phenyl group is longer (4.8 Å) than the tert-butyl group (2.8 Å) and therefore compound **I-38** would favor the formation of *M* helicity leading to the observed negative signal.

In summary, porphyrin tweezers can function as reporters of chirality for molecules with two sites of attachment as well as for molecules where a secondary binding element could be appended via derivatization. Furthermore, Borhan and coworkers devised a new host system **I-Zn-MAPOL 34** that allows for the chiroptical sensing of chiral molecules lacking suitable site for derivatization. The high sensitivity and fast response time offer a microscale, rapid and non-empirical solution for the absolute stereochemical determination of chiral organic molecules.

## REFERENCES

1. Hyttel, J.; Bogeso, K. P.; Perregaard, J.; Sanchez, C., *J. Neural. Transm. Gen. Sect.* **1992**, *88*, 157-160.
2. Stephens, T. D.; Brynner, R. *Dark Remedy: The Impact of Thalidomide and its Revival as a Vital Medicine*; Perseus Publishing: Cambridge, MA, 2001.
3. Smith, G.; Kennard, C. H. L.; White, A. H.; Hodgson, P. G., *Acta. Crystallogr. B.* **1980**, *36*, 992-994.
4. Flack, H. D.; Bernardinelli, G., *Chirality* **2008**, *20*, 681-690.
5. Dale, J. A.; Mosher, H. S., *J. Am. Chem. Soc.* **1973**, *95*, 512-519.
6. Seco, J. M.; Quinoa, E.; Riguera, R., *Tetrahedron: Asymmetry* **2000**, *11*, 2781-2791.
7. Seco, J. M.; Quinoa, E.; Riguera, R., *Chem. Rev.* **2012**, *112*, 4603-4641.
8. Blazewska, K. M.; Gajda, T., *Tetrahedron: Asymmetry* **2009**, *20*, 1337-1361.
9. Pirkle, W. H., *J. Am. Chem. Soc.* **1966**, *88*, 1837.
10. Uccello-Barretta, G.; Balzano, F., *Top. Curr. Chem.* **2013**, *341*, 69-131.
11. Harada, N.; Chen, S. L.; Nakanishi, K., *J. Am. Chem. Soc.* **1975**, *97*, 5345-5352.
12. Berova, N.; Polavarapu, P. L.; Nakanishi, K.; Woody, R. W. *Comprehensive Chiroptical Spectroscopy, Vol. 2. Applications in Stereochemical Analysis of Synthetic Compounds, Natural Products, and Biomolecules*; Wiley: Hoboken, NJ, 2012.
13. Harada, N.; Nakanishi, K. *Circular Dichroic Spectroscopy - Exciton Coupling in Organic Stereochemistry*; University Science Books: Mill Valley, CA, 1983.
14. Borovkov, V. V.; Hembury, G. A.; Inoue, Y., *Acc. Chem. Res.* **2004**, *37*, 449-459.
15. Lu, H.; Kobayashi, N., *Chem. Rev.* **2016**, *116*, 6184-6261.
16. Pasini, D.; Nitti, A., *Chirality* **2016**, *28*, 116-123.
17. You, L.; Zha, D.; Anslyn, E. V., *Chem. Rev.* **2015**, *115*, 7840-7892.

18. Liu, M.; Zhang, L.; Wang, T., *Chem. Rev.* **2015**, *115*, 7304-7397.
19. Huang, X. F.; Rickman, B. H.; Borhan, B.; Berova, N.; Nakanishi, K., *J. Am. Chem. Soc.* **1998**, *120*, 6185-6186.
20. Berova, N.; Pescitelli, G.; Petrovic, A. G.; Proni, G., *Chem. Commun.* **2009**, 5958-5980.
21. Dhamija, A.; Mondal, P.; Saha, B.; Rath, S. P., *Dalton Trans* **2020**, *49*, 10679-10700.
22. Pescitelli, G.; Di Bari, L.; Berova, N., *Chem. Soc. Rev.* **2014**, *43*, 5211-5233.
23. Valderrey, V.; Aragay, G.; Ballester, P., *Coord. Chem. Rev.* **2014**, *258*, 137-156.
24. Li, X.; Tanasova, M.; Vasileiou, C.; Borhan, B., *J. Am. Chem. Soc.* **2008**, *130*, 1885-1893.
25. Li, X.; Borhan, B., *J. Am. Chem. Soc.* **2008**, *130*, 16126-16127.
26. Li, X.; Burrell, C. E.; Staples, R. J.; Borhan, B., *J. Am. Chem. Soc.* **2012**, *134*, 9026-9029.
27. Huang, X.; Fujioka, N.; Pescitelli, G.; Koehn, F. E.; Williamson, R. T.; Nakanishi, K.; Berova, N., *J. Am. Chem. Soc.* **2002**, *124*, 10320-10335.
28. Kurtan, T.; Nesnas, N.; Li, Y. Q.; Huang, X.; Nakanishi, K.; Berova, N., *J. Am. Chem. Soc.* **2001**, *123*, 5962-5973.
29. Yang, Q.; Olmsted, C.; Borhan, B., *Org. Lett.* **2002**, *4*, 3423-3426.
30. Tanasova, M.; Anyika, M.; Borhan, B., *Angew. Chem., Int. Ed.* **2015**, *54*, 4274-4278.
31. Borovkov, V. V.; Lintuluoto, J. M.; Inoue, Y., *J. Am. Chem. Soc.* **2001**, *123*, 2979-2789.
32. Anyika, M.; Gholami, H.; Ashtekar, K. D.; Acho, R.; Borhan, B., *J. Am. Chem. Soc.* **2014**, *136*, 550-553.
33. Eelkema, R.; Feringa, B. L., *J. Am. Chem. Soc.* **2005**, *127*, 13480-13481.
34. Eelkema, R.; Feringa, B. L., *Org. Lett.* **2006**, *8*, 1331-1334.

35. Gholami, H.; Anyika, M.; Zhang, J.; Vasileiou, C.; Borhan, B., *Chemistry* **2016**, *22*, 9235-9239.
36. Gholami, H.; Zhang, J.; Anyika, M.; Borhan, B., *Org. Lett.* **2017**, *19*, 1722-1725.

CHAPTER II: ABSOLUTE STEREOCHEMICAL ASSIGNMENT OF  $\alpha$ -AMINO AND  $\alpha$ -HYDROXYPHOSPHONATES EMPLOYING A SINGLE CHIROPTICAL SENSOR



## II-1 Introduction

$\alpha$ -Amino and  $\alpha$ -hydroxyphosphonates constitute an important family of biologically active molecules because of their desirable pharmacological properties.<sup>1-5</sup> In particular,  $\alpha$ -aminophosphonic acids are considered as structural analogues of natural  $\alpha$ -amino acids, and thus are used as bioisosters in drug discovery platforms. Their structural similarity with the tetrahedral transition state for amide and ester hydrolysis has led to the development of  $\alpha$ -amino and  $\alpha$ -hydroxyphosphonates as potent enzyme inhibitors.<sup>6-7</sup> Furthermore, their importance as antiviral and anticancer agents, antibiotics, neuro-modulators, plant growth regulators, herbicides, and many other applications<sup>8-10</sup> (Figure II-1) has drawn significant attention from medicinal as well as synthetic chemists for their streamlined asymmetric preparation. It is thus not surprising that the efficacy and potency of this class of molecules is often determined by their absolute stereochemistry since it is

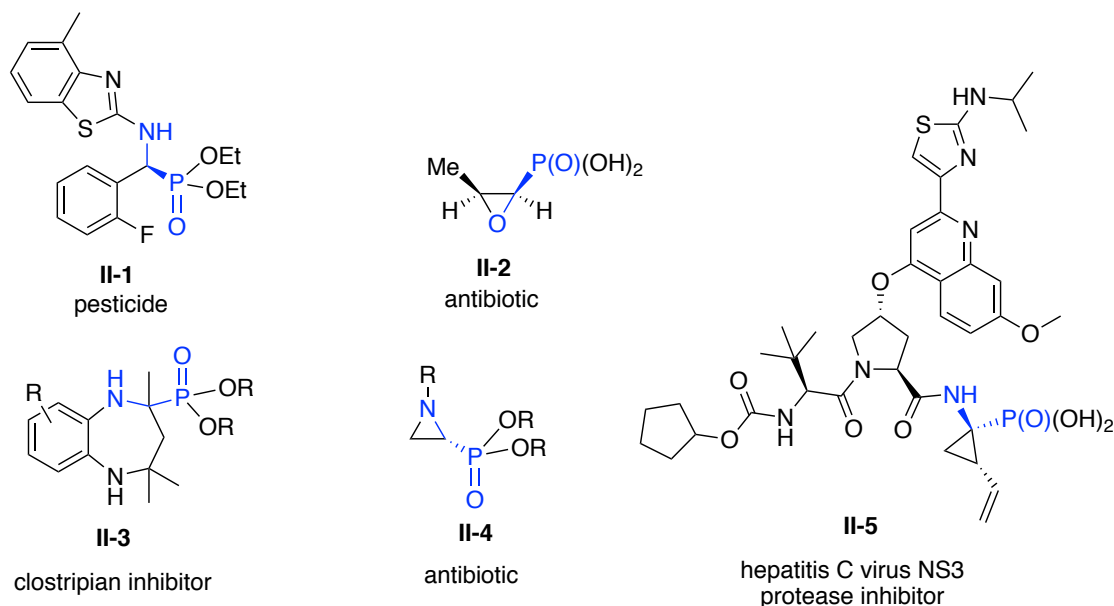


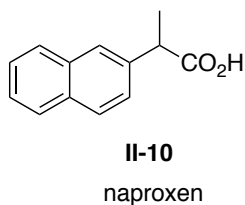
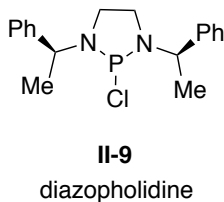
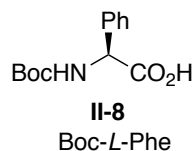
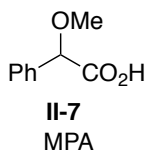
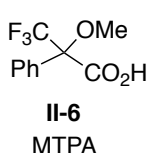
**Figure II-1.** Representative examples of important  $\alpha$ -amino and hydroxyphosphonates.

their interactions with proteins and enzymes that is the key to their biological activity. The recent advancements in asymmetric synthesis have resulted in a plethora of enantioselective methods to access this class of compounds.<sup>11-14</sup> Despite synthetic advances in this area, strategies, and methodologies for rapid determination of their absolute stereochemistry is less developed and remains as a critical bottleneck for structural analysis.

## II-2 Background

Current strategy for the absolute stereochemical assignment of  $\alpha$ -amino and  $\alpha$ -hydroxyphosphonates heavily relies on Mosher ester (or amide) analysis.<sup>15</sup> This protocol necessitates the formation of both Mosher diastereomers with the chiral analyte and subsequent analysis of their  $^1\text{H}$  and  $^{31}\text{P}$  NMR. Often, conformational analysis of the diastereomers is required to predict changes in the NMR data based on optimized conformations of the molecules. Typically for the absolute stereochemical determination of alcohols and amines, MTPA or MPA esters or amides are preferably used (Figure II-

a. Chiral Derivatizing agents



b. Chiral Solvating agents

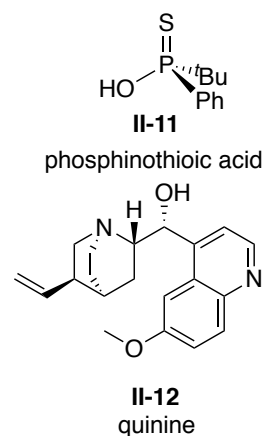


**Figure II-2.** NMR based reagents to elucidate the stereochemistry of  $\alpha$ -amino and hydroxyphosphonates.

2a), whereas for amino and hydroxyphosphonates the naproxen system **II-10** is the only one that has been studied thoroughly (Figure II-2a).<sup>15</sup> Furthermore, these studies are supported by theoretical calculations and low temperature NMR experiments. According to Gajda et al.<sup>15-16</sup> naproxen esters and amides exist mainly in two conformers separated by the rotation around  $C_{\alpha}$ -C(CO) bond. The most stable conformer is the *ap* conformer, where  $C_{\alpha}$ -H bond is anti-periplanar to the  $C_{\alpha}$ -C(CO) bond and is in the same plane as  $C^1$ -H. Despite the success of this naproxen-based method, the overall process is slow, requiring chemical derivatization and chromatographic separation prior to analysis and limited to secondary stereocenters.

Chiral solvating agents (CSA), (Figure II-2b) that form diastereomers via non-

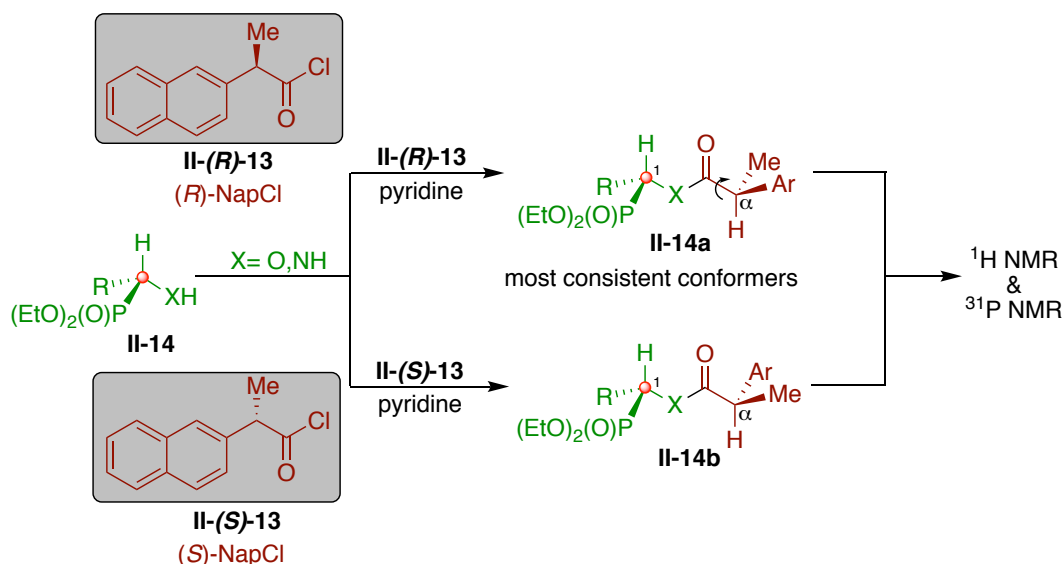


**Figure II-3.** Assignment of the absolute configuration of the  $\alpha$ -amino and hydroxyphosphonates by double derivatization with **II-(R)-13** and **II-(S)-13**.

covalent interactions has also been employed for the absolute stereochemical determination of  $\alpha$ -amino and  $\alpha$ -hydroxyphosphonates. Nonetheless, they do not provide a general solution for this class of compounds as the changes in  $^1H$ -NMR are empirical

and cannot be readily predicted. For example, the application of phosphinothionic acid **II-11**<sup>17</sup> and quinines **II-12**<sup>18-20</sup> is limited to hydroxy phosphonates only.

### **II-3 Absolute stereochemical determination of $\alpha$ -aminophosphonates**

A general chiroptical protocol that can determine the absolute stereochemistry of both  $\alpha$ -amino and  $\alpha$ -hydroxyphosphonates in a rapid manner has remained elusive. To this end, we sought to take advantage of the supramolecular host-guest chemistry where translation of chirality from a chiral guest molecule to the host-guest complex would result in a predictable circular dichroic output. This led to the development of a rapid, general, micro-scale, derivatization-free chiroptical procedure to assign the absolute stereochemistry of  $\alpha$ -amino and  $\alpha$ -hydroxyphosphonates in a non-empirical fashion utilizing the principles of Exciton Coupled Circular Dichroism (ECCD).

In particular, the porphyrin tweezer methodology pioneered by Nakanishi,<sup>21</sup> provided a general solution for the absolute stereochemical determination of chiral molecules that do not possess the required chromophores for exciton coupling. This methodology has been implemented successfully for the stereochemical determination of a variety of molecular families such as alcohols, amines, diols, diamines, amino acids, amino alcohols, epoxy alcohols, carboxylic acid, etc.<sup>22-27</sup> Through bidentate coordination of its Zn-metallo centers with chiral guest molecule, the achiral porphyrin tweezer adopts a specific helicity that yields a significant ECCD signal. The observed signal is the direct consequence of the induced helicity, which in turn depends on the chirality of the guest molecule. Thus, the observed signal can be correlated with the absolute stereochemistry of the guest molecule in a non-empirical fashion. Molecules typically used as guests for

this protocol can be divided in two groups; those with two sites of attachment that can interact in a bidentate fashion with the porphyrin tweezer, and others with only one coordinating site available requiring alternate strategies for complexation with porphyrin tweezers or must rely on the use of different host molecules altogether.  $\alpha$ -Amino and  $\alpha$ -hydroxyphosphonates fall in the first category, where the phosphonate oxygen atom can provide one binding site and the nitrogen or oxygen atom in  $\alpha$ -amino and  $\alpha$ -hydroxyphosphonates, respectively, provide the second binding element. Our prior investigations with porphyrin tweezers have shown that success of this protocol in producing consistent ECCD signals is dependent on limiting the number of possible conformations upon host-guest complexation. To achieve the latter, two strategies have emerged; 1. Large binding affinity ensures a strong host-guest complexation, reducing energetically close-lying conformations that can complicate the ECCD spectrum; and 2. A smaller and/or rigid linker between the two porphyrin rings reduces conformational

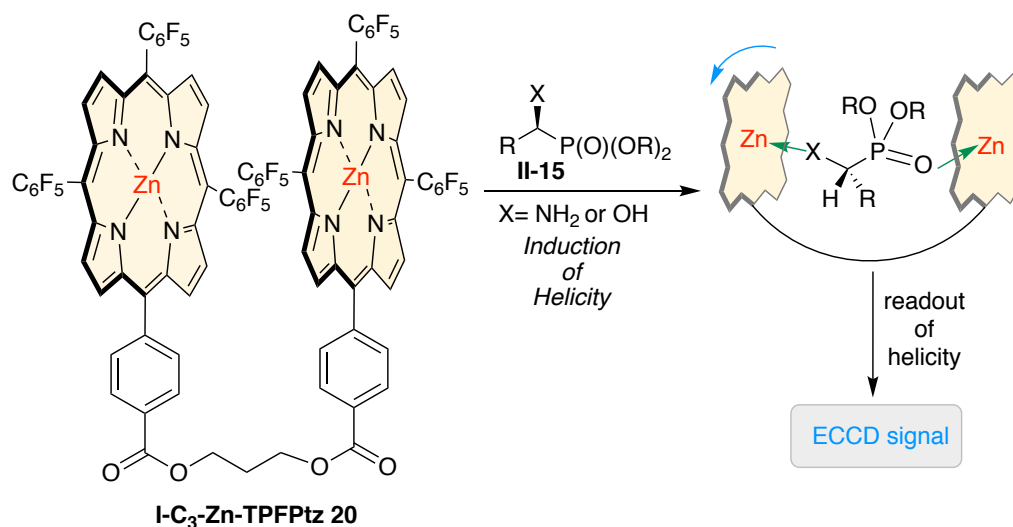
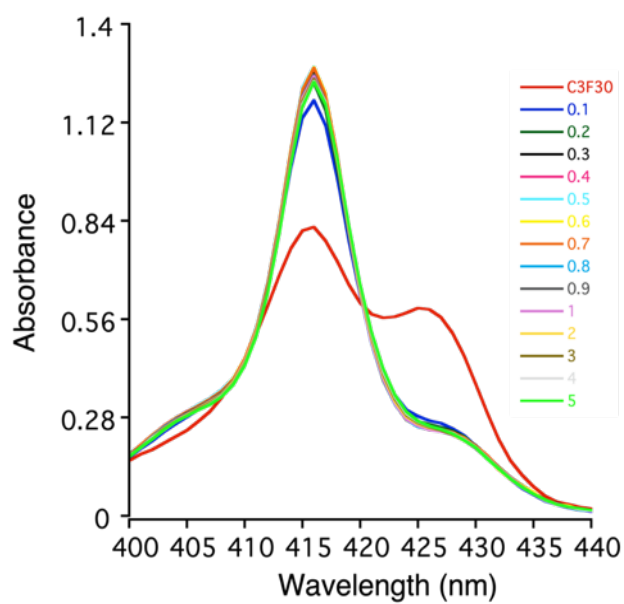


**Figure II-4.** Induction of helicity in host **I-C<sub>3</sub>-Zn-TPFPtz 20** via transfer of chirality from **II-15** through strong host-guest complexation.

flexibility. To this end, we envisioned the use of the fluorinated **I-C<sub>3</sub>-Zn-TPFPtz-20**,<sup>24</sup> where the porphyrin rings are connected by a short C<sub>3</sub> linker (Figure II-4). The fluorinated aryl rings lead to a more Lewis acidic Zn metal center that enhances the binding affinity with  $\alpha$ -amino and  $\alpha$ -hydroxyphosphonates.

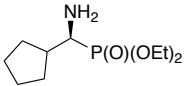
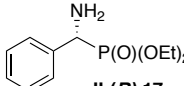
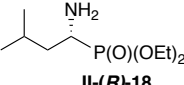
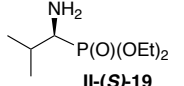
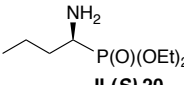
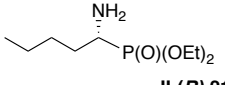
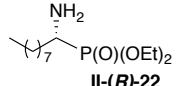
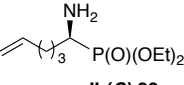
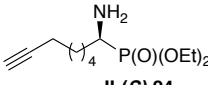
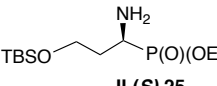
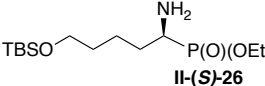
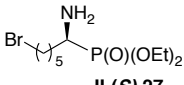
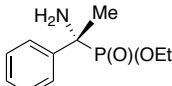
Gratifyingly, a strong positive ECCD signal ( $A = +264$ ) was observed when only 5 equivalents of compound **II-(S)-16** was complexed with C<sub>3</sub>-Zn-TPFPtz-1 (1  $\mu$ M) in hexane at 0 °C (Table II-1). Hexane was chosen as the solvent as it neither competes with the guest molecule in binding with the host, nor does it interact with the guest molecule to diminish the host-guest interaction. Figure II-5 depicts the binding titration of compound **II-(S)-16** with the host. A closer inspection at the spectra reveals almost no shift of the absorbance maxima. It is known in the literature, that a bathochromic shift of ~12 nm for amine and ~8-10 nm for phosphonates are expected when they coordinate to Zn porphyrin.<sup>25, 27</sup> Additionally, these two functional groups can bind to Zn porphyrin strongly, bringing the porphyrins in close proximity. Furthermore, it has been demonstrated, as the two porphyrins come closer a hypsochromic shift in their absorption spectra occurs. Presence of such opposing effects in the same system could explain the observed discrepancy. The successful binding of **II-(S)-16** with **I-C<sub>3</sub>-Zn-TPFPtz-20** that resulted in a strong ECCD signal was followed with the examination of a number of structurally diverse aminophosphonates exhibiting branched alkyl or aryl groups (Table II-1). Next, the system was challenged with aminophosphonates that featured linear alkyl groups of different chain lengths, as well as alkene, alkyne and heteroatoms (Table II-1).

The binding of all of aminophosphonates with **I-C<sub>3</sub>-Zn-TPFPtz-20** led to substantial ECCD signals without any complications.



**Figure II-5.** UV-vis titration of **I-C<sub>3</sub>-ZnTPFPtz 20** (1  $\mu$ M) with **II-(S)-16** at 0  $^{\circ}$ C in hexane.

**Table II-1.** ECCD of  $\alpha$ -aminophosphonates with **I-C<sub>3</sub>-Zn-TPFPtz-20**

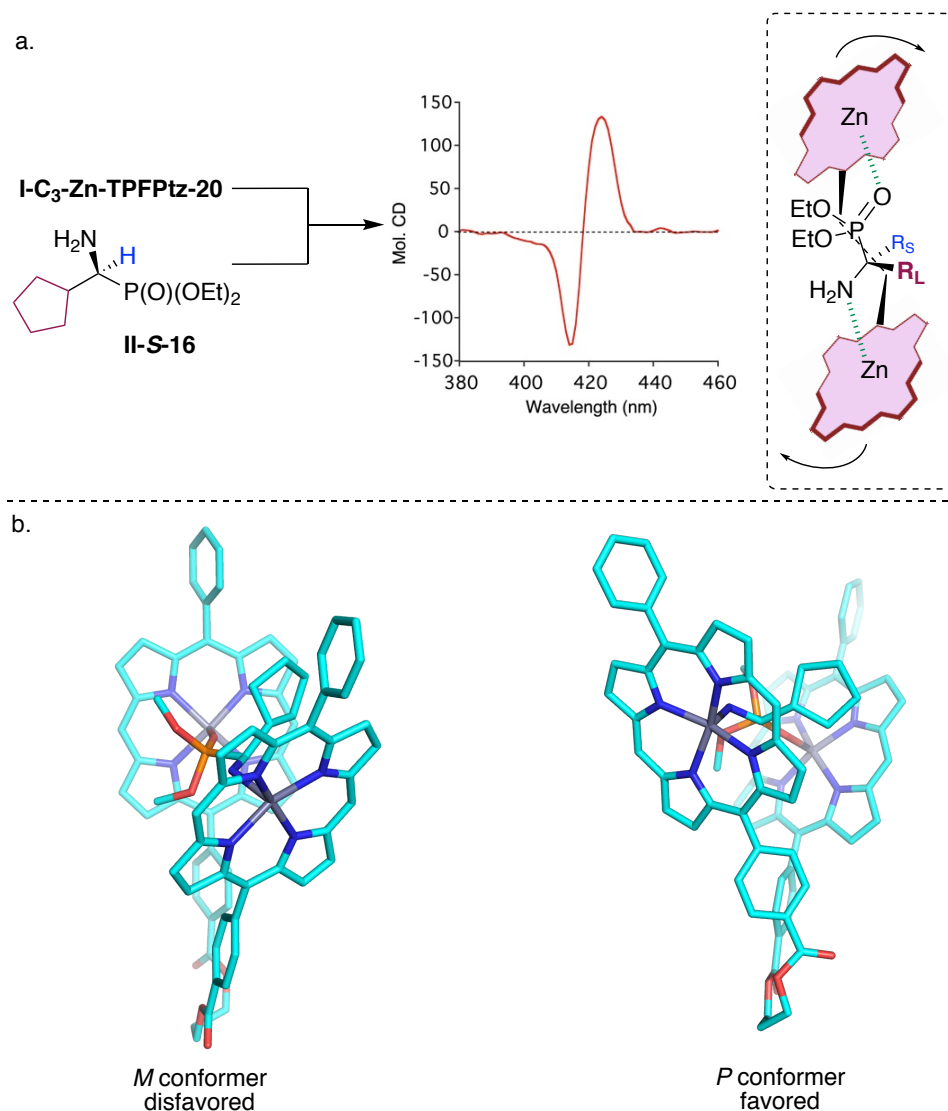
Phosphonate	Predicted sign	$\lambda$ , nm ( $\Delta\epsilon$ )	$A/A_{\text{corr}}$
 <b>II-(S)-16</b>	positive	424, +133 412, -131	+264 <sup>b</sup> /+372
 <b>II-(R)-17</b>	negative	425, -117 414, +81	-198 <sup>b</sup> /-220
 <b>II-(R)-18</b>	negative	424, -117 415, +136	-253 <sup>b</sup> /-278
 <b>II-(S)-19</b>	positive	421, +106 414, -77	+183 <sup>b</sup> /+229
 <b>II-(S)-20</b>	positive	426, +32 417, -25	+57 <sup>b</sup> /+64
 <b>II-(R)-21</b>	negative	422, -27 415, +27	-54 <sup>b</sup> /-60
 <b>II-(R)-22</b>	negative	422, -28 415, +26	-54 <sup>c</sup> /-67
 <b>II-(S)-23</b>	positive	426, +52 414, -36	+88 <sup>b</sup> /+100
 <b>II-(S)-24</b>	positive	425, +21 416, -45	+66 <sup>c</sup> /+72
 <b>II-(S)-25</b>	positive	425, +87 413, -56	+143 <sup>b</sup> /+172
 <b>II-(S)-26</b>	positive	426, +144 416, -96	+240 <sup>a</sup> /+282
 <b>II-(S)-27</b>	positive	426, +122 416, -93	+215 <sup>a</sup> /+247
 <b>II-(R)-28</b>	negative	425, -150 414, +185	-335 <sup>a</sup>

a. 1 equiv of guest   b. 5 equiv of guest   c. 10 equiv of guest



In general, (*R*)  $\alpha$ -aminophosphonates produced a negative ECCD signal whereas (*S*)  $\alpha$ -aminophosphonates generated a positive signal. We believe that stereochemical differentiation that leads to the induced ECCD of the host is driven by steric considerations of the guest substituents, yet caution is warranted as Cahn-Ingold-Prelog stereochemical assignment may not always follow steric preferences. In all examples listed in Table II-1 the larger substituent based on A strain values also has the third priority (phosphonate first and amino being second) by CIP rule. Correlation of the sign of the ECCD spectra for complexes generated between **I-C<sub>3</sub>-Zn-TPFPtz-20** and the aminophosphonates with their known absolute stereochemistry provided the opportunity to derive a simple predictive binding mnemonic (Figure II-6a). A bidentate coordination between the phosphonate oxygen and nitrogen atom with the Zn-metallo centers would place compound **II-(S)-16** between the two porphyrin rings. As depicted in Figure II-6a, the porphyrin coordinated to the oxygen atom does not dictate the helicity of the host-guest complex as the adjacent P center is achiral. The other porphyrin that binds the nitrogen atom is close to the asymmetric center. An energetically favorable conformer would dictate the smaller H atom towards the linker and place the larger cyclopentyl group (larger substituent based on A strain value), away from the nitrogen bound porphyrin ring in the open quadrant. Such orientation of the chromophores would result in a *P* helicity and a positive ECCD signal is expected. Indeed, substrate **II-(S)-16** yielded a positive ECCD spectrum (Figure II-6a). Computational study (B3LYP/6-31G\*) also agrees with the same intuitive reasoning as the conformer that adopts *P*-helicity is 0.83 kcal/mol more stable as compared to the *M*-helical conformer. The predicted signs of all  $\alpha$ -

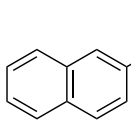
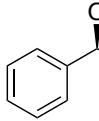
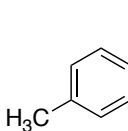
aminophosphonates presented in Table II-1 are consistent with the proposed binding model. In general, compounds with branched alkyl groups and aromatic substituents lead to a stronger ECCD signal. This can be rationalized based on the greater steric differentiation between the larger substituent and the H atom (based on the A strain value).



**Figure II-6.** a. Proposed binding pnemonic to correlate the observed ECCD signal with the guest stereochemistry. b. Optimized (B3LYP/6-31G\* level) *P* and *M* conformer of compound **II-S-16** complexed with **I-C<sub>3</sub>-Zn-TPFPtz-20**. The calculation predicts *P* conformer to be 0.83 kcal/mol lower in energy. Phenyl groups at 10,20 positions are not shown here for clarity.

With the initial success of **I-C<sub>3</sub>-Zn-TPFPtz-20** in determining the absolute stereochemistry of secondary  $\alpha$ -aminophosphonates, the host system was then challenged with the tertiary aminophosphonate **II-(R)-28**. Notably, Mosher model is limited to a secondary chiral center and cannot be extended directly to determine the absolute configuration of a tertiary center. To determine the absolute chirality of **II-(R)-28** via MTPA ester, Hammerschmidt et al.<sup>28</sup> considered the Me group to be on the same plane as the carbonyl of the corresponding MTPA amide of **II-(R)-28**. Although the difference in <sup>1</sup>H chemical shift matched with the model, the <sup>31</sup>P NMR chemical shift difference turned out exactly the opposite to that expected from the predicted model. Furthermore, Mosher ester method has never been used as a general method to determine the absolute stereochemistry of tertiary aminophosphonates. When treated with **I-C<sub>3</sub>-Zn-TPFPtz-20** under identical conditions compound **II-(R)-28** yielded an ECCD signal consistent with the ECCD signal. The observed signal is in accordance with mnemonic (Figure II-6a) where

**Table II-2.** ECCD of  $\alpha$ -hydroxyphosphonates with **I-C<sub>3</sub>-ZnTPFPtz-20**

Phosphonate	Predicted sign	$\lambda$ nm ( $\Delta\epsilon$ )	A/A <sub>corr</sub>
 <b>II-(S)-29</b>	positive	424, +122 412, -72	+194/+198
 <b>II-(S)-30</b>	positive	424, +81 412, -30	+111/+173
 <b>II-(S)-31</b>	positive	424, +40 413, +11	+ 51/+88
----- a. 1 equiv. of guest			

the smaller Me group is pointed towards the linker and porphyrin slides away from the Ph group. This demonstrates the generality of our developed methodology.

#### **II-4 Absolute stereochemical determination of $\alpha$ -hydroxyphosphonates**

The successful implementation of **I-C<sub>3</sub>-Zn-TPFPtz-20** as a “reporter of chirality” for the  $\alpha$ -aminophosphonates prompted us to expand the generality of the methodology for  $\alpha$ -hydroxyphosphonates. We surmised that **I-C<sub>3</sub>-Zn-TPFPtz-20** should bind  $\alpha$ -hydroxyphosphonates in a similar fashion with the hydroxyl oxygen serving as the secondary binding element. Thus, **II-(S)-30** can be considered as the pseudo-enantiomer of **II-(R)-17**, since the *R*-amino group is replaced with an *S*-hydroxyl group, while the rest of the substituents are the same. As predicted, complexation of **II-(S)-30** with **I-C<sub>3</sub>-Zn-TPFPtz-20** leads to a negative ECCD signal, which is opposite to that observed with **II-(R)-17**. The observed ECCD spectra with **II-(S)-29** and **II-(S)-31** are also in full agreement with the predicted signs based on the proposed mnemonic (Table II-2).

In summary, we have demonstrated a simple chiroptical procedure for the determination of absolute stereochemistry of  $\alpha$ -aminophosphonates and  $\alpha$ -hydroxy phosphonates. This protocol does not require derivatization or chromatographic separation prior to analysis. Strong host-guest complex formation leads to a discernable ECCD signal at a micromolar level. A simple binding model based on the size of the substituents can easily correlate the chirality of the guest with the observed ECCD spectra.

## II-5 Experimental section

### II-5-1 Materials and general instrumentation

Anhydrous solvents used for CD measurements were purchased from Aldrich and were spectra grade. Unless otherwise mentioned, solvents were purified as follows. CH<sub>2</sub>Cl<sub>2</sub> was dried over CaH<sub>2</sub>. CD spectra were recorded on a JASCO J-810 spectropolarimeter, equipped with a temperature controller (Neslab 111) for low temperature studies, and are reported as Mol. CD /  $\lambda$  [nm]. UV-vis spectra were recorded on an Agilent, Cary 100 UV-visible spectrophotometer equipped with temperature controller. UV-vis spectra were collected with scan rate of 100 nm/min. All the amino and hydroxyphosphonates were synthesized following literature procedure.<sup>11, 29-30</sup> Compound **I-C3-ZnTPFP-20** was synthesized following the protocol developed in our lab.<sup>24</sup>

### II-5-2 General procedure for UV measurements

**I-C3-ZnTPFP-20** (1.0  $\mu$ L of a 0.001M solution in anhydrous dichloromethane, 1.0  $\mu$ mol) was added to hexane (1.0 mL) in a 1.0 cm UV-cell. The background spectrum was recorded from 350 nm to 480 nm at a scan rate of 100 nm/min. Chiral guests (1 up to 100 equivalents) from three different stock solutions in anhydrous dichloromethane [0.01M (for 10-100 equiv), 0.001M (for 1-10 equiv), 0.0001M (for 0.1-1 equiv)] were then added to the **I-C3-ZnTPFP-20** solution. The UV-vis spectra were collected after each addition at 0 °C.

### II-5-3 General procedure for CD measurements

**I-C3-ZnTPFP-20** (1.0  $\mu$ L of a 0.001M solution in anhydrous dichloromethane, 1.0  $\mu$ mol) was added to hexane (1.0 mL) in a 1.0 cm CD cell (cooled to 0  $^{\circ}$ C) to obtain a 1.0  $\mu$ M solution. The background spectrum was recorded from 350 nm to 480 nm with a scan rate of 100 nm/min at 0  $^{\circ}$ C. Chiral aminophosphonate and hydroxyphosphonate from a stock solution in anhydrous dichloromethane (0.001 M for 1-10 equiv and 0.01 M for 10-20 equiv) was added to the prepared host solution to afford the host-guest complex. The CD spectra were measured immediately (10 scans). The resultant ECCD spectra recorded in millidegrees were converted the molecular CD (Mol. CD) considering the host concentration of 1.0  $\mu$ M.

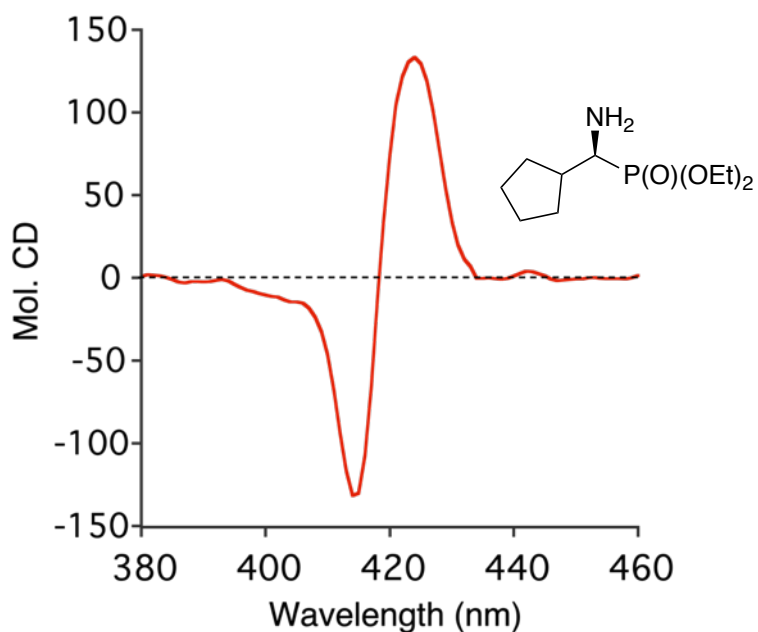


**Figure II-7.** Positive EECDD spectrum of **I-C3-ZnTPFP-20** complexed with 5 equiv of **II-(S)-16** at 0 °C in hexane.

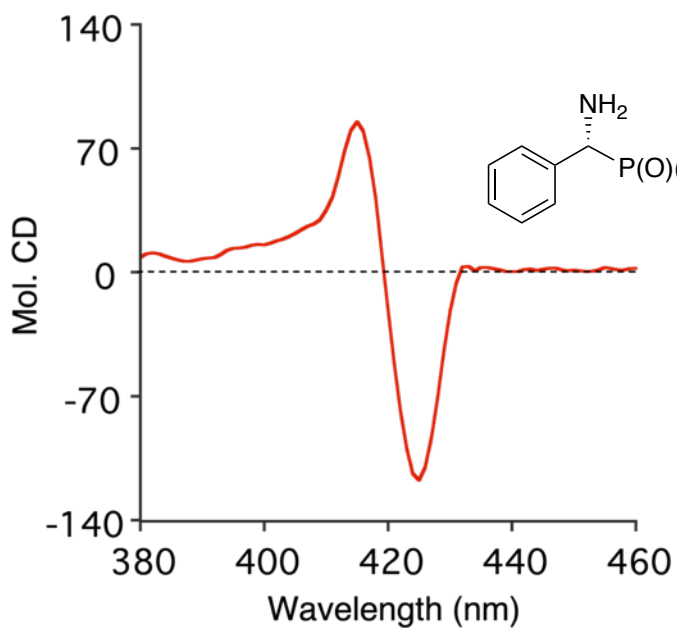


**Figure II-8.** Negative EECDD spectrum of **I-C3-ZnTPFP-20** complexed with 5 equiv of **II-(R)-17** at 0 °C in hexane.

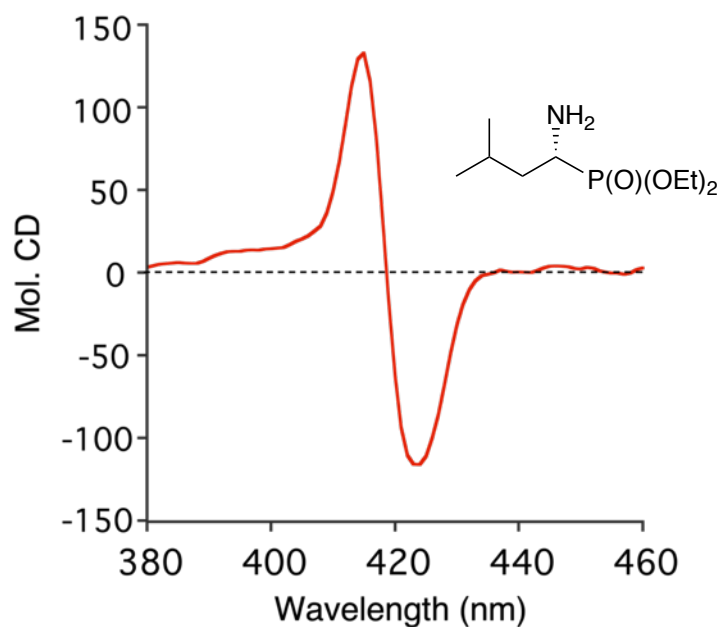


**Figure II-9.** Negative ECCD spectrum of **I-C3-ZnTPFP-20** complexed with 5 equiv of **II-(R)-18** at 0 °C in hexane.

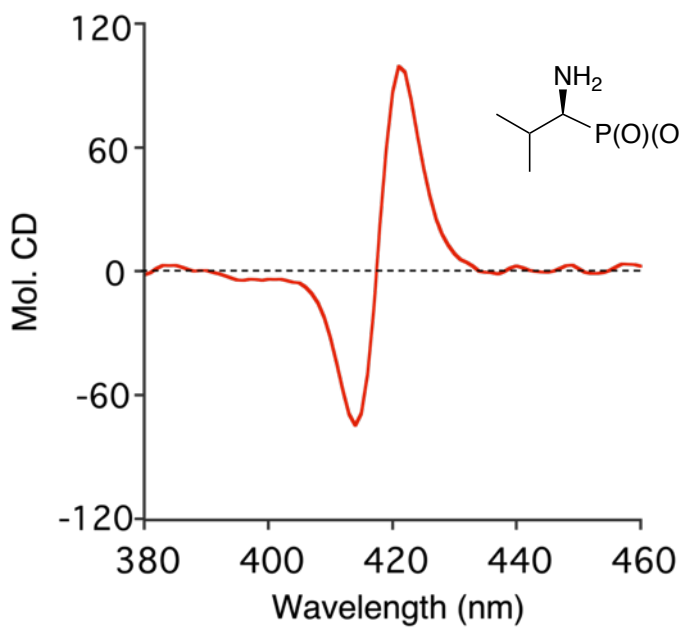


**Figure II-10.** Positive ECCD spectrum of **I-C3-ZnTPFP-20** complexed with 5 equiv of **II-(S)-19** at 0 °C in hexane.



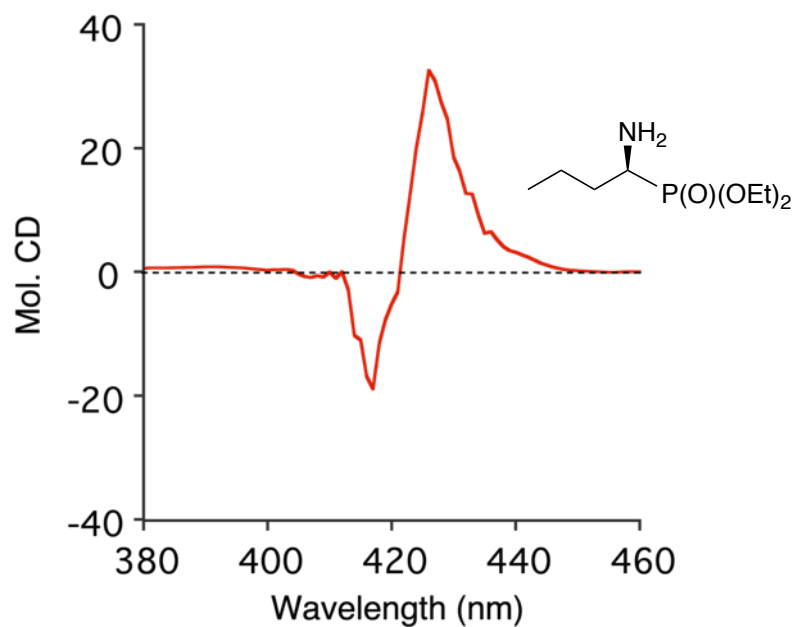


**Figure II-11.** Positive ECD spectrum of **I-C3-ZnTPFP-20** complexed with 5 equiv of **II-(S)-20** at 0 °C in hexane.

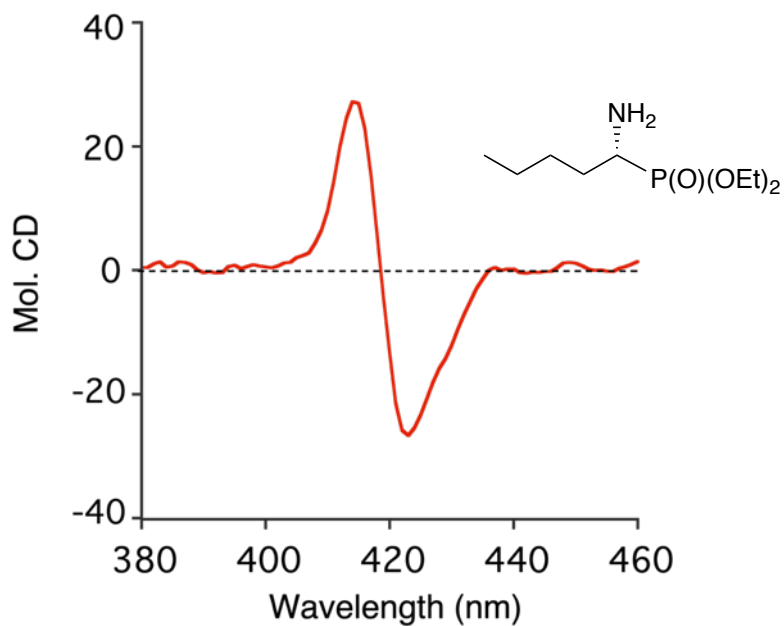


**Figure II-12.** Negative ECD spectrum of **I-C3-ZnTPFP-20** complexed with 5 equiv of **II-(R)-21** at 0 °C in hexane.

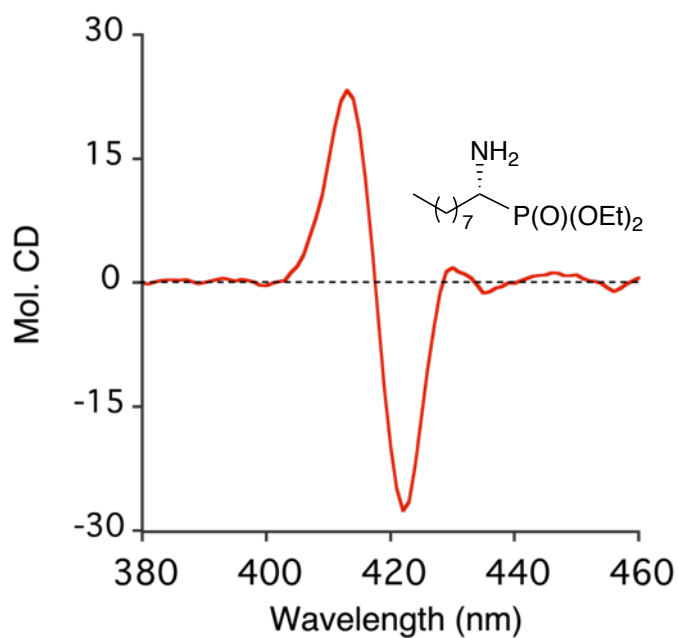


**Figure II-13.** Negative ECCD spectrum of **I-C3-ZnTPFP-20** complexed with 10 equiv of **II-(*R*)-22** at 0 °C in hexane.

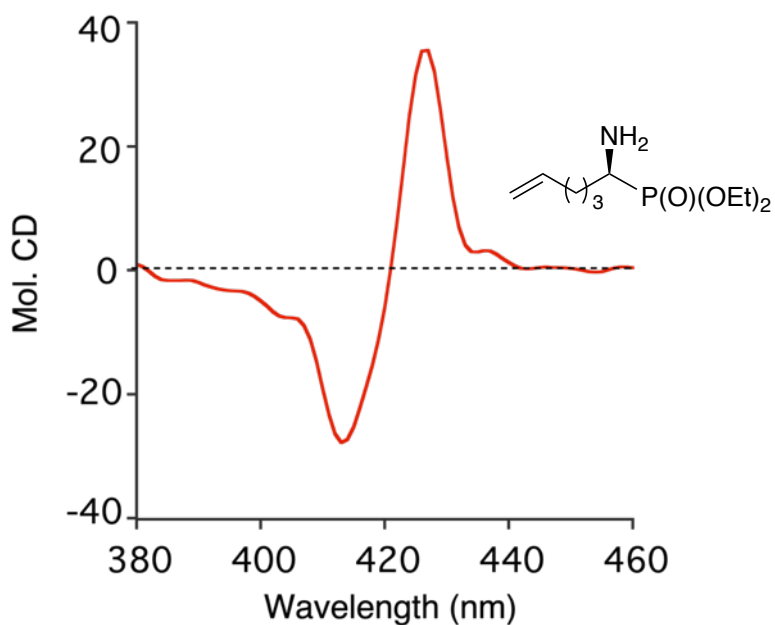


**Figure II-14.** Positive ECCD spectrum of **I-C3-ZnTPFP-20** complexed with 5 equiv of **II-(*S*)-23** at 0 °C in hexane.

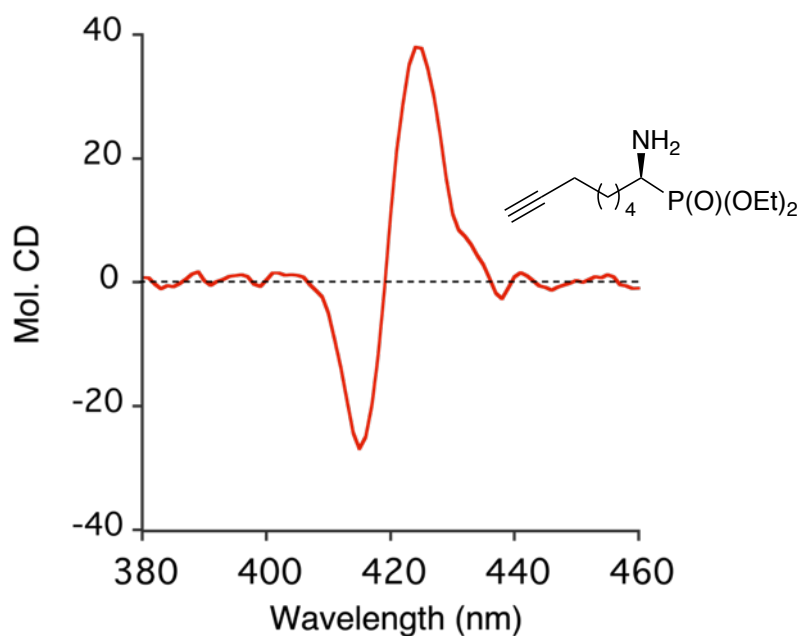


**Figure II-15.** Positive ECCD spectrum of **I-C3-ZnTPFP-20** complexed with 10 equiv of **II-(*R*)-24** at 0 °C in hexane.

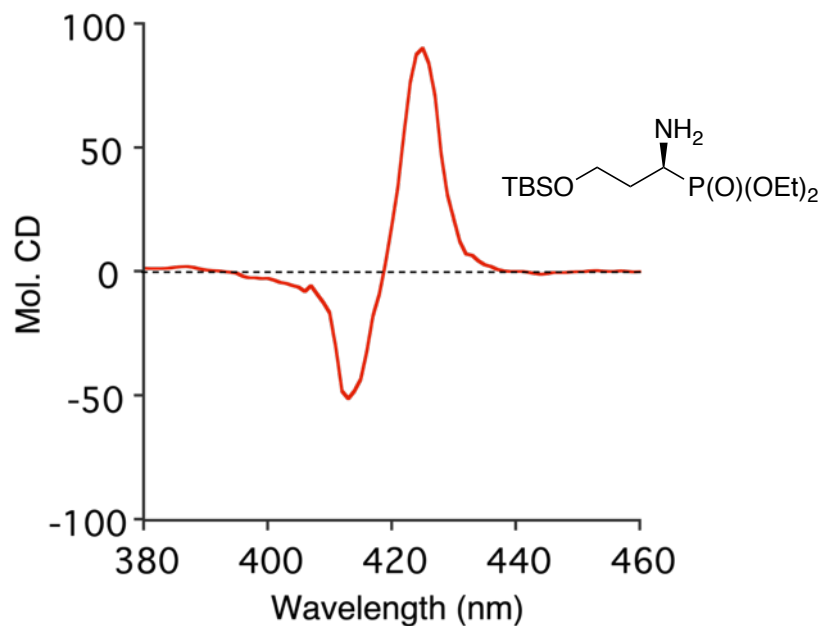


**Figure II-16.** Positive ECCD spectrum of **I-C3-ZnTPFP-20** complexed with 5 equiv of **II-(*R*)-25** at 0 °C in hexane.

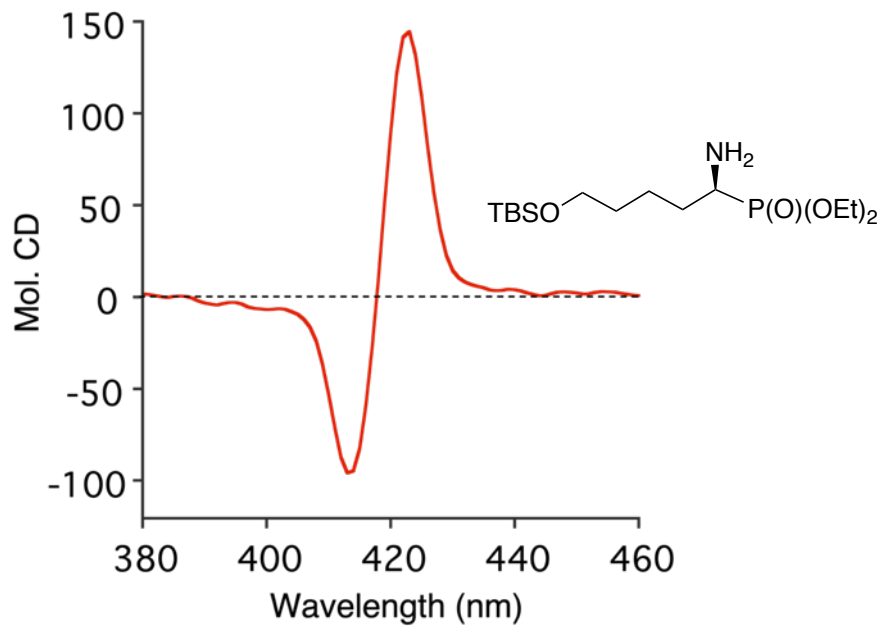


**Figure II-17.** Positive ECCD spectrum of **I-C3-ZnTPFP-20** complexed with 1 equiv of **II-(R)-26** at 0 °C in hexane.

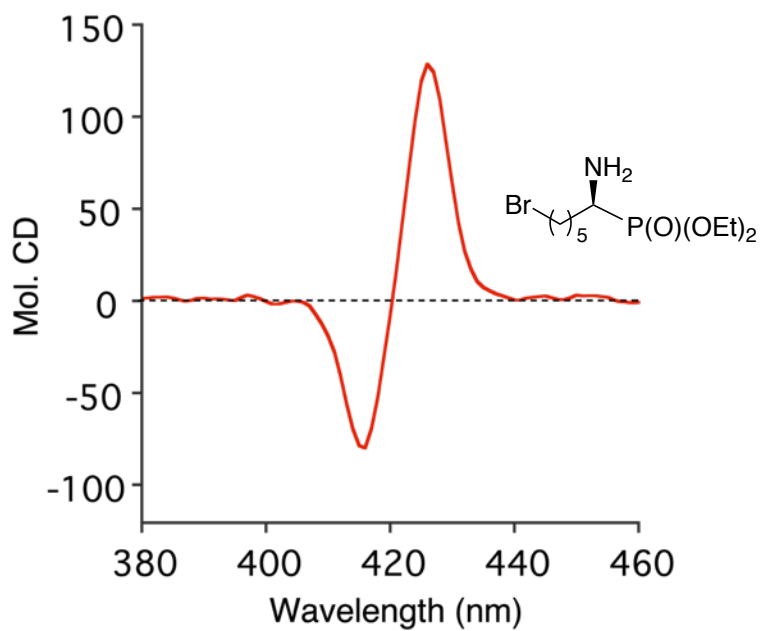


**Figure II-18.** Positive ECCD spectrum of **I-C3-ZnTPFP-20** complexed with 1 equiv of **II-(R)-27** at 0 °C in hexane.

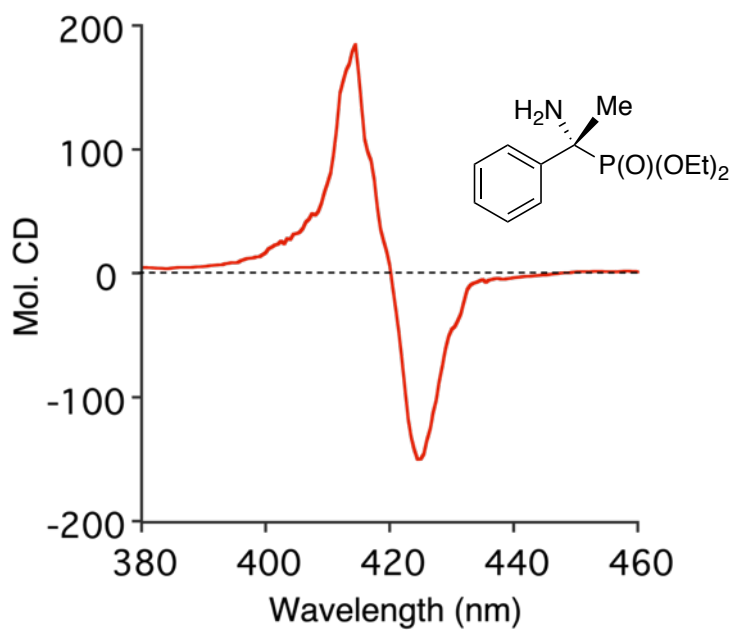


**Figure II-19.** Negative ECCD spectrum of **I-C3-ZnTPFP-20** complexed with 1 equiv of **II-(*R*)-28** at 0 °C in hexane.

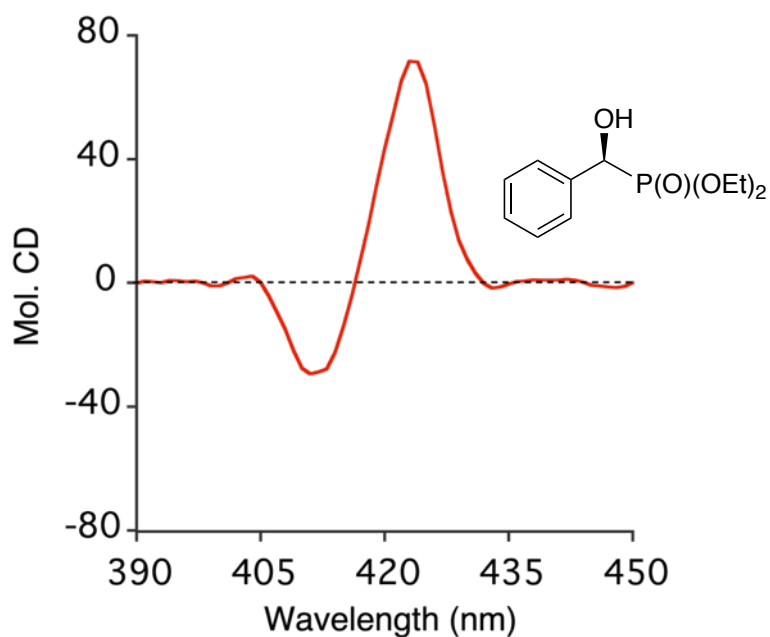


**Figure II-20.** Positive ECCD spectrum of **I-C3-ZnTPFP-20** complexed with 1 equiv of **II-(*S*)-29** at 0 °C in hexane.

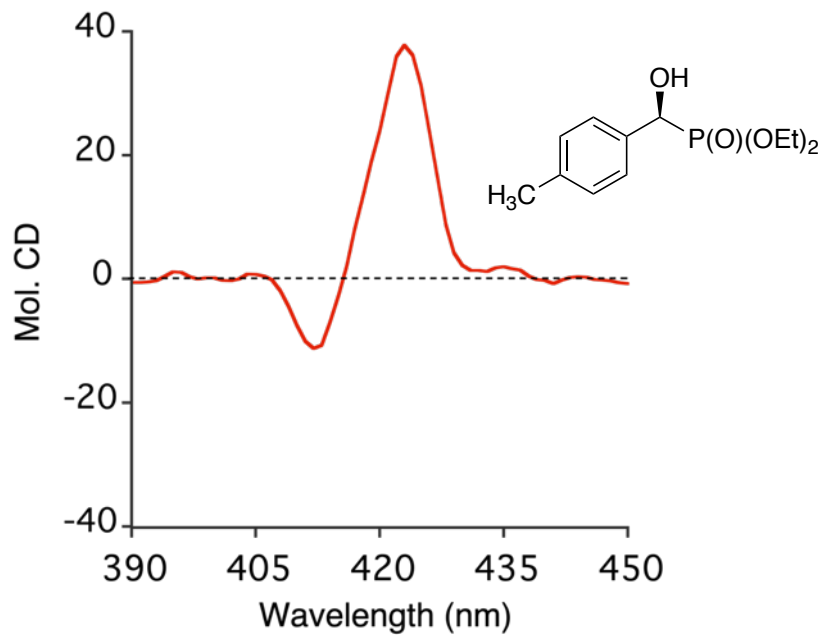


**Figure II-21.** Positive ECCD spectrum of **I-C3-ZnTPFP-20** complexed with 1 equiv of **II-(S)-30** at 0 °C in hexane.

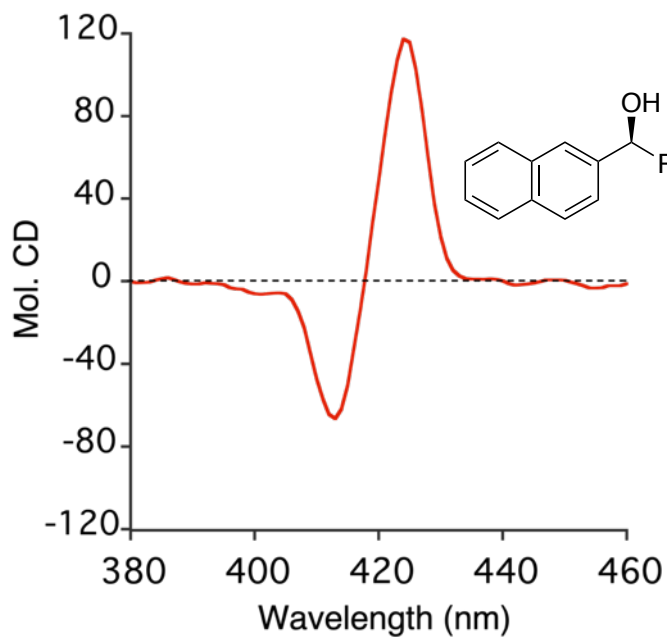


**Figure II-22.** Positive ECCD spectrum of **I-C3-ZnTPFP-20** complexed with 1 equiv of **II-(S)-31** at 0 °C in hexane.

## REFERENCES

1. Seto, H.; Kuzuyama, T., *Nat. Prod. Rep.* **1999**, *16*, 589-596.
2. Moonen, K.; Laureyn, I.; Stevens, C. V., *Chem. Rev.* **2004**, *104*, 6177-6215.
3. Palacios, F.; Alonso, C.; de Los Santos, J. M., *Chem. Rev.* **2005**, *105*, 899-931.
4. Kolodiazhnyi, O. I., *Tetrahedron: Asymmetry* **2005**, *16*, 3295-3340.
5. Groger, H.; Hammer, B., *Chem. Eur. J.* **2000**, *6*, 943-948.
6. Giannousis, P. P.; Bartlett, P. A., *J. Med. Chem.* **1987**, *30*, 1603-1609.
7. Ikeda, S.; Ashley, J. A.; Wirsching, P.; Janda, K. D., *J. Am. Chem. Soc.* **1992**, *114*, 7604-7606.
8. Giordano, C.; Castaldi, G., *Journal of Organic Chemistry* **1989**, *54*, 1470-1473.
9. Glamkowski, E. J.; Gal, G.; Purick, R.; Davidson, A. J.; Sletzinger, M., *J. Org. Chem.* **1970**, *35*, 3510-3512.
10. Guan, H. P.; Qiu, Y. L.; Ksebati, M. B.; Kern, E. R.; Zemlicka, J., *Tetrahedron* **2002**, *58*, 6047-6059.
11. Dai, Y.; Zheng, L.; Chakraborty, D.; Borhan, B.; Wulff, W. D., *Chem. Sci.* **2021**, *12*, 12333-12345.
12. Joly, G. D.; Jacobsen, E. N., *J. Am. Chem. Soc.* **2004**, *126*, 4102-4103.
13. Saito, B.; Egami, H.; Katsuki, T., *J. Am. Chem. Soc.* **2007**, *129*, 1978-1986.
14. Ordonez, M.; Viveros-Ceballos, J. L.; Cativiela, C.; Sayago, F. J., *Tetrahedron* **2015**, *71*, 1745-1784.
15. Blazewska, K. M.; Gajda, T., *Tetrahedron: Asymmetry* **2009**, *20*, 1337-1361.
16. Blazewska, K.; Paneth, P.; Gajda, T., *J. Org. Chem.* **2007**, *72*, 878-887.
17. Hammerschmidt, F.; Lindner, W.; Wuggenig, F.; Zarbl, E., *Tetrahedron: Asymmetry* **2000**, *11*, 2955-2964.
18. Skwarczynski, M.; Lejczak, B.; Kafarski, P., *Chirality* **1999**, *11*, 109-114.
19. Ward, C. V.; Jiang, M. L.; Kee, T. P., *Tetrahedron Lett.* **2000**, *41*, 6181-6184.

20. Li, Y.; Yang, G. H.; He, C. Q.; Li, X.; Houk, K. N.; Cheng, J. P., *Org. Lett.* **2017**, *19*, 4191-4194.
21. Harada, N.; Chen, S. L.; Nakanishi, K., *J. Am. Chem. Soc.* **1975**, *97*, 5345-5352.
22. Huang, X. F.; Rickman, B. H.; Borhan, B.; Berova, N.; Nakanishi, K., *J. Am. Chem. Soc.* **1998**, *120*, 6185-6186.
23. Li, X.; Borhan, B., *J. Am. Chem. Soc.* **2008**, *130*, 16126-16127.
24. Li, X.; Burrell, C. E.; Staples, R. J.; Borhan, B., *J. Am. Chem. Soc.* **2012**, *134*, 9026-9029.
25. Li, X.; Tanasova, M.; Vasileiou, C.; Borhan, B., *J. Am. Chem. Soc.* **2008**, *130*, 1885-1893.
26. Tanasova, M.; Anyika, M.; Borhan, B., *Angew. Chem. Int. Ed.* **2015**, *54*, 4274-4278.
27. Gholami, H.; Chakraborty, D.; Zhang, J.; Borhan, B., *Acc. Chem. Res.* **2021**, *54*, 654-667.
28. Kuliszewska, E.; Hanbauer, M.; Hammerschmidt, F., *Chem. Eur. J.* **2008**, *14*, 8603-8614.
29. Davis, F. A.; Lee, S.; Yan, H.; Titus, D. D., *Org. Lett.* **2001**, *3*, 1757-1760.
30. Davis, F. A.; Zhang, Y. L.; Andemichael, Y.; Fang, T. A.; Fanelli, D. L.; Zhang, H. M., *J. Org. Chem.* **1999**, *64*, 1403-1406.



CHAPTER III: A CHIROPTICAL APPROACH FOR THE ABSOLUTE  
STEREOCHEMICAL DETERMINATION OF P-STEREOGENIC  
CENTER

### III-1 Introduction

Optically active P-stereogenic compounds have been widely applied as chiral ligands, organocatalysts and versatile synthons.<sup>1-4</sup> Furthermore, several biologically active molecules, agrochemicals and pharmaceuticals possess P-chirogenic center (Figure III-1).<sup>1</sup> Recently, phostine **III-3**, a P-chirogenic mimic of glucoside has shown promising activity in cancer treatment.<sup>1</sup> With the advancement in asymmetric synthesis, a plethora of catalytic asymmetric methodologies has evolved over the years to access P-stereogenic compounds.<sup>5-15</sup> Despite these recent progresses, there is a dearth of straightforward methods for the rapid stereochemical determination of P-stereogenic centers impeding further development of novel catalytic asymmetric methodologies.

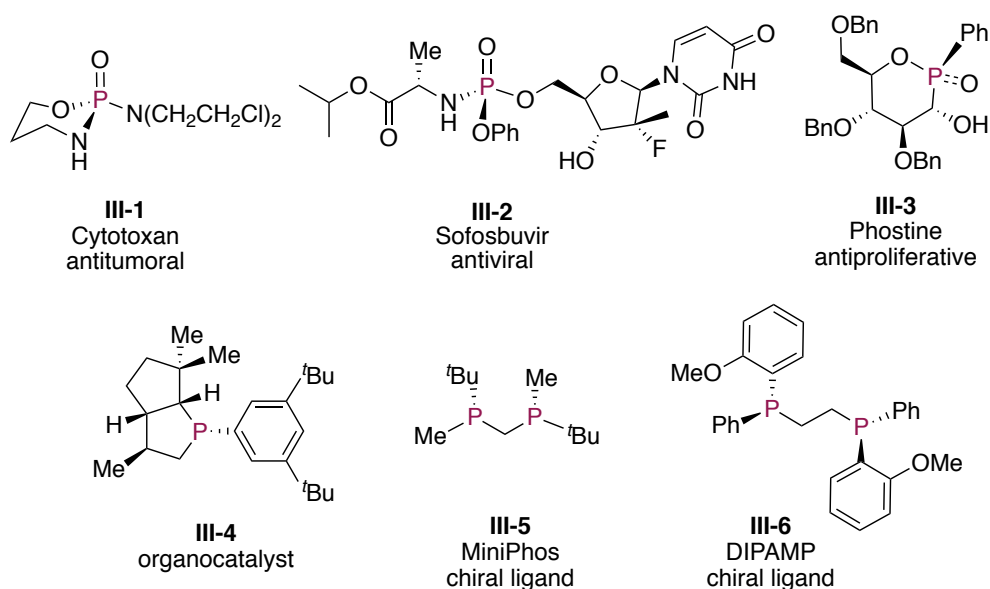
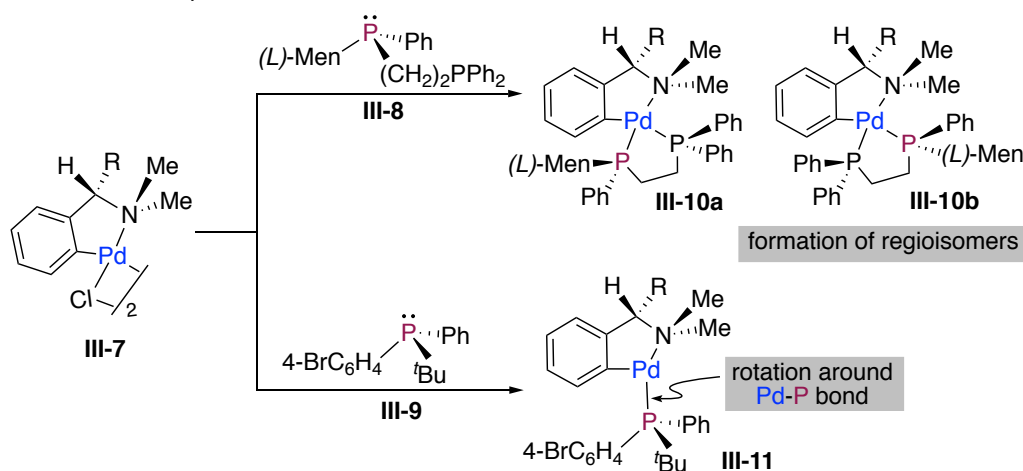


**Figure III-1.** Representative examples important P-chiral compounds.

## III-2 Background

Current methods for the absolute stereochemical determination of P-chiral centers rely on X-ray crystallography, optical rotation, 2D NMR spectroscopy and chemical derivatization to a known compound.<sup>16-22</sup> These methods are generally slow and not a simple solution for most cases. Well diffracting crystals are required for X-ray analysis, a slow and laborious process that depends on the propensity of the molecule to form crystals. Over the years the Mosher ester method has been successfully employed for the determination of absolute stereochemistry of chiral amines and alcohols. One of the

a. 2D NMR technique:



b. Chiroptical technique:

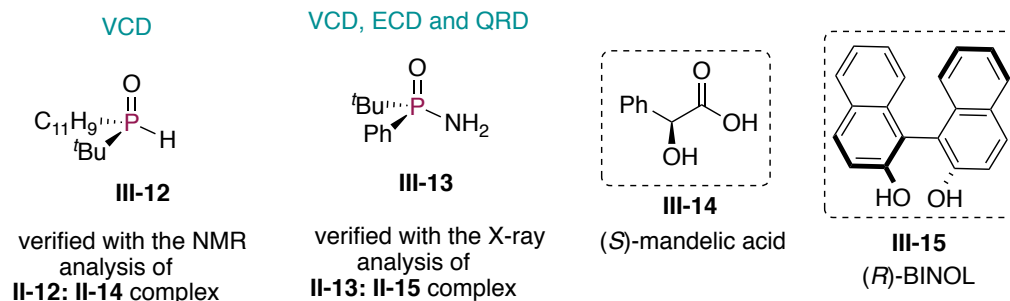


**Figure III-2.** Current techniques and their challenges to the assignment of absolute configuration.

major limitations of this methodology is the requirement of derivatization to form diastereomers. Often, P-chiral compounds do not possess convenient handles to functionalize, hence they are well suited for Mosher ester method. Homochiral *ortho*-palladated complexes **III-7** have been implemented as a “reporter complex” to establish the stereochemistry of P-chiral compounds using 2D NMR spectroscopy (Figure III-2a).<sup>16,</sup>  
<sup>22</sup> These complexes bind with chiral phosphines, leading to diastereomeric forms, which are then separated. Their unique <sup>1</sup>H NMR signals are analyzed to assign the absolute stereochemistry at the P center. Although this methodology has enjoyed some success, it is limited to symmetrically substituted bis or polydentate phosphines. Binding of non-symmetric bisphosphines leads to the formation of regioisomers that complicates the absolute stereochemical determination (Figure III-2a). Chiral mono-phosphines i.e; **III-9** were initially envisaged to avoid regioisomer problem, however their high rotameric lability (free rotation around Pd-P bond) leads to ambiguous determination of their absolute stereochemistry (Figure III-2a).

Less attention has been paid to unravel this problem using common chiroptical techniques. In 2002, Zygo *et al.*<sup>23</sup> utilized VCD (Vibrational Circular Dichroism) to solve the absolute stereochemistry of a single substrate (*S*)-*tert*-butyl-1-(2-methylnaphthyl) phosphine oxide **III-12** (Figure 2b). The absolute configuration was separately confirmed via NMR analysis of the complex formed between the substrate **III-12** and (*S*)-mandelic acid **III-14** (Figure 2b).

Very recently, Drabowicz *et al.*<sup>24</sup> exploited a combination of three different chiroptical techniques namely VCD (Vibrational Chiroptical Dichroism), ECD (Electronic

Circular Dichroism) and ORD (Optical Rotatory Dispersion) in determining the absolute configuration of (*R*)-*tert*-butylphenylphosphinoamidate **III-13** (Figure 2b). The absolute configuration was independently verified via X-ray analysis of the complex formed between (*R*)-BINOL **III-15** and the chiral analyte of interest **III-13**. Although chiroptical methods has gained a limited success (only two substrates), they are yet to become a routine method for this class of compounds. These chiroptical techniques are empirical in nature and require a consistent quantum mechanically predicted theoretical spectra to be matched with the experimentally observed data. The difficulty often stems from the inability to predict an accurate set of solution phase conformers and their respective theoretical spectrum, due to the flexibility of the molecules and complexity of their structures.

### **III-3 Absolute stereochemical determination of tertiary phosphine oxides**

With our prior experience in using porphyrin-based hosts as reporters of chirality, we set our goal to develop a simple, rapid, direct (derivatization free), and micro-scale methodology to assign the chirality of P-stereogenic compounds. We envisioned utilizing the principles of Exciton Coupled Circular Dichroism (ECCD) to develop a procedure that addresses this long-standing problem. The porphyrin tweezer methodology, a host-guest interacting system, has been used successfully for the absolute stereochemical determination of various functionalities as discussed earlier. A major limitation in using this strategy is the requirement for bidentate coordination between the metal centers and the chiral guest molecule to induce helicity within the host/guest complex. Monophosphines inherently lack the presence of a secondary coordination site and in most of

the cases do not possess a suitable functional group to append the required secondary binding element. Recently, our group has developed a new host system **I-MAPOL-32**,<sup>25</sup> having a rigid bis-phenol backbone that brings the two porphyrin rings closer in proximity compared to a traditional tweezer, thus creating a cavity between the two porphyrin units. **I-MAPOL-32**, remains as a 1:1 mixture of its *P* and *M* stereoisomers at room temperature (Figure III-3). It is assumed that the intramolecular hydrogen bonding between the two hydroxy groups keep **I-MAPOL 32** in its *syn* conformation where the porphyrins face each other. This equilibrium is shifted in one direction through its interaction with a chiral guest molecule. The induced chirality is analyzed via Circular

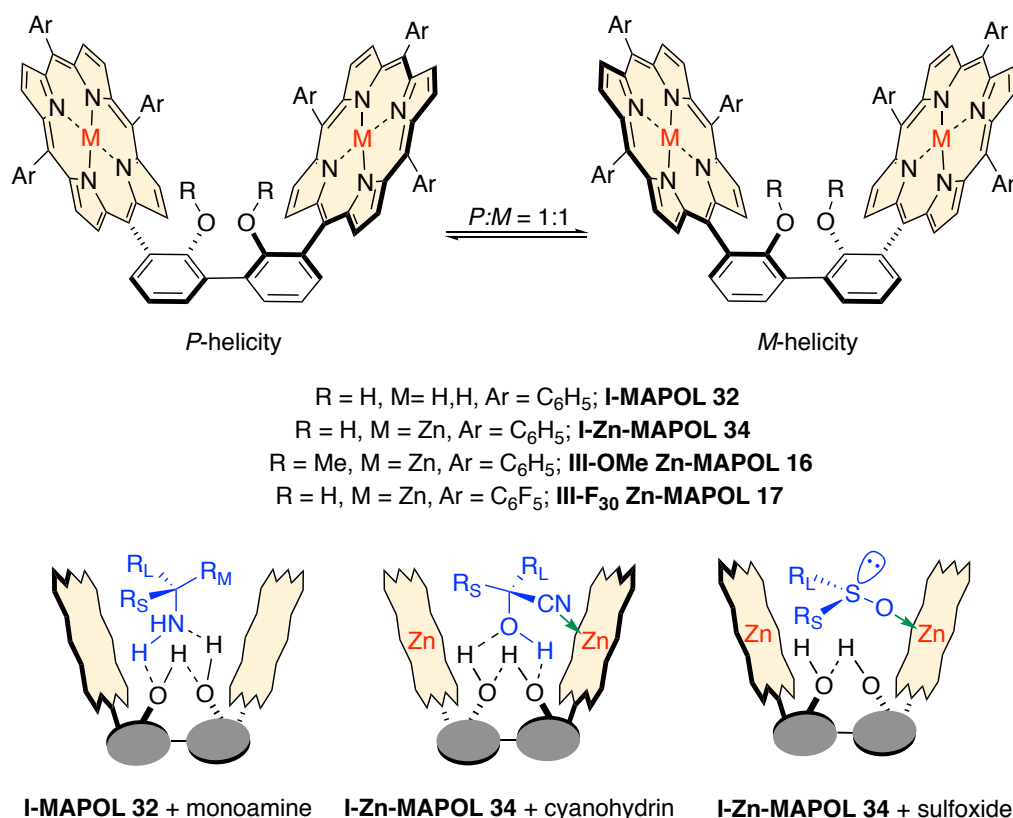


**Figure III-3.** MAPOL and its analogs, used in the absolute stereochemical determination of chiral amines, cyanohydrins, and sulfoxides.

Dichroism (CD) spectroscopy and correlated with the absolute chirality of the guest molecule. Using this concept, **I-MAPOL 32** was initially employed as a reporter of chirality for chiral monoamines.<sup>25</sup> Translation of point to axial chirality through hydrogen bonding interaction between the phenolic hydrogen atoms in the host with the chiral amine guest was key to its success. Host **I-MAPOL 32** can function as both H-bond donor and as well as H-bond acceptor, thus forming a strong ECCD active host-guest complex with monoamines. On the other hand, **I-Zn-MAPOL 34**, the zincated version of host **I-MAPOL 32** bears two orthogonal binding elements *i.e.*, similar hydrogen bonding with phenolic moieties and additional ligand to metal coordination can take place with the zinc metallo centers embedded in the porphyrin core (Figure III-3). These properties made **I-Zn-MAPOL 34**, an excellent host to bind with chiral cyanohydrin molecules. In similarity with the monoamines, the hydroxyl group interacts with bi-phenolic moiety through H-bonding whereas the cyano group coordinates to the Zn metal. Although for cyanohydrin<sup>26</sup> dual binding was necessary, S-chiral sulfoxides required coordination of the sulfoxide oxygen atom to the Zn metal to induce helicity in **I-Zn-MAPOL 34** (Figure III-3).<sup>27</sup> Intrigued by the results observed with S-chiral sulfoxides and literature preceding of phosphonates coordination with metallo mono-porphyrins<sup>28-31</sup> we realized that a similar approach might provide an effective chiroptical solution for the absolute stereochemical assignment of P-chiral phosphorus oxides. Coordination between the Zn metal and the oxygen atom should yield a strongly bound host-guest complex, leading to the induction of helicity in the host-guest complex. Furthermore, phosphines do not bind strongly with Zn-porphyrins and alkyl phosphines are prone to aerobic oxidation. With recent advances in conversion

of phosphine oxides to phosphines with stereochemical fidelity,<sup>11-13</sup> a routine method for the absolute stereochemical determination of phosphine oxides would automatically solve the problem with phosphines.

First, we turned our attention to UV-vis measurements to explore the binding of phosphine oxides to **I-Zn-MAPOL 34**. Addition of phosphine oxide **III-Rp-19** to **I-Zn-MAPOL 34** led to a redshift from 413 nm to 423 nm, indicating the binding event between the host and the guest molecules (Figure III-4). Gratifyingly, a strong negative ECCD signal ( $A = -667$ ) was observed when only 5 equivalents of compound **III-Rp-19** were added to a solution of **I-Zn-MAPOL 34** (1  $\mu\text{M}$ ) in hexane at 0  $^{\circ}\text{C}$  (Figure III-5). This low detection limit along with 10 nm redshift in the UV-vis is indicative of the strong binding

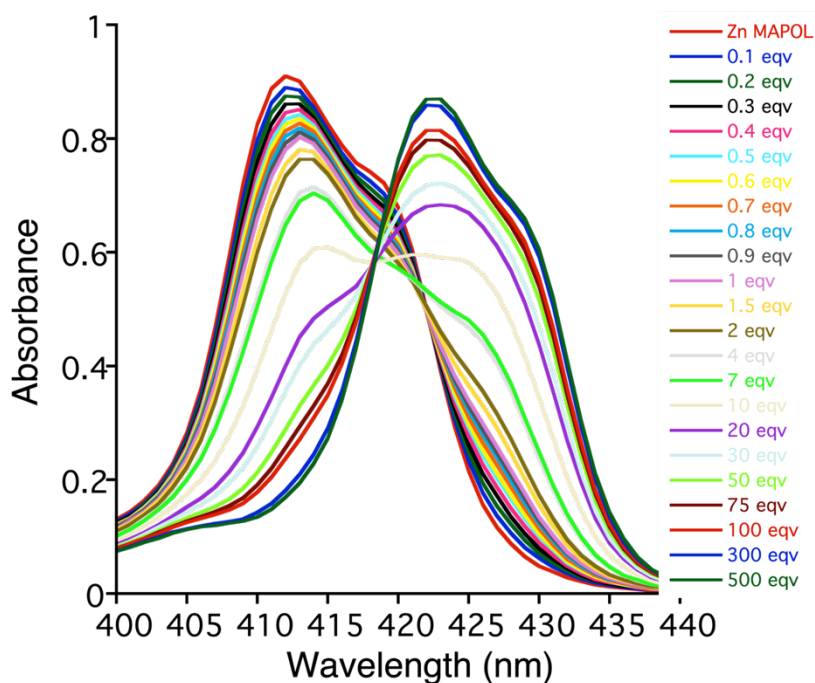


**Figure III-4.** UV-vis titration of **I-Zn-MAPOL 34** (1  $\mu\text{M}$ ) with **III-Rp-19** at 0  $^{\circ}\text{C}$  in hexane.



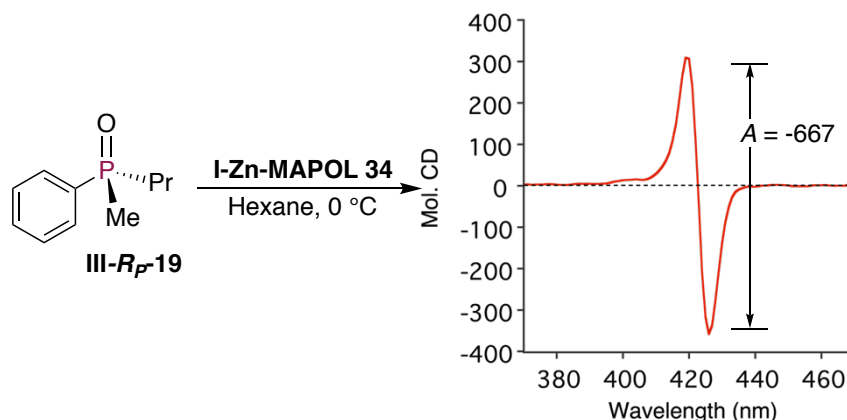


**Figure III-5.** Strong ECCD signal is observed upon binding of **III-R<sub>P</sub>-19** (5 equiv) to **I-Zn-MAPOL 34**

affinity for phosphine oxides with **I-Zn-MAPOL 34**. As anticipated, a positive ECCD signal was observed for **III-S<sub>P</sub>-19**, the enantiomer of **III-R<sub>P</sub>-19**, with nearly similar intensity under identical conditions (Table III-1). The strength of the ECCD signal was found to be sensitive to the temperature of measurement. Expectedly, the ECCD amplitude decreased with increasing temperature (Figure III-6). Nevertheless, a significant signal is observed even at 45 °C, further corroborating the strong binding between the host and

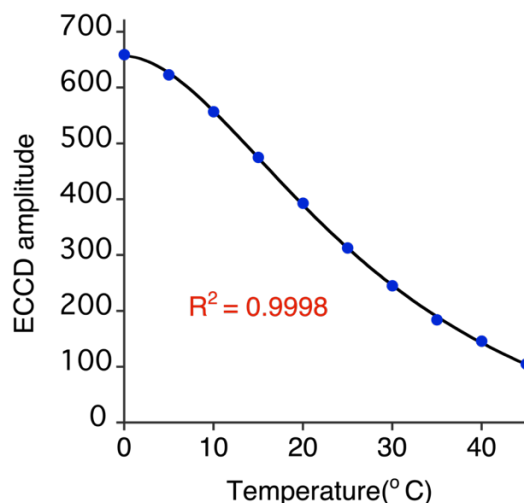


**Figure III-6.** Temperature dependence on the amplitude of the ECCD signal of **I-Zn-MAPOL 34** complexed with 5 equiv of **III-R<sub>P</sub>-19** in hexane.

guest molecule. To test the sensitivity of the host system to different solvent impurities, the host-guest complex was titrated with different equivalents of acetone and ethyl acetate and their respective CD intensities were measured. Acetone and ethyl acetate showed diminution of signal only after 2000 equivalents. These data further support the intense binding between the host and the guest. Job's plot analysis indicated the formation of a 1:1 complex (Figure III-7a). Titration of **I-Zn-MAPOL 34** with excess of **III-R<sub>P</sub>-19** provided a binding isotherm revealing a  $K_{\text{assoc}}$  of  $\sim 2.7 \times 10^5 \text{ M}^{-1}$  in hexane confirming our initial evidence of strong binding affinity (Figure III-7b). With these preliminary results in hand, a variety of molecules possessing an asymmetric phosphorous oxide moiety with different alkyl and aryl substituents were synthesized according to reported procedures.<sup>5</sup> Complexation of these P-stereogenic compounds with **I-Zn-MAPOL 34** resulted in strong ECCD signals centered around the Soret band of the host system (Table III-1). In general, all *S<sub>P</sub>* phosphorous oxides produce positive ECCD

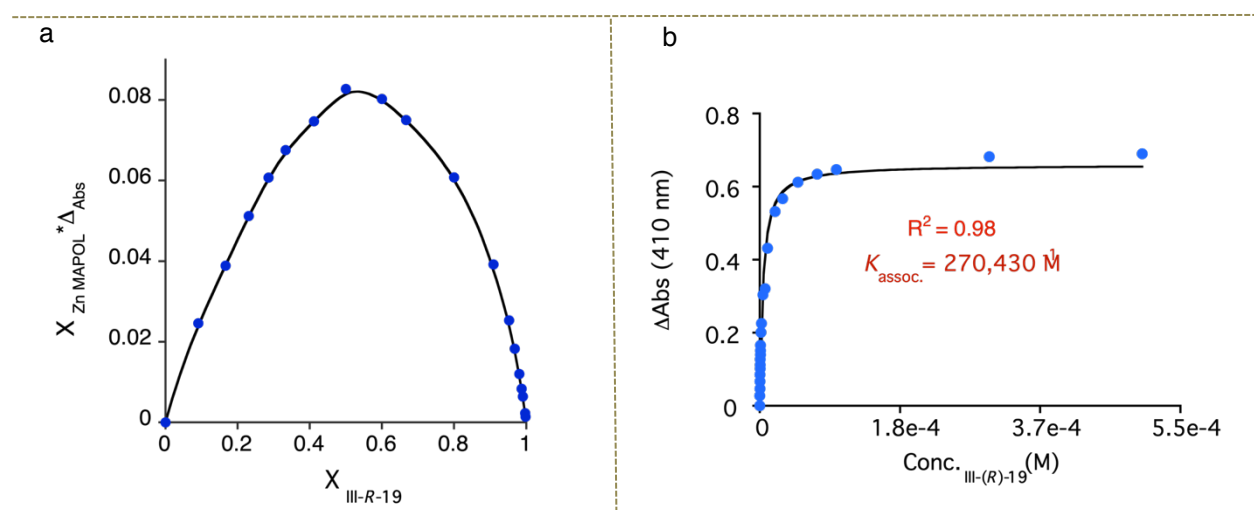
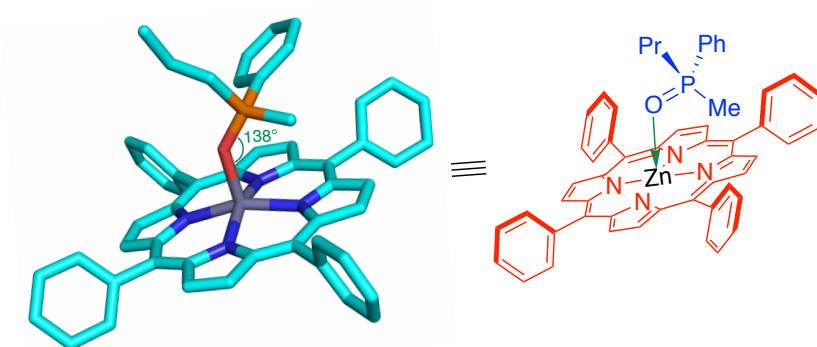


**Figure III-7.** a. Jobs plot of **I-Zn-MAPOL 34** with **III-R<sub>P</sub>-19** at 410 nm. b. Binding affinity measurement for **III-R<sub>P</sub>-18** with **I-Zn MAPOL 34**.

spectra while  $R_P$  phosphorous oxides yield negative ECCD spectra. In order to correlate the observed ECCD signal with the asymmetry of the phosphine oxides few more experiments were performed.

1. Attempts to obtain a single crystal of any of the host-guest complexes were unfruitful. Nonetheless, the crystal structure of the phosphine oxide **III- $R_P$ -19** bound to the Zn-tetraphenylporphyrin (Zn-TPP) as a mimic of the porphyrin ring in **I-Zn-MAPOL 34** was obtained (Figure III-9). The crystal structure confirmed the coordination between the oxygen atom in phosphine oxide and the zinc metal of the metal porphyrin. It was also evident that upon coordinating the zinc center, the chiral phosphine oxide **III- $R_P$ -19** projects its smallest substituent (the methyl group) towards the porphyrin ring (Zn-O-P bond angle is  $138^\circ$ ), thus pushing the medium and larger group away (Figure III-8).

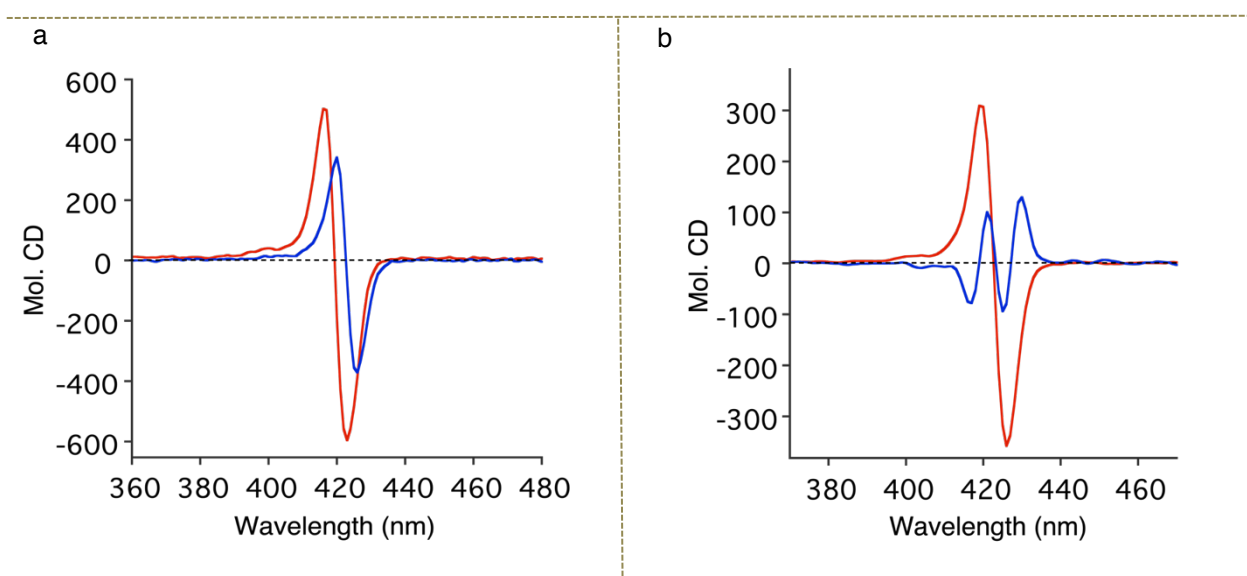
2. A stronger CD signal ( $A = -1098$  vs  $A = -667$ ) was observed when **III- $R_P$ -19** was complexed with **III-F<sub>30</sub> Zn-MAPOL 17** (Figure III-9a). The larger amplitude is expected because of the higher binding affinity with the more Lewis acidic Zn metallo-center of the



**Figure III-8.** The crystal structure of **III- $R_P$ -19** bound to Zn-TPP.

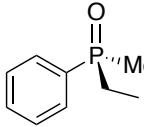
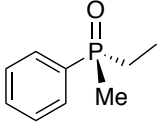
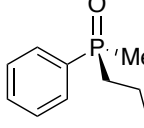
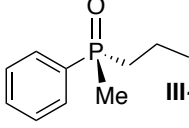
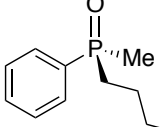
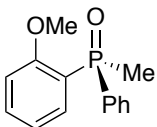
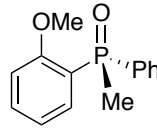
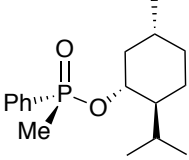
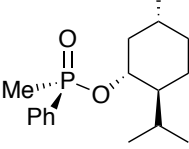
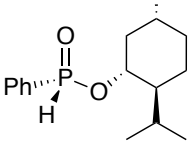
fluorinated porphyrin. This observation further corroborates the oxygen to zinc coordination as the main binding element.

3. Binding of **III-R<sub>P</sub>-19** with **III-OMe Zn-MAPOL 16** produced a complex spectrum, (Figure III-9b) suggesting the presence of the hydroxyl groups in host **I-Zn-MAPOL 34** is essential to yield a consistent ECCD signal. This observation can be justified because the intramolecular hydrogen bonding between the hydroxyl groups at the 2,2' positions of



**Figure III-9.** a. ECCD of **III-R<sub>P</sub>-19** bound to **III-F<sub>30</sub> Zn-MAPOL 17** (red) and **I-Zn-MAPOL 34** (blue). b. ECCD of **III-R<sub>P</sub>-19** bound to **III-OMe Zn-MAPOL 16** (blue) and **I-Zn-MAPOL 34** (red).

**Table III-1.** ECCD of chiral phosphine oxides bound to **I-Zn MAPOL**

entry	predicted sign	$\lambda$ nm, $\Delta\epsilon$	$A/A_{\text{corr}}^a$
 <b>III-S<sub>P</sub>-18</b>	positive	426, +127 419, -96	+223 <sup>b</sup> /+301
 <b>III-R<sub>P</sub>-18</b>	negative	426, -126 419, +107	-233 <sup>b</sup> /-347
 <b>III-S<sub>P</sub>-19</b>	positive	426, +279 419, -218	+497 <sup>b</sup> /+742
 <b>III-R<sub>P</sub>-19</b>	negative	426, -358 419, +309	-667 <sup>b</sup> /-844
 <b>III-S<sub>P</sub>-20</b>	positive	426, +308 419, -253	+561 <sup>b</sup> /+837
 <b>III-S<sub>P</sub>-21</b>	positive	426, +74 419, -70	+144 <sup>c</sup> /+202
 <b>III-R<sub>P</sub>-21</b>	negative	426, -203 419, +208	-411 <sup>c</sup> /-561
 <b>III-R<sub>P</sub>-22</b>	negative	426, -561 419, +462	-1023 <sup>b</sup>
 <b>III-S<sub>P</sub>-23</b>	positive	426, +287 419, -214	+501/+590 <sup>b</sup>
 <b>III-R<sub>P</sub>-24</b>	negative	425, -434 418, +351	-785/-872 <sup>c</sup>

<sup>a</sup>A corresponds to the amplitude for the ECCD spectrum, while  $A_{\text{corr}}$  is the amplitude after correction for the enantiopurity. <sup>b</sup>5 equiv of phosphine oxide.

<sup>c</sup>20 equiv of phosphine oxide.

the host system helps in rigidifying the favored CD active helical conformer, thereby reducing the number of other possible conformers for the host-guest complex. Based on these observations, a mnemonic was proposed to correlate the absolute stereochemistry of the host molecule with the observed CD signal. As depicted in Figure III-10, coordination of the oxygen lone pair with the Lewis acidic Zn center places the guest molecule **III-*R<sub>P</sub>*-19** in the pocket between the two porphyrin rings of **I-Zn-MAPOL 34**. Minimization of steric interactions, between the substituents at the asymmetric P center and the porphyrin ring leads to **I-Zn-MAPOL 34** adopting a specific helicity. After the initial O-Zn coordination the smallest group (Me) is projected towards the bound porphyrin and the other two substituents of the chiral center are pointed towards the unbound porphyrin ring. An energetically minimized conformer would be achieved by placing the larger

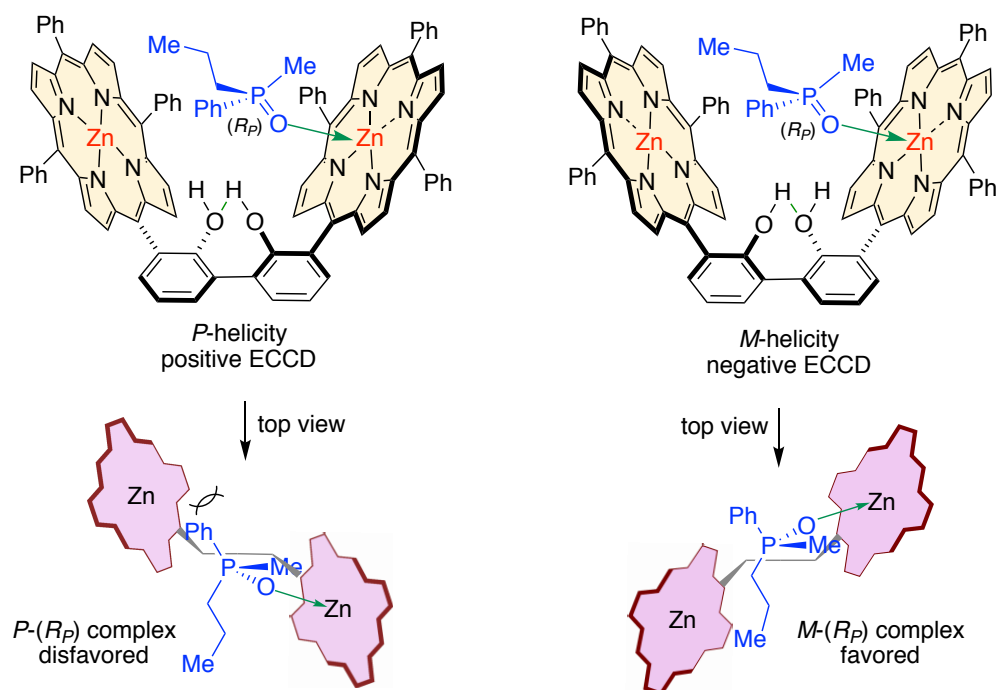


**Figure III-10.** Proposed working model to correlate the observed signal with the stereochemistry of the guest phosphine oxide.

phenyl group (based on A strain values) in a less sterically hindered space, that is away from the unbound porphyrin. Such spatial arrangement would lead to the *M*-(*R*<sub>P</sub>) complex and a negative ECCD signal is anticipated. The latter speculation agrees with the observed ECCD signal for the complex of **III-*R*<sub>P</sub>-19** with **I-Zn-MAPOL 34** (Table III-1). The predicted signs of all phosphine oxides, based on their A strain values, are in full agreement with the experimentally observed values (Table III-1). The **I-Zn-MAPOL 34** host system is capable of discerning small differences in relative size of the P-substituents with ease. For example, steric differentiation of methyl and ethyl, or phenyl and o-anisyl, leads to large ECCD signals, although their sizes are not significantly different (Table III-1). It is also worth mentioning here that the length parameter **L**, that was used for the S-chiral sulfoxide molecules cannot predict the observed ECCD spectra. Based on the **L** values of the substituents, (<sup>n</sup>Bu > Ph > Me) a negative ECCD spectra is expected for compound **III-*S*<sub>P</sub>-20**. Nonetheless, a positive spectrum is observed relating their A values i.e; Ph > <sup>n</sup>Bu > Me.

The successful application of **I-Zn-MAPOL 34** to determine the absolute configuration of tertiary mono-phosphine oxides prompted the investigation of more complex substrates to examine the generality and applicability of our developed methodology. In this pursuit, compound **III-*R*<sub>P</sub>-22** and its epimer **III-*S*<sub>P</sub>-23** (differing chirality at P center only) both bearing multiple chiral centers was synthesized. Nonetheless, they produced opposite ECCD signals when complexed with **I-Zn-MAPOL 34**, thus highlighting the sensitivity of the host system to the asymmetry at the P-chiral center (Figure III-11a). Similar binding model (Figure III-10) can also predict the chirality

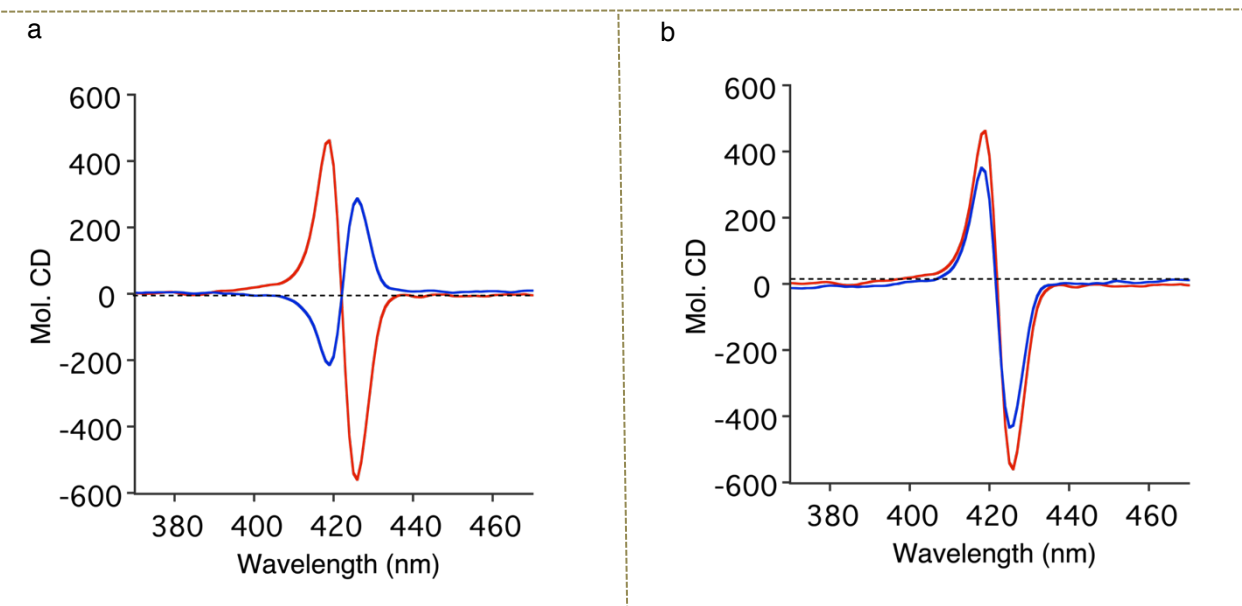


**Figure III-11.** a. ECD spectra of **I-Zn-MAPOL 34** with 5 equiv of **III-Rp-22** (red) and **III-Sp-23** (blue). b. ECD spectra of **I-Zn-MAPOL 34** with 5 equiv of **III-Rp-22** (red) and **III-Rp-24** (blue).

of these two epimers considering the size of the substituents (based on A strain values) in the order of Ph > OMen > Me. Compound **III-Rp-24** (Ph > OMen > H) replacing Me group with a H atom, produced similar signal as **III-Rp-22** (Figure III-11b) reinforces our proposed binding model.

#### III-4 Absolute stereochemical determination of P-chiral center of Sofosbuvir

Next, the system was challenged with molecules that not only contain multiple stereocenters, but also have coordinating functionalities, which has the potential to bind with the zincated porphyrin. This would demonstrate the practical use of **I-Zn-MAPOL 34** with a pharmaceutical API with a complex structure. Hence, we decided to analyze Sofosbuvir **III-2**, a commercial antiviral agent, widely used for the treatment of hepatitis C virus (HCV).<sup>15</sup> In addition to the phosphoramidate functionality, sofosbuvir contains hydroxyl, ester, fluoride, and imide moieties, which could potentially bind to the zincated



porphyrin. Nonetheless, we posited that the strong binding affinity for phosphorous oxide complexation with the zincated porphyrin ( $\sim 270,000 \text{ M}^{-1}$ ) would still make this coordination as the primary binding mode. As a point of comparison, to date we have found amines and sulfoxides as the strongest binders of Zn-TPP, with binding affinities of  $\sim 11,000\text{-}15,000 \text{ M}^{-1}$ .<sup>27, 34</sup> Complexation of Sofosbuvir **III-2** with **I-Zn-MAPOL 34** resulted in strong positive ECCD signal in hexane. Surprisingly, *epi*-Sofosbuvir (**III-*epi*-2**), epimeric only at the P-stereocenter, also resulted in a positive ECCD signal, albeit with lower amplitude (Figure III-12). We proposed that although various functional groups in sofosbuvir **III-2**, such as the ester, imide, fluoride, or hydroxyl, would have a substantially reduced binding affinity in comparison to the phosphoramidate, the presence of the second metalloporphyrin does not preclude the potential dual binding of other functional groups. In fact, the initial strong binding of the phosphoramidate would entropically favor the binding of another functional group with the second porphyrin leading to a bidentate coordination.

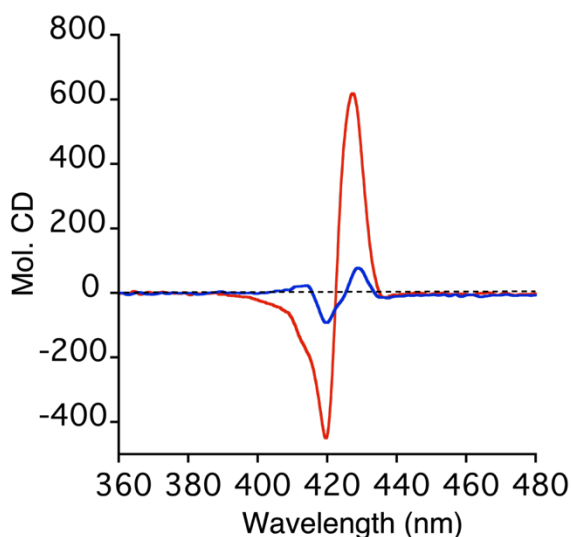


**Figure III-12.** ECCD spectra of **I-Zn-MAPOL 34** complexed with 1 equiv of **III-2** (red) and **III-*epi*-2** (blue) in hexane.

We surmised that the use of the non-interacting solvent, hexane, increases the availability for binding of a second functionality. It is noteworthy that the metalloporphyrin strategy (i.e., the porphyrin tweezer methodology or the Zn-MAPOL system for absolute stereochemical determination of most functional groups fails in polar solvents, presumably because of the attenuated binding affinities, either as a result of solvation of the functional group, and/or competing solvent coordination with the metalloporphyrin. Nonetheless, the high binding affinity of the phosphoramidate moiety with the zincated

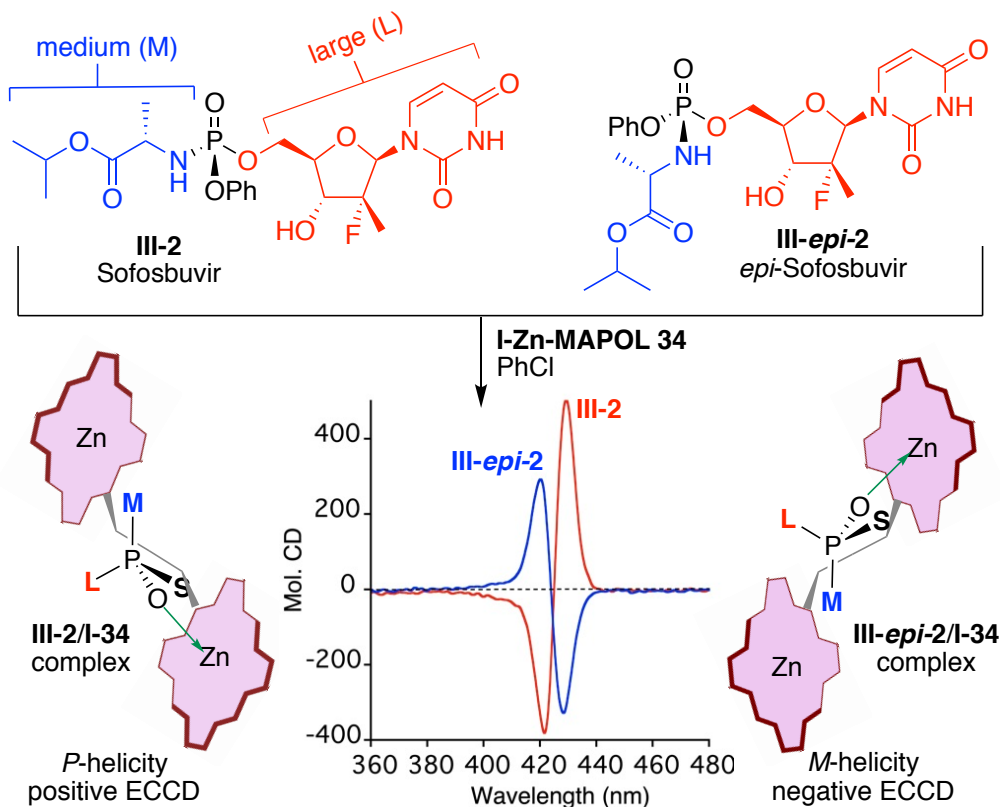


**Figure III-13.** Sofosbuvir **III-2** and **III-epi-2** bound to **I-Zn-MAPOL 34** lead to positive and negative ECCD respectively in chlorobenzene.

porphyrin suggests a solution to remove secondary interactions that originate from less efficient binding functionalities. The use of a more polar solvent would not only solvate

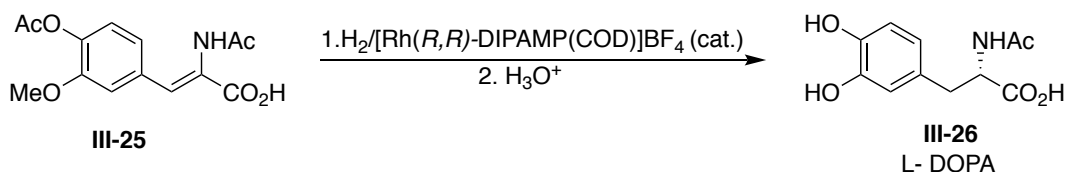
the interfering groups, but also, would decrease their binding affinity with the zincated porphyrin. This would eliminate the secondary interaction that interferes with desired sole stereo-differentiation based on the asymmetry of the P chiral center.

After a quick survey, chlorinated solvents, such as dichloromethane, chloroform, and chlorobenzene provided the best balance, where sofosbuvir **III-2**, maintained its positive ECCD signal when bound to **I-Zn-MAPOL 34**, while complexation of **III-*epi*-2** resulted in a negative ECCD signal (Figure III-13). The binding model follows the mnemonic proposed in Figure III-10, in which the smallest group (phenoxy) on the P-stereogenic center points towards the bound porphyrin ring, while the medium (amino ester) and large (uracil) substituents on the phosphorus atom project towards the unbound porphyrin ring. To minimize steric interaction, the unbound porphyrin resides away from the larger group favoring *P*-helicity. This leads to the prediction of a positive ECCD signal for **III-2**, as observed experimentally. Expectedly, a counterclockwise twist would be favored in the binding of **III-*epi*-2** with **I-Zn-MAPOL 34**, yielding a negative ECCD signal. Indeed, the measured ECCD signals are in full agreement with the proposed binding scenario (Figure III-13).

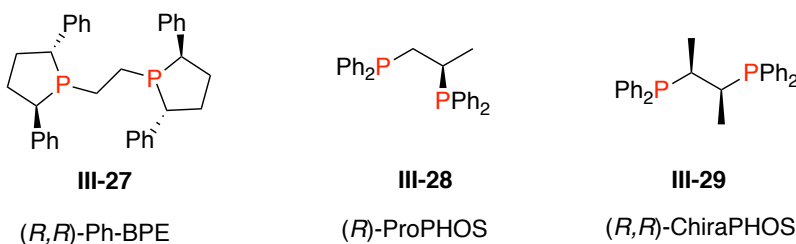
### III-5 Absolute stereochemical determination of chiral bis-phosphine oxide

After the primary accomplishment with mono-dentate P-chiral phosphine oxides, we envisaged that a similar treatment could provide an efficient protocol to determine the stereochemistry of bidentate P stereogenic ligands, a class of ligands used extensively in the literature for transition metal mediated homogeneous catalysis.<sup>1</sup> The chiral ligand DIPAMP was first used in 1970 for an asymmetric hydrogenation to synthesize L-DOPA by Knowles at Monsanto (Figure III-14a).<sup>35</sup> It was envisaged that the presence of the bis Zn-metallo center would lead to a bidentate coordination, yielding stronger complex formation in comparison to their monodentate analogues. As anticipated, the binding affinity of bisphosphine oxides with **I-Zn-MAPOL 34** are much higher (300 times) as compared to their corresponding mono-phosphine oxide analogues ( $8.2 \times 10^7 \text{ M}^{-1}$  in

a. DIPAMP ligand for asymmetric hydrogenation:



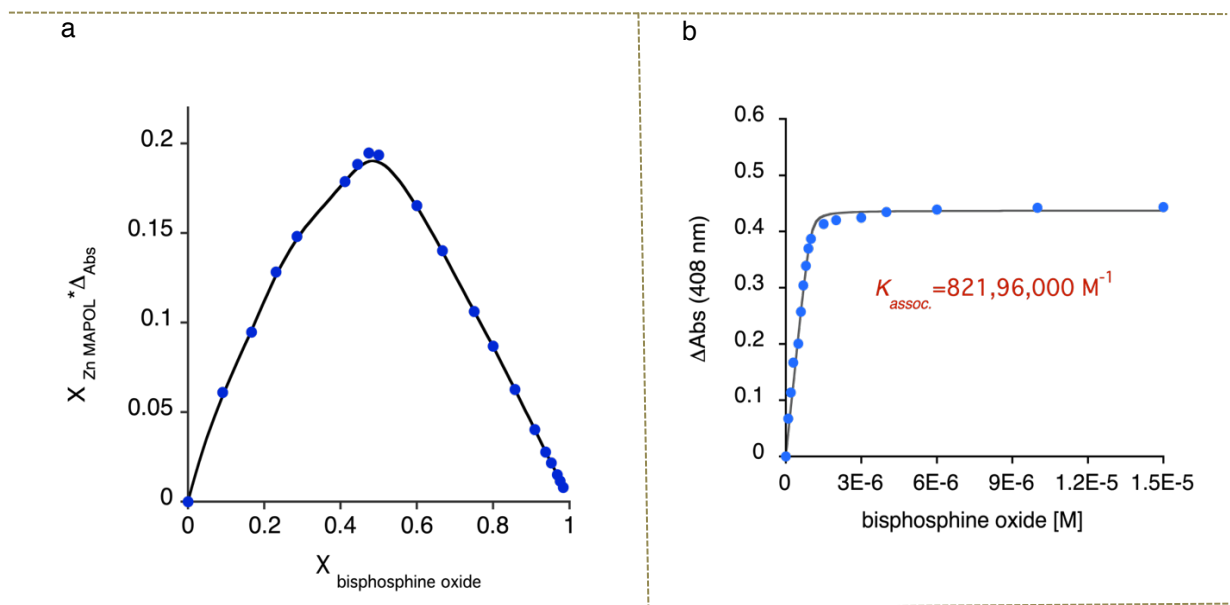
b.  $\alpha$ -chiral bis-phosphine ligands:



**Figure III-14.** a. Asymmetric hydrogenation to synthesize L-DOPA using DIPAMP ligand. b. Examples of important  $\alpha$ -chiral bis-phosphine ligands used in transition metal catalyzed reactions.

comparison with  $\sim 2.7 \times 10^5 \text{ M}^{-1}$ ). The stoichiometry of the complex was found to be 1:1 employing the Job's analysis (Figure III-15a).

The investigation of the chirality was initiated with **III-*R<sub>P</sub>,R<sub>P</sub>*-30**, the corresponding

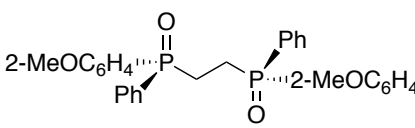
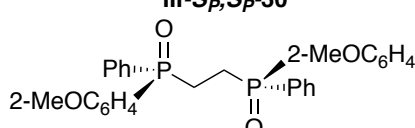
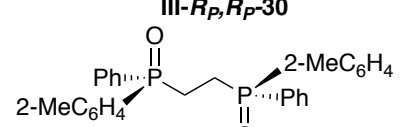
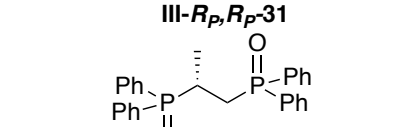
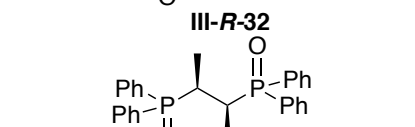
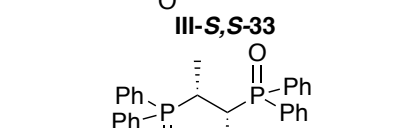
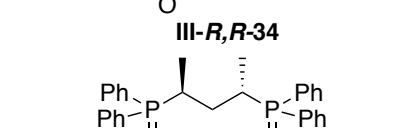


**Figure III-15.** a. Jobs plot of **I-Zn-MAPOL 34** with DPPOE at 408 nm. b. Binding affinity measurement of DPPOE with **I-Zn-MAPOL 34**.

oxide of commercially available *R<sub>P</sub>,R<sub>P</sub>*-DIPAMP. Gratifyingly only 1 equivalent of **III-*R<sub>P</sub>,R<sub>P</sub>*-30** can produce strong ECCD signal in hexane (Table III-2). This low detection limit is consistent with its strong binding affinity to the Zn metallo centers. As predicted, the enantiomer **III-*S<sub>P</sub>,S<sub>P</sub>*-30** produces the opposite signal. The concept was then extended to compound **III-*R<sub>P</sub>,R<sub>P</sub>*-31**, showcasing the practicality of our developed methodology. Figure III-17a depicts the proposed mnemonic for the stereodifferentiation that leads to the observed ECCD spectra. It was assumed that each asymmetric phosphorus center plays its part in orienting the attached porphyrin independently, leading to the preferred helicity of the host system.

Each porphyrin is bound to the phosphorus center in a way to minimize steric interactions with the larger of the two substituents (2-Me-C<sub>6</sub>H<sub>4</sub> vs. Ph, **III-*R<sub>P</sub>*,*R<sub>P</sub>*-31**). In the proposed mnemonic the chain connecting the two phosphorus centers is not part of the stereodifferentiation. Also important is the fact that the two substituents on the phosphorus center are moved away from the biphenol linker to reduce steric interactions

**Table III-2.** ECCD of chiral bisphosphine oxides with **I-Zn-MAPOL 34**

entry	predicted sign	$\lambda$ nm, $\Delta\epsilon$	$A^{[a]}$
 <b>III-<i>S<sub>P</sub></i>,<i>S<sub>P</sub></i>-30</b>	positive	427, +416 418, -196	+612
 <b>III-<i>R<sub>P</sub></i>,<i>R<sub>P</sub></i>-30</b>	negative	427, -426 418, +228	-654
 <b>III-<i>R<sub>P</sub></i>,<i>R<sub>P</sub></i>-31</b>	negative	429, -1838 420, +1622	-3460
 <b>III-<i>R</i>-32</b>	positive	429, +332 421, -254	+586
 <b>III-<i>S</i>,<i>S</i>-33</b>	negative	427, -1646 419, +1124	-2770
 <b>III-<i>R</i>,<i>R</i>-34</b>	positive	427, +1862 419, -1248	+3110
 <b>III-<i>S</i>,<i>S</i>-35</b>	negative	427, -1350 418, +804	-2154

a. A corresponds to the amplitude of the ECCD spectrum with one equiv of guest.

with the linker. Such orientation would lead to the negative ECCD signal which is in accordance with the observed signal (Figure III-16a).

So far, all the examples have demonstrated ‘chiral sensing’ of molecules with an asymmetric phosphorus center. Nonetheless, an important subset of the bidentate phosphorus ligands is not asymmetric at the P-center, rather at the adjacent carbon center (Figure III-16b).<sup>36-37</sup> We envisaged that strong bidentate coordination between bisphosphine oxide and **I-Zn-MAPOL 34** might allow us to determine the absolute chirality at the adjacent carbon center. Gratifyingly a strong positive ECCD signal is observed

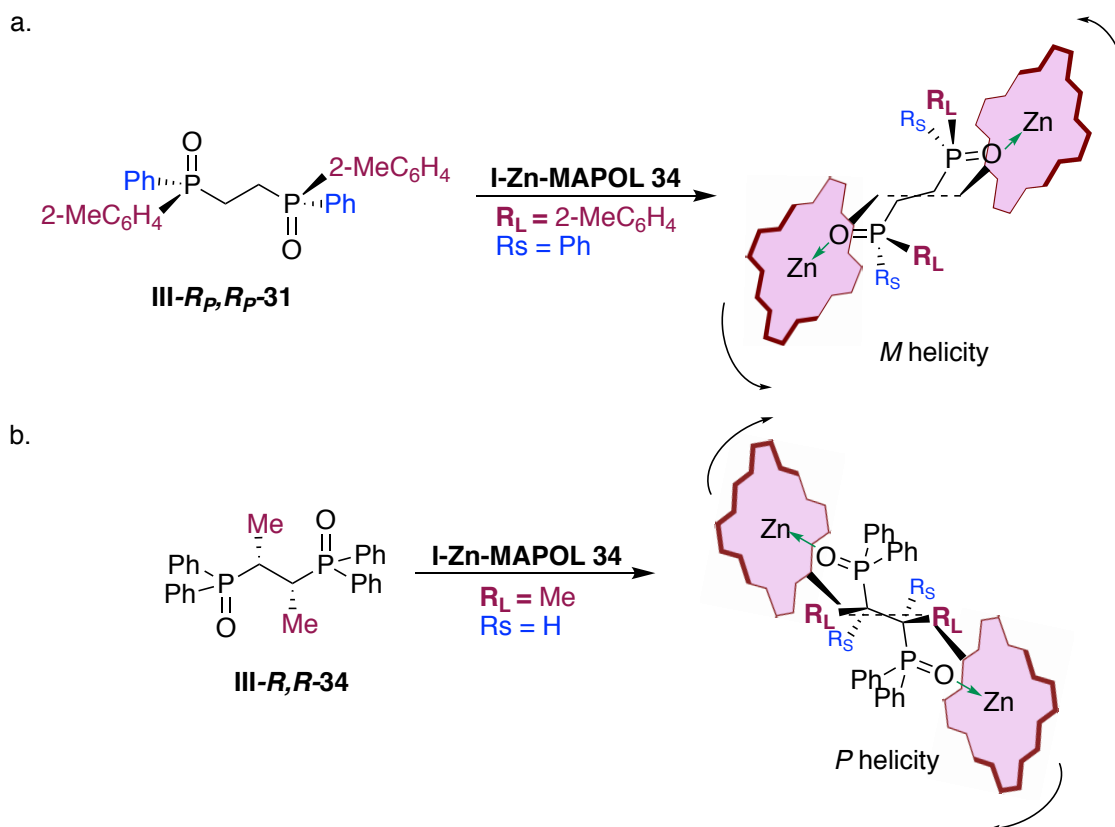


**Figure III-16.** Proposed working model to correlate the chirality of the bisphosphine oxides with the observed ECCD signal.

when compound **III- $R,R$ -34** was treated with **I-Zn-MAPOL 34** under identical conditions.

Table III-2 lists a number of these molecules complexed with **I-Zn-MAPOL 34**, where

consistently strong ECCD signals were observed. Figure III-16b depicts the proposed binding model that predicts helicity of the complex. As depicted, we believe the chirality at each carbon center is responsible for the helical twist of its adjacent porphyrin. The phenyl substituents on each phosphorus atom are placed in the most sterically open space, while between R<sub>L</sub> and R<sub>S</sub>, (the large and small  $\alpha$ -carbon substituents, respectively) it is the smaller R<sub>S</sub> (H atom) that is oriented towards the linker. In this manner each porphyrin slides away from R<sub>L</sub> (phenyl) group placing it in the least sterically hindered space. Such an orientation leads to a clockwise (*P*-helical) helicity for **III-*R,R*-34**, that indeed matches with the observed positive ECCD signal.

In summary, we have developed a simple chiroptical protocol for the direct assignment of absolute stereochemistry of chiral phosphorus compounds without the need for derivatization. The protocol is suitable for the stereochemical determination of phosphorus stereocenters in monophosphine oxides, phosphinates, phosphoramidates, as well as bis-phosphine oxides, chiral at either the P-center or the  $\alpha$ -carbon. High binding affinities enable the detection of stereochemistry for P-stereogenic center of molecules with multiple functionalities that could also bind with the zincated porphyrin. Simple mnemonics for each class of molecules correlates the observed ECCD signal with the stereochemistry. Based on the strong binding affinities between the phosphine oxide and Zn metallo center we surmise that this work could be extended in future to  $\alpha$ -chiral as well as distal chiral mono phosphine oxides.



### III-6 Experimental Section

#### III-6.1. Materials and general instrumentations

Anhydrous solvents used for CD measurements were purchased from Aldrich and were spectra grade. Unless otherwise mentioned, solvents were purified as follows.  $\text{CH}_2\text{Cl}_2$  was dried over  $\text{CaH}_2$  whereas THF and  $\text{Et}_2\text{O}$  were dried over sodium (dryness was monitored by colorization of benzophenone ketyl radical); they were freshly distilled prior to use. NMR spectra were obtained using 500 MHz Varian NMR spectrometers and referenced using the residual  $^1\text{H}$  peak from the deuterated solvent for the proton NMR, the carbon shift of the solvent (77.0 ppm for  $\text{CDCl}_3$ ) for the  $^{13}\text{C}$ -NMR, and phosphoric acid (as the internal standard reference for the  $^{31}\text{P}$ -NMR measurements. Column chromatography was performed using Silicycle 60 Å, 35-75  $\mu\text{m}$  silica gel. Pre-coated 0.25 mm thick silica gel 60 F254 plates were used for analytical TLC and visualized using UV light, *p*-anisaldehyde stain or phosphomolybdic acid in EtOH stain. CD spectra were recorded on a JASCO J-810 spectropolarimeter, equipped with a temperature controller (Neslab 111) for low temperature studies, and are reported as Mol. CD /  $\lambda$  [nm]. UV-vis spectra were recorded on an Agilent, Cary 100 UV-visible spectrophotometer equipped with temperature controller. UV spectra were collected with scan rate of 100 nm/min. Sofosbuvir and *epi*-sofosbuvir were generously gifted from Merck, Inc.

### III-6.2. General procedure for UV-vis measurements, binding affinity calculations and Job plot analysis

UV-vis measurement: **I-Zn-MAPOL 34** (1.0  $\mu\text{L}$  of a 0.001M solution in anhydrous dichloromethane, 1.0  $\mu\text{mol}$ ) was added to hexane (1.0 mL) in a 1.0 cm UV-cell. The background spectrum was recorded from 350 nm to 480 nm at a scan rate of 100 nm/min. Chiral phosphorus oxides (1 up to 500 equivalents) from four different stock solutions in anhydrous dichloromethane [0.1M (for 100-500 equiv), 0.01M (for 10-100 equiv), 0.001M (for 1-10 equiv), 0.0001M (for 0.1-1 equiv)] were then added to the **I-Zn-MAPOL 34** solution. The UV spectra were collected after each addition. A representative UV-vis titration graph is shown in Figure III-17.

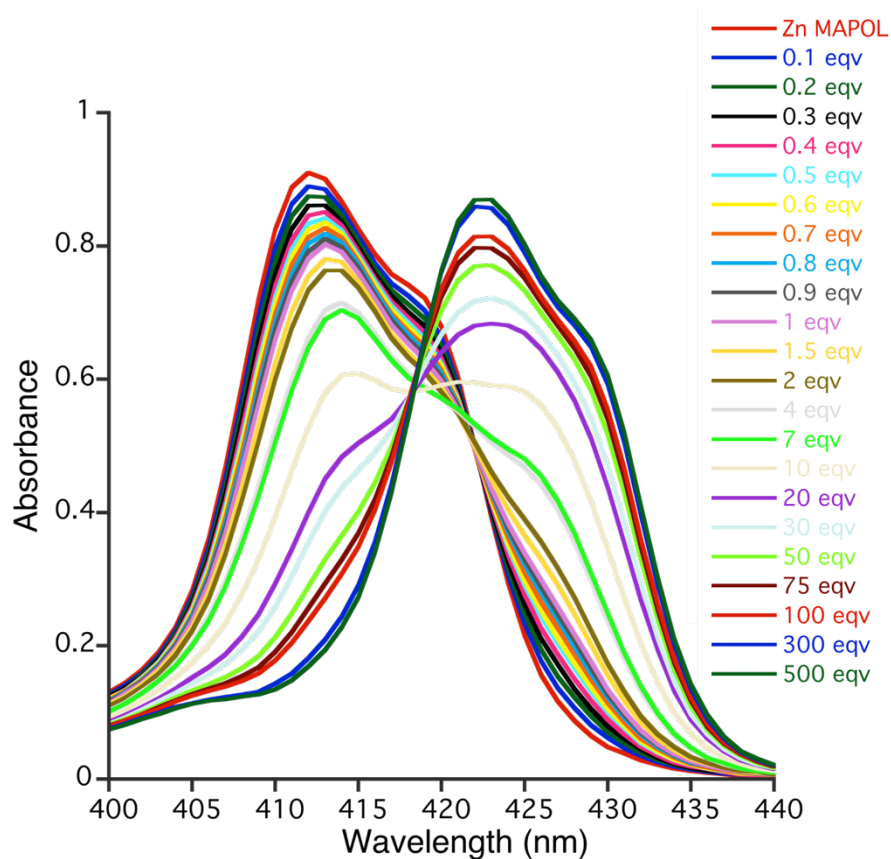


**Figure III-17.** UV-vis titration of **I-Zn-MAPOL 34** (1 $\mu\text{M}$ ) with **III-RP-19** at 0 °C in hexane.

Binding affinity measurements: The binding affinity was derived by fitting the UV-vis data (Fig- III-17) to the non-linear least square equation as reported by Shoji et. al.<sup>38</sup> Figure III-18 depicts the binding affinity measured for **III-*R<sub>P</sub>*-19**.

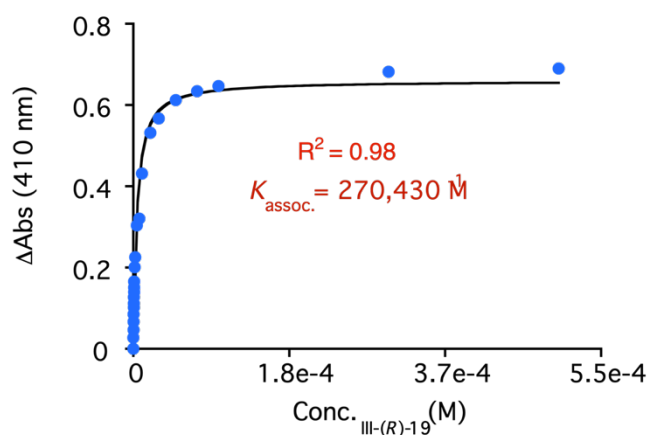


**Figure III-18.** Binding affinity measurement for **III-*R<sub>P</sub>*-19** titration with **I-Zn-MAPOL 34**.

Jobs plot analysis: Job's plot analysis was performed by measuring the changes in the UV-vis absorbance of **I-Zn-MAPOL 34** upon addition of **III-*R<sub>P</sub>*-19**. Changes in the UV-vis absorbance ( $\Delta A_{\text{abs}}$ ) were calculated by subtracting the absorbance at each titration point from the absorbance of free **I-Zn-MAPOL 34** at 410 nm. The molar fraction of **I-Zn-MAPOL 34** ( $X_{\text{Zn-MAPOL}}$ ) was then multiplied with the change in the UV-vis absorbance ( $\Delta A_{\text{abs}}$ ) for each titration point and was plotted against the molar fraction of **III-*R<sub>P</sub>*-19**. The

maxima at 0.5 **III-R<sub>P</sub>-19** confirms the formation of a 1:1 complex between **I-Zn-MAPOL 34** and phosphine oxide **III-R<sub>P</sub>-19**.

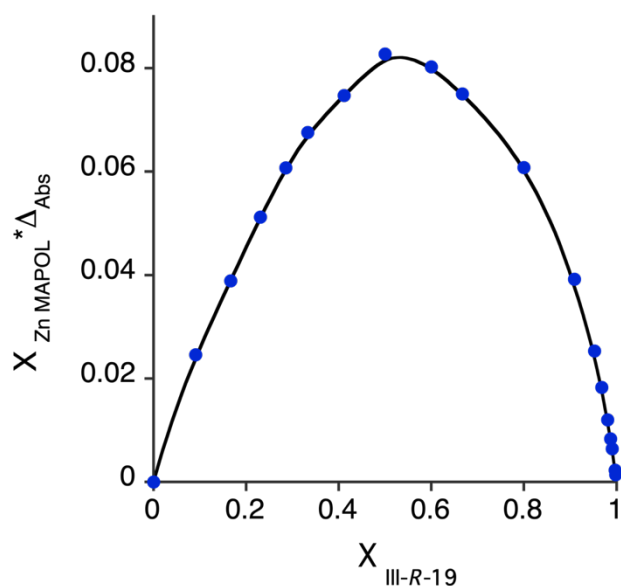


**Figure III-19.** Job plot of **I-Zn-MAPOL 34** with **III-R<sub>P</sub>-19** at 410 nm.

### III-6.3. General procedure for CD measurement

**I-Zn-MAPOL 34** (1.0  $\mu\text{L}$  of a 0.001M solution in anhydrous dichloromethane, 1.0  $\mu\text{mol}$ ) was added to hexane (1.0 mL) in a 1.0 cm CD cell (cooled to 0  $^{\circ}\text{C}$ ) to obtain a 1.0  $\mu\text{M}$  solution. The background spectrum was recorded from 350 nm to 480 nm with a scan rate of 100 nm/min at 0  $^{\circ}\text{C}$ . Chiral phosphine oxide from a stock solution in anhydrous dichloromethane (0.001 M for 1-10 equiv and 0.01 M for 10-20 equiv) was added to the prepared host solution to afford the host-guest complex. The CD spectra were measured immediately (10 scans). The resultant ECCD spectra recorded in millidegrees were converted the molecular CD (Mol. CD) considering the host concentration of 1.0  $\mu\text{M}$ .

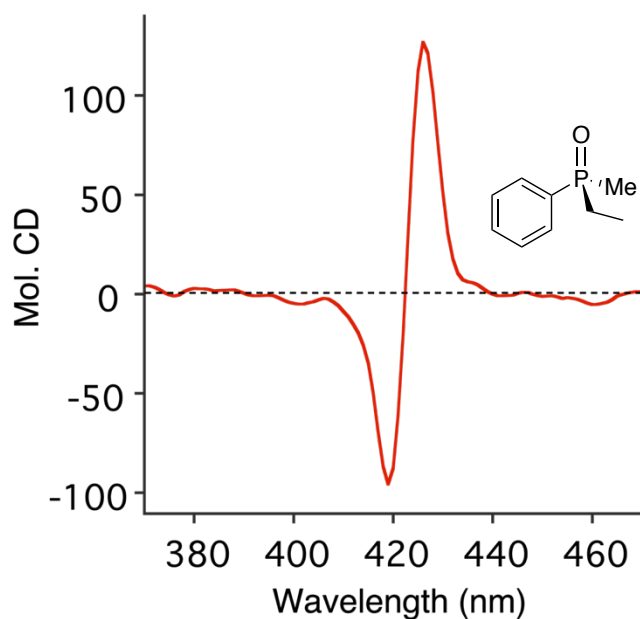


**Figure III-20.** Positive ECD spectrum of **I-Zn-MAPOL 34** complexed with 5 equiv of **III-S-P-18** at 0 °C in hexane.

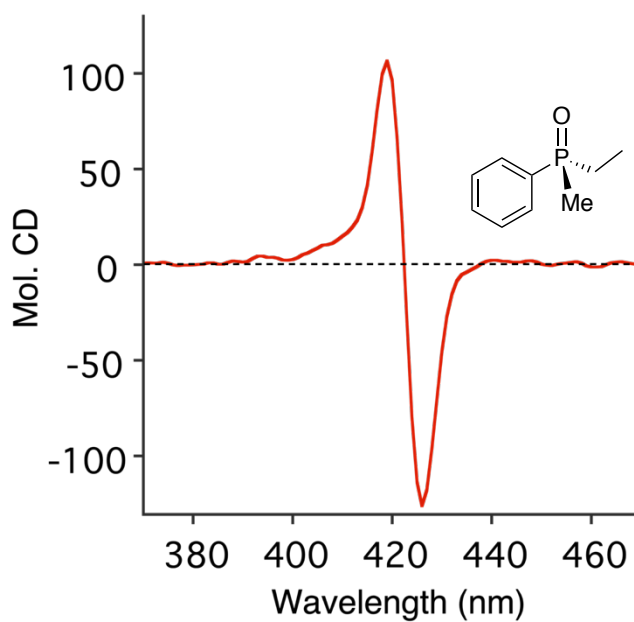


**Figure III-21.** Negative ECD spectrum of **I-Zn-MAPOL 34** complexed with 5 equiv of **III-R-P-18** at 0 °C in hexane.

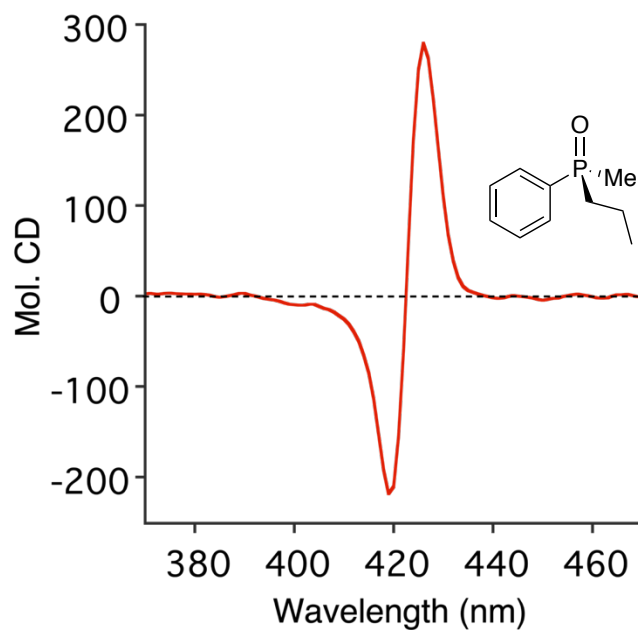


**Figure III-22.** Positive ECCD spectrum of **I-Zn-MAPOL 34** complexed with 5 equiv of **III-SP-19** at 0 °C in hexane.

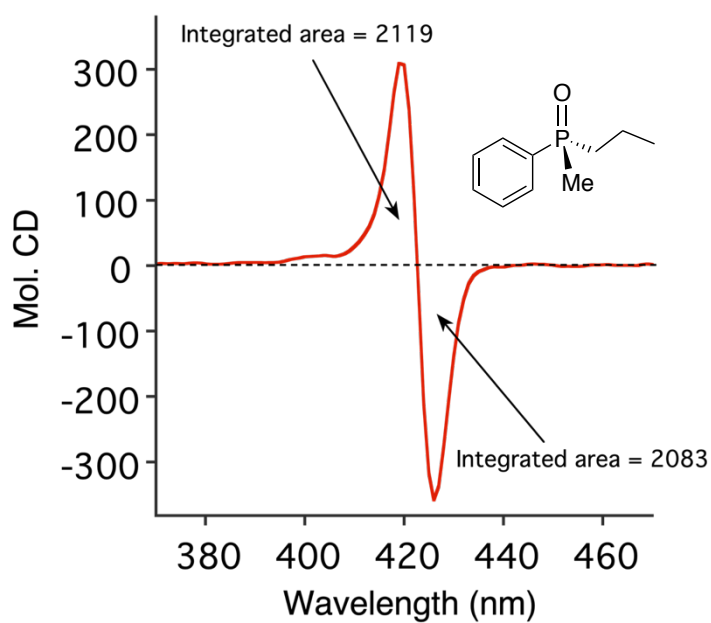


**Figure III-23.** Negative ECCD spectrum of **I-Zn-MAPOL 34** complexed with 5 equiv of **III-RP-19** at 0 °C in hexane.

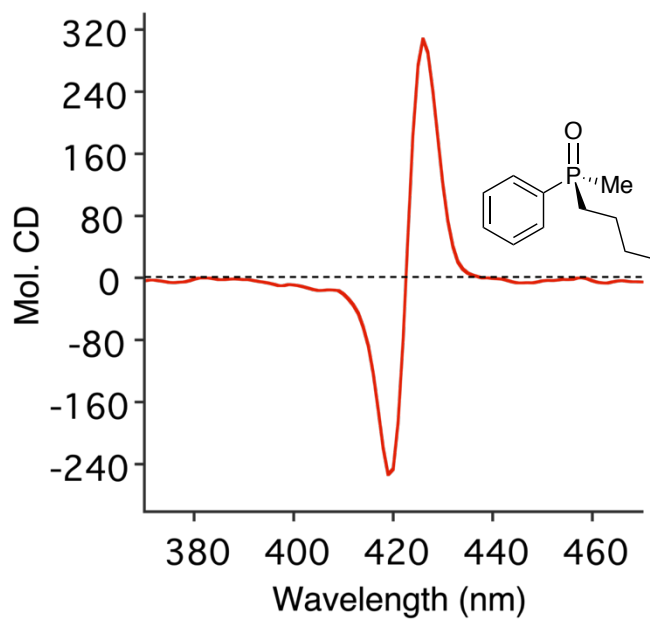


**Figure III-24.** Positive ECD spectrum of **I-Zn-MAPOL 34** complexed with 5 equiv of **III-SP-20** at 0 °C in hexane.

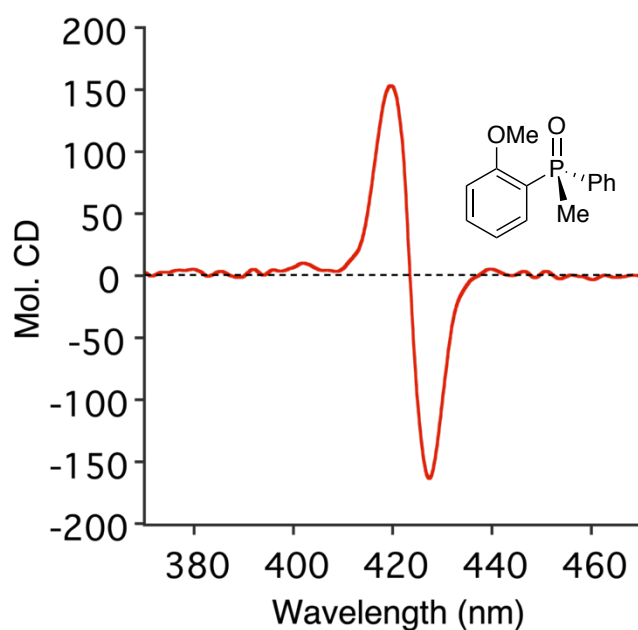


**Figure III-25.** Negative ECD spectrum of **I-Zn-MAPOL 34** complexed with 5 equiv of **III-RP-21** at 0 °C in hexane.

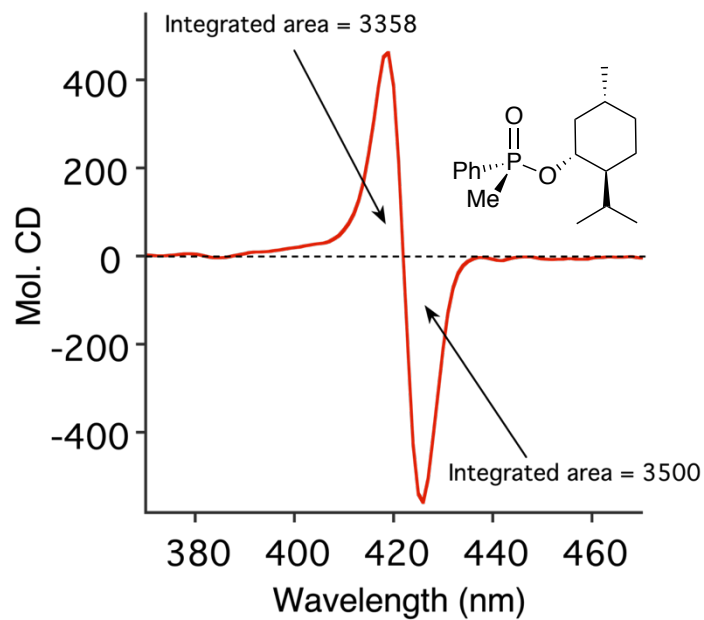


**Figure III-26.** Positive EECDD spectrum of **I-Zn-MAPOL 34** complexed with 5 equiv of **III-*R<sub>P</sub>*-22** at 0 °C in hexane.

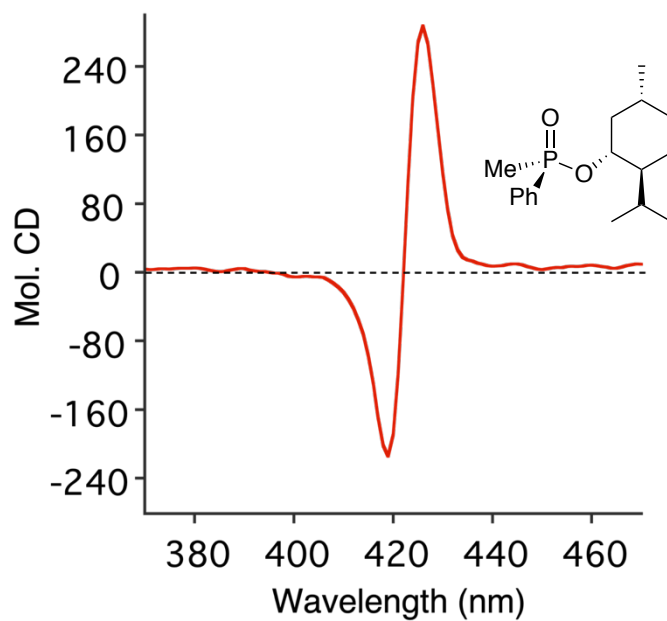


**Figure III-27.** Negative EECDD spectrum of **I-Zn-MAPOL 34** complexed with 5 equiv of **III-*S<sub>P</sub>*-23** at 0 °C in hexane.



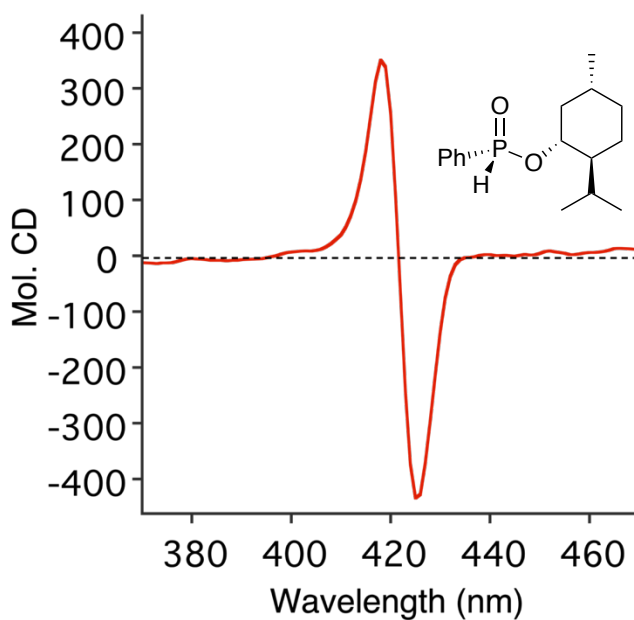


**Figure III-28.** Negative ECD spectrum of **I-Zn-MAPOL 34** complexed with 5 equiv of **III-RP-24** at 0 °C in hexane.

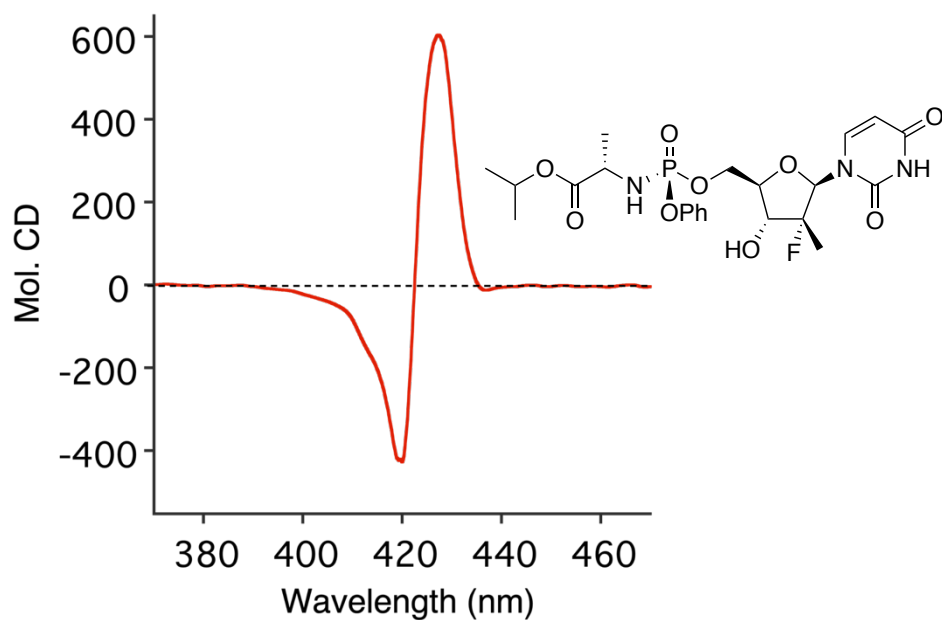


**Figure III-29.** Positive ECD spectrum of **I-Zn-MAPOL 34** complexed with 1 equiv of **III-2** at 0 °C in hexane.

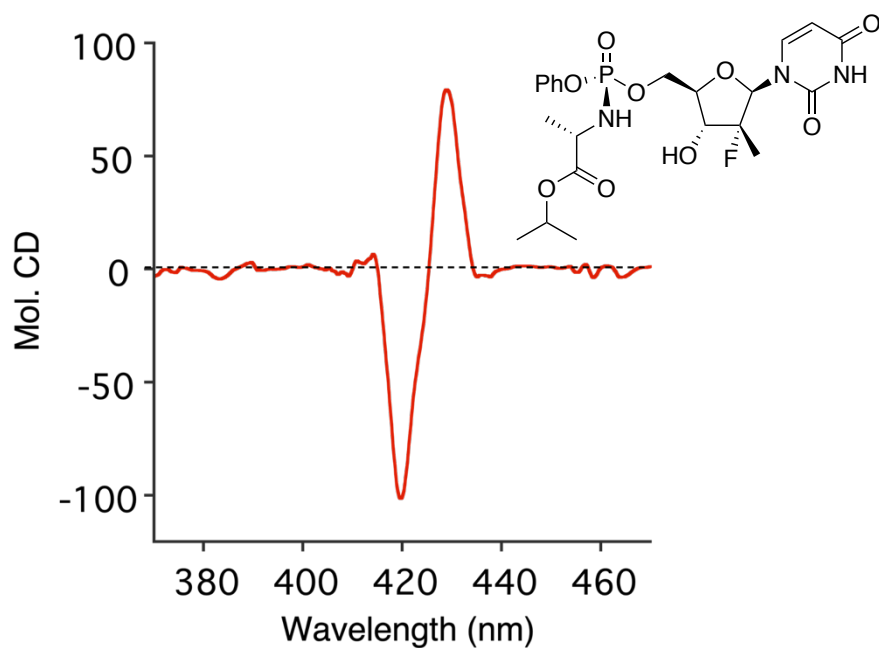


**Figure III-30.** Positive ECCD spectrum of **I-Zn-MAPOL 34** complexed with 1 equiv of **III-*epi*-2** at 0 °C in hexane.

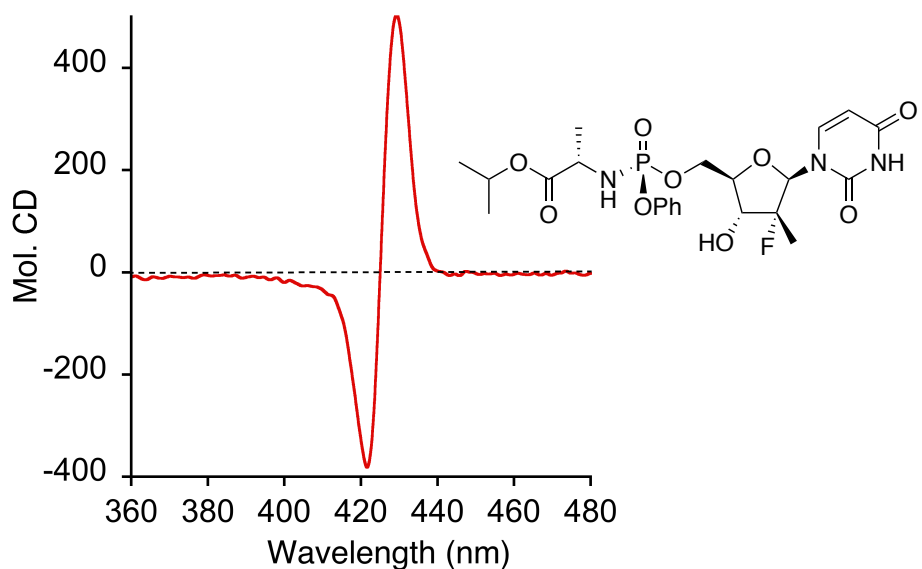


**Figure III-31.** Positive ECCD spectrum of **I-Zn-MAPOL 34** complexed with 20 equiv of **III-2** at 0 °C in chlorobenzene.

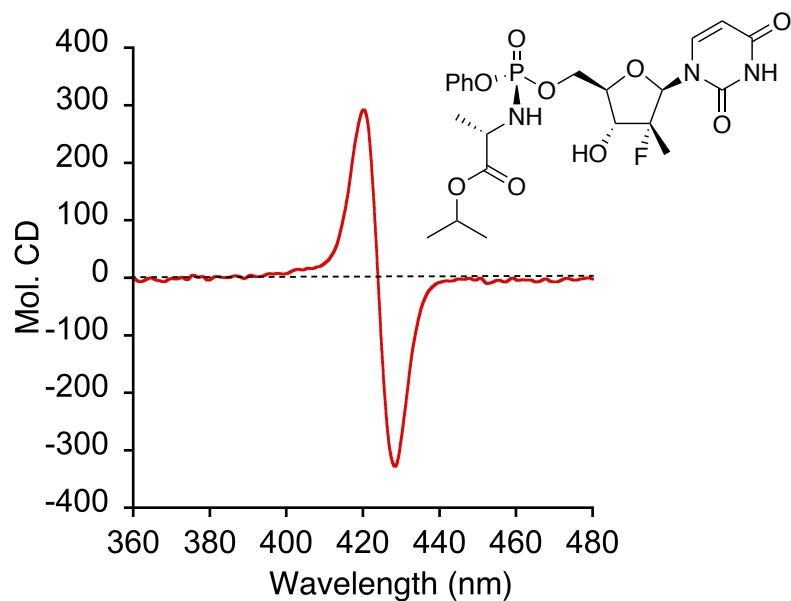


**Figure III-32.** Negative ECD spectrum of **I-Zn-MAPOL 34** complexed with 20 equiv of **III-*epi*-2** at 0 °C in chlorobenzene.

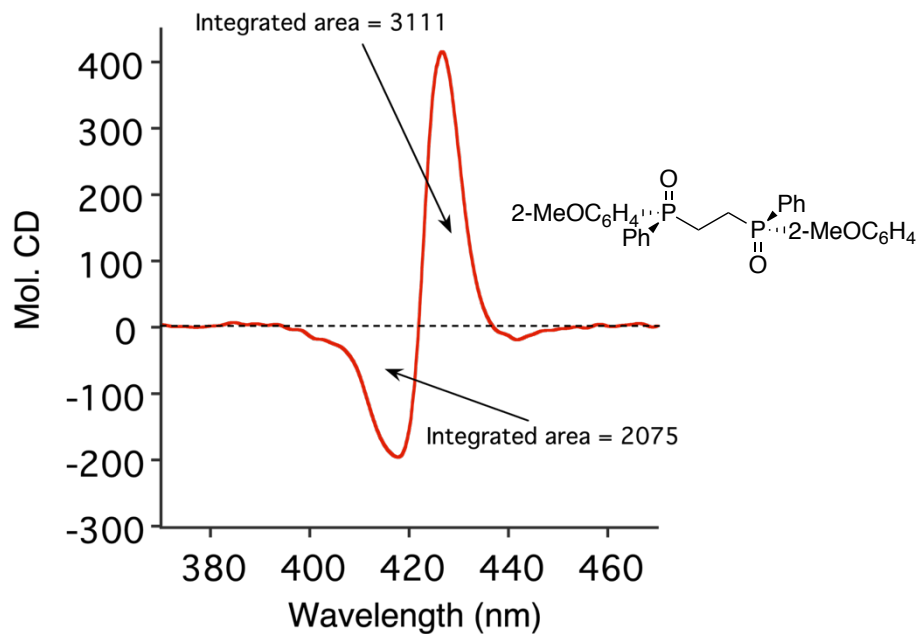


**Figure III-33.** Positive ECD spectrum of **I-Zn-MAPOL 34** complexed with 1 equiv of **III-*S<sub>P</sub>,S<sub>P</sub>*-30** at 0 °C in hexane.

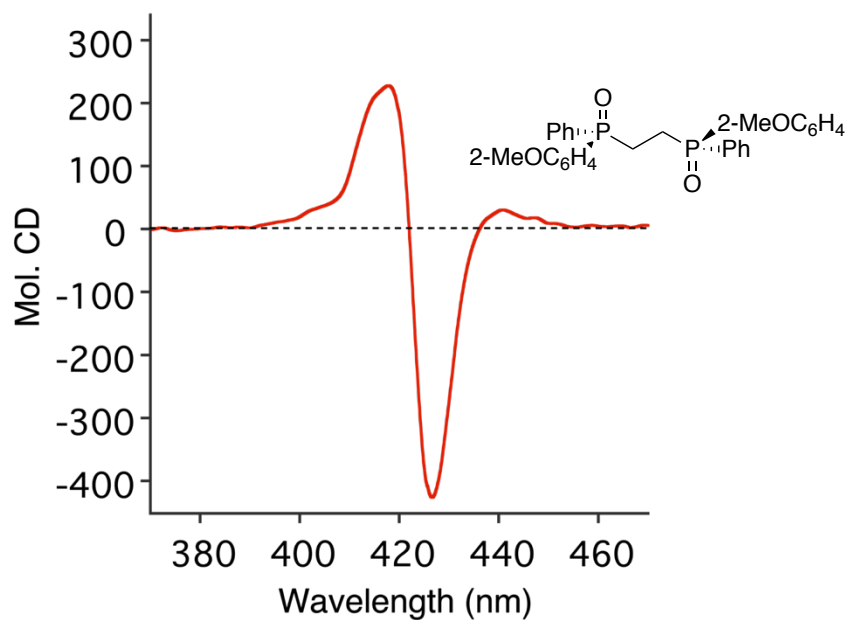


**Figure III-34.** Negative ECCD spectrum of **I-Zn-MAPOL 34** complexed with 1 equiv of **III-*R<sub>P</sub>*,*R<sub>P</sub>*-30** at 0 °C in hexane.

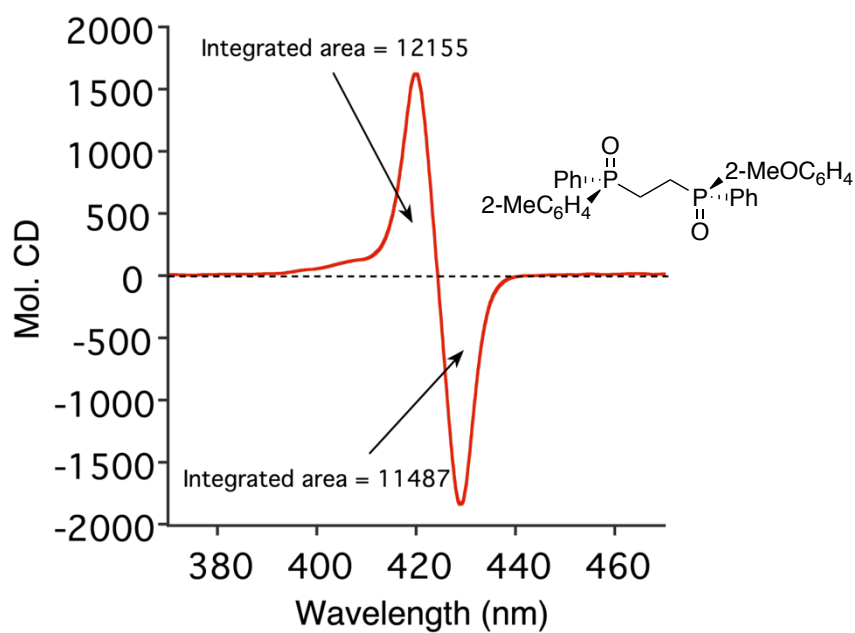


**Figure III-35.** Negative ECCD spectrum of **I-Zn-MAPOL 34** complexed with 1 equiv of **III-*R<sub>P</sub>*,*R<sub>P</sub>*-31** at 0 °C in hexane.

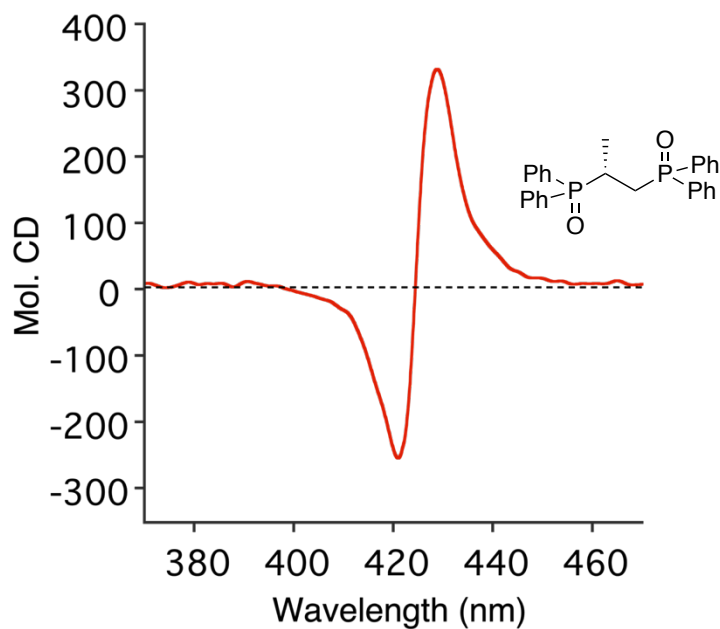


**Figure III-36.** Positive ECCD spectrum of **I-Zn-MAPOL 34** complexed with 1 equiv of **III-R-32** at 0 °C in hexane.

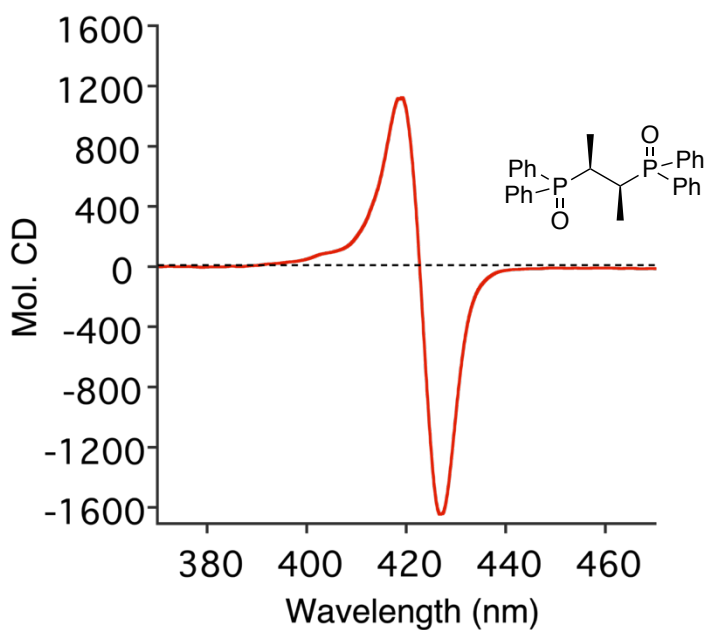


**Figure III-37.** Negative ECCD spectrum of **I-Zn-MAPOL 34** complexed with 1 equiv of **III-S,S-33** at 0 °C in hexane.

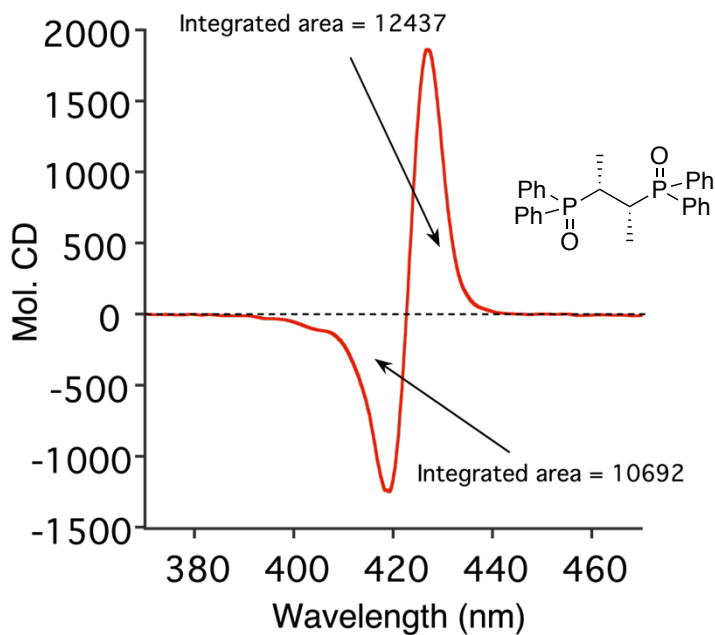


**Figure III-38.** Positive ECD spectrum of **I-Zn-MAPOL 34** complexed with 1 equiv of **III-*R,R*-34** at 0 °C in hexane.

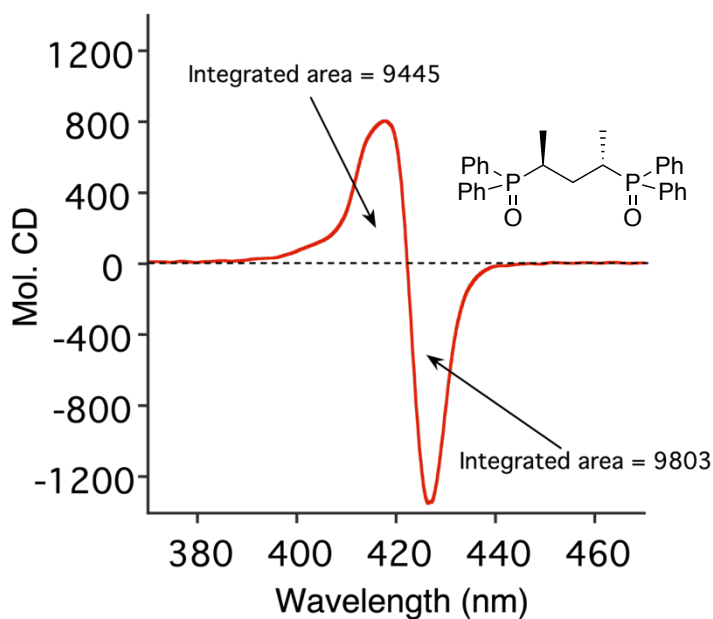


**Figure III-39.** Negative ECD spectrum of **I-Zn-MAPOL 34** complexed with 1 equiv of **III-*S,S*-35** at 0 °C in hexane.

#### III-6.4. Temperature dependence on the amplitude of the ECCD signal for I-Zn-MAPOL 34 complexed with III-*R<sub>P</sub>*-19

I-Zn-MAPOL 34 (1.0  $\mu$ M) was complexed with 5 equiv of III-*R<sub>P</sub>*-19 (5.0  $\mu$ mol) in hexane. With the increase in temperature the ECCD signal drops gradually, although significant signal is observed even at 45 °C. The same ECCD active solution at 45 °C increases signal intensity when cooled down to 0 °C with an intensity similar to the ECCD signal of the original complex at 0 °C.

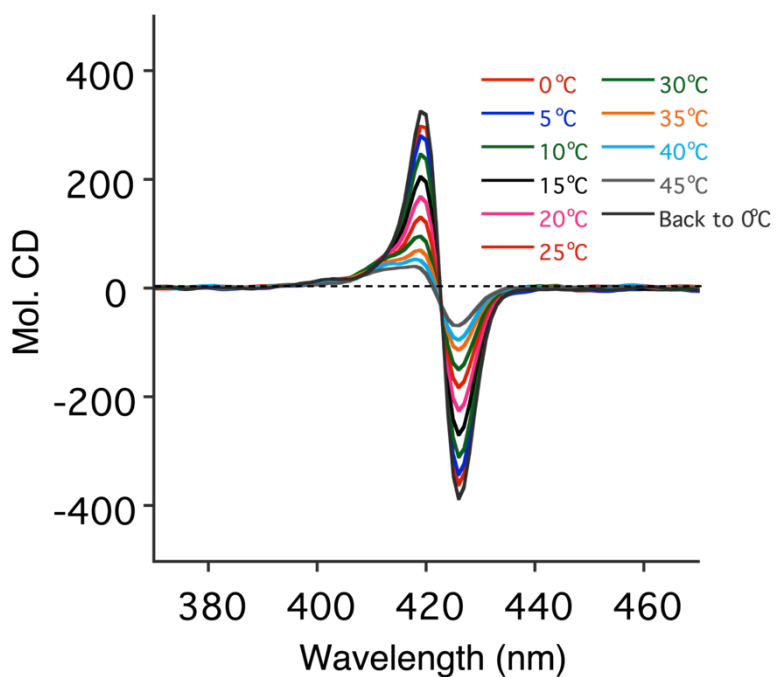


**Figure III-40.** Change in ECCD signal of I-Zn-MAPOL 34 complexed with 5 equiv of III-*R<sub>P</sub>*-19 in hexane at different temperatures.

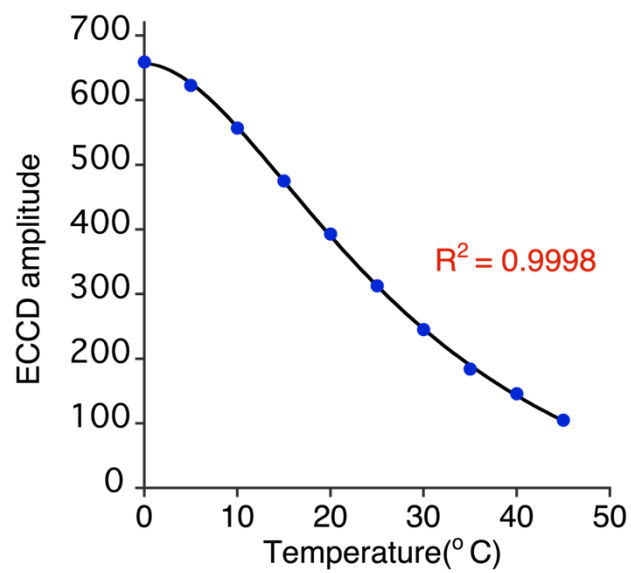


**Figure III-41.** Temperature dependence on the amplitude of the ECCD signal of **I-Zn-MAPOL 34** complexed with 5 equiv of **III-*R<sub>P</sub>*-19** in hexane.



### III-6.5. Solvent screening for I-Zn-MAPOL 34 complexed with III-*R<sub>P</sub>*-19 and III-*R<sub>P</sub>*-22

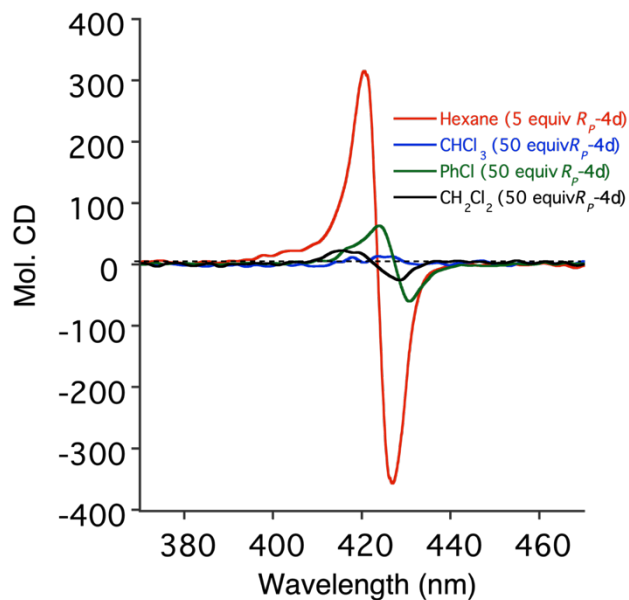


**Figure III-42.** ECCD spectra of I-Zn-MAPOL 34 complexed with III-*R<sub>P</sub>*-19 at 0 °C in different solvents.

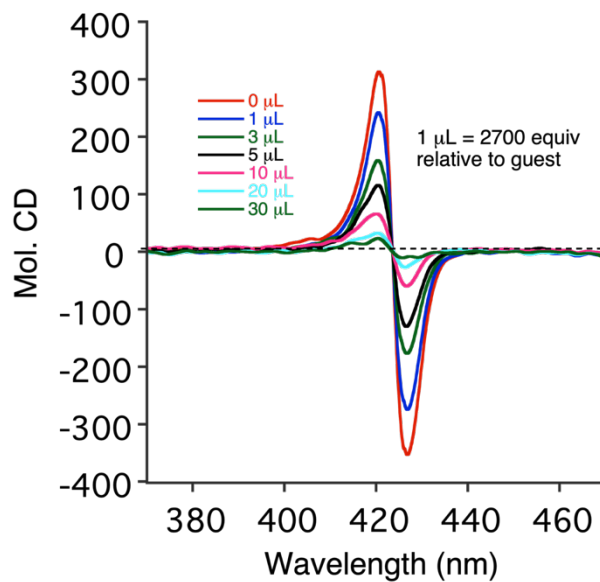


**Figure III-43.** ECCD titration of I-Zn-MAPOL 34 complexed with 5 equiv of III-*R<sub>P</sub>*-19 at 0 °C with acetone.

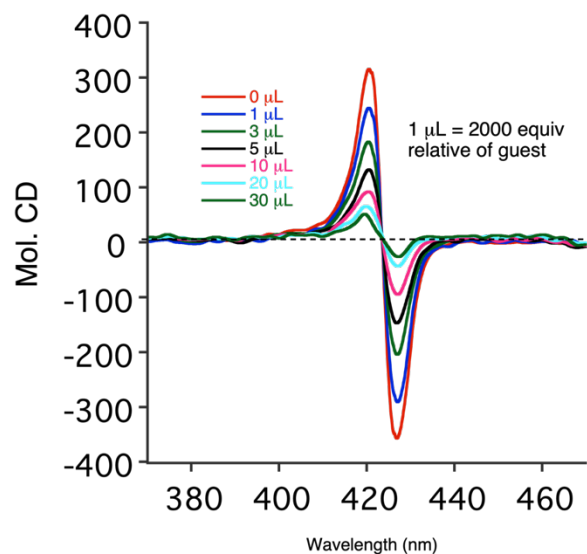


**Figure III-44.** ECCD titration of **I-Zn-MAPOL 34** complexed with 5 equiv of **III-RP-19** at 0 °C with ethyl acetate.

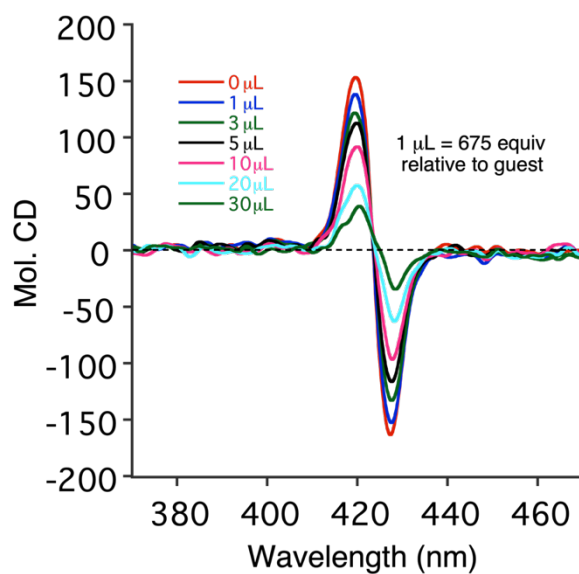


**Figure III-45.** ECCD titration of **I-Zn-MAPOL 34** complexed with 20 equiv of **III-RP-22** at 0 °C with acetone.

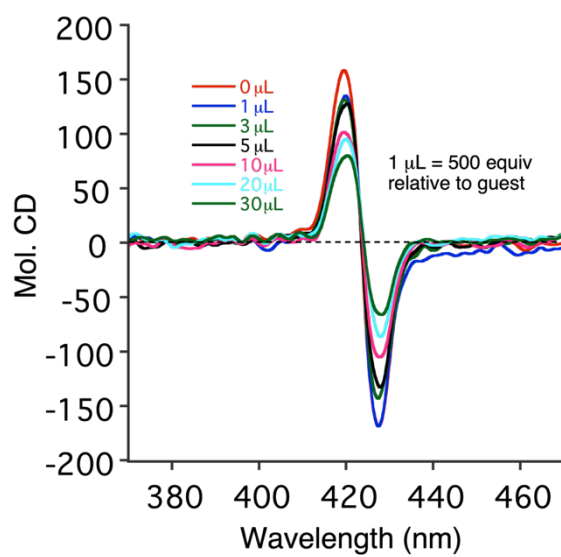


**Figure III-46.** ECCD titration of **I-Zn-MAPOL 34** complexed with 20 equiv of **III-RP-22** at 0 °C in ethyl acetate.

### III-6.6. ECCD of III-MeO-Zn-MAPOL 16 complexed with chiral phosphorous oxide

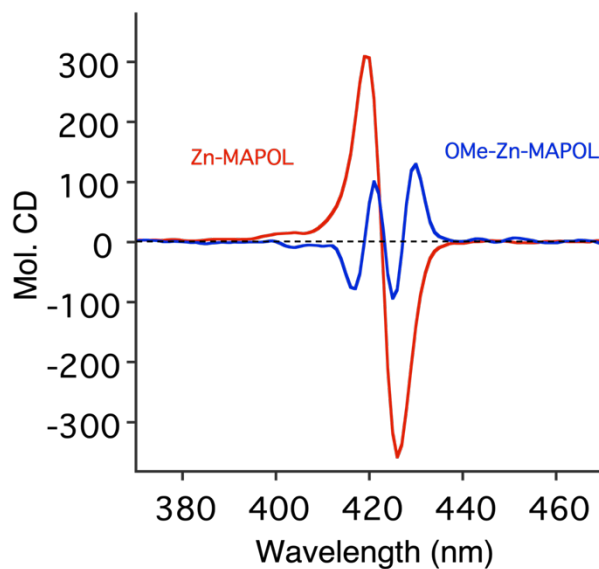


**Figure III-47.** ECCD of **I-Zn-MAPOL 34** (red curve) and **III-MeO-Zn-MAPOL 16** (blue curve) complexed with 5 equiv of **III-*R<sub>P</sub>*-19** at 0 °C in hexane.

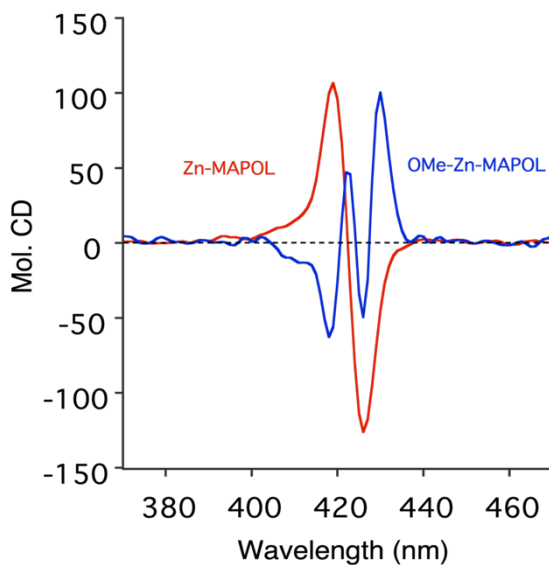


**Figure III-48.** ECCD of **I-Zn-MAPOL 34** (red curve) and **III-MeO-Zn-MAPOL 16** (blue curve) complexed with 5 equiv of **III-*R<sub>P</sub>*-18** at 0 °C in hexane.

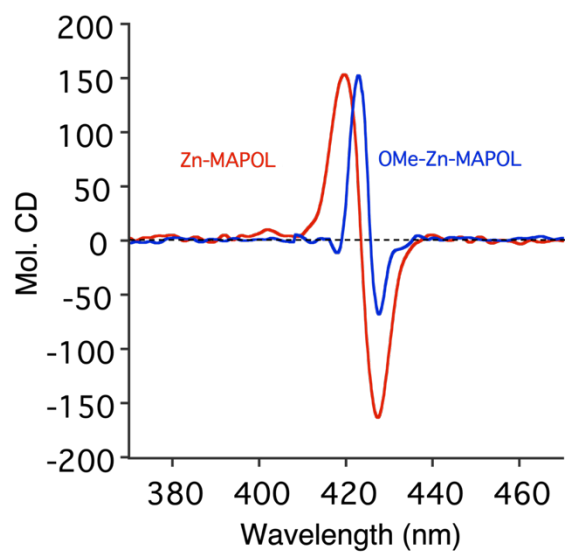


**Figure III-49.** ECCD of **I-Zn-MAPOL 34** (red curve) and **III-MeO-Zn-MAPOL 16** (blue curve) complexed with 20 equiv of **III-*R<sub>P</sub>*-21** at 0 °C in hexane.

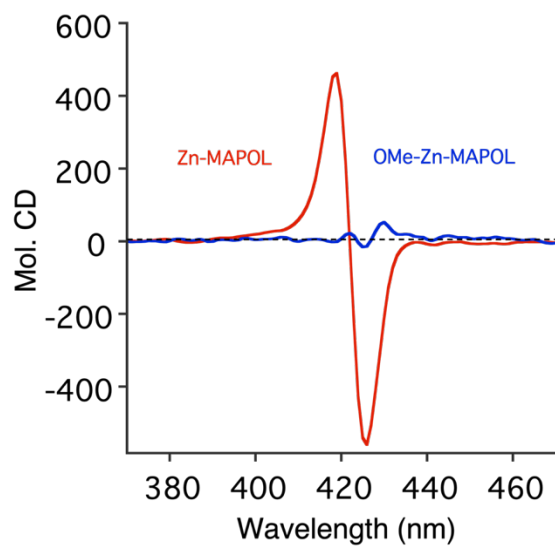


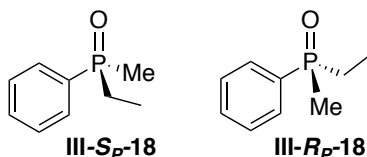
**Figure III-50.** ECCD of **I-Zn-MAPOL 34** (red curve) and **III-MeO-Zn-MAPOL 16** (blue curve) complexed with 5 equiv of **III-*R<sub>P</sub>*-22** at 0 °C in hexane.

### III-6.7. Synthesis of P-chiral phosphine oxides

P-chiral phosphine oxides were synthesized following literature procedures.<sup>5, 18-19, 32-33</sup>

Optical purity was measured comparing their optical rotation values with the reported values.

#### ethyl(methyl)(phenyl)phosphine oxide:



**III-S<sub>P</sub>-18** enantiomer:

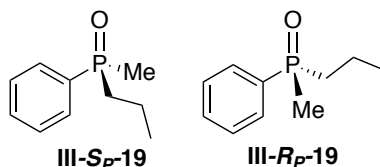
$[\alpha]_D = -16.7$  ( $c = 1.0$ , MeOH);  $ee = 68\%$

**III-R<sub>P</sub>-18** enantiomer:

$[\alpha]_D = +18.1$  ( $c = 1.0$ , MeOH);  $ee = 74\%$

$^1\text{H}$  NMR (500 MHz,  $\text{CDCl}_3$ )  $\delta$  7.72 – 7.67 (m, 2H), 7.54 – 7.46 (m, 3H), 2.03 – 1.83 (m, 2H), 1.69 (dd,  $J = 12.7, 1.4$  Hz, 3H), 1.15 – 1.08 (m, 3H).  $^{13}\text{C}$  NMR (126 MHz,  $\text{CDCl}_3$ )  $\delta$  133.62, 132.86, 131.61 (d,  $J = 2.7$  Hz), 130.07 (d,  $J = 9.3$  Hz), 128.64 (d,  $J = 11.4$  Hz), 24.64 (d,  $J = 71.4$  Hz), 15.40 (d,  $J = 69.6$  Hz), 5.73 (d,  $J = 5.1$  Hz).  $^{31}\text{P}$  NMR (202 MHz,  $\text{CDCl}_3$ )  $\delta$  39.11.

#### methyl(phenyl)(propyl)phosphine oxide:



**III-*S<sub>P</sub>*-19** enantiomer:

$[\alpha]_D = -13.2$  ( $c = 1.0$ , MeOH);  $ee = 78\%$

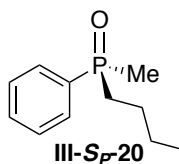
**III-*R<sub>P</sub>*-19** enantiomer:

$[\alpha]_D = +15.5$  ( $c = 1.0$ , MeOH);  $ee = 92\%$

$^1\text{H}$  NMR (500 MHz,  $\text{CDCl}_3$ )  $\delta$  7.73 – 7.69 (m, 2H), 7.53 – 7.48 (m, 3H), 2.00 – 1.81 (m, 3H), 1.69 (d,  $J = 12.7$  Hz, 3H), 1.67 – 1.47 (m, 2H), 0.99 (td,  $J = 7.3, 1.1$  Hz, 3H).

$^{13}\text{C}$  NMR (126 MHz,  $\text{CDCl}_3$ )  $\delta$  134.15, 133.99, 131.55 (d,  $J = 2.6$  Hz), 129.99 (d,  $J = 9.3$  Hz), 128.63 (d,  $J = 11.4$  Hz), 33.91 (d,  $J = 70.4$  Hz), 16.32, 15.73 (d,  $J = 11.9$  Hz), 15.56, 15.42 (d,  $J = 3.8$  Hz).  $^{31}\text{P}$  NMR (202 MHz,  $\text{CDCl}_3$ )  $\delta$  37.11.

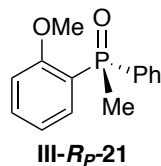
**butyl(methyl)(phenyl)phosphine oxide:**



$[\alpha]_D = -11.5$  ( $c = 1.0$ , MeOH);  $ee = 69\%$

$^1\text{H}$  NMR (500 MHz,  $\text{CDCl}_3$ )  $\delta$  7.70 – 7.67 (m, 2H), 7.59 – 7.41 (m, 3H), 2.02 – 1.81 (m, 2H), 1.70 (d,  $J = 12.7$  Hz, 3H), 1.66 – 1.42 (m, 2H), 1.42 – 1.32 (m, 2H), 0.87 (t,  $J = 7.3$  Hz, 3H).  $^{13}\text{C}$  NMR (126 MHz,  $\text{CDCl}_3$ )  $\delta$  134.16, 133.40, (131.55 (d,  $J = 2.8$  Hz), 130.02 (d,  $J = 9.1$  Hz), 128.64 (d,  $J = 11.4$  Hz), 31.52 (d,  $J = 70.5$  Hz), 24.03 (d,  $J = 15.2$  Hz), 23.68 (d,  $J = 4.3$  Hz), 16.04 (d,  $J = 69.5$  Hz), 13.58.  $^{31}\text{P}$  NMR (202 MHz,  $\text{CDCl}_3$ )  $\delta$  37.39

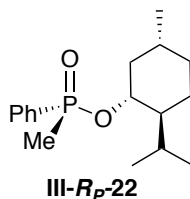
**2-methoxyphenyl(methyl)(phenyl)phosphine oxide:**



$[\alpha]_D = +18.8$  ( $c = 1.0$ , MeOH);  $ee = 71\%$

$^1\text{H}$  NMR (500 MHz,  $\text{CDCl}_3$ )  $\delta$  7.97 (ddd,  $J = 13.1, 7.5, 1.8$  Hz, 1H), 7.79 – 7.68 (m, 2H), 7.55 – 7.45 (m, 2H), 7.44 – 7.40 (m, 2H), 7.11 (tdd,  $J = 7.5, 1.8, 0.9$  Hz, 1H), 6.89 (ddd,  $J = 8.5, 5.4, 0.9$  Hz, 1H), 3.73 (s, 3H), 2.08 (d,  $J = 14.0$  Hz, 3H).  $^{13}\text{C}$  NMR (126 MHz,  $\text{CDCl}_3$ )  $\delta$  133.97 (d,  $J = 6.1$  Hz), 133.88 (d,  $J = 2.8$  Hz), 131.25 (d,  $J = 2.9$  Hz), 130.26 (d,  $J = 10.4$  Hz), 128.20 (d,  $J = 12.4$  Hz), 121.04 (d,  $J = 11.3$  Hz), 110.84 (d,  $J = 6.6$  Hz), 55.28, 16.17 (d,  $J = 75.2$  Hz).  $^{31}\text{P}$  NMR (202 MHz,  $\text{CDCl}_3$ )  $\delta$  28.33.

**(1*R*,2*S*,5*R*)-2-isopropyl-5-methylcyclohexyl (*R<sub>P</sub>*)-methyl(phenyl) phosphinate:**

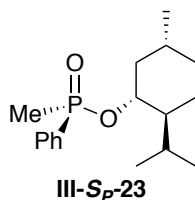


$^1\text{H}$  NMR (500 MHz,  $\text{CDCl}_3$ )  $\delta$  7.85 – 7.75 (m, 2H), 7.56 – 7.50 (m, 1H), 7.49 – 7.44 (m, 2H), 4.27 (tdd,  $J = 10.7, 8.2, 4.5$  Hz, 1H), 2.23 – 2.17 (m, 1H), 1.83 – 1.79 (m, 1H), 1.71 – 1.55 (m, 5H), 1.39 – 1.29 (m, 2H), 1.04 – 0.97 (m, 2H), 0.96 (d,  $J = 7.1$  Hz, 3H), 0.88 (d,  $J = 6.9$  Hz, 3H), 0.85 – 0.79 (m, 1H), 0.76 (d,  $J = 6.6$  Hz, 3H).  $^{13}\text{C}$  NMR (126 MHz,  $\text{CDCl}_3$ )  $\delta$  131.89 (d,  $J = 2.8$  Hz), 130.82 (d,  $J = 10.1$  Hz), 128.40 (d,  $J = 12.8$  Hz), 76.37 (d,  $J =$



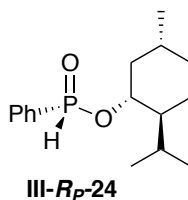
7.1 Hz), 48.75 (d,  $J = 6.2$  Hz), 43.21, 34.09, 31.43, 25.85, 22.95, 21.91, 21.10, 16.95, 16.14, 15.83.  $^{31}\text{P}$  NMR (202 MHz,  $\text{CDCl}_3$ )  $\delta$  39.81.

**(1*R*,2*S*,5*R*)-2-isopropyl-5-methylcyclohexyl (*S<sub>P</sub>*)-methyl(phenyl) phosphinate:**



$^1\text{H}$  NMR (500 MHz,  $\text{CDCl}_3$ )  $\delta$  7.83 – 7.79 (m, 2H), 7.58 – 7.51 (m, 1H), 7.51 – 7.45 (m, 2H), 3.97 (tdd,  $J = 10.5, 7.9, 4.5$  Hz, 1H), 2.45 – 2.33 (m, 1H), 1.94 – 1.88 (m, 1H), 1.72 (d,  $J = 14.5$  Hz, 3H), 1.65 – 1.55 (m, 2H), 1.43 – 1.37 (m, 1H), 1.35 – 1.19 (m, 3H), 0.92 (d,  $J = 6.5$  Hz, 3H), 0.86 (d,  $J = 10.3$  Hz, 1H), 0.83 (d,  $J = 7.1$  Hz, 1H), 0.31 (d,  $J = 6.9$  Hz, 3H).  $^{13}\text{C}$  NMR (126 MHz,  $\text{CDCl}_3$ )  $\delta$  131.97 (d,  $J = 2.6$  Hz), 131.12 (d,  $J = 10.0$  Hz), 128.41 (d,  $J = 12.8$  Hz), 76.69, 48.76 (d,  $J = 6.8$  Hz), 43.87, 34.07, 31.54, 25.36, 22.67, 21.98, 21.08, 16.96, 16.14, 15.15.  $^{31}\text{P}$  NMR (202 MHz,  $\text{CDCl}_3$ )  $\delta$  40.49.  $dr = 12.5 : 1$

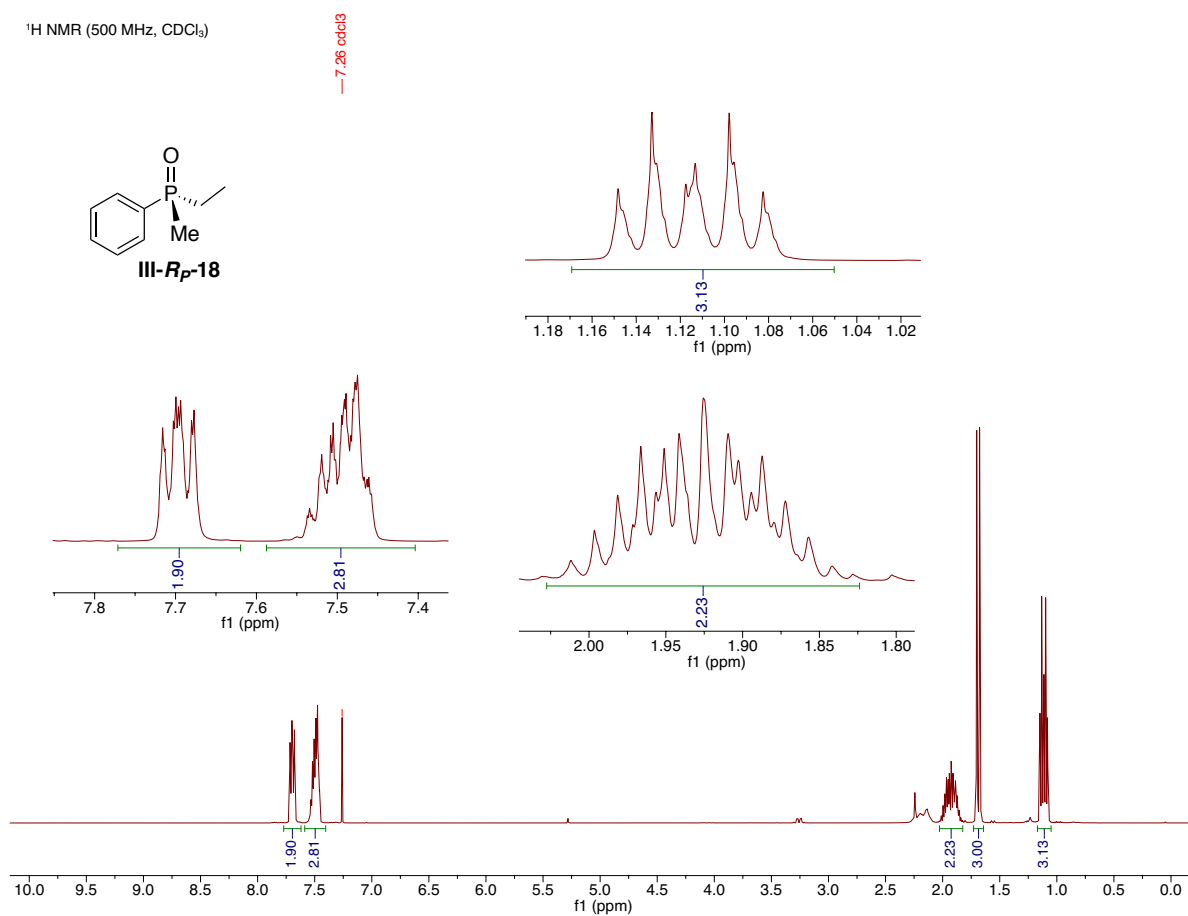
**(1*R*,2*S*,5*R*)-2-isopropyl-5-methylcyclohexyl (*R<sub>P</sub>*)-phenyl phosphinate:**



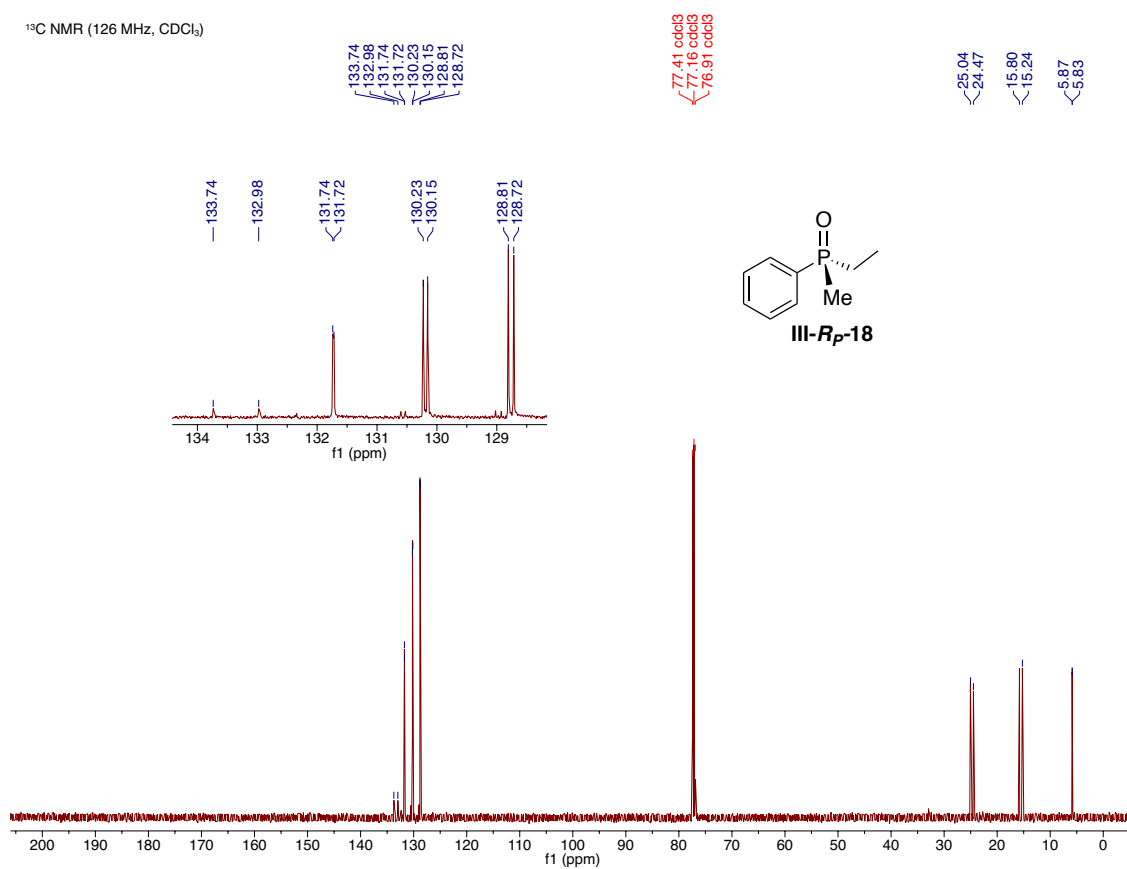
$^1\text{H}$  NMR (500 MHz,  $\text{CDCl}_3$ )  $\delta$  8.20 (s, 1H), 7.80 – 7.75 (m, 2H), 7.65 (d,  $J_{\text{HP}} = 550$  Hz, 1H), 7.60 – 7.57 (m, 1H), 7.52 – 7.48 (m, 2H), 4.25 (qd,  $J = 10.5, 4.5$  Hz, 1H), 2.24 – 2.15

(m, 2H), 1.71 – 1.65 (m, 2H), 1.48 – 1.42 (m, 2H), 1.24 (q,  $J = 10.0$  Hz, 1H), 1.04 (qd, ,  $J = 15$  Hz, 5 Hz, 1H), 0.95 (d,  $J = 7.0$  Hz, 3H), 0.87 (m, 7H),  $^{13}\text{C}$  NMR (126 MHz,  $\text{CDCl}_3$ )  $\delta$  132.91 (d,  $J = 2.9$  Hz), 130.63, (d,  $J = 11.8$  Hz), 128.67 (d,  $J = 13.8$  Hz), 78.96 (d,  $J = 7.4$  Hz), 48.69 (d,  $J = 6.2$  Hz), 43.49 (d,  $J = 1.1$  Hz), 33.91, 31.63, 25.76, 22.89, 21.86, 20.99, 15.73.  $^{31}\text{P}$  NMR (202 MHz,  $\text{CDCl}_3$ )  $\delta$  24.73.  $dr = 19:1$

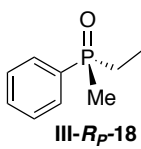
### III-6.8. NMR Spectra:



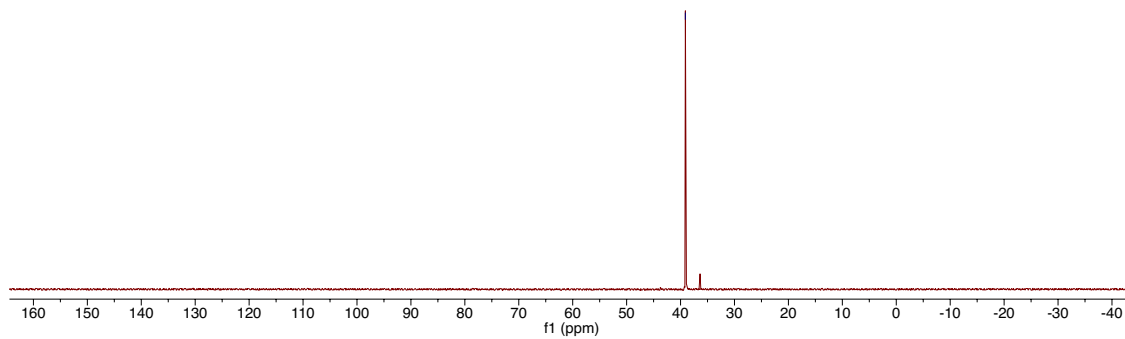
<sup>13</sup>C NMR (126 MHz, CDCl<sub>3</sub>)



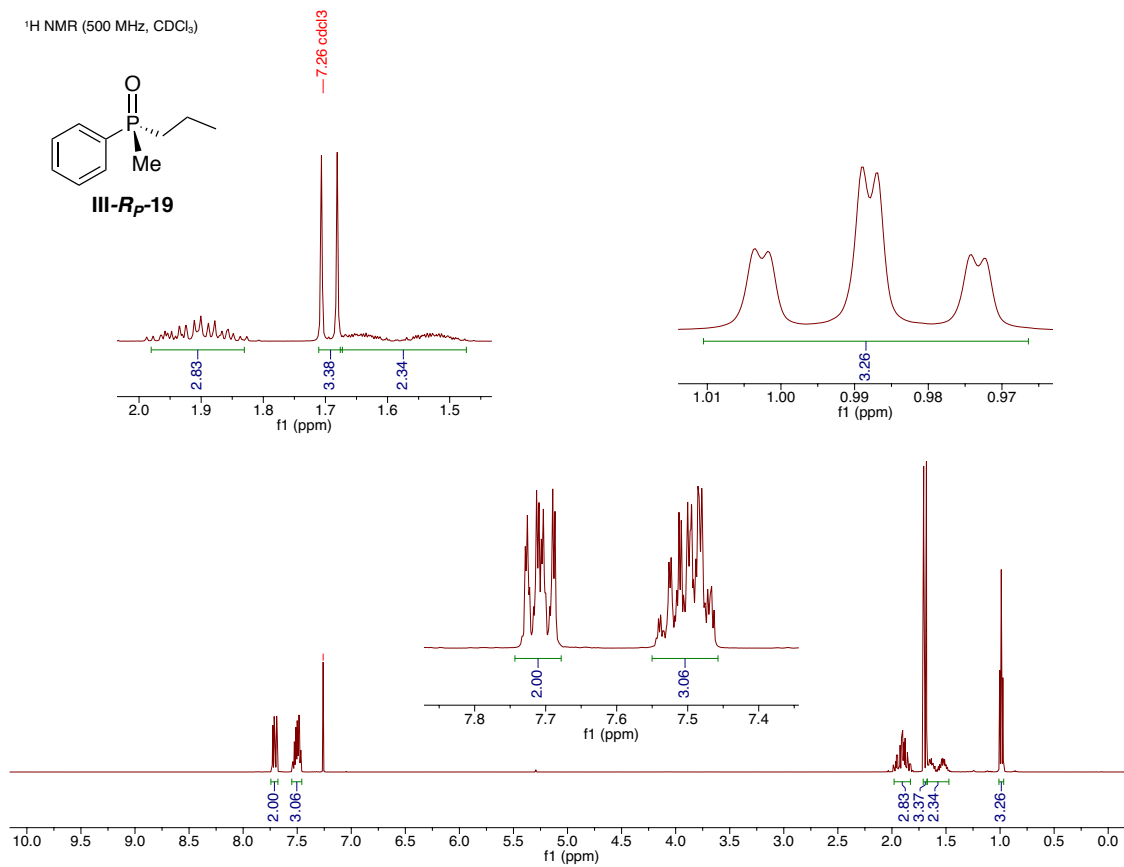
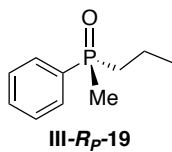
$^{31}\text{P}$  NMR (202 MHz,  $\text{CDCl}_3$ )

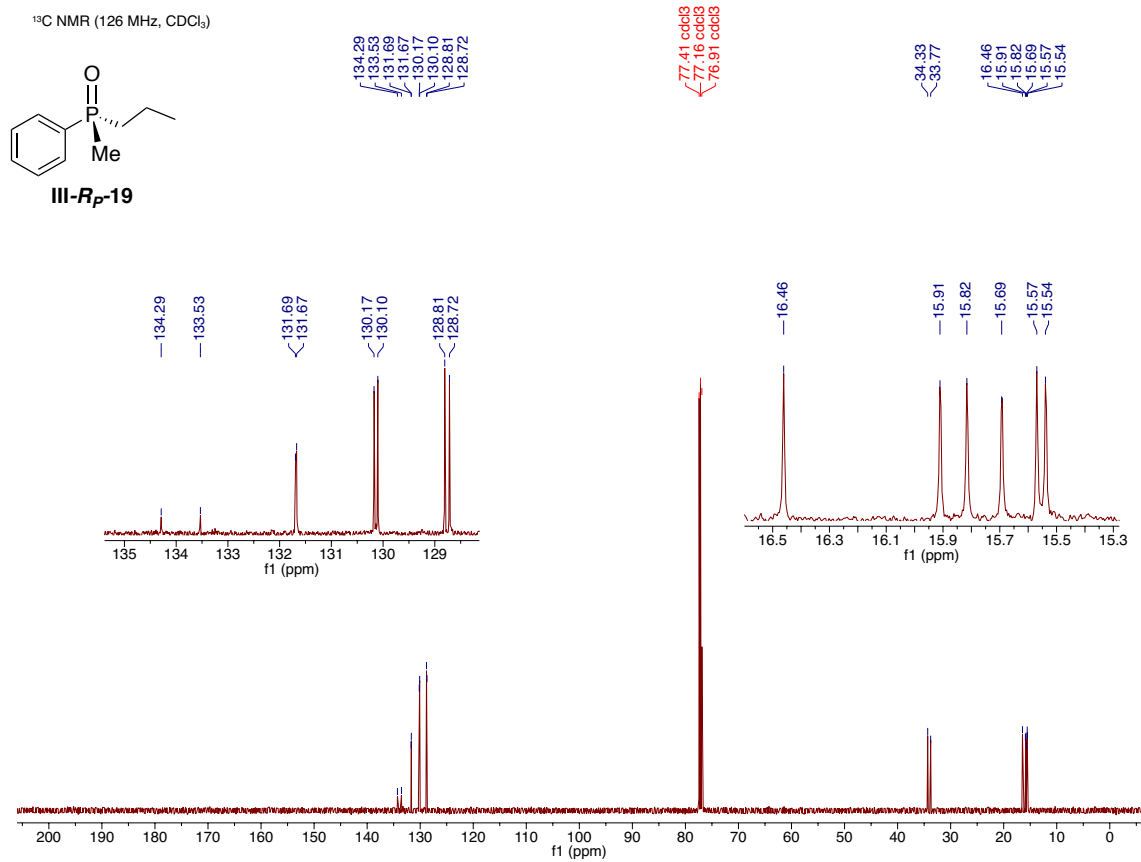


—39.11



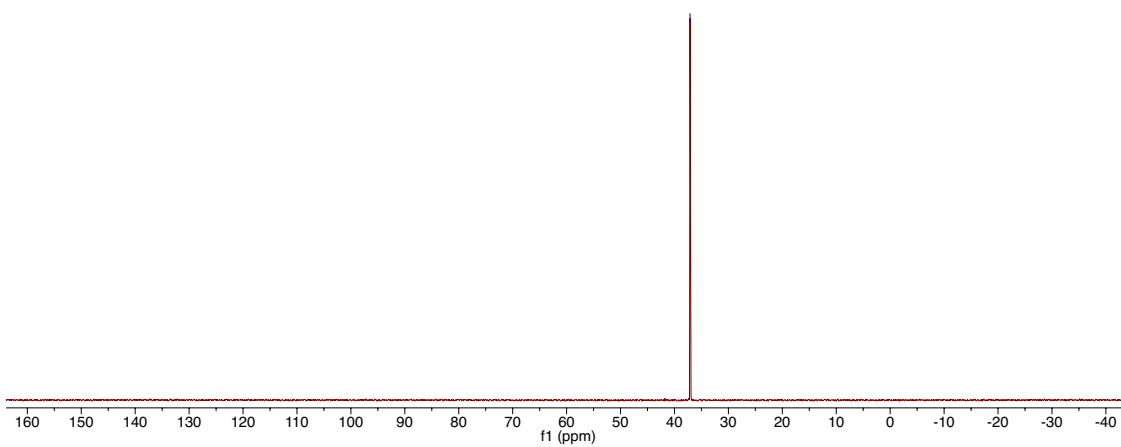
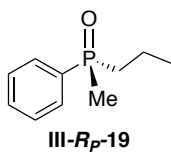
<sup>1</sup>H NMR (500 MHz, CDCl<sub>3</sub>)



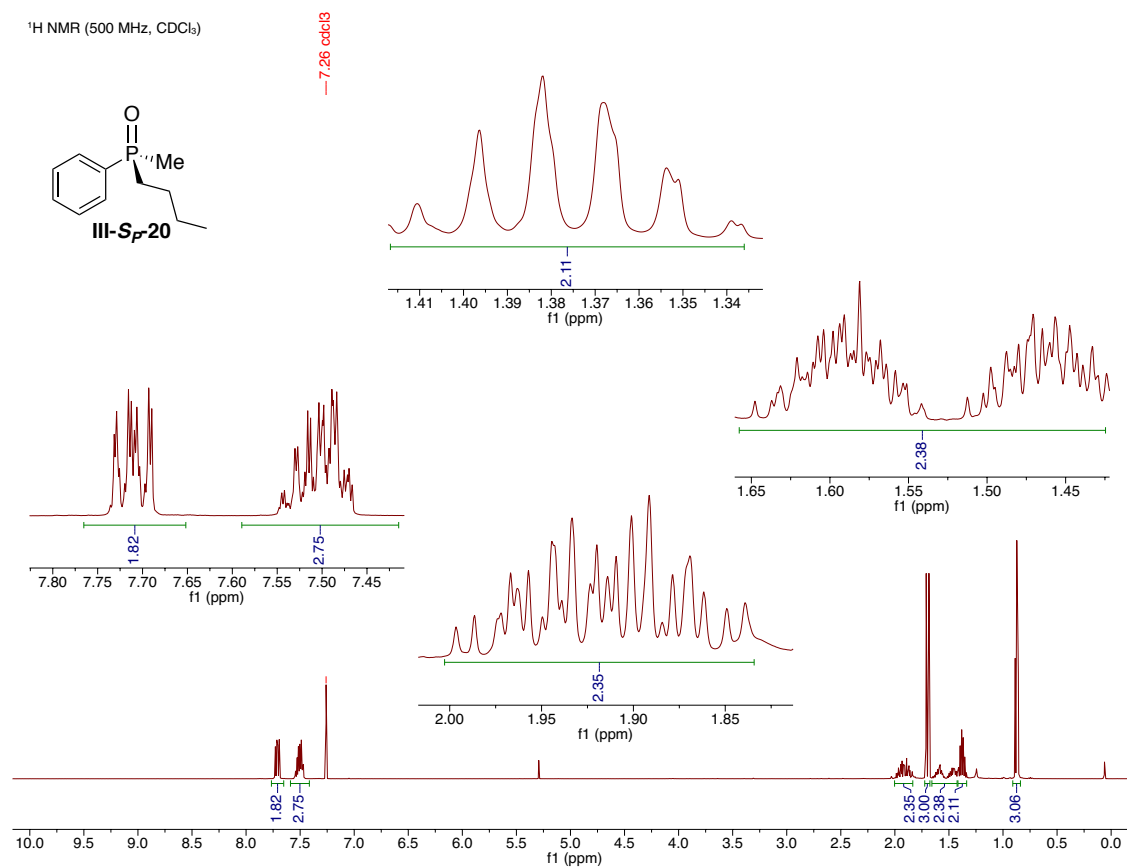
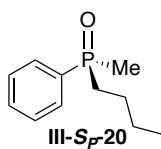


$^{31}\text{P}$  NMR (202 MHz,  $\text{CDCl}_3$ )

— 37.11

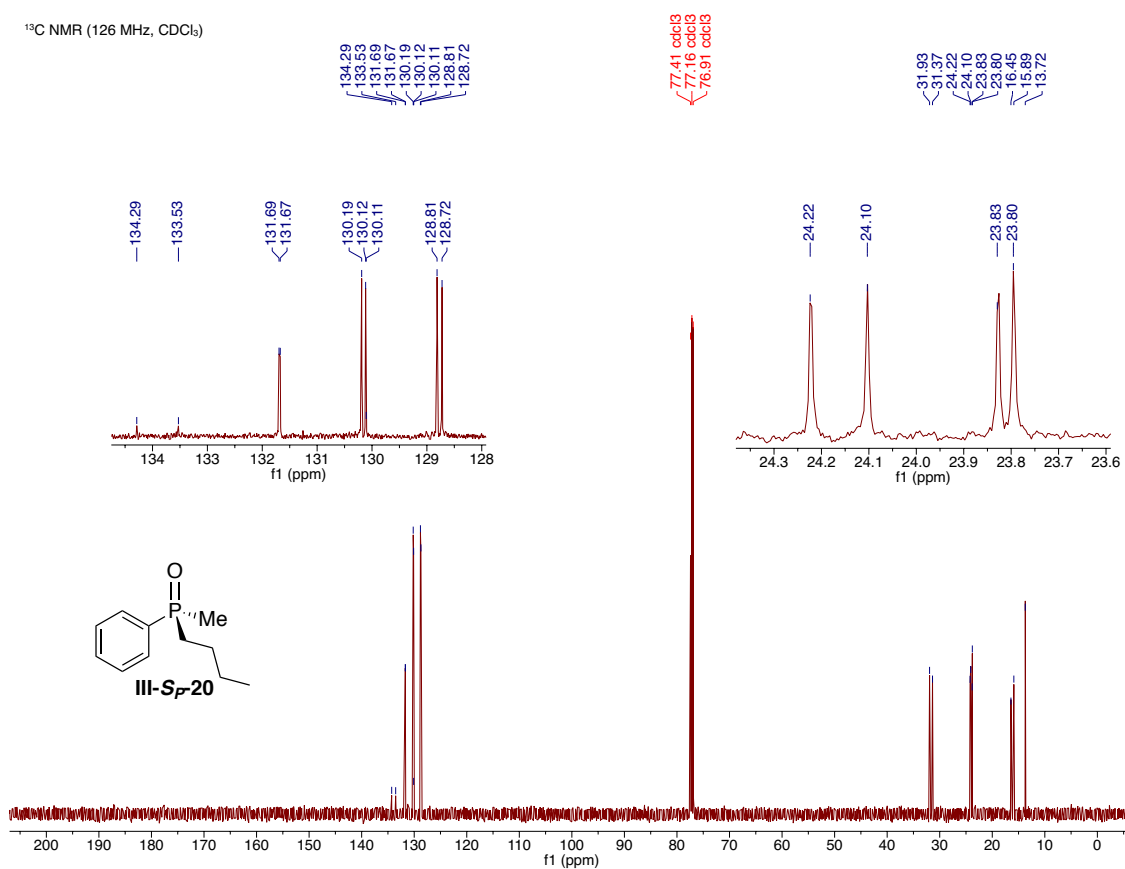


<sup>1</sup>H NMR (500 MHz, CDCl<sub>3</sub>)



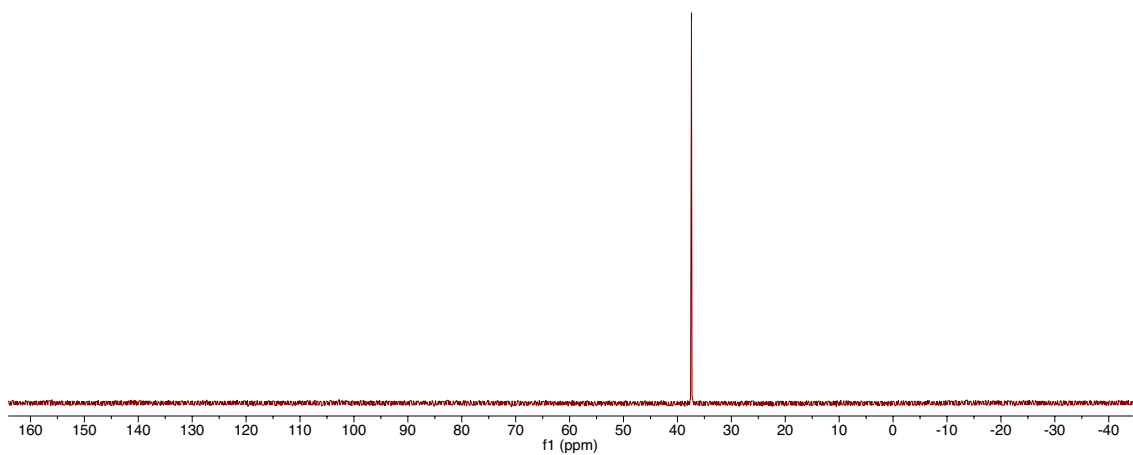
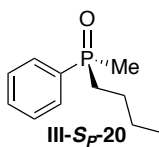


<sup>13</sup>C NMR (126 MHz, CDCl<sub>3</sub>)



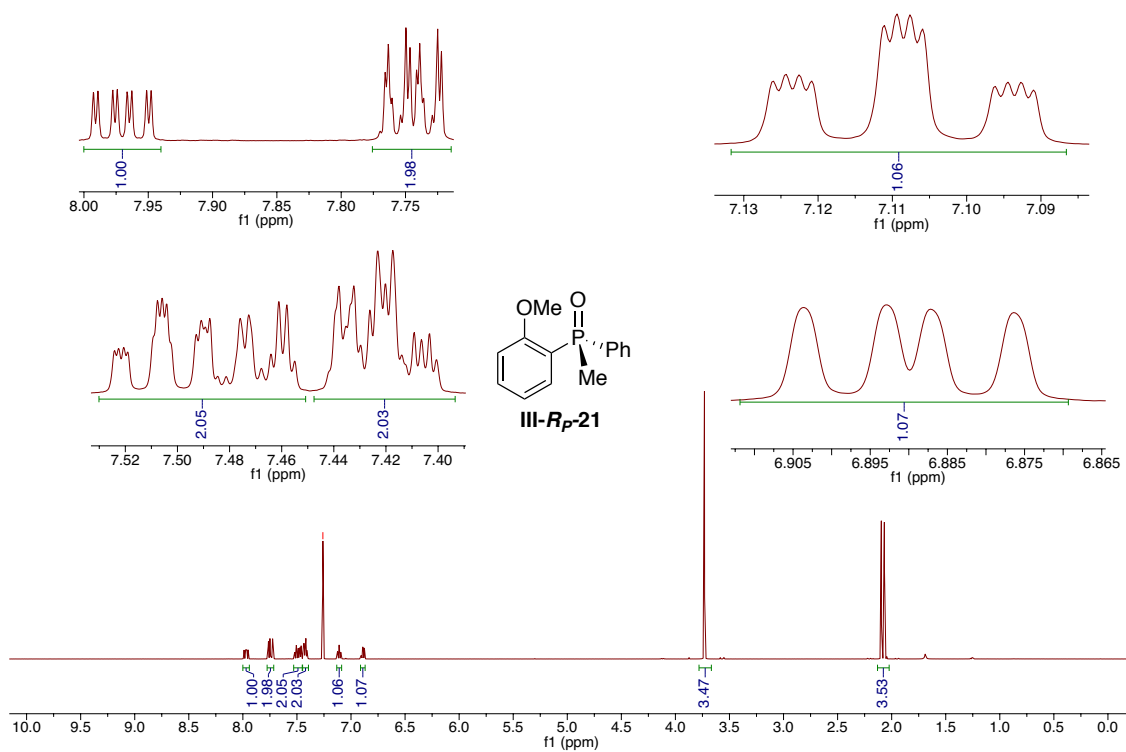
$^{31}\text{P}$  NMR (202 MHz,  $\text{CDCl}_3$ )

— 37.39

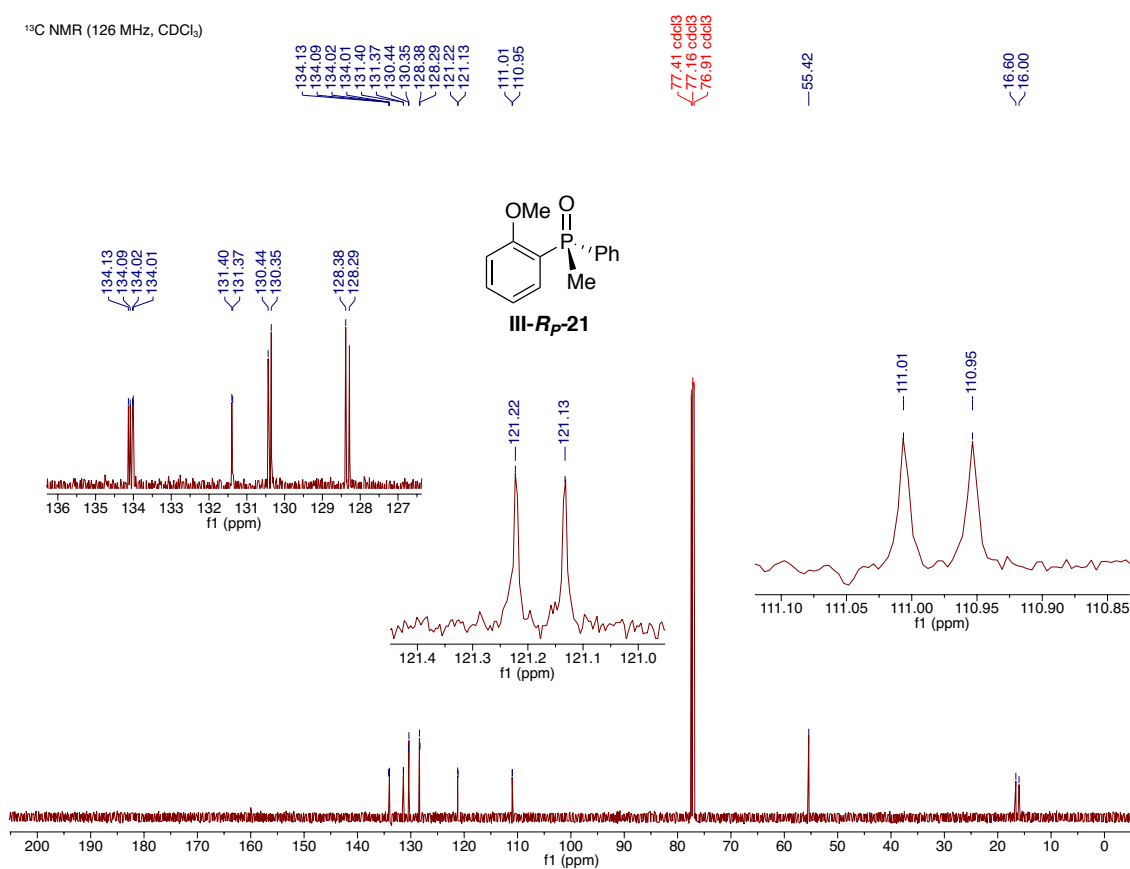


<sup>1</sup>H NMR (500 MHz, CDCl<sub>3</sub>)

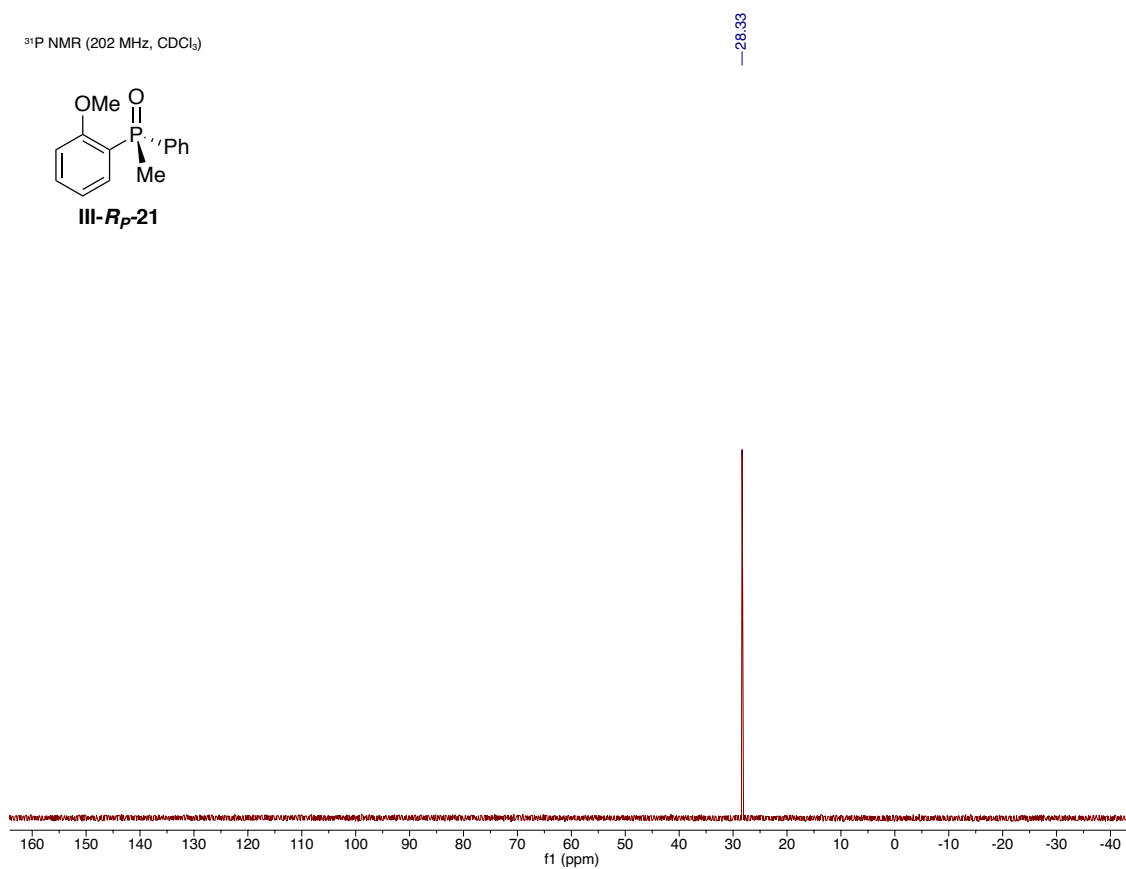
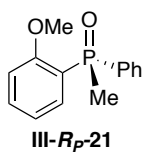
— 7.26 odd3



<sup>13</sup>C NMR (126 MHz, CDCl<sub>3</sub>)

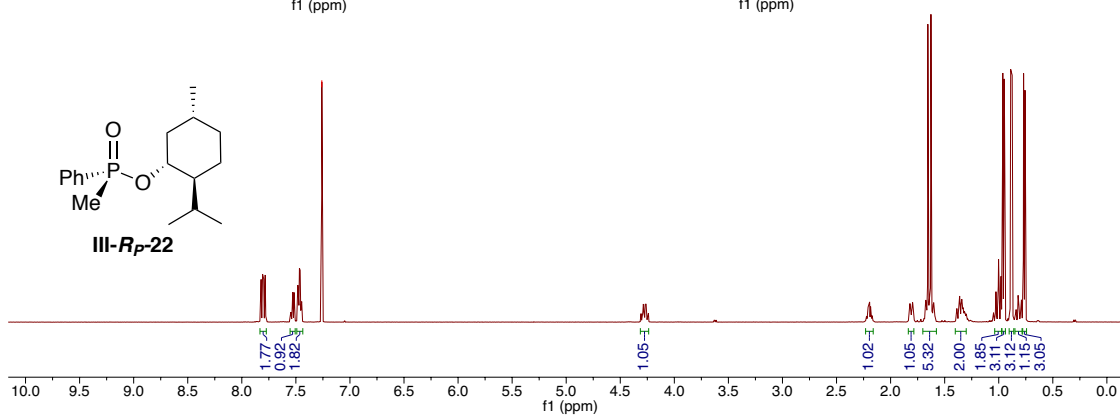
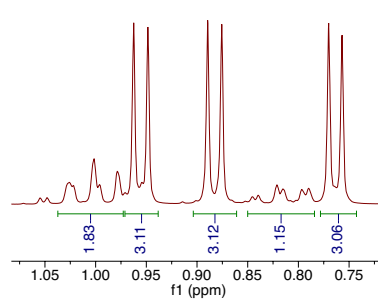
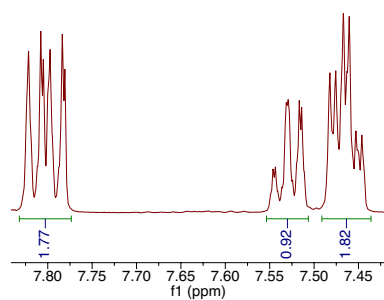


$^{31}\text{P}$  NMR (202 MHz,  $\text{CDCl}_3$ )

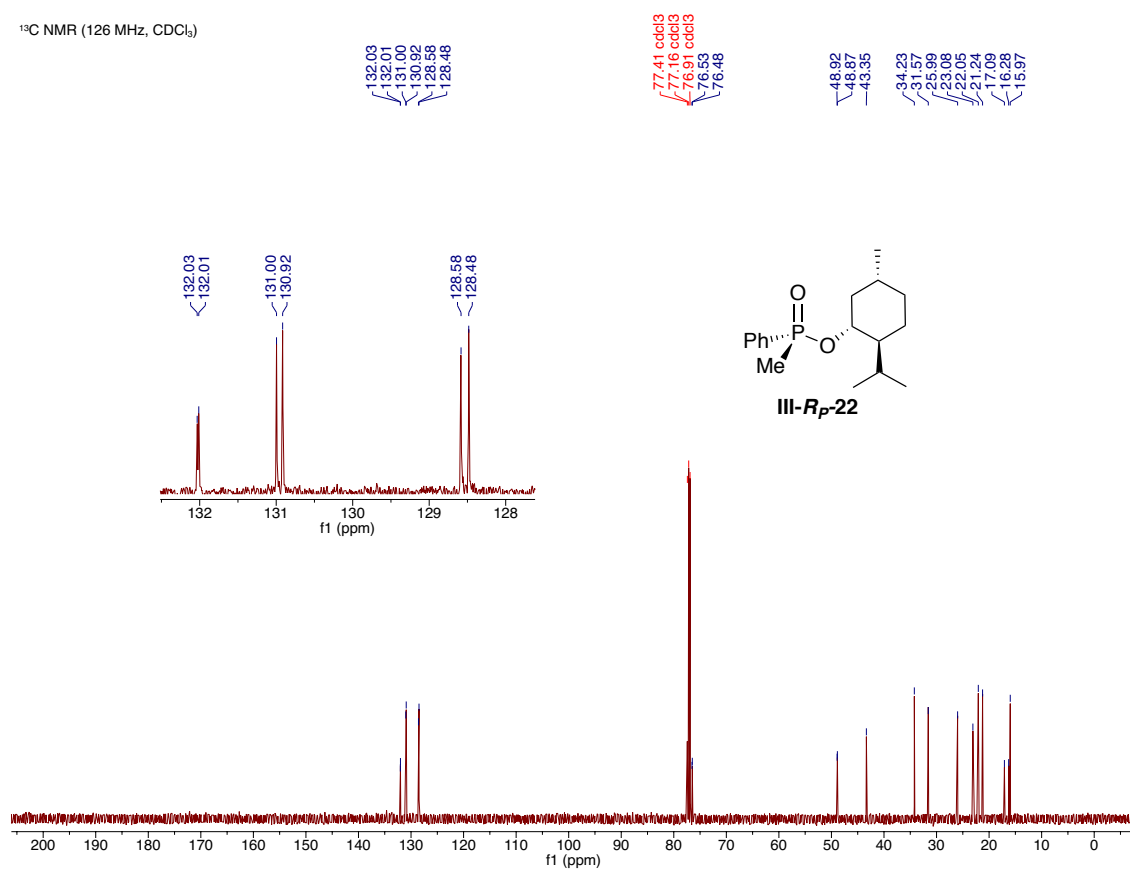


<sup>1</sup>H NMR (500 MHz, CDCl<sub>3</sub>)

—7.26 cdcl<sub>3</sub>

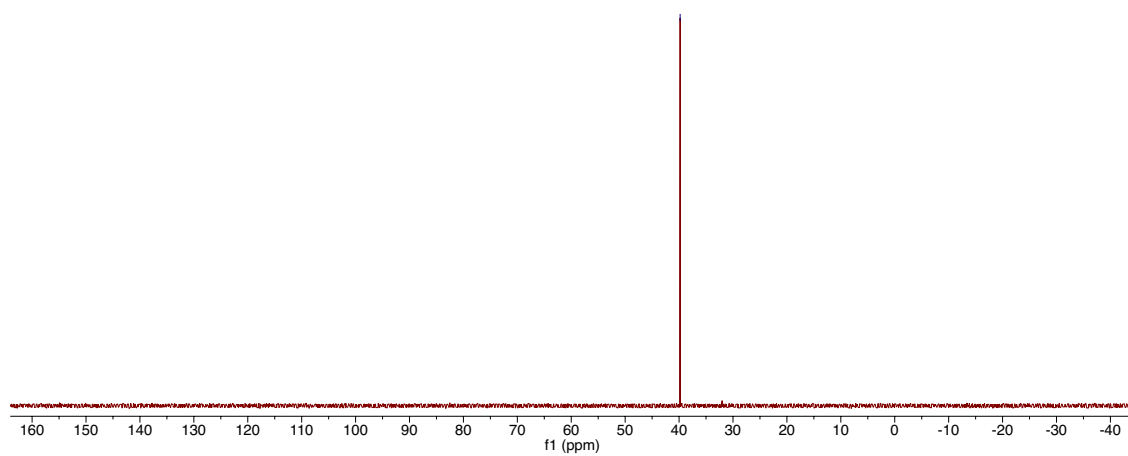
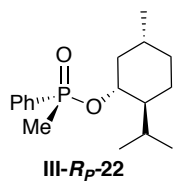


$^{13}\text{C}$  NMR (126 MHz,  $\text{CDCl}_3$ )



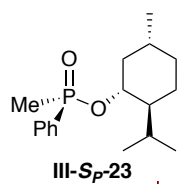
$^{31}\text{P}$  NMR (202 MHz,  $\text{CDCl}_3$ )

—39.81

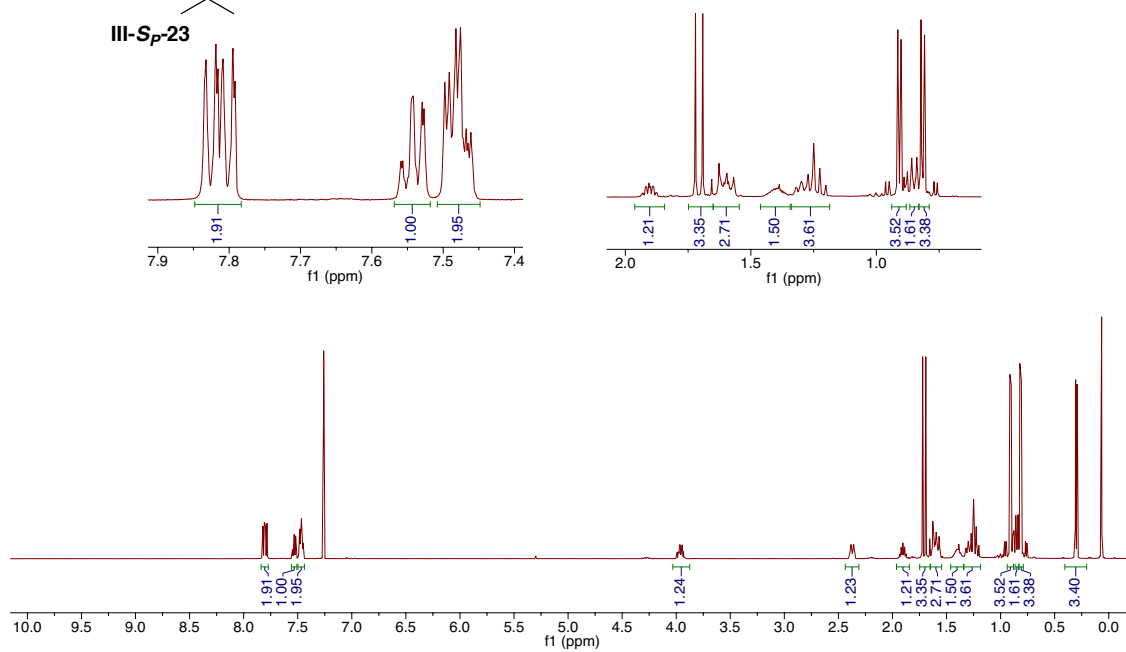




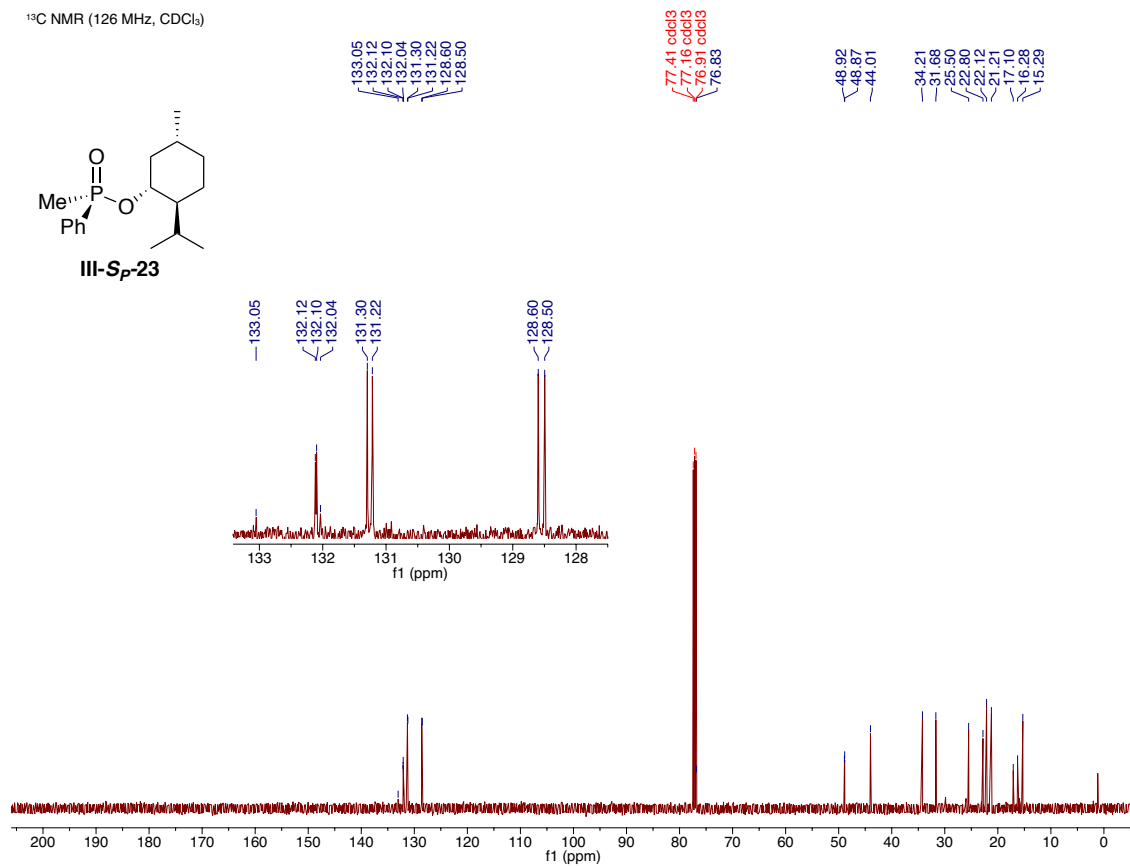
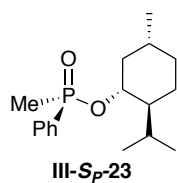
<sup>1</sup>H NMR (500 MHz, CDCl<sub>3</sub>)



—7.26 cdd3

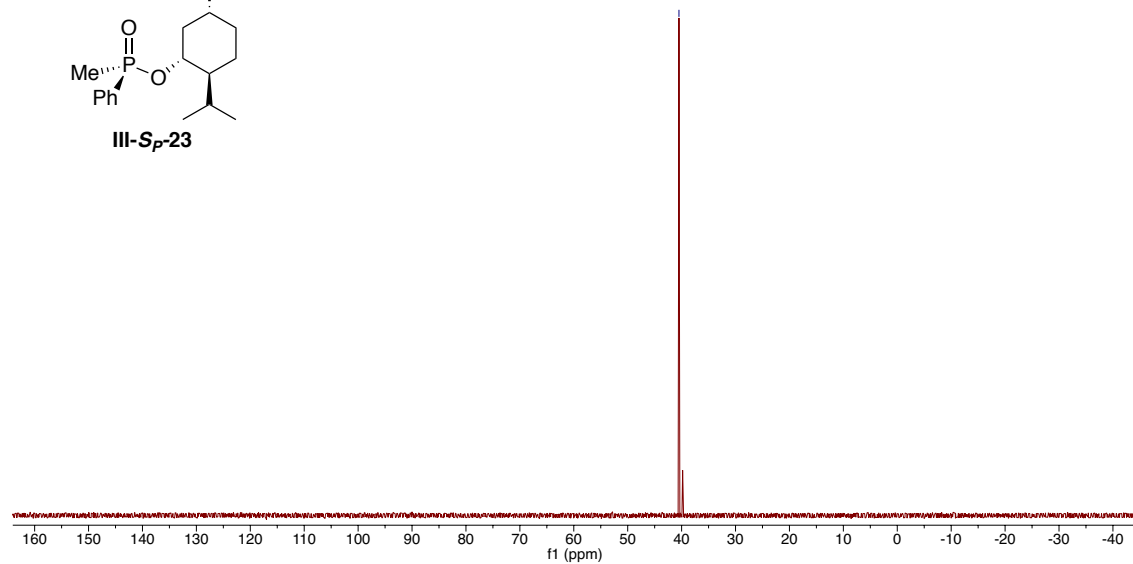
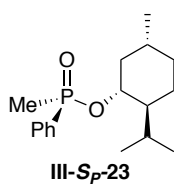


<sup>13</sup>C NMR (126 MHz, CDCl<sub>3</sub>)

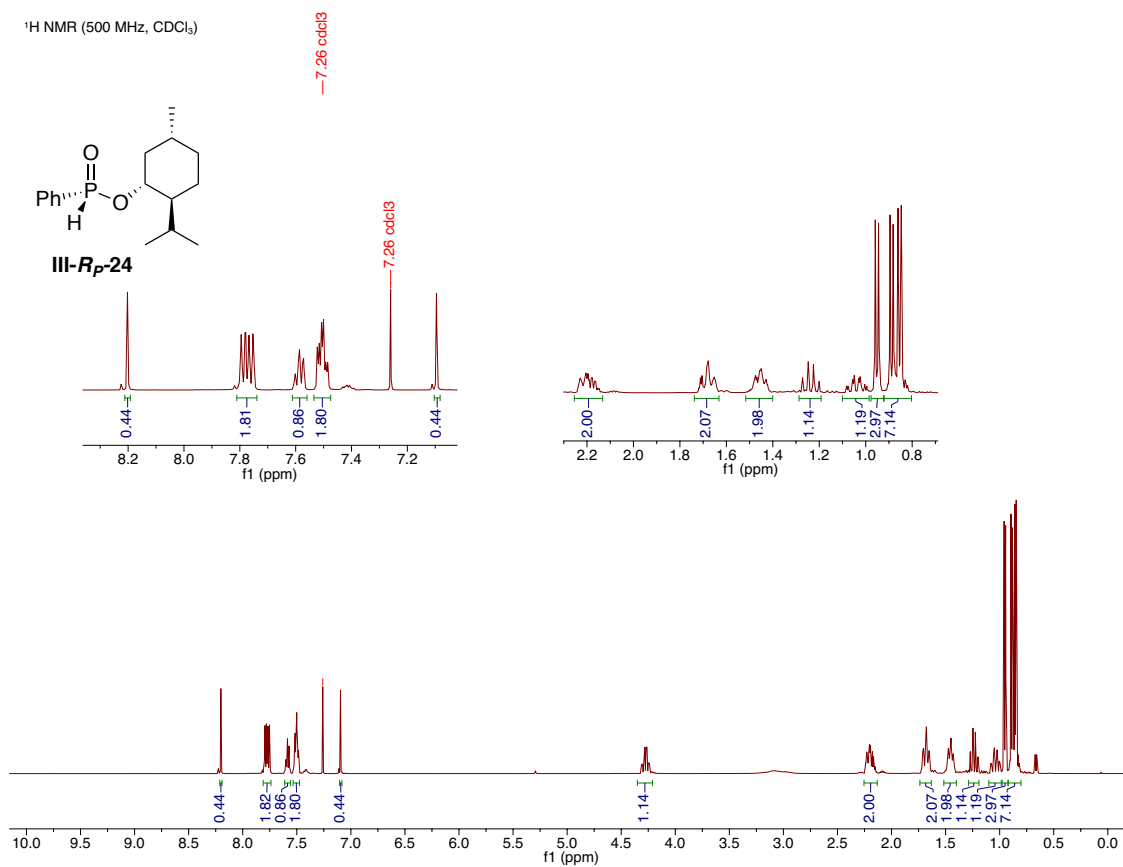


<sup>31</sup>P NMR (202 MHz, CDCl<sub>3</sub>)

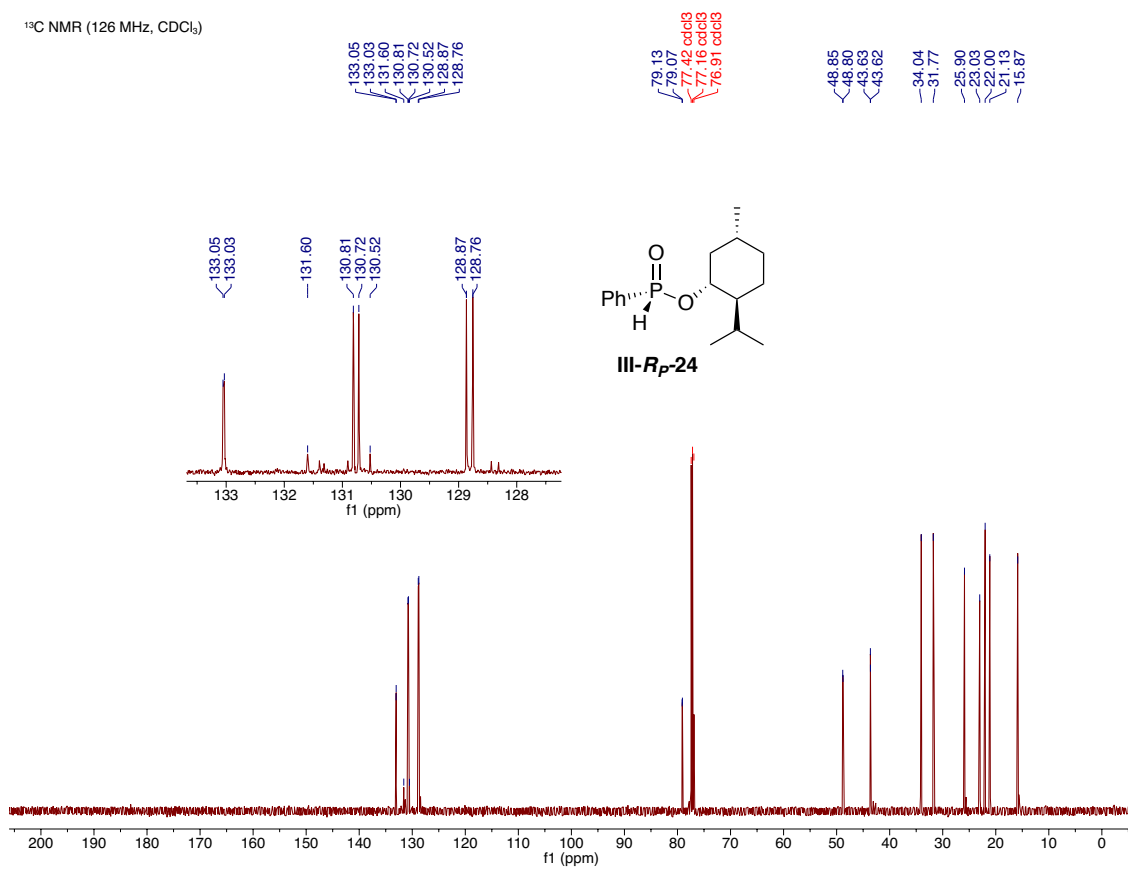
40.49



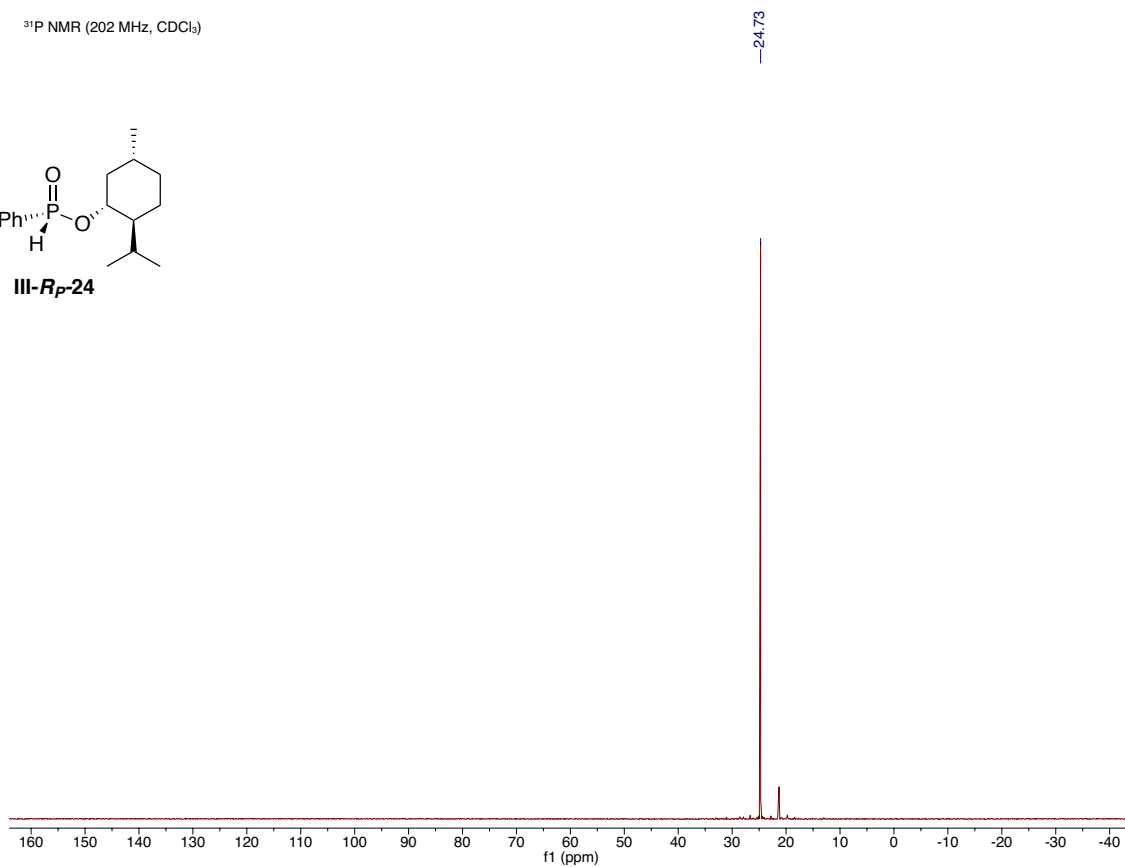
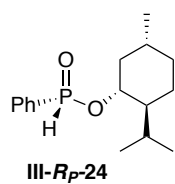
<sup>1</sup>H NMR (500 MHz, CDCl<sub>3</sub>)



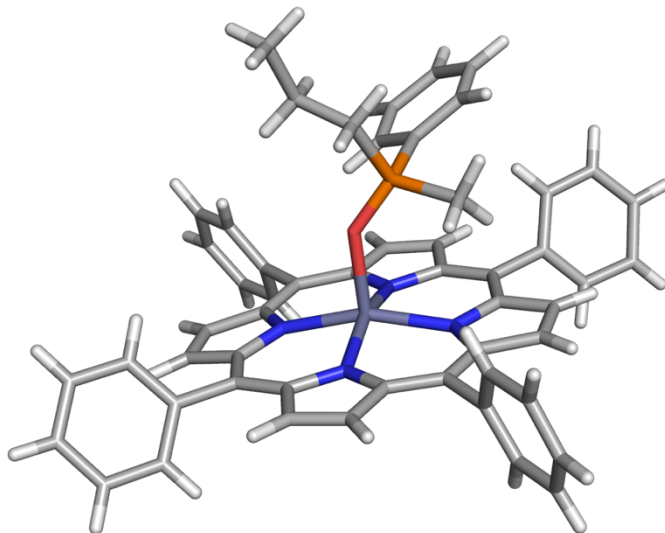
<sup>13</sup>C NMR (126 MHz, CDCl<sub>3</sub>)



$^{31}\text{P}$  NMR (202 MHz,  $\text{CDCl}_3$ )



### III-6.9. Crystal structure of III-*R<sub>P</sub>*-19 bound to Zn-TPP



**Experimental.** Single purple needle-shaped crystals of were used as received. A suitable crystal (0.43×0.07×0.03) mm<sup>3</sup> was selected and mounted on a nylon loop with paratone oil on a Bruker APEX-II CCD diffractometer. The crystal was kept at  $T = 173(2)$  K during data collection. Using **Olex2** the structure was solved with the **olex2.solve** structure solution program, using the Charge Flipping solution method. The model was refined with version of **XL** using Least Squares minimization.

**Crystal Data.** C<sub>55.17</sub>H<sub>44.33</sub>N<sub>4</sub>OPZn,  $M_r = 875.62$ , hexagonal, P6<sub>1</sub> (No. 169),  $a = 28.1290(8)$  Å,  $b = 28.1290(8)$  Å,  $c = 10.2773(4)$  Å,  $\alpha = 90^\circ$ ,  $\beta = 90^\circ$ ,  $\gamma = 120^\circ$ ,  $V = 7042.4(5)$  Å<sup>3</sup>,  $T = 173(2)$  K,  $Z = 6$ ,  $Z' = 1$ ,  $\mu(\text{CuK}\alpha) = 1.376$ , 21473 reflections measured, 8298 unique ( $R_{\text{int}} = 0.2745$ ) which were used in all calculations. The final  $wR_2$  was 0.2611(all data) and  $R_1$  was 0.0880 ( $I > 2(I)$ ).

Formula	C <sub>55.17</sub> H <sub>44.33</sub> N <sub>4</sub> OPZn
$D_{calc.}/\text{g cm}^{-3}$	1.239
$\mu/\text{mm}^{-1}$	1.376
Formula Weight	875.62
Colour	purple
Shape	needle
Size/mm <sup>3</sup>	0.43×0.07×0.03
$T/\text{K}$	173(2)
Crystal System	hexagonal
Flack Parameter	0.07(4)
Hooft Parameter	0.05(4)
Space Group	P6 <sub>1</sub>
$a/\text{\AA}$	28.1290(8)
$b/\text{\AA}$	28.1290(8)
$c/\text{\AA}$	10.2773(4)
$\alpha/^\circ$	90
$\beta/^\circ$	90
$\gamma/^\circ$	120
$V/\text{\AA}^3$	7042.4(5)
$Z$	6
$Z'$	1
Wavelength/ $\text{\AA}$	1.541838



Radiation type	CuK $_{\alpha}$
$\theta_{min}^{\circ}$	1.813
$\theta_{max}^{\circ}$	68.215
Measured Refl.	21473
Independent Refl.	8298
Reflections Used	3791
$R_{int}$	0.2745
Parameters	556
Restraints	8
Largest Peak	0.831
Deepest Hole	-0.468
GooF	0.957
$wR_2$ (all data)	0.2611
$wR_2$	0.2059
$R_1$ (all data)	0.1980
$R_1$	0.0880

A purple needle-shaped crystal with dimensions  $0.43 \times 0.07 \times 0.03 \text{ mm}^3$  was mounted on a nylon loop with paratone oil. Data were collected using a Bruker APEX-II CCD diffractometer equipped with an Oxford Cryosystems low-temperature device, operating at  $T = 173(2) \text{ K}$ .

Data were measured using  $\omega$  of  $1.00^\circ$  per frame for 495.00 s using  $\text{CuK}\alpha$  radiation (sealed tube, 40 kV, 30 mA). The total number of runs and images was based on the strategy calculation from the program **COSMO** (BRUKER, V1.61, 2009). The achieved resolution was  $\theta = 68.215$ .

Cell parameters were retrieved using the **SAINT** (Bruker, V8.34A, after 2013) software and refined using **SAINT** (Bruker, V8.34A, after 2013) on 1949 reflections, 9% of the observed reflections. Data reduction was performed using the **SAINT** (Bruker, V8.34A, after 2013) software which corrects for Lorentz polarization. The final completeness is 99.20 out to  $68.215$  in  $\theta$ . A multi-scan absorption correction was performed using SADABS-2012/1 (Bruker, 2012) was used for absorption correction.  $wR_2(\text{int})$  was 0.0778 before and 0.0604 after correction. The Ratio of minimum to maximum transmission is 0.7866. The  $\lambda/2$  correction factor is 0.0015. The absorption coefficient  $\mu$  of this material is  $1.376 \text{ mm}^{-1}$  at this wavelength ( $\lambda = 1.54178 \text{ \AA}$ ) and the minimum and maximum transmissions are 0.5924 and 0.7531. SADABS-2012/1 (Bruker, 2012) was used for absorption correction.  $wR_2(\text{int})$  was 0.0778 before and 0.0604 after correction. The Ratio of minimum to maximum transmission is 0.7866. The  $\lambda/2$  correction factor is 0.0015.

The structure was solved in the space group  $P6_1$  by Charge Flipping using the

**olex2.solve** structure solution program. The structure was refined by Least Squares using version 2014/6 of **XL** incorporated in **Olex2**. All non-hydrogen atoms were refined anisotropically. Hydrogen atom positions were calculated geometrically and refined using the riding model.

There is a single molecule in the asymmetric unit, which is represented by the reported sum formula. In other words: Z is 6 and Z' is 1.

The Flack parameter was refined to 0.07(4). Determination of absolute structure using Bayesian statistics on Bijvoet differences using the Olex2 results in 0.05(4). Note: The Flack parameter is used to determine chirality of the crystal studied, the value should be near 0, a value of 1 means that the stereochemistry is wrong, and the model should be inverted. A value of 0.5 means that the crystal consists of a racemic mixture of the two enantiomers.

## REFERENCES

1. Dutartre, M.; Bayardon, J.; Juge, S., *Chem. Soc. Rev.* **2016**, *45*, 5771-5794.
2. Grabulosa, A.; Granell, J.; Muller, G., *Coord. Chem. Rev.* **2007**, *251*, 25-90.
3. Warner, C. J. A.; Reeder, A. T.; Jones, S., *Tetrahedron: Asymmetry* **2016**, *27*, 136-141.
4. Loup, J.; Muller, V.; Ghorai, D.; Ackermann, L., *Angew. Chem. Int. Ed.* **2019**, *58*, 1749-1753.
5. Adams, H.; Collins, R. C.; Jones, S.; Warner, C. J. A., *Org. Lett.* **2011**, *13*, 6576-6579.
6. Beaud, R.; Phipps, R. J.; Gaunt, M. J., *J. Am. Chem. Soc.* **2016**, *138*, 13183-13186.
7. Bergin, E.; O'Connor, C. T.; Robinson, S. B.; McGarrigle, E. M.; O'Mahony, C. P.; Gilheany, D. G., *J. Am. Chem. Soc.* **2007**, *129*, 9566-9567.
8. Han, Z. X. S.; Goyal, N.; Herbage, M. A.; Sieber, J. D.; Qu, B.; Xu, Y. B.; Li, Z. B.; Reeves, J. T.; Desrosiers, J. N.; Ma, S. L.; Grinberg, N.; Lee, H.; Mangunuru, H. P. R.; Zhang, Y. D.; Krishnamurthy, D.; Lu, B. Z.; Song, J. H. J.; Wang, G. J.; Senanayake, C. H., *J. Am. Chem. Soc.* **2013**, *135*, 2474-2477.
9. Huang, Z. J.; Huang, X.; Li, B. S.; Mou, C. L.; Yang, S.; Song, B. A.; Chi, Y. R., *J. Am. Chem. Soc.* **2016**, *138*, 7524-7527.
10. Jang, Y. S.; Wozniak, L.; Pedroni, J.; Cramer, N., *Angew. Chem. Int. Ed.* **2018**, *57*, 12901-12905.
11. Dai, Q.; Li, W. B.; Lo, Z. M.; Zhang, J. L., *J. Am. Chem. Soc.* **2019**, *141*, 20556-20564.
12. Trost, B. M.; Spohr, S. M.; Rolka, A. B.; Kalnmals, C. A., *J. Am. Chem. Soc.* **2019**, *141*, 14098-14103.
13. Xu, D.; Rivas-Bascon, N.; N, M. P.; Knouse, K. W.; Zheng, B.; Vantourout, J. C.; Schmidt, M. A.; Eastgate, M. D.; Baran, P. S., *J. Am. Chem. Soc.* **2020**, *142*, 5785-5792.
14. Knouse, K. W.; deGruyter, J. N.; Schmidt, M. A.; Zheng, B.; Vantourout, J. C.; Kingston, C.; Mercer, S. E.; McDonald, I. M.; Olson, R. E.; Zhu, Y.; Hang, C.; Zhu,

- J.; Yuan, C.; Wang, Q.; Park, P.; Eastgate, M. D.; Baran, P. S., *Science* **2018**, *361*, 1234-1238.
15. DiRocco, D. A.; Ji, Y. N.; Sherer, E. C.; Klapars, A.; Reibarkh, M.; Dropinski, J.; Mathew, R.; Maligres, P.; Hyde, A. M.; Limanto, J.; Brunskill, A.; Ruck, R. T.; Campeau, L. C.; Davies, I. W., *Science* **2017**, *356*, 426-429.
  16. Jiang, Q. Z.; Ruegger, H.; Venanzi, L. M., *J. Organomet. Chem.* **1995**, *488*, 233-240.
  17. Karle, I. L.; Karle, J. M.; Egan, W.; Zon, G.; Brandt, J. A., *J. Am. Chem. Soc.* **1977**, *99*, 4803-4807.
  18. Korpium, O.; Mislow, K., *J. Am. Chem. Soc.* **1967**, *89*, 4784-4786.
  19. Korpiun, O.; Lewis, R. A.; Chickos, J.; Mislow, K., *J. Am. Chem. Soc.* **1968**, *90*, 4842-4846.
  20. Lewis, R. A.; Korpiun, O.; Mislow, K., *J. Am. Chem. Soc.* **1968**, *90*, 4847-4853.
  21. Lewis, R. A.; Mislow, K., *J. Am. Chem. Soc.* **1969**, *91*, 7009-7012.
  22. Dunina, V. V.; Kuz'mina, L. G.; Rubina, M. Y.; Grishin, Y. K.; Veits, Y. A.; Kazakova, E. I., *Tetrahedron: Asymmetry* **1999**, *10*, 1483-1497.
  23. Wang, F.; Wang, Y.; Polavarapu, P. L.; Li, T. Y.; Drabowicz, J.; Pietrusiewicz, K. M.; Zygo, K., *J. Org. Chem.* **2002**, *67*, 6539-6541.
  24. Petrovic, A. G.; Polavarapu, P. L.; Lopusinski, A.; Krasowska, D.; Wieczorek, W.; Szyrej, M.; Blaszczyk, J.; Drabowicz, J., *J. Org. Chem.* **2020**, *85*, 14456-14466.
  25. Anyika, M.; Gholami, H.; Ashtekar, K. D.; Acho, R.; Borhan, B., *J. Am. Chem. Soc.* **2014**, *136*, 550-553.
  26. Gholami, H.; Anyika, M.; Zhang, J.; Vasileiou, C.; Borhan, B., *Chem. Eur. J.* **2016**, *22*, 9235-9239.
  27. Gholami, H.; Zhang, J.; Anyika, M.; Borhan, B., *Org. Lett.* **2017**, *19*, 1722-1725.
  28. Fang, Y.; Jiang, X.; Kadish, K. M.; Nefedov, S. E.; Kirakosyan, G. A.; Enakieva, Y. Y.; Gorbunova, Y. G.; Tsivadze, A. Y.; Stern, C.; Bessmertnykh-Lemeune, A.; Guillard, R., *Inorg. Chem.* **2019**, *58*, 4665-4678.
  29. Officer, D. L.; Lodato, F.; Jolley, K. W., *Inorg. Chem.* **2007**, *46*, 4781-4783.

30. Matano, Y.; Matsumoto, K.; Terasaka, Y.; Hotta, H.; Araki, Y.; Ito, O.; Shiro, M.; Sasamori, T.; Tokitoh, N.; Imahori, H., *Chem. Eur. J.* **2007**, *13*, 891-901.
31. Maza, W. A.; Vetromile, C. M.; Kim, C.; Xu, X.; Zhang, X. P.; Larsen, R. W., *J. Phys. Chem. A* **2013**, *117*, 11308-11315.
32. Fernandez, I.; Khair, N.; Roca, A.; Benabra, A.; Alcudia, A.; Espartero, J. L.; Alcudia, F., *Tetrahedron. Lett.* **1999**, *40*, 2029-2032.
33. Xu, Q.; Zhao, C. Q.; Han, L. B., *J. Am. Chem. Soc.* **2008**, *130*, 12648-12655.
34. Li, X.; Tanasova, M.; Vasileiou, C.; Borhan, B., *J. Am. Chem. Soc.* **2008**, *130*, 1885-1893.
35. Vineyard, B. D.; Knowles, W. S.; Sabacky, M. J.; Bachman, G. L.; Weinkauff, D. J., *J. Am. Chem. Soc.* **1977**, *99*, 5946-5952.
36. Chan, A. S. C.; Pluth, J. J.; Halpern, J., *J. Am. Chem. Soc.* **1980**, *102*, 5952-5954.
37. Yamaguchi, M.; Shima, T.; Yamagishi, T.; Hida, M., *Tetrahedron: Asymmetry* **1991**, *2*, 663-666.
38. Shoji, Y.; Tashiro, K.; Aida, T., *J. Am. Chem. Soc.* **2006**, *128*, 10690-10691.

## CHAPTER IV: POINT-TO-AXIAL-TO-POINT CHIRALITY TRANSFER: DESIGN AND DEVELOPMENT OF A PROGRAMMABLE ORGANOCATALYST

## IV-1 Introduction

Over the past few years interest in the design and synthesis of supramolecular catalysts that can mimic the catalytic efficacy of enzymes has intensified. In particular, the area of artificial switchable metal catalyst and organocatalyst have witnessed tremendous progress in the past decade.<sup>1-5</sup> The most exciting part of this area of research is the control over catalyst's reactivity. The catalyst can be triggered 'ON' or 'OFF' simply by an external stimulus that ranges from light, heat, acidity of the medium, solvent, coordination of a ligand, redox to mechanical force. Within this realm of switchable catalysis, only a few offer the possibility of dynamic control in the stereochemistry of the chiral catalyst itself.<sup>6-8</sup> The chiral switchable catalyst kinetically favors the formation of a particular enantiomer of the product, whereas in its enantiomeric state, opposite enantiomer of the product is favored. Asymmetric organic synthesis has evolved over the years from employing stoichiometric chiral auxiliaries to the use of chiral catalyst. A common thread for either strategy has been the utilization of enantiomeric mediators to access antipodal products. The switchable chiral catalyst offers a new paradigm in this area, as it would eliminate the necessity of the availability of both the enantiomers of the same catalyst. From a practical standpoint, this strategy would eliminate the unnecessary steps required to synthesize both the enantiomeric forms of the catalyst. From a design point of view, different external effectors that can control the stereochemistry of the catalyst in a predictable manner are discussed below.



## IV-2 Light, and heat driven chiral switchable catalyst

In 2011, Nobel laureate Feringa and co-workers designed a unidirectional molecular motor and employed that as a chiral switchable catalyst in the sulfa-Michael addition to  $\alpha,\beta$ -unsaturated ketone (Figure IV-1).<sup>9-10</sup> The bifunctional chiral catalyst contains a Bronsted acidic site to activate the ketone moiety, as well as a Bronsted basic

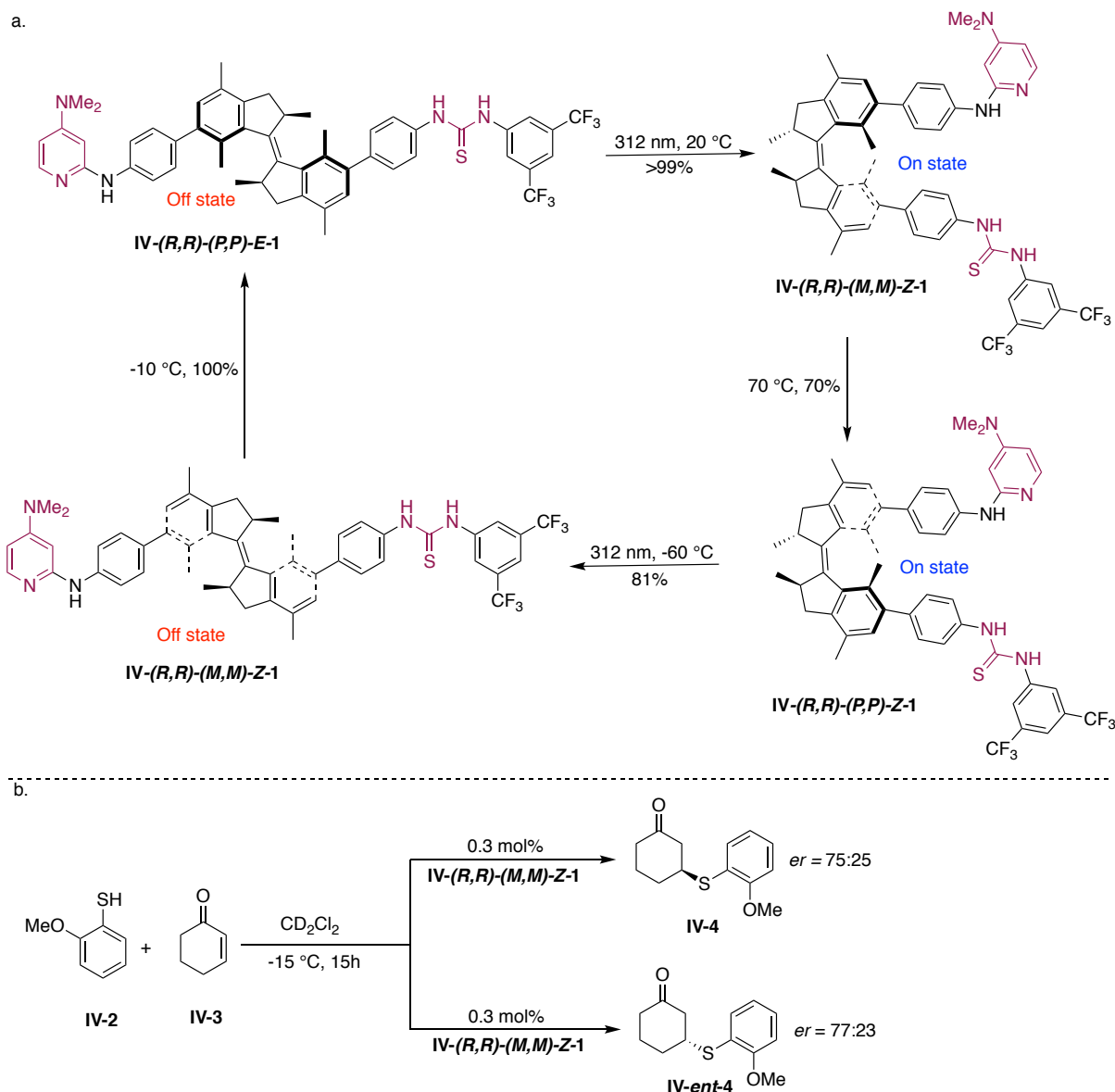


**Figure IV-1.** a. Design of a light driven unidirectional molecular motor. b. Example of a light driven switchable catalysis in a Michael addition reaction.

site to generate the nucleophilic sulfa anion. The catalyst in its **IV-(R,R)-(P,P)-E-1** form is inactive as its catalytic sites are far away from each other and therefore cannot activate both the electrophilic as well as nucleophilic components simultaneously. Irradiation of

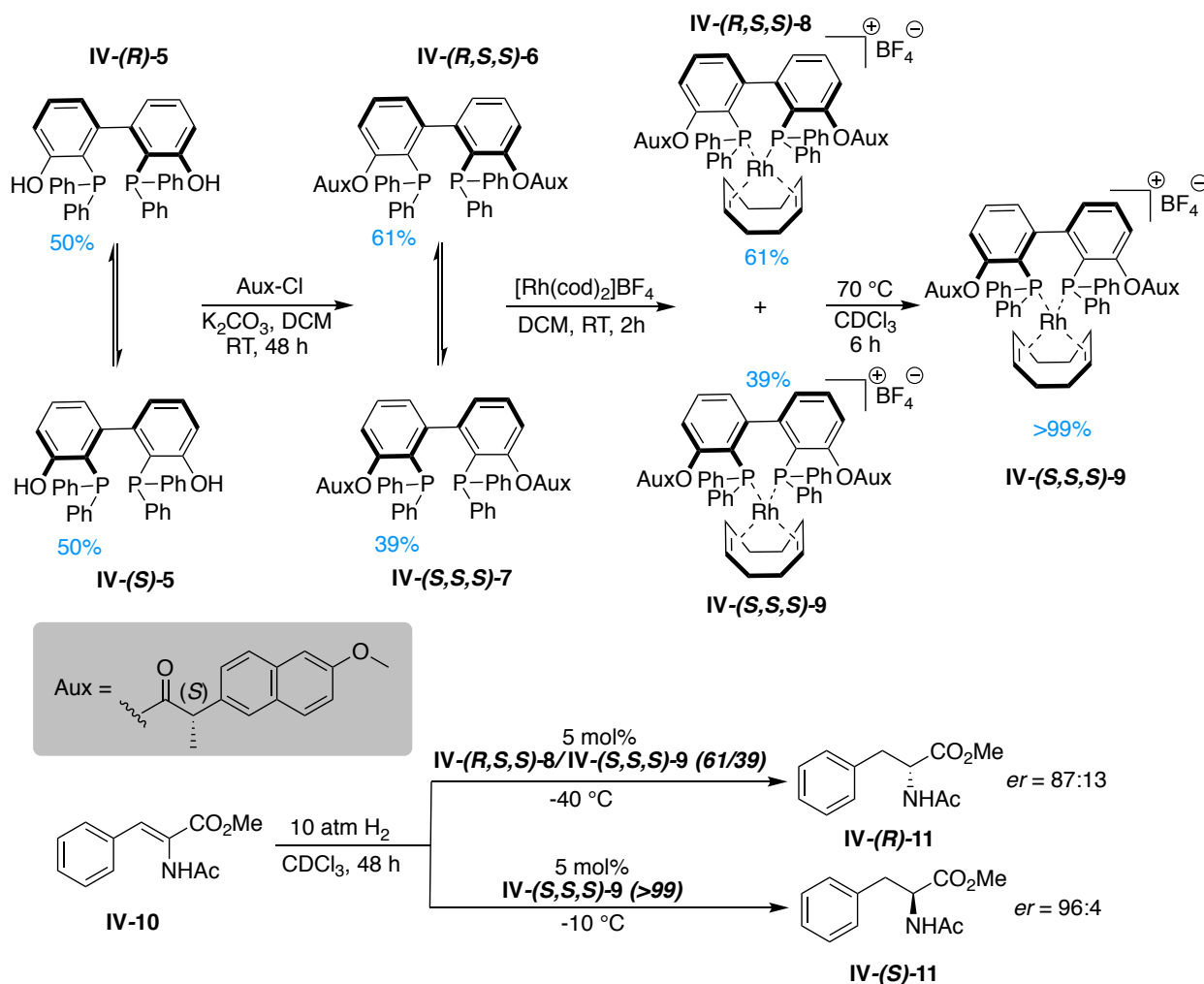


**Figure IV-2.** Design and application of a temperature driven chiral switchable catalyst.

**IV-(R,R)-(P,P)-E-1** with light (312 nm) at 20 °C led to *E-Z* photoisomerization and a helix inversion. The newly formed **IV-(R,R)-(M,M)-Z-1** state can perform bifunctionally as it brings both of the active sites in closer proximity. A thermal helix inversion of the latter leads to **IV-(R,R)-(P,P)-Z-1** (Figure IV-1a). A final photoirradiation, followed by thermal

inversion brings the molecular motor to its original state. When **IV-(*R,R*)-(M,M)-Z-1** was subjected to the reaction condition, **IV-4** was observed with 50% *ee*. On the other hand, **IV-(*R,R*)-(P,P)-Z-1** led to the formation of the enantiomer **IV-*ent*-4** with almost identical enantioselectivity (Figure IV-1b). Since their pioneering work, Feringa and coworkers have developed several other switchable molecular motors and employed them as programmable organocatalysts in many different asymmetric reactions.<sup>8</sup>

In 2015, Storch and Trapp developed a chiral switchable catalytic system where the temperature was employed as an external stimulus (Figure IV-2).<sup>11</sup> Functionalization of the racemic *tropos* BIPHEP ligand with a chiral auxiliary perturbed the equilibrium and favored the formation of one diastereomer over the other (61:39). The point chirality of the appended chiral auxiliary was translated to the chiral axis of the biphenyl core. Complexation of the equilibrium mixture with Rh(I) restricted the free rotation around the chiral axis. Intriguingly, when this mixture was heated at 70 °C for 6 h, the equilibrium shifted completely towards the minor diastereomer **IV-(*S,S,S*)-9** and did not change even after prolonged cooling. The catalytic properties of the mixture or the pure minor diastereomer was then tested in the asymmetric hydrogenation of a prochiral cinnamate **IV-10**. Interestingly, for the mixture a non-linear chiral amplification of the product enantioselectivity was observed.

### IV-3 Redox driven chiral switchable catalyst

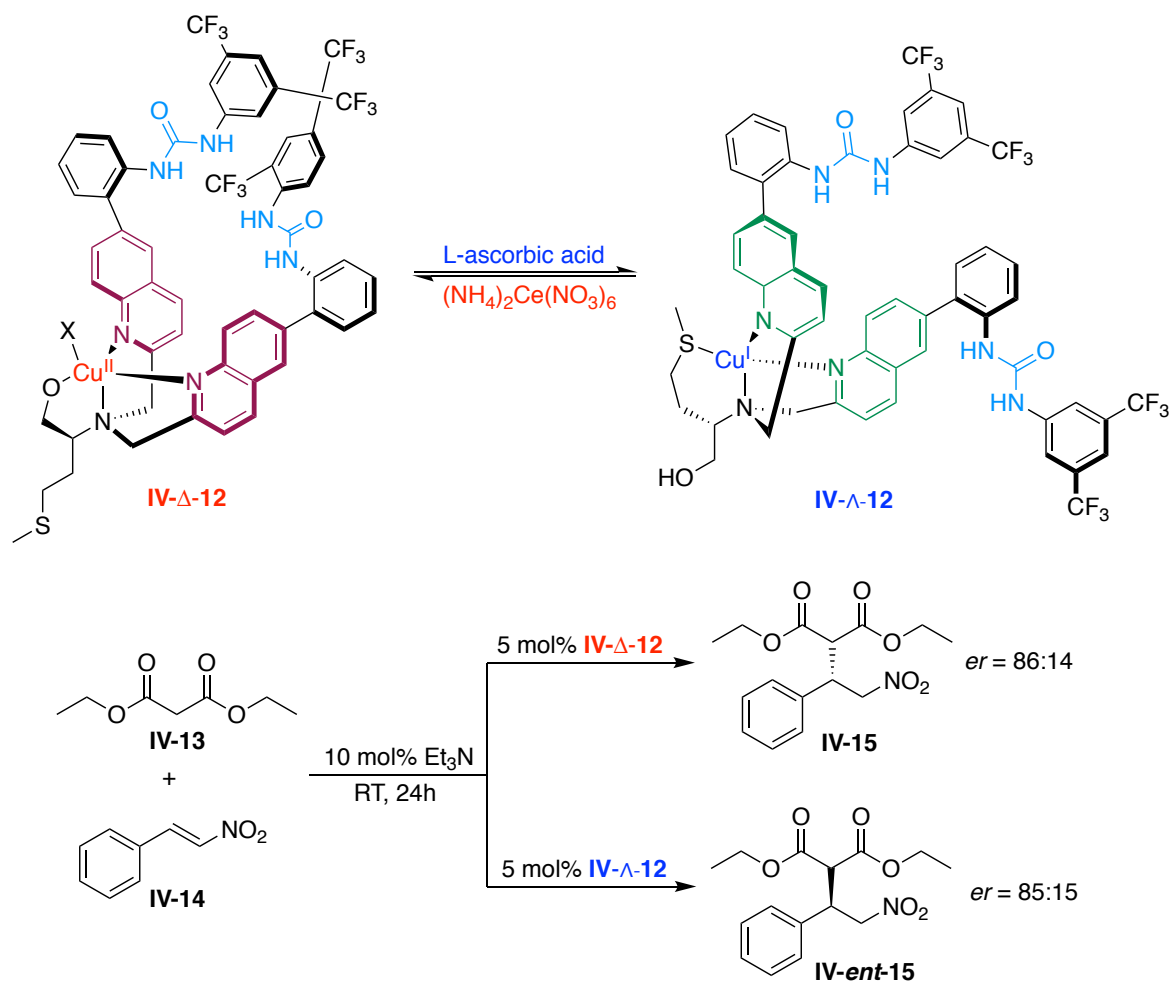


**Figure IV-3.** Design and application of a redox driven chiral switchable catalyst.

In 2012, Canary and coworkers reported a redox driven programmable chiral catalyst (Figure IV-3).<sup>12</sup> Inspired from their own work,<sup>13</sup> they designed a multidentate ligand attached with a bis-urea site that can potentially act as an organocatalyst. The hard carboxylate group of the methionine derived ligand coordinates to Cu (II). Such coordination resulted in a negative helicity of the quinolines. When the Cu (II) is reduced to Cu (I) by ascorbic acid, a reorganization around the metal center occurs. Now the soft Cu(I) metal center is coordinated via the soft sulfide atom. As a result, the chirality

between the quinolines is inverted and positive helicity is formed. This system could be reversed back to its original form simply by oxidizing the metal center via ceric ammonium nitrate. The enantiomeric forms of the catalyst were able to deliver the antipodal products in a nitro-Michael addition reaction with almost equal but opposite enantioselectivity.

#### IV-4 Solvent driven chiral switchable catalyst

Suginome and co-workers showed a solvent dependent helical inversion of polymeric ligands.<sup>14</sup> In particular, the polymer **IV-16** containing chiral ether side chains and diphenyl phosphino pendants exhibited switching of helicity from *P* to *M* as the solvent was switched from cyclooctane to *n*-octane (Figure IV-4). The Pd-catalyzed hydrosilylation of styrene with ligand **IV-(P)-16** afforded the product **IV-(S)-17** with 90% *ee* in cyclooctane. When the same reaction was carried out in *n*-octane with ligand **IV-**

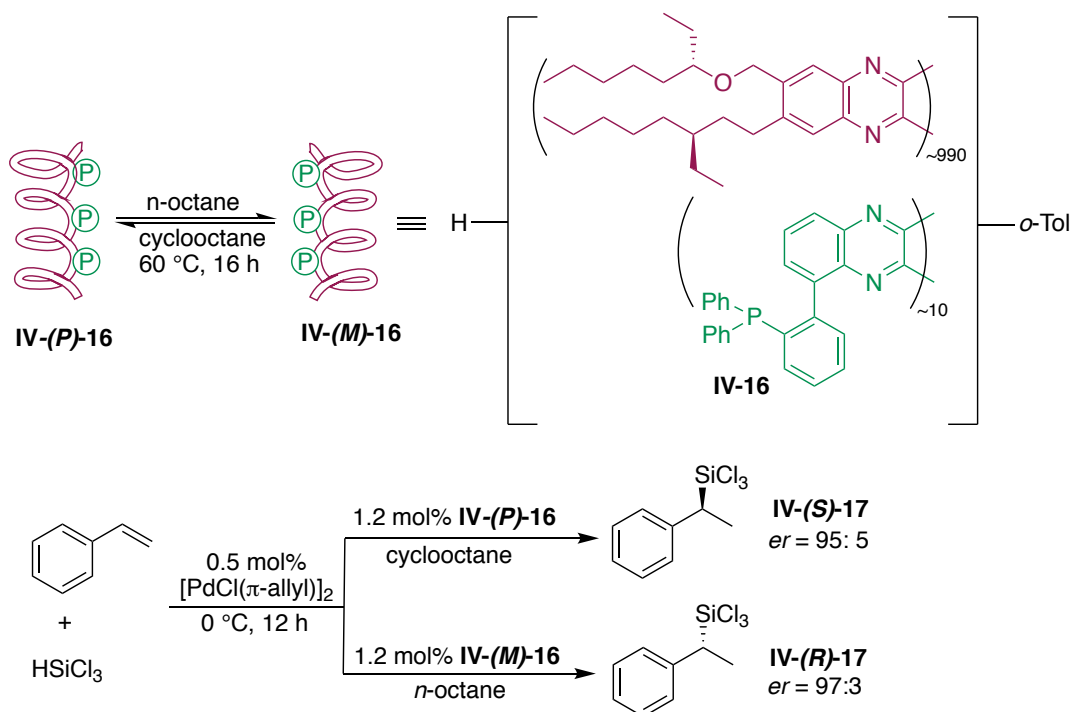
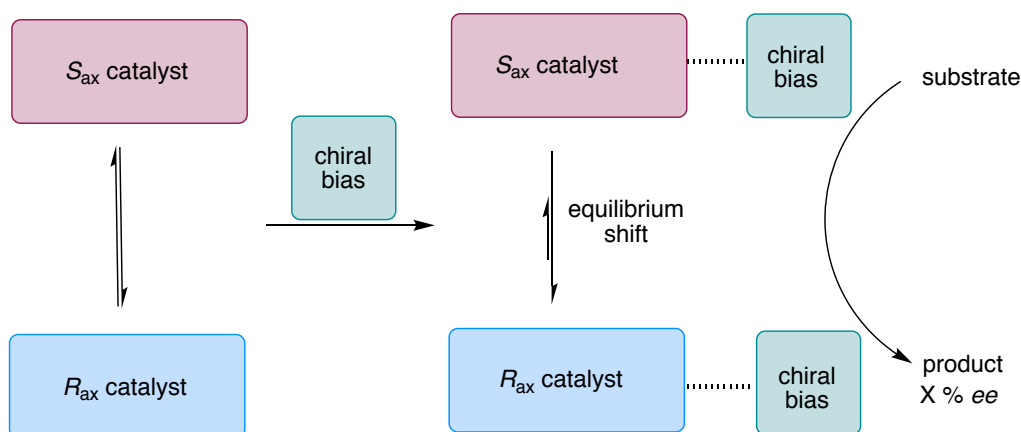


**Figure IV-4.** Example of a solvent driven chiral switchable catalyst.

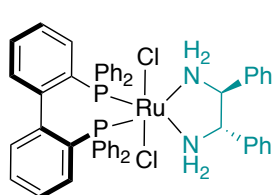
(*M*)-16, that resulted in the formation of IV-(*R*)-17 with opposite but similar enantioselectivity.

#### IV-5 Ligand driven chirality switching of catalyst

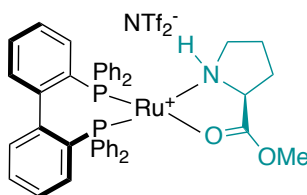
The examples of switchable catalysis discussed so far contain the asymmetric element within the catalyst. Biphenyl ligands are easily synthesized without any asymmetric synthesis and *tropos* in nature, can freely rotate around its dynamic chiral axis. To generate enantioenriched biphenyl ligands for asymmetric catalysis an external trigger is required. This could be achieved by interaction of the racemic ligands with a chiral stimulus (Figure IV-5). The energetic difference between the diastereomeric adducts would allow the system to re-equilibrate favoring the formation of one adduct over the other. There are two possible ways to access this- 1. Employment of a chiral



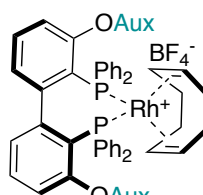
Examples:



IV-(*S*)-18



IV-(*S*)-19



IV-(*S*)-20

**Figure IV-5.** Design and examples of chiral ligand driven switchable catalysts.

ligand that could interact via non-covalent interactions. 2. Attachment of a chiral moiety with the ligands. In both instances, the chiral information of the external trigger must be transferred to the chiral axis of the biphenyl to perturb the initial equilibrium mixture. In 1999, Mikami<sup>15</sup> and later other groups<sup>8, 11, 16</sup> developed such system where a co-ligand transferred its chiral information to the biphenyl axis through a shared metal center (Figure IV-5). One of the major disadvantages of such strategy is that the external ligand

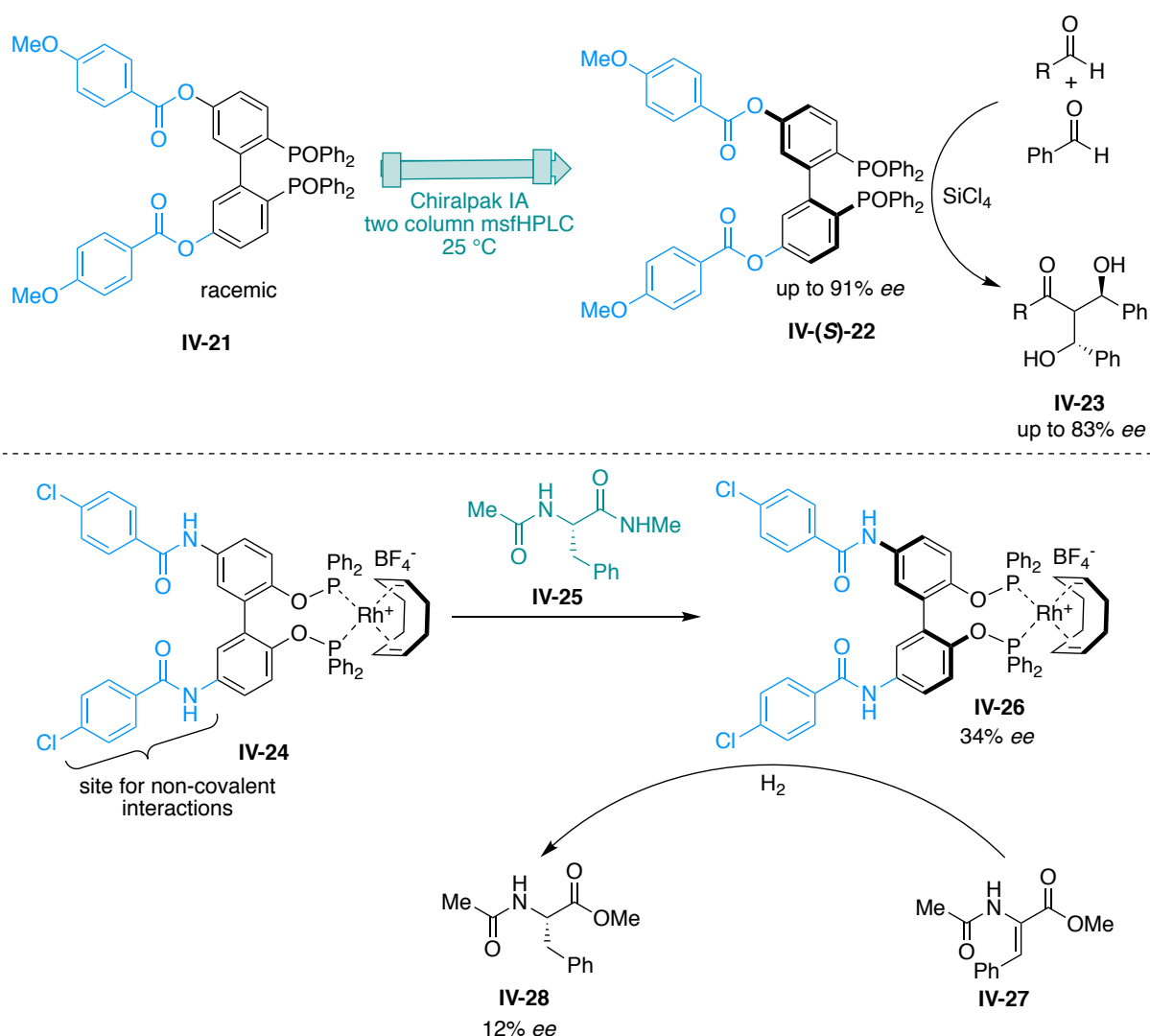


**Figure IV-6.** Examples of chiral switchable catalysts where catalytic site and chirality induction site are in opposite part of the catalyst.

was playing a key role in the reactivity and selectivity of the catalyst at the same time as it was coordinating to the reactive metal site.

In 2014, Trapp group redesigned a new type of *tropos* ligand.<sup>17</sup> Electron rich aromatic units were attached to the backbone of the ligands that can non-covalently interact with the external chiral stimulus. This would allow the transfer of chirality without the participation of the original catalytic site. Initially, they used a two-step multi stopped flow chiral HPLC technique to isolate the enantioenriched ligand and directly used the enantiopure bisphosphine oxide catalyst in an asymmetric reaction at lower temperature to prevent any racemization (Figure IV-6). Recently, Trapp group reported on the deracemization of the *tropos* ligand in situ and were only able to achieve 12% *ee* in the product (Figure IV-6).<sup>18</sup>

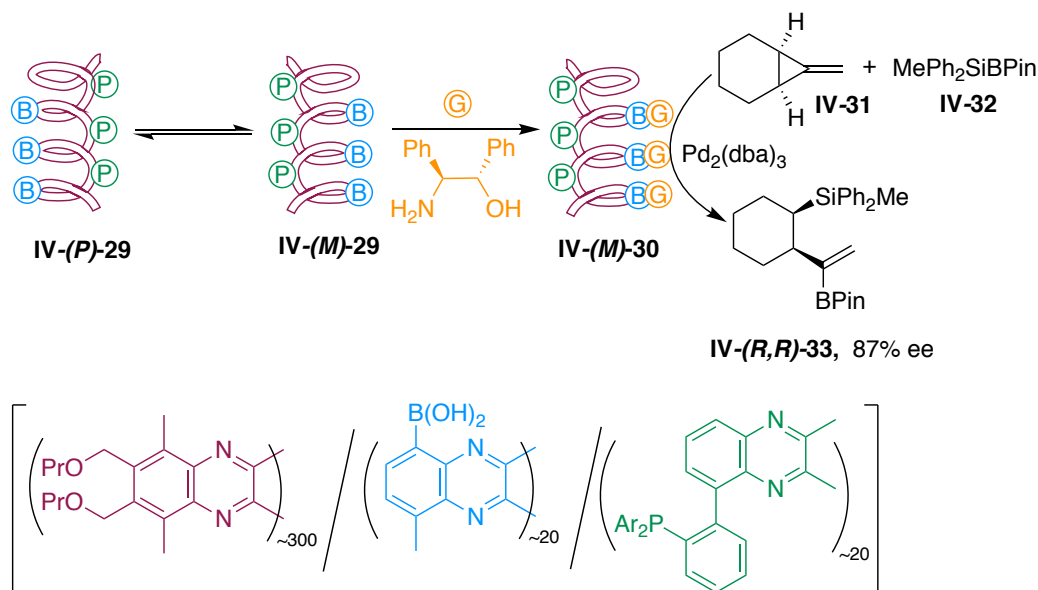


**Figure IV-7.** Induction of chirality to polymeric dynamic racemic ligands and its application to silaboration of an alkene.



In 2018, Suginome and coworkers employed a similar strategy for their polymeric dynamically racemic ligands.<sup>19</sup> Helical chirality was induced within poly(quinoxaline-2,3-diyl) via condensation of the chiral diol or aminoalcohols on the pendant boronyl group at the 5-position of the quinoxaline ring (Figure IV-7). The induced chirality of the ligand was then translated to the product via a palladium catalyzed asymmetric silaboration of meso-methylenecyclopropene.

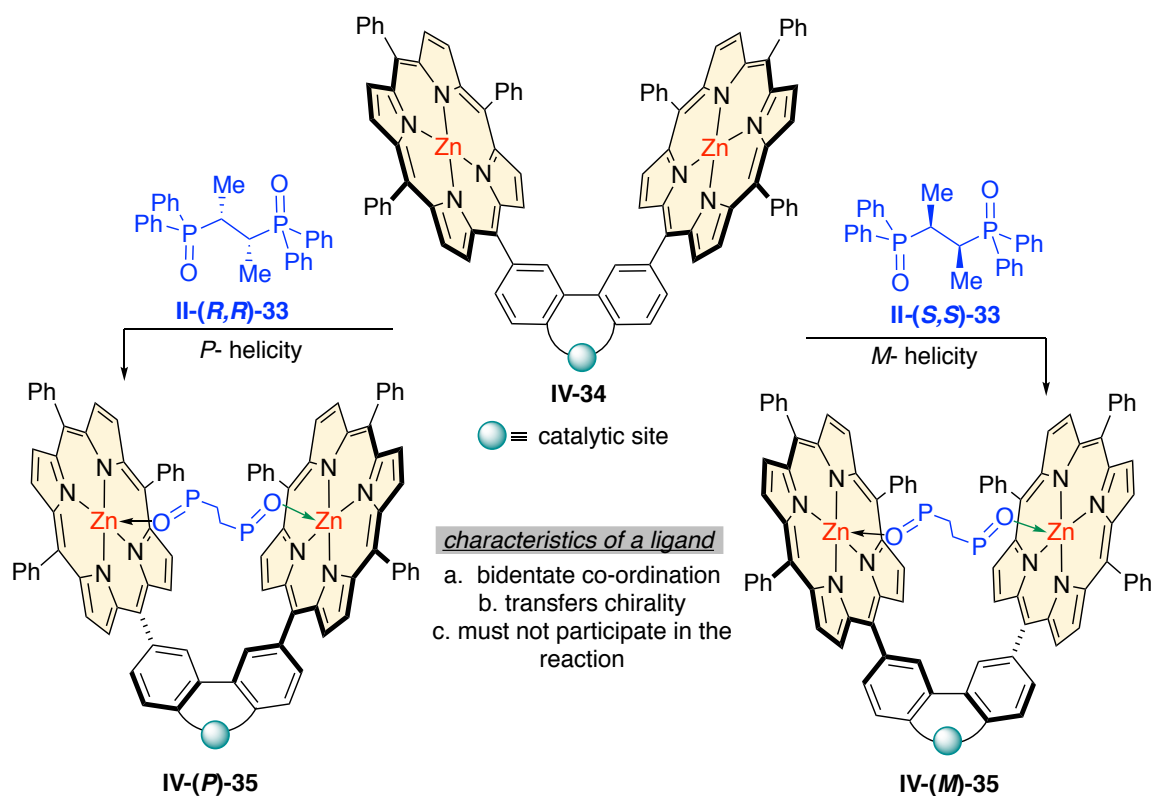


**Figure IV-8.** Design of a bis-porphyrin based chiral bis-phosphineoxide driven programmable catalyst.

## IV-6 Design and application of a ligand driven enantiodivergent programmable organocatalyst

Based on our work with the MAPOL host system<sup>20-23</sup> and inspired from the work of Trapp<sup>17-19</sup> and Suginome<sup>19</sup> on ligand driven chiral switchable catalyst, we were intrigued to design a bis porphyrin *tropos* organocatalyst **IV-34** that could be deracemized in situ, through its interaction with an external chiral ligand (Figure IV-8). The strong host-guest complexation through a ligand to metal coordination would facilitate the transfer of the point chirality to the chiral axis of the catalyst. Since the stereochemical identity of the catalyst is dictated by the asymmetry of the ligand, it could be switched easily by changing ligand's chirality. Intrigued by the strong binding affinity of bisphosphine oxides with **I-Zn-**

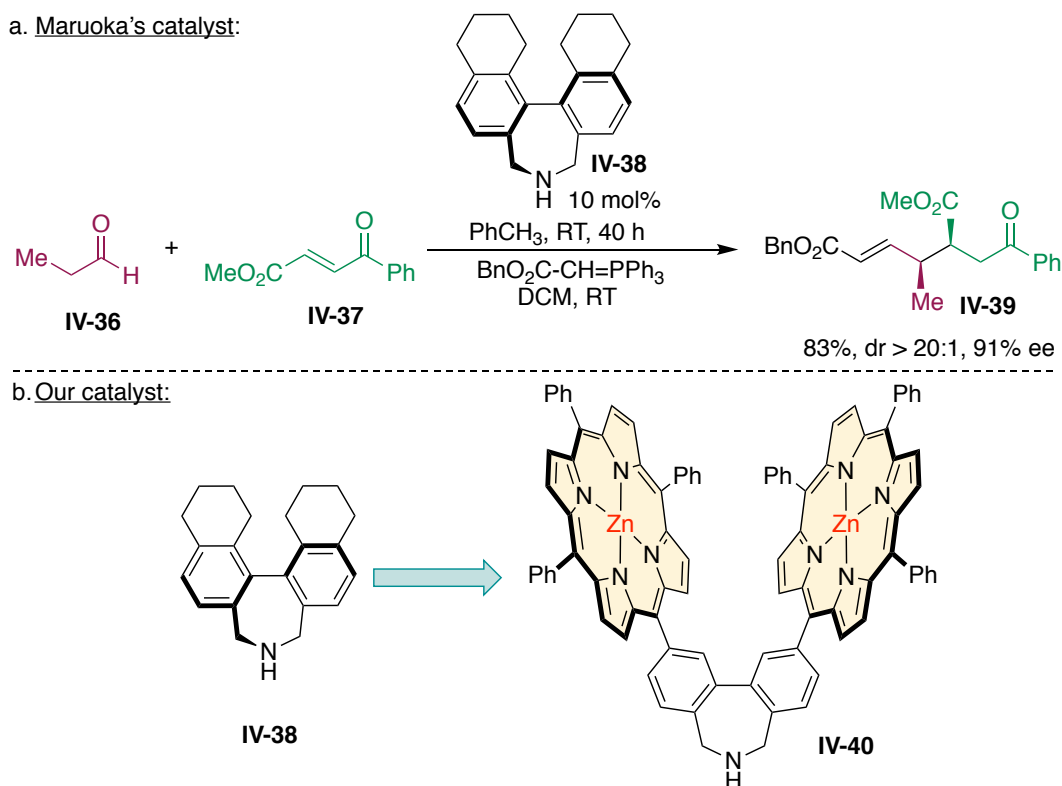
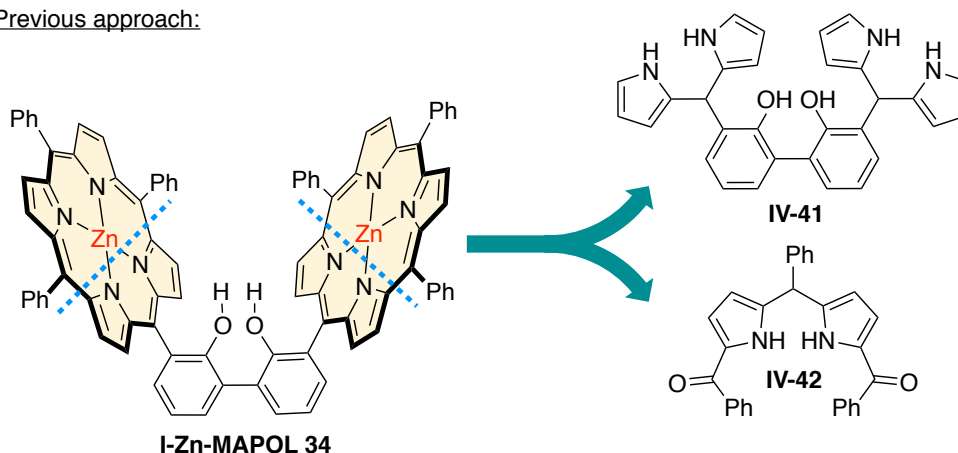


**Figure IV-9.** a. Stereoselective conjugate addition of aldehydes to electron deficient olefins developed by Maruoka. b. Our designed programmable organocatalyst **IV-40** inspired from Maruoka's catalyst **IV-38**.

**MAPOL 34**, we quickly surmised that the bisphosphine oxide could serve the purpose of the desired chiral ligand. Such a strong interaction would not only enable efficient chirality transfer, but it would also hold the induced chirality under the reaction condition in presence of other interferences i.e; substrates, products etc. (Figure IV-8).

Drawing inspiration from Maruoka's enamine catalyst **IV-38** (Figure IV-9a),<sup>24</sup> we designed our programmable catalyst **IV-40** (Figure IV-9b). Our proposed catalyst contains

Previous approach:



Current approach:

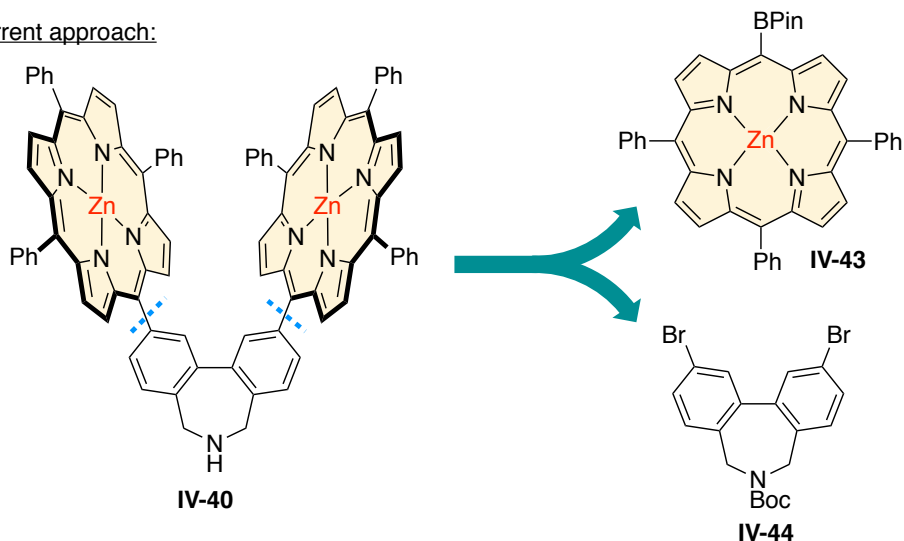


**Figure IV-10.** Newly designed retrosynthetic approach for the synthesis of **IV-40**.

a secondary amine unit as its catalytic site for the enamine catalysis and the bis-porphyrin receptors that will serve the purpose of a host for the ligand. Considering the chiral ligands might interfere with the stereochemical outcome of the product, the catalytic amine unit and porphyrin receptors are placed in the opposite direction.

However, we realized the difficulties in scaling up the synthesis of the catalyst. Typically, **I-Zn-MAPOL 34** is synthesized following a literature procedure developed in our group (Figure IV-10).<sup>22</sup> The bis-pyrromethane unit **IV-41** is made initially and then the porphyrin units are built upon that core through acid catalyzed condensation with **IV-42**, which is made separately. This last step of the synthesis is challenging and the overall yield for this route was low (<4%). To enable a more practical synthesis of our proposed catalyst **IV-40**, we revised our synthetic strategy for the bis-porphyrin receptors. We envisioned a convergent route i.e; synthesis of the mono-porphyrin unit **IV-43** separately

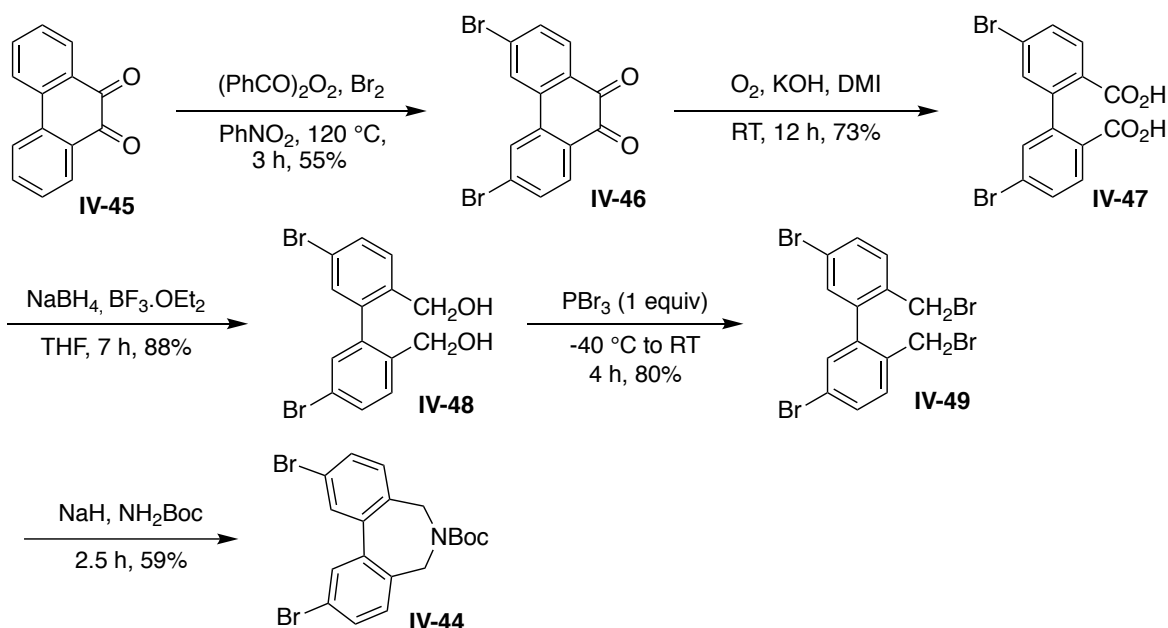


**Figure IV-11.** Forward synthesis of the coupling partner **IV-44**.

and then coupling with the backbone partner **IV-44** would circumvent the multiple bond formation in the key step unlike our previous strategy.

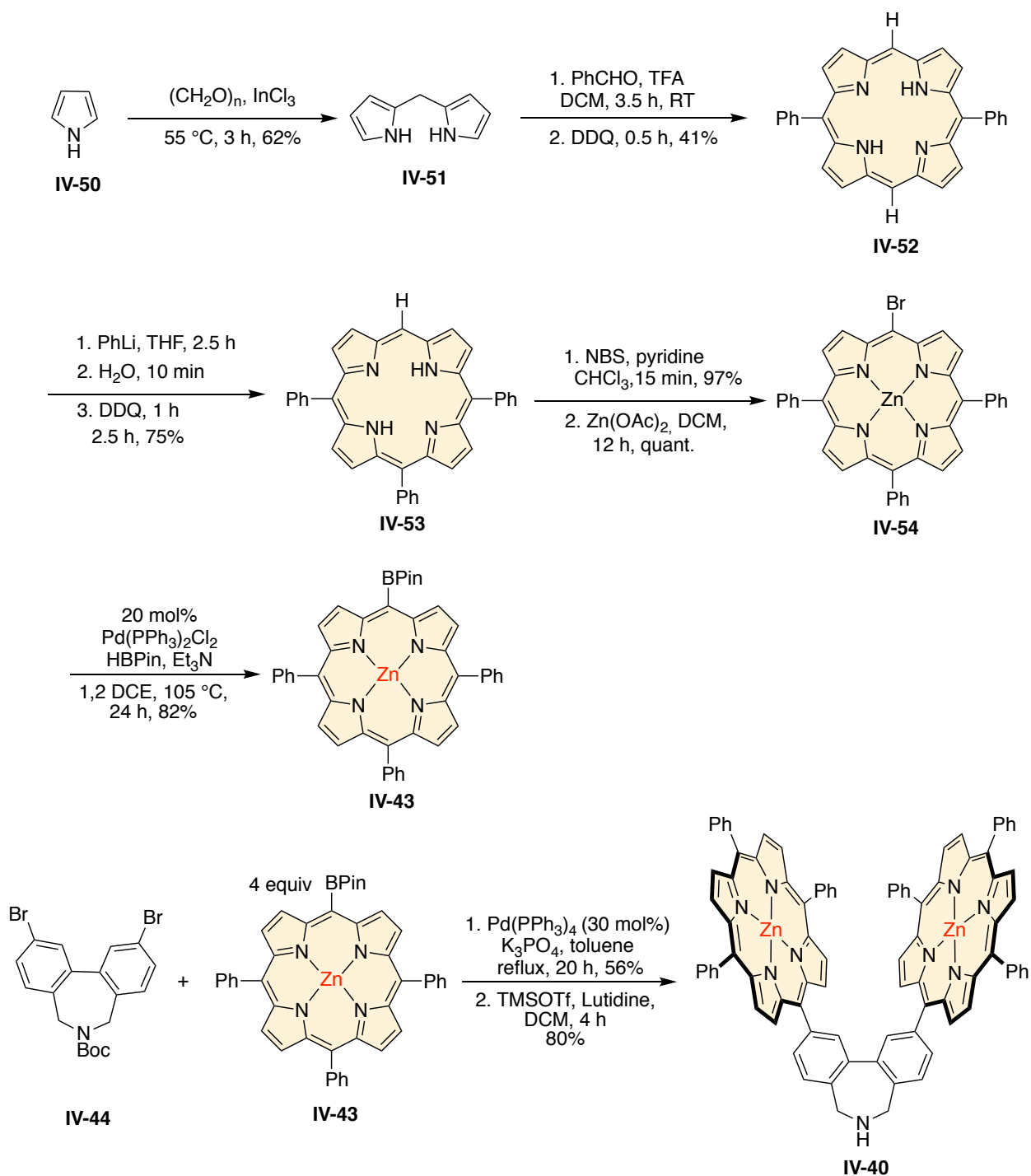


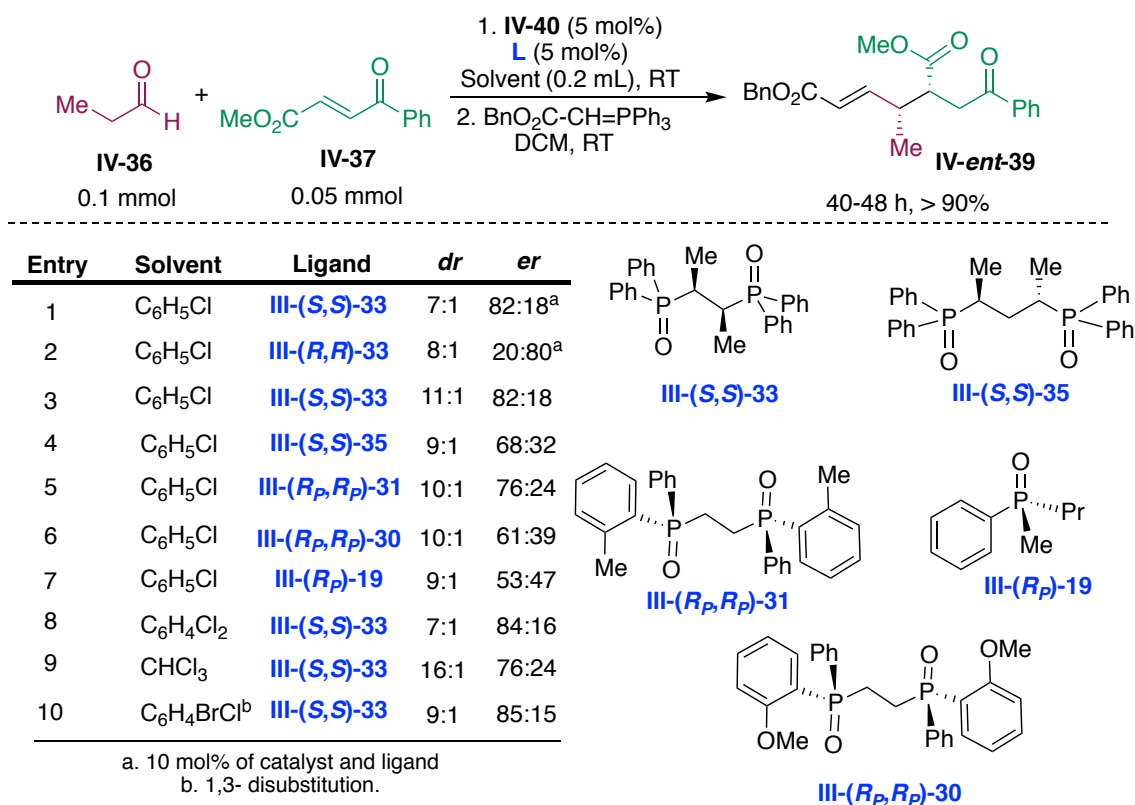
**Figure IV-12.** Forward synthesis of the coupling partner **IV-43** and final steps for the synthesis of **IV-40**.

The synthesis of the fragment **IV-44** commenced with commercially available **IV-45** (Figure IV-11). The dibromination of **IV-45** followed by an oxidative cleavage with H<sub>2</sub>O<sub>2</sub> gave rise to compound **IV-46** in 73% yield.<sup>25</sup> A subsequent reduction with sodium borohydride, followed by a di-bromination and finally a cyclization with Boc carbamate resulted in the desired product **IV-44**.

The borylated counterpart **IV-43** was synthesized following a literature procedure with little modification (Figure IV-12).<sup>26</sup> Condensation of pyrrole **IV-50** with paraformaldehyde in presence of indium chloride gave rise to dipyrromethene **IV-51** in 62% yield. The dipyrromethene was then converted to mono-porphyrin **IV-52** with 41% yield. A subsequent nucleophilic addition of phenyllithium to **IV-52**, followed by oxidation with DDQ produced compound **IV-53** in 75% yield.<sup>27</sup> Bromination of **IV-53** with NBS, a quantitative zincation followed by Miyaura borylation yielded the desired boronic ester **IV-43**.<sup>26</sup> Two coupling partners were then subjected to Suzuki-Miyaura coupling conditions to provide the Boc protected catalyst **IV-NBoc-40**.<sup>28</sup> Initial attempts to drop the Boc group under acidic condition led to the concomitant removal of the Zn metal from the porphyrin core. Finally, the Boc group was deprotected under basic conditions to produce the desired catalyst **IV-40** keeping the Zn metals intact (Figure IV-12).

With both the catalyst **IV-40** and chiral bis-phosphine oxide **III-(S,S)-33** in hand, we tested the exact reaction conditions as Maruoka's.<sup>24</sup> Gratifyingly, the anticipated *syn* diastereomer was formed in 45% *ee* in our initial trial in toluene. After an extensive evaluation of solvents, the enantiomeric excess increased to 64% in chlorobenzene (Scheme IV-1, entry 1). Notably, no enantioinduction in the product was observed when the reaction was run in solvents like THF or methanol. These solvents can potentially

coordinate to the Zn metal center and outcompete the bis-phosphine oxides as they are present in a large excess. To test the ligand driven switchability of our designed catalyst **IV-40**, the reaction was run with **III-(*R,R*)-33**. As anticipated, enantiomeric product was formed with almost identical enantioselectivity (Scheme IV-1, entry 2). Furthermore, we explored different phosphine oxides with chirality at phosphorus, chirality at carbon with various chain lengths. Unfortunately, the enantioselectivity did not increase (Scheme IV-1, entries 4-6). The mono-phosphine oxide **III-*R<sub>P</sub>*-19** led to nearly racemic product (Scheme IV-1, entry 7). We attribute this interesting observation to the binding of mono-phosphine oxide from the outside of the porphyrin cavity, and therefore, not inducing any preferred helicity for the host-guest complex. It also corroborates the fact that a bidentate



**Scheme IV-1.** Selected optimization studies of the Michael addition reaction with our designed programmable catalyst **IV-40** and bisphosphine oxide ligands.

coordination is necessary to deracemize the catalyst during the reaction. Further optimization of the reaction led to the 5 mol% of the catalyst and 1,3 chlorobromobenzene as the optimal condition with the desired enantiomer forming in 70% *ee* (Scheme IV-1, entry 10).

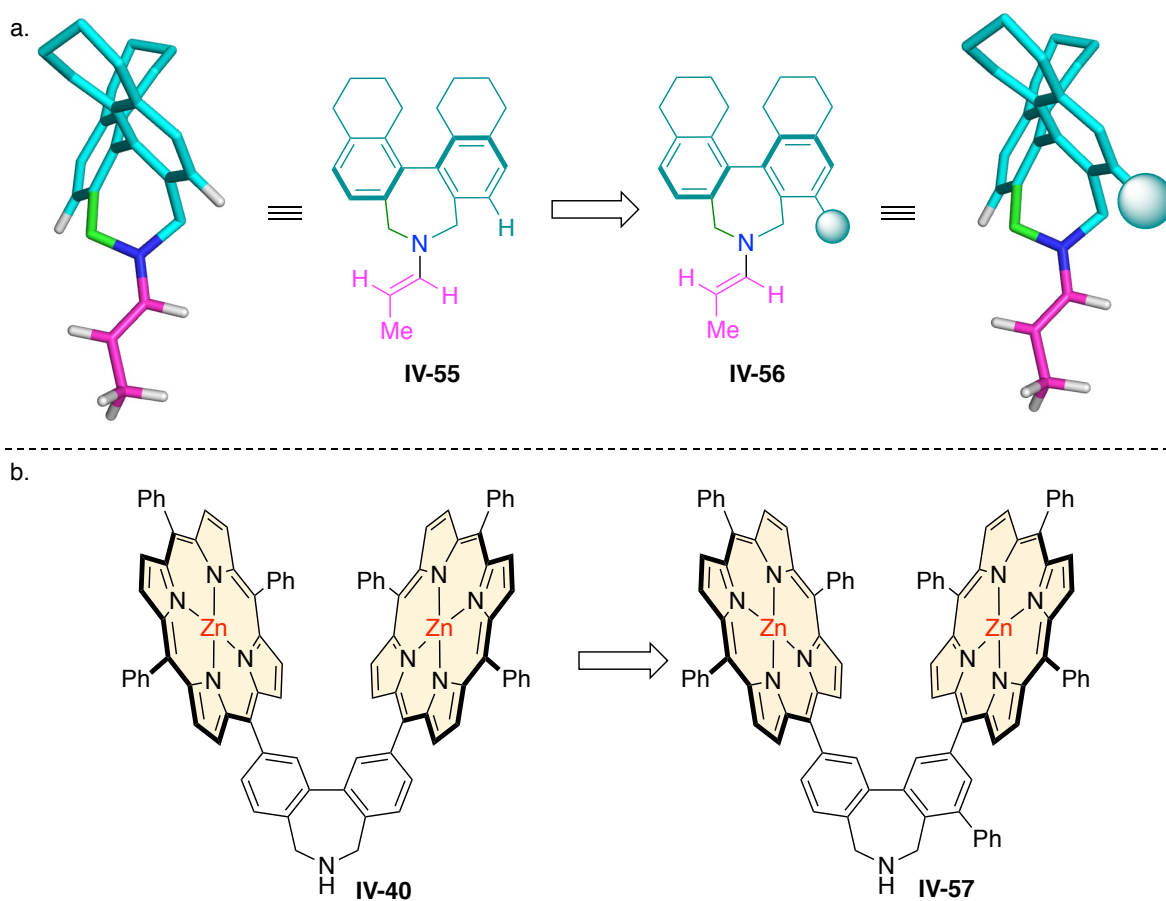


**Figure IV-13.** a. Predicted approach of the electrophile in the enantioinduction step for Maruoka's enamine catalysis. b. Design of a Ph substituted C<sub>1</sub> catalyst **IV-57**.



## IV-7 Steric manipulation of the programmable catalyst

In comparison to Maruoka's catalyst the ee's from our programmable catalyst was low. We began by evaluating the steric influence of substituents to improve the selectivity. Our modeling study with Maruoka's system revealed how the facial selectivity is attained in the enantioinduction step (Figure IV-13a). It was realized that the *Re* face of the intermediate enamine **IV-55**, formed after the initial condensation between the amine and aldehyde, is blocked by the unsubstituted C-3 position of the catalyst (Figure IV-13a). Therefore, the Michael acceptor **IV-37** approaches the enamine from its less sterically encumbered bottom face i.e; the *Si* face. We postulated that substitution at one of the C-

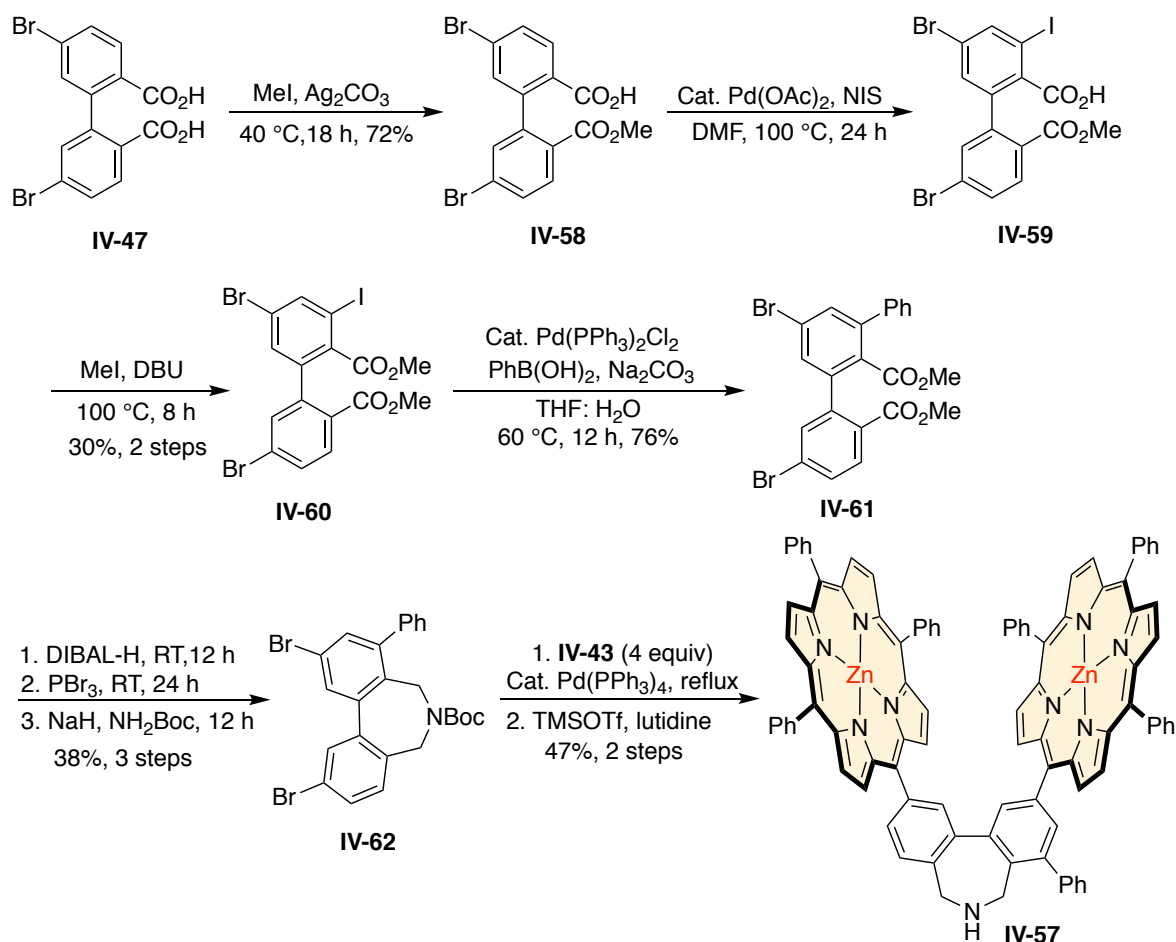
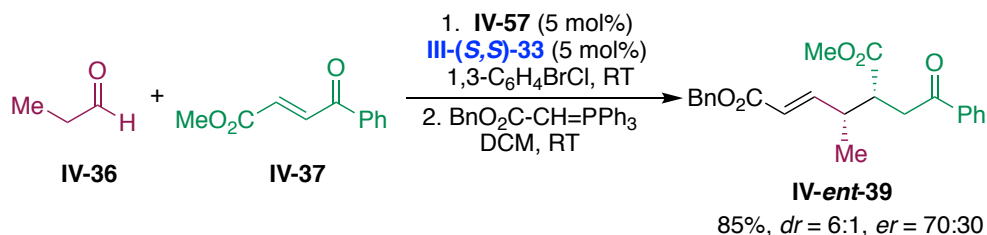


**Figure IV-14.** Synthesis of the Ph substituted C<sub>1</sub> catalyst **IV-57**.

3 position of the catalyst could further prevent the approach of the electrophile **IV-37** from the *Re* face and might enhance the enantioselectivity. To this end, we redesigned our parent catalyst **IV-40** and specifically substituted at the C-3 position with a phenyl group



**Scheme IV-2.** Syn selective conjugate addition with catalyst **IV-57** and **III-(S,S)-33**.

(Figure IV-13b). The Ph group was chosen initially for the ease of synthesis. The newly designed C<sub>1</sub> catalyst **IV-57** were synthesized following the similar protocol as the parent catalyst **IV-40** (Figure IV-14). Mono-methylation of the previously synthesized **IV-47** with MeI afforded compound **IV-58** in 72% yield. A subsequent carboxylic acid directed C-H iodination resulted in **IV-59**, which was then converted to the diester without further purification. The diester **IV-60** was converted to the coupling partner **IV-62** following routine procedures in 3 steps. Finally, a Suzuki-Miyaura coupling and a Boc deprotection

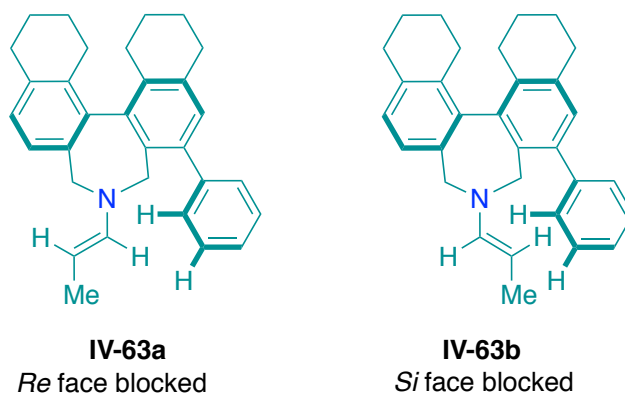


**Figure IV-15.** Two energetically close conformers (1 kcal/mol) of the mimic **IV-63** catalyst block the opposite faces of the enamine.

afforded the final catalyst **IV-57**. Surprisingly, a decrease in enantioselectivity to 40% *ee* was observed when the **IV-57** was subjected to the reaction condition. To gain insight into this undesired outcome, a conformational study was done with a mimic of Maruoka's catalyst **IV-63** (Figure IV-15). The study revealed that the undesired conformer **IV-63b** blocks the desired *Si* face of the intermediate and is only 1 kcal/mol higher in energy (DFT/B3LYP/6-31G\*) as compared to the desired conformer **IV-63a**. Concomitant presence of both the conformers in the reaction could be one of the many reasons of lowered enantioselectivity in this case. At this point, we were also uncertain of the *P/M*

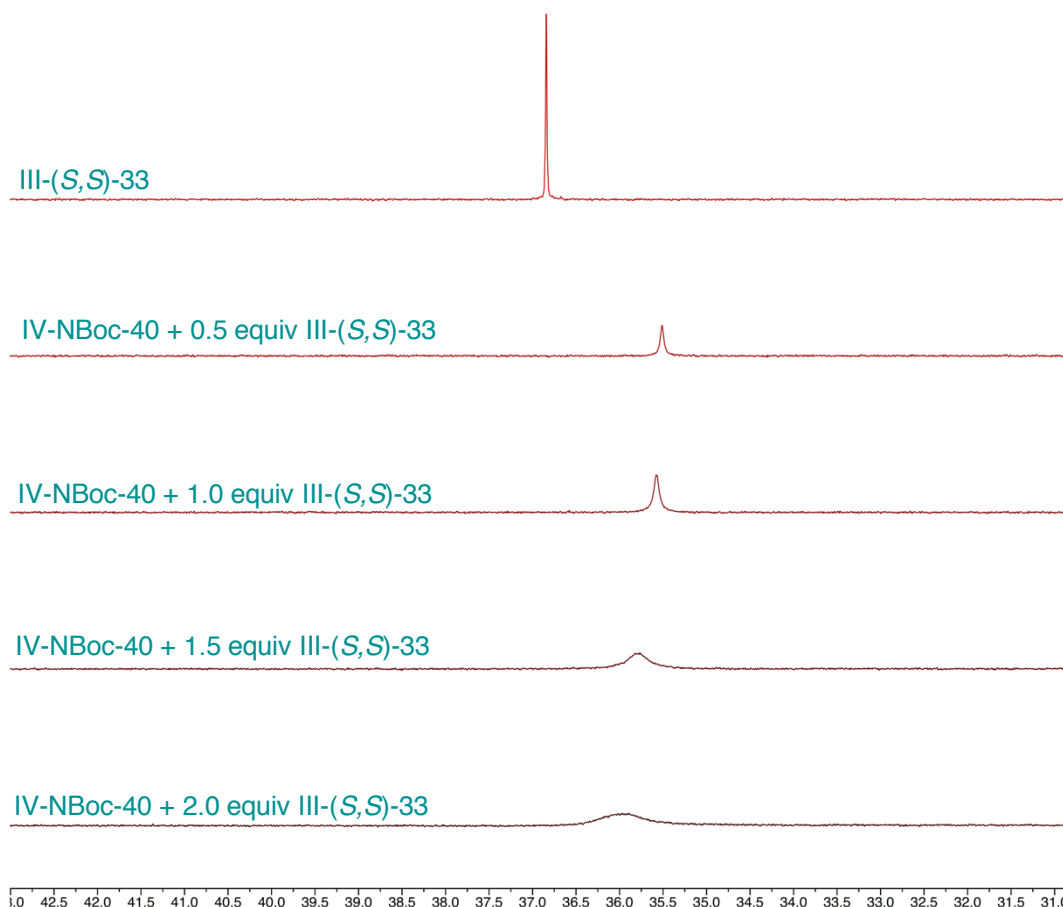


**Figure IV-16.**  $^{31}\text{P}$  NMR titration studies of **IV-NBoc-40** (6mM) with **III-(S,S)-33** at room temperature in  $\text{CDCl}_3$ .

helicity ratio in any of our actual catalytic system. Knowing this ratio is critically important as it would suggest if the observed selectivity were the result of the *P/M* ratio, or it was inherent under the conditions used for an enantiopure catalyst.

#### IV-8 Electronic manipulation of the catalyst

From the  $^{31}\text{P}$  NMR studies of the Boc protected catalyst **IV-NBoc-40** complexed with **III-(S,S)-33**, it was evident that the coordination of the bis-phosphine oxide with the Zn metal is dynamic in nature.<sup>29-31</sup> Figure IV-16 displays the  $^{31}\text{P}$  NMR spectra at room temperature in  $\text{CDCl}_3$  resulting from the complexation between **IV-NBoc-40** and **III-(S,S)-33**. The free ligand **III-(S,S)-33** appears at  $\sim 36.8$  ppm. As the complex is formed, an upfield chemical shift in the  $^{31}\text{P}$  NMR is observed. With the increase in the equivalents of the ligand, only broad  $^{31}\text{P}$  peak at  $\sim 36$  ppm, instead of two distinct peaks, one for the bound and one for the unbound ligand, was witnessed. Cooling the mixture down to  $-80^\circ\text{C}$  did not change the scenario. The broad chemical shift represents the weighted average of the two sets of phosphorus nuclei because of fast exchange between the coordinated and non-coordinated phosphine oxide. This result suggested that the binding between the catalyst and the ligand may not be as strong as desired. This might lead to a certain degree of ligand-unbound catalyst, that could potentially drive the background reaction and lower the enantioselectivity. To saturate the catalyst with ligand, we envisaged to increase the amount of the ligand in the reaction. Unfortunately, increasing the ligand amount led to poor enantioselectivity presumably due to the formation of 1:2 or 2:3 type catalyst:ligand complex where the ligand binds from the outside of the cavity and therefore, no helicity would be preferred. To this end, we planned to increase the binding affinity between the host catalyst and the guest ligand. The role of electronics of

the porphyrin ring to increase the binding affinity was evaluated. From our prior experience,<sup>32</sup> we surmised that the per-fluorination of the porphyrin ring would lower the LUMO energy at the Zn center, making it strongly Lewis acidic. To test our hypothesis, a new catalyst with per-fluorinated bis-porphyrin **IV-70** was designed and synthesized

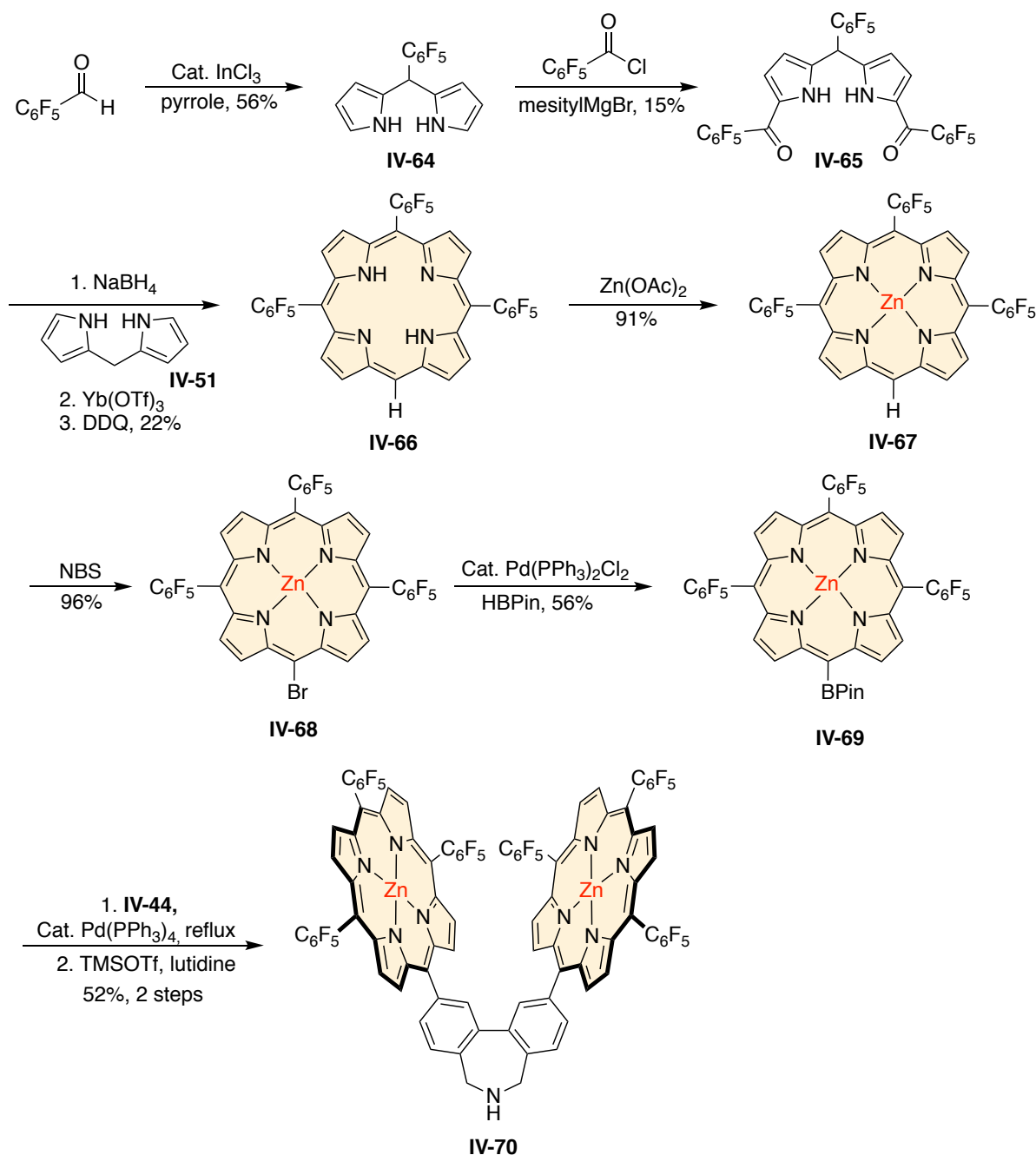


**Figure IV-17.** Synthesis of the per-fluorinated highly Lewis acidic Zn center containing catalyst **IV-70**.

following a similar strategy as the other catalysts (Figure IV-17). Our investigation began with the  $^{31}\text{P}$  NMR studies between **IV-70** and the ligand **III-(S,S)-33**. As depicted in Figure IV-18, addition of 0.6 equivalent of **III-(S,S)-33** to a  $\text{CDCl}_3$  solution of **IV-70** led to a 2 ppm shift of **III-(S,S)-33** in the  $^{31}\text{P}$  NMR confirming their binding. In presence of excess ligand, two separate peaks for bound and unbound ligand appeared. It is worth mentioning that similar studies with catalyst **IV-40** only showed the presence of a broad single peak. The CD study (Figure IV-19) further confirmed that **III-(S,S)-33** binds stronger to **IV-70** ( $A=2229$  vs  $A=1322$ , larger ECCD amplitude) in comparison to the non-fluorinated one **IV-40**. Unfortunately, when the catalyst **IV-70** was subjected to the reaction condition, none of the desired product was formed. Instead, the Michael acceptor **IV-37** was recovered completely. NMR studies (Figure IV-20) between **IV-71** and **IV-72** disclosed

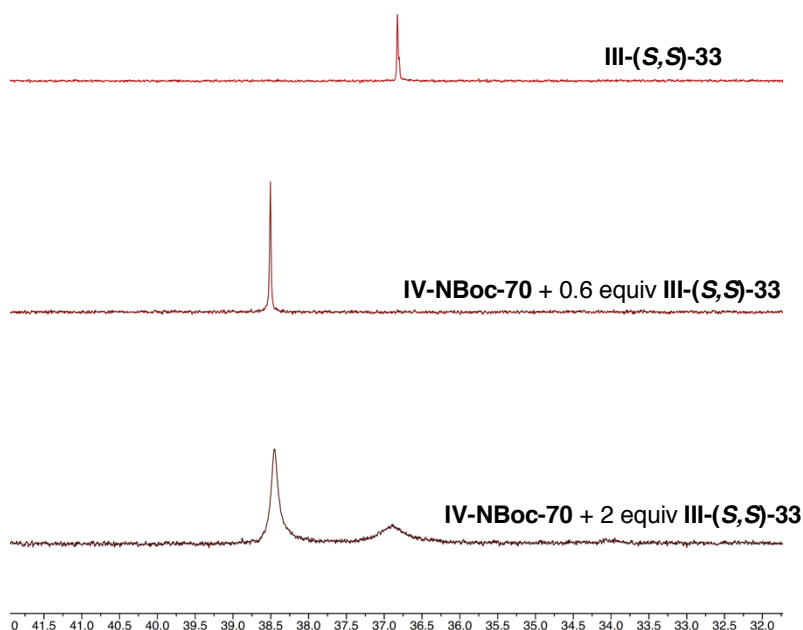


**Figure IV-18.**  $^{31}\text{P}$  NMR titration studies of **IV-NBoc-70** (6mM) with **III-(S,S)-33** at room temperature.

that the secondary amine of the catalyst tightly coordinates to the Zn metallo center of Zn-TPP. Such coordination is further strengthened in catalyst **IV-70** due to the presence of the highly Lewis acidic Zn metal center. This observation led us to the conclusion that

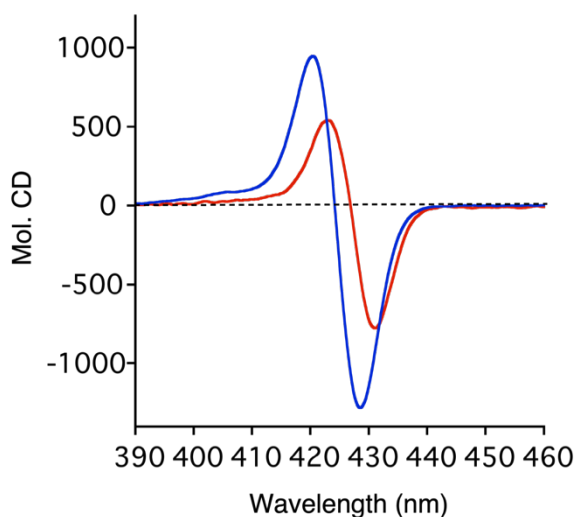


**Figure IV-19.** ECCD spectrum of **IV-70** (blue) and **IV-40** (red) complexed with 1 equivalent of **III-(S,S)-33** at room temperature in PhCl.

such a strong coordination is preventing the amine in **IV-70** to react with the aldehyde **IV-36** to form the initial iminium ion that isomerizes to enamine. Therefore, enhancement of the Lewis acidity on the Zn metal center is not a solution to the problem. To circumvent this fundamental challenge, we explored the possibility of employing other metallo porphyrins with oxophilic property. Mg porphyrins bind stronger to oxygen nucleophiles compared to nitrogen nucleophiles due to their high oxophilicity.<sup>33-35</sup> Therefore, a Mg based catalyst provides two major advantages- 1. It would enhance the binding affinity between the catalyst and the bis-phosphine oxide ligands. 2. The intermolecular amine-Mg porphyrin coordination would be reduced. To explore the binding of Mg porphyrin with

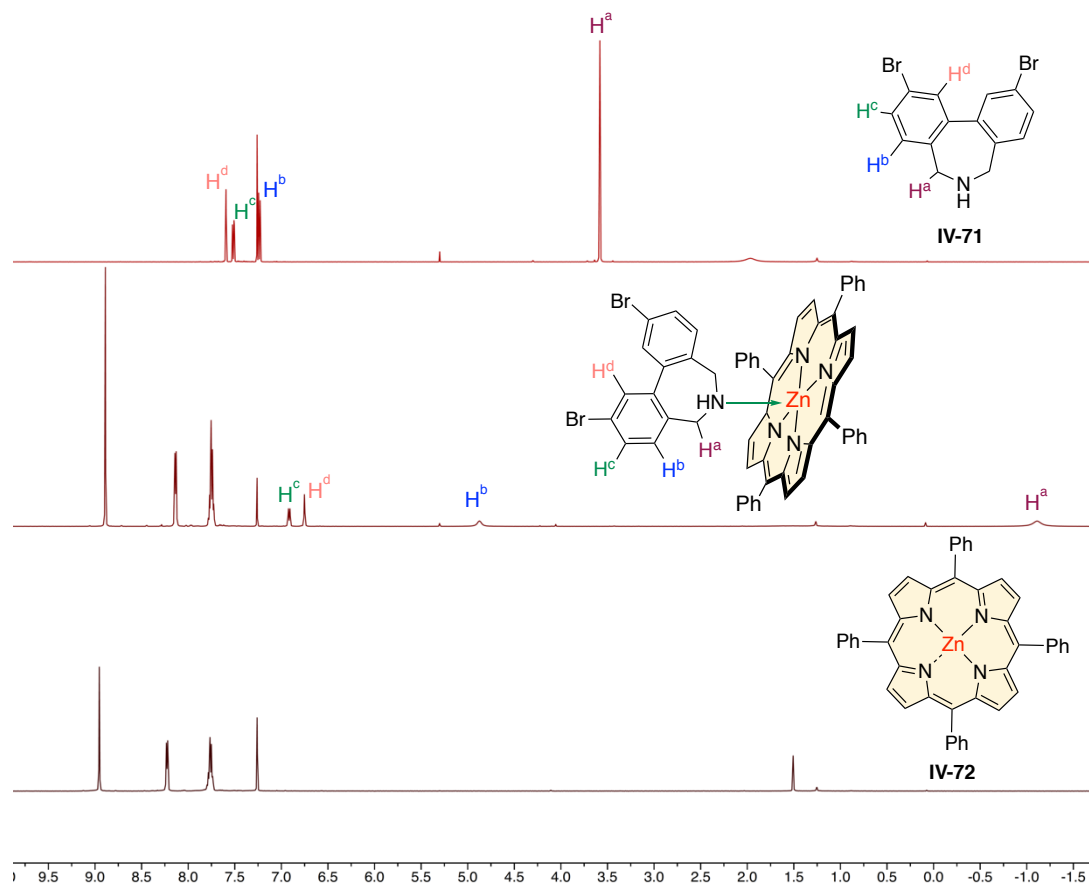


**Figure IV-20.** Room temperature  $^1\text{H}$  NMR studies in  $\text{CDCl}_3$  show the ligand to metal coordination between **IV-71** and **IV-72** (Zn-TPP).

phosphine oxides, a  $^{31}\text{P}$  NMR study was performed (Figure IV-21). Zn-TPP bound to excess triphenyl phosphine oxide shows the presence of only one NMR peak that is probably the average of the bound and unbound phosphine oxide. Notably, two separate peaks were observed when Mg-TPP was complexed with 1.5 equivalent of triphenylphosphine oxide. The peak at 29.3 ppm clearly matches with the unbound one, whereas the new peak at 25.5 ppm is from the phosphine oxide bound to Mg-TPP. It is worth mentioning here that the upfield chemical shift of phosphine oxide upon



coordination is due to the diamagnetic anisotropy of the porphyrin ring. Synthesis of **IV-Mg-40** is currently underway.

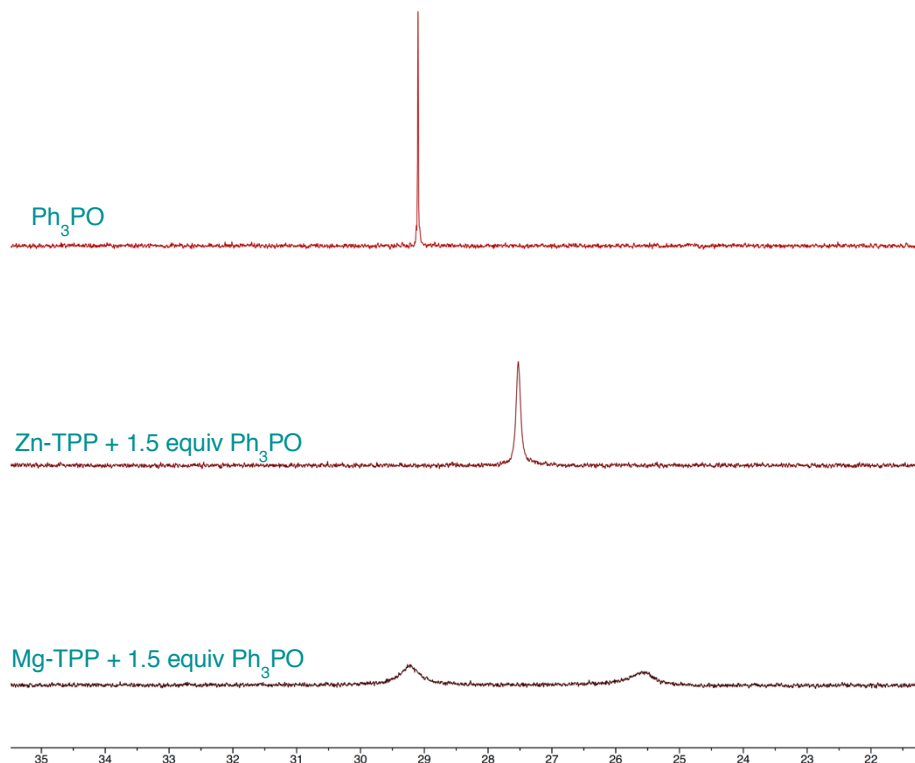


**Figure IV-21.** Room temperature  $^{31}\text{P}$  NMR studies of triphenylphosphine oxide with Zn-TPP and Mg-TPP.

#### IV-9 Binding affinity enhancement using bipyridine ligands

In parallel, we explored the possibility of enhancing the binding strength by increasing the donor ability of the ligand. This would allow us to enhance the binding affinity without changing the metal or the electronics of the metal. This hypothesis could be tested either by changing the substituents on the phosphine oxide ligands or changing to a completely new set of ligands with different coordinating group that binds stronger

than phosphine oxides to Zn metallo porphyrin. After a quick survey of literature, it appeared that pyridine binds stronger to Zn mono-porphyrin than triphenylphosphine

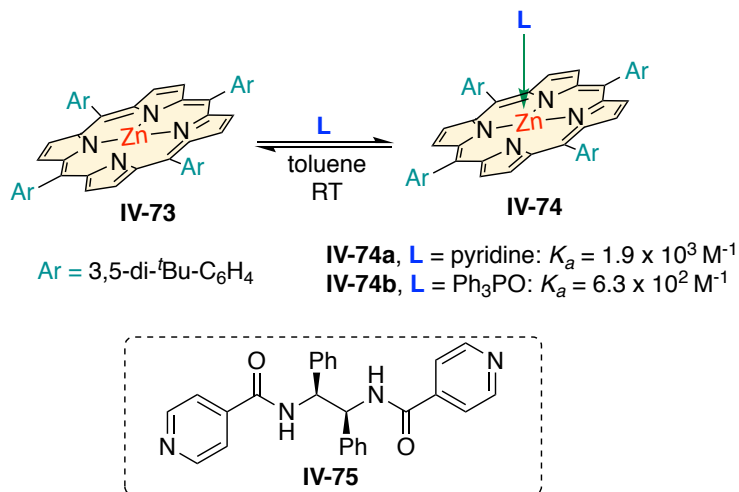


**Figure IV-22.** Pyridine binds stronger to Zn porphyrins than the triphenylphosphine oxide. Rath's bi-pyridine ligand **IV-75**.

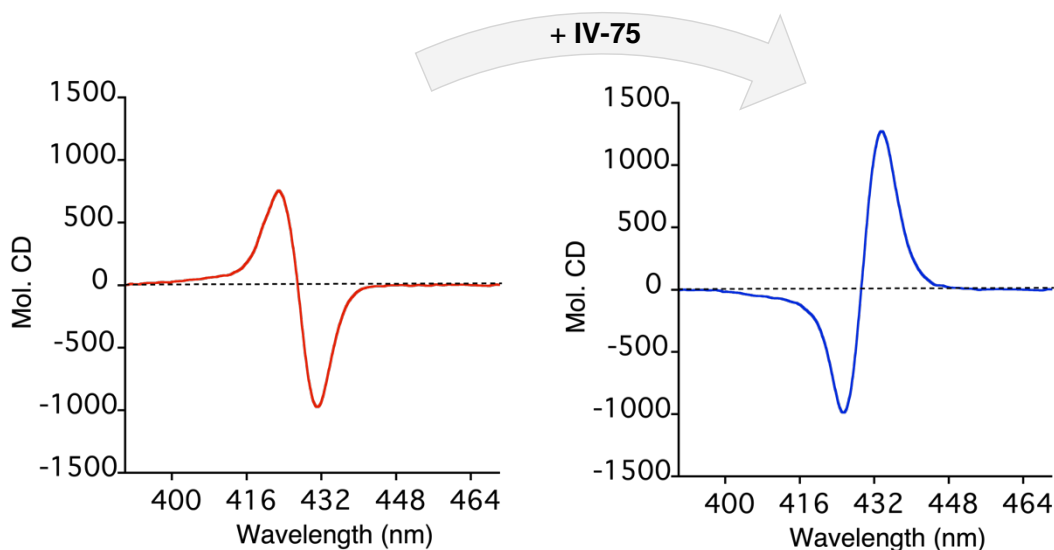
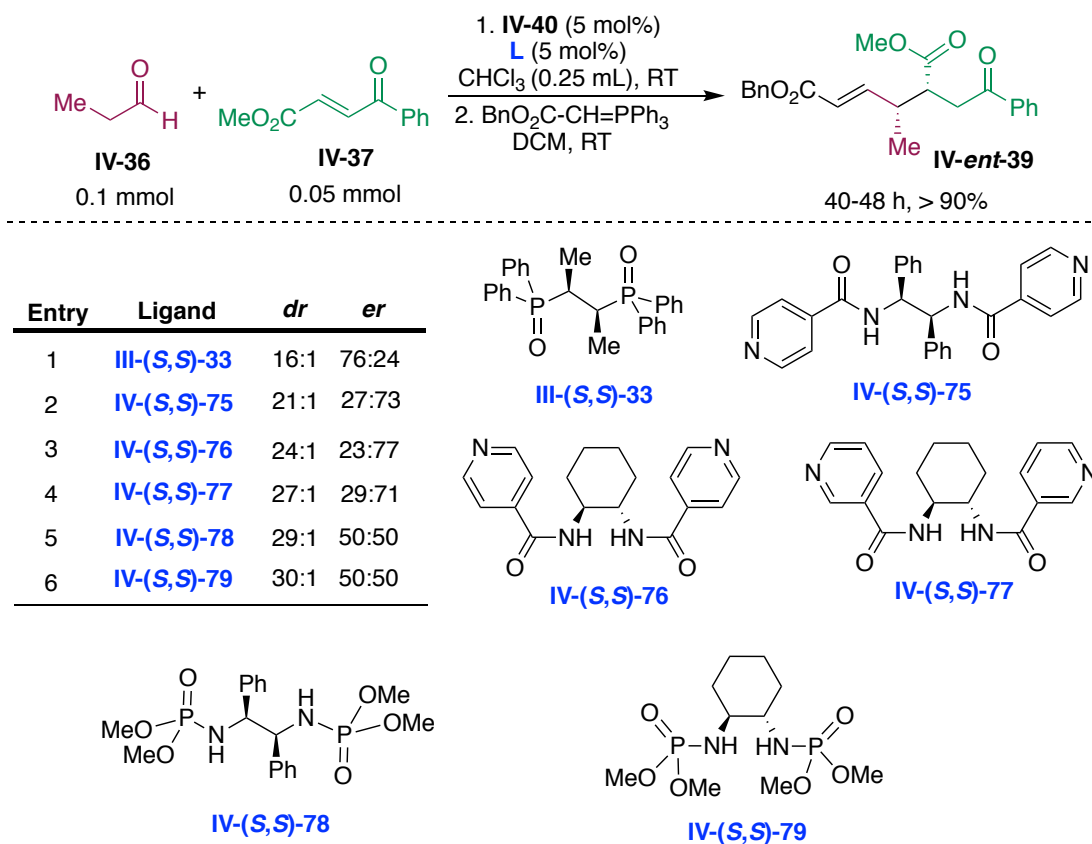


**Figure IV-23.** ECD spectrum (red) of **IV-40** complexed with 1 equivalent of **III-(S,S)-33** in PhCl. The helicity completely switches (blue) as 1 equivalent of **IV-75** was added to the mixture.

oxide (Figure IV-22).<sup>29</sup> Inspired from the work of Rath and co-workers,<sup>36</sup> a series of bis-pyridine ligands were synthesized following literature protocols.

To test our hypothesis, an initial ECCD study was performed with the bispyridine ligand. When 1 equivalent of **IV-(S,S)-75** ligand was added to a preformed 1:1 complex of **IV-40** and **III-(S,S)-33** a complete switch in the ECCD signal from negative to positive is observed (Figure IV-23). This newly formed signal is consistent with the positive ECCD signal observed with the 1:1 complex of **IV-40** and **IV-(S,S)-75** albeit lower intensity. These observations led us to two conclusions- 1. **IV-(S,S)-75** ligand binds stronger to **IV-40** than **III-(S,S)-33**. 2. Coordination of **III-(S,S)-33** ligand to the catalyst **IV-40** is dynamic in nature, again consistent with our NMR results (Figure IV-16).



**Scheme IV-3.** Optimization studies with bis-pyridine and bis-phosphoramidate ligands.

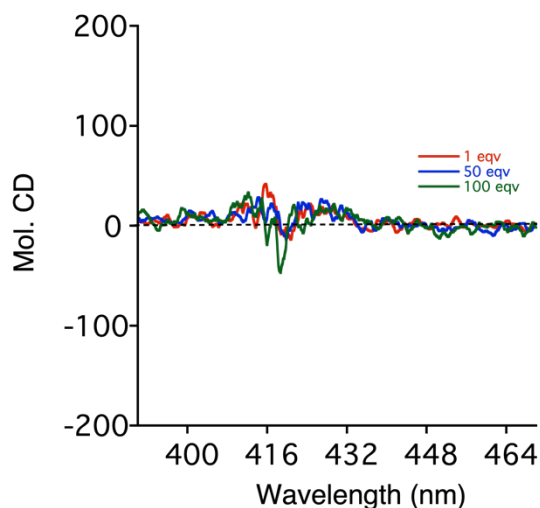


**Figure IV-24.** ECD titration of **IV-40** with different equivalents of **IV-(S,S)-79** in  $\text{CHCl}_3$  at room temperature.

With this initial data in hand, different bis-pyridine and bis-phosoramidate ligands were tested under the reaction condition (Scheme IV-3). Notably, all these reactions were performed in chloroform as these ligands were insoluble in 1,3-bromochlorobenzene. The

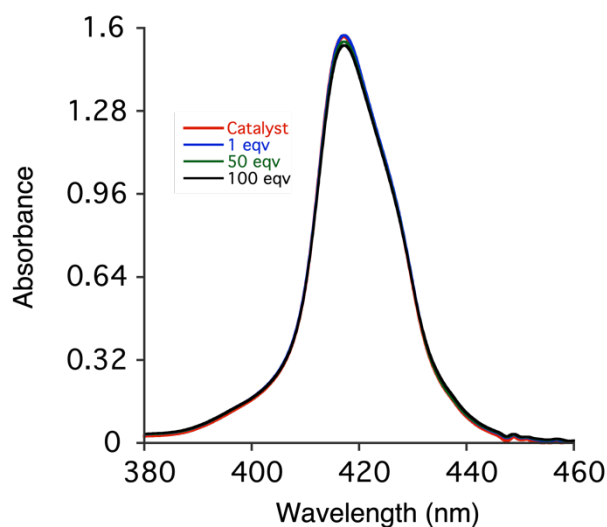


**Figure IV-25.** UV-vis titration of **IV-40** with different equivalents of **IV-(S,S)-79** in  $\text{CHCl}_3$  at room temperature.

best enantioselectivity was observed with **IV-(S,S)-76** (Entry 3). Surprisingly, **IV-(S,S)-78** and **IV-(S,S)-79** afforded completely racemic product. To gain insight into these unexpected outcomes, we studied the host-guest complex formation between these ligands and the catalyst **IV-40** via UV-vis and circular dichroism experiments. As shown in Figure IV-24, ligand **IV-(S,S)-79** was unable to induce any helicity in the catalyst. Furthermore, UV-vis study reveals no shift in the absorption maxima (Figure IV-25). Based on the studies, it is evident no coordination between the ligand and the metal has taken place. We attribute such discrepancies to the presence of C-H...O hydrogen bonding between the phosphoramidite oxygen and the acidic C-H of chloroform. The putative hydrogen bonding would prevent the ligand to coordinate to the Zn center and therefore the catalyst **IV-40** would remain racemic throughout the reaction. Observation of similar hydrogen bonding of phosphine oxide in chloroform has been reported in the literature.<sup>37</sup> Further screening of these type of ligands is currently underway.

In summary, we have developed an enantiodivergent programmable catalyst. Enantiomeric products can be afforded from a single racemic entity. Our catalyst eliminates the requirement of two enantiomeric catalysts to afford antipodal products. The asymmetry in the racemic catalyst can be introduced through coordination with ligands and therefore can be programmed at will. Different types of other catalysts are currently being explored to showcase the generality of our developed methodology.

## IV-10 Experimental Section

### IV-10.1. Materials and general instrumentations

Anhydrous solvents used for CD measurements were purchased from Aldrich and were spectra grade. Unless otherwise mentioned, solvents were purified as follows.  $\text{CH}_2\text{Cl}_2$  was dried over  $\text{CaH}_2$  whereas THF and  $\text{Et}_2\text{O}$  were dried over sodium (dryness was monitored by colorization of benzophenone ketyl radical); they were freshly distilled prior to use. NMR spectra were obtained using 500 MHz Varian NMR spectrometers and referenced using the residual  $^1\text{H}$  peak from the deuterated solvent for the proton NMR, the carbon shift of the solvent (77.0 ppm for  $\text{CDCl}_3$ ) for the  $^{13}\text{C}$ -NMR, and phosphoric acid as the internal standard reference for the  $^{31}\text{P}$ -NMR measurements. Column chromatography was performed using Silicycle 60 Å, 35-75  $\mu\text{m}$  silica gel. Pre-coated 0.25 mm thick silica gel 60 F254 plates were used for analytical TLC and visualized using UV light, *p*-anisaldehyde stain or phosphomolybdic acid in EtOH stain. CD spectra were recorded on a JASCO J-810 spectropolarimeter, equipped with a temperature controller (Neslab 111) for low temperature studies, and are reported as Mol. CD /  $\lambda$  [nm]. UV-vis spectra were recorded on an Agilent, Cary 100 UV-visible spectrophotometer equipped with temperature controller. UV-vis spectra were collected with scan rate of 100 nm/min.

#### IV-10.2. General procedure for UV-vis and CD measurements

UV-vis measurement: The host **IV-40** (1.0  $\mu\text{L}$  of a 0.001M solution in anhydrous dichloromethane, 1.0  $\mu\text{mol}$ ) was added to the solvent (1.0 mL) in a 1.0 cm UV-cell. The background spectrum was recorded from 350 nm to 500 nm at a scan rate of 100 nm/min. The guest molecule (1 up to 500 equivalents) from four different stock solutions in anhydrous dichloromethane [0.1M (for 100-500 equiv), 0.01M (for 10-100 equiv), 0.001M (for 1-10 equiv), 0.0001M (for 0.1-1 equiv)] were then added to the **IV-40** solution. The UV-vis spectra were collected after each addition at room temperature.

CD measurement: **IV-40** (1.0  $\mu\text{L}$  of a 0.001M solution in anhydrous dichloromethane, 1.0  $\mu\text{mol}$ ) was added to the solvent (1.0 mL) in a 1.0 cm CD cell to obtain a 1.0  $\mu\text{M}$  solution. The background spectrum was recorded from 350 nm to 500 nm with a scan rate of 100 nm/min. at room temperature. The guest from a stock solution in anhydrous dichloromethane (0.001 M for 1-10 equiv and 0.01 M for 10-20 equiv) was added to the prepared host solution to afford the host-guest complex. The CD spectra were measured immediately (10 scans). The resultant ECCD spectra recorded in millidegrees were converted the molecular CD (Mol. CD) considering the host concentration of 1.0  $\mu\text{M}$ .

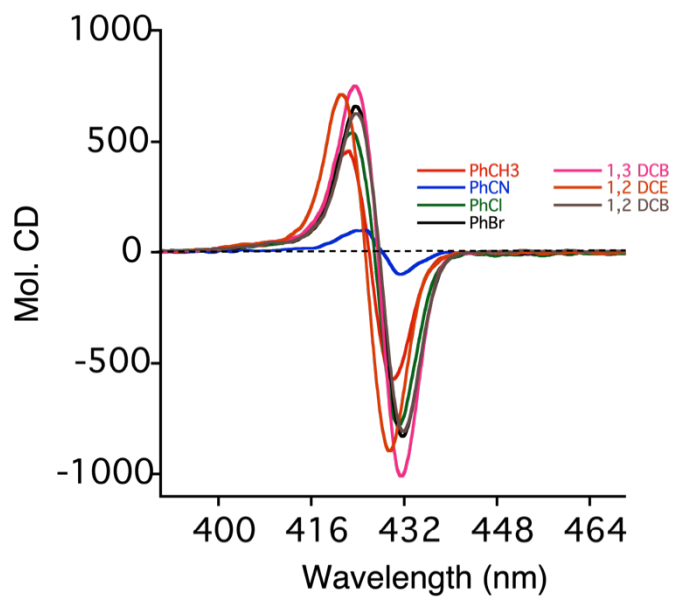


**Figure IV-26.** ECD spectrum of **IV-40** (1  $\mu$ M) complexed with one equivalent of **III-(S,S)-33** in different solvents at room temperature.

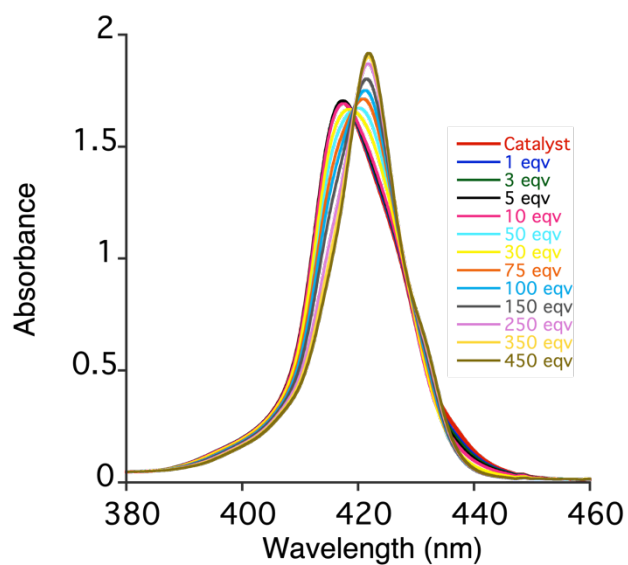


**Figure IV-27.** UV-vis titration of **IV-40** (1  $\mu$ M) with different equivalents of **III-(S,S)-33** in  $\text{CHCl}_3$  at room temperature.



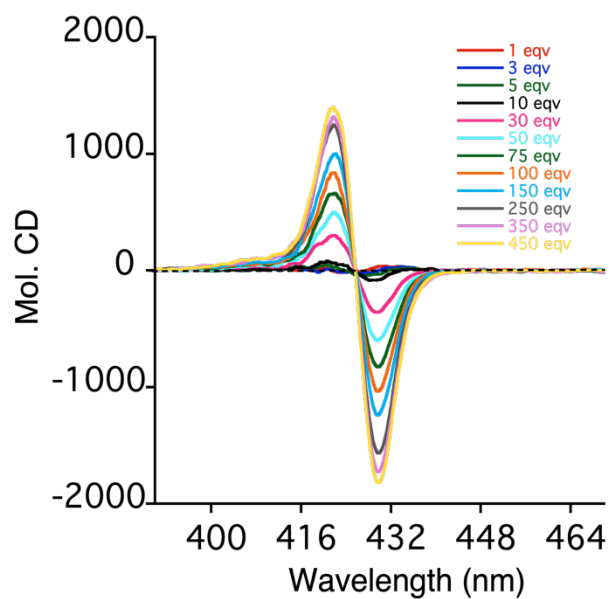


**Figure IV-28.** ECD titration of **IV-40** (1  $\mu\text{M}$ ) with different equivalents of **III-(S,S)-33** in  $\text{CHCl}_3$  at room temperature.

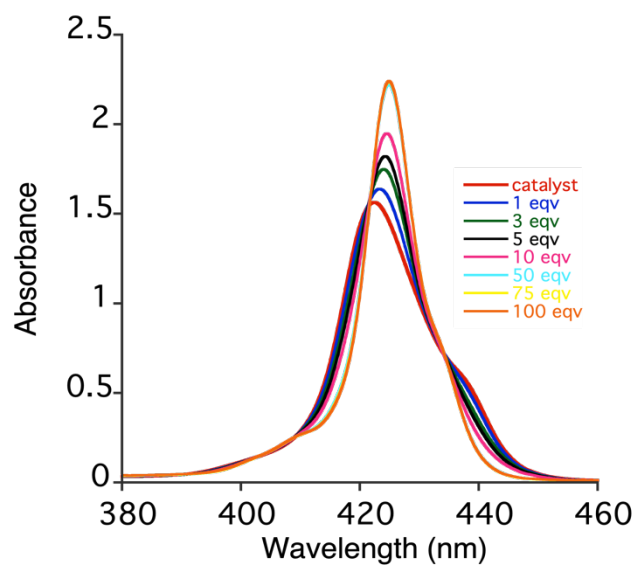


**Figure IV-29.** UV-vis titration of **IV-40** (1  $\mu\text{M}$ ) with different equivalents of **III-(S,S)-33** in 1,3-bromochlorobenzene at room temperature.

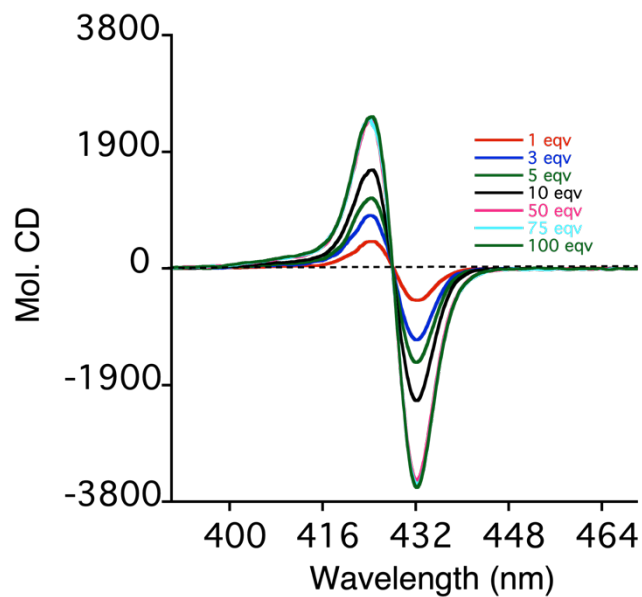


**Figure IV-30.** ECCD titration of **IV-40** (1 μM) with different equivalents of **III-(S,S)-33** in 1,3-bromochlorobenzene at room temperature.

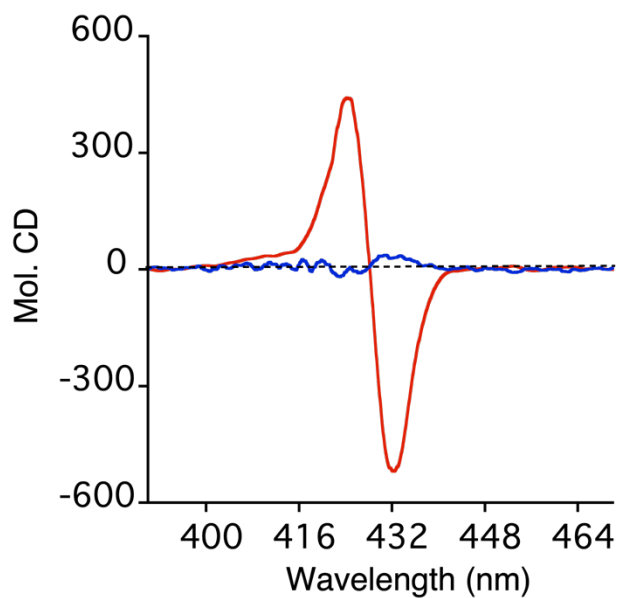


**Figure IV-31.** ECCD spectrum of **IV-40** (1 μM) with one equivalent of **III-(S,S)-33** in 1,3-bromochlorobenzene (red) and chloroform (blue) at room temperature.

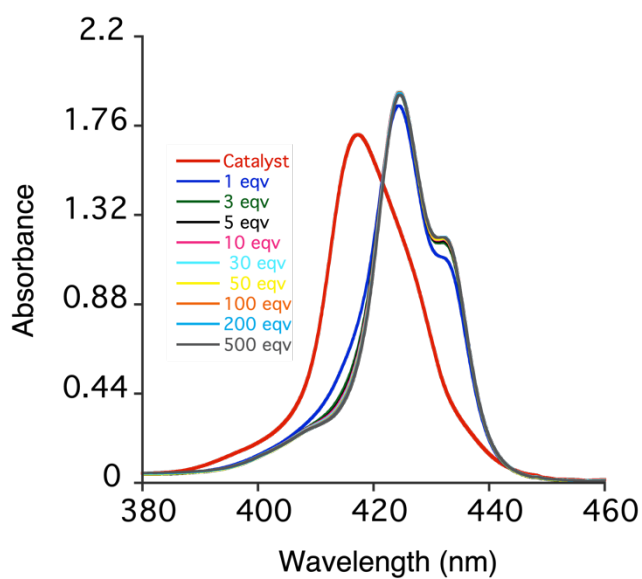


**Figure IV-32.** UV-vis titration of **IV-40** (1  $\mu$ M) with different equivalents of **IV-(S,S)-76** in  $\text{CHCl}_3$  at room temperature.

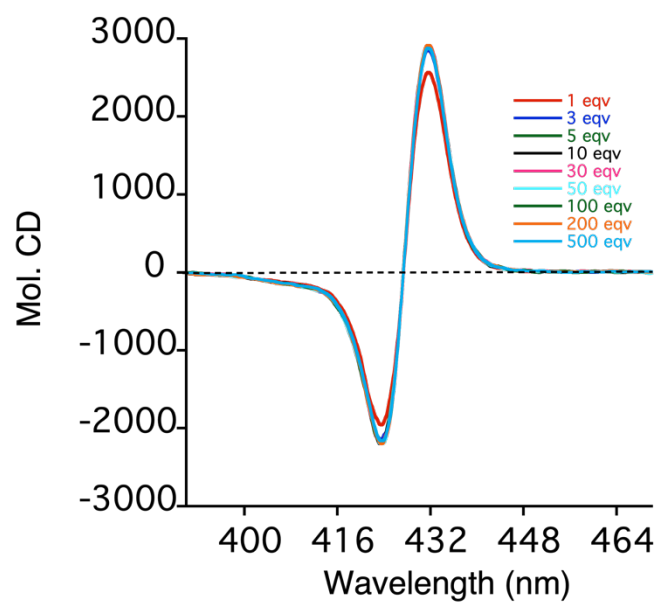
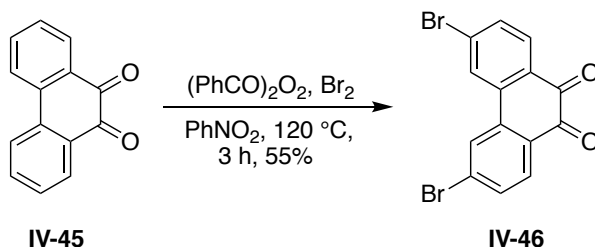


**Figure IV-33.** ECCD titration of **IV-40** (1  $\mu$ M) with different equivalents of **IV-(S,S)-76** in  $\text{CHCl}_3$  at room temperature.

### IV-10.3. Synthesis of catalyst IV-40

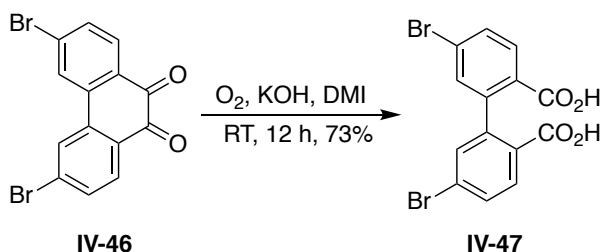


**Synthesis of IV-46:**<sup>38</sup> A mixture of **IV-45** (5.0 g, 0.21 mol), (PhCO)<sub>2</sub>O<sub>2</sub> (500 mg, 21 mmol) and bromine (0.6 mL) in nitrobenzene (40 mL) was heated to 120 °C. After initiation of the reaction, additional bromine (2 mL) was added dropwise. The reaction mixture was stirred for 3 h and then allowed to cool down to RT. Hexane (40 mL) was added to the mixture. The precipitate was filtered, washed with hexane, and dried under vacuum to afford the desired product **IV-46** in 55% yield.

<sup>1</sup>H NMR (500 MHz, Chloroform-*d*) δ 8.12 (d, *J* = 1.7 Hz, 2H), 8.07 (d, *J* = 8.3 Hz, 2H), 7.67 (dd, *J* = 8.3, 1.7 Hz, 2H).

<sup>13</sup>C NMR (126 MHz, Chloroform-*d*) δ 178.93, 136.01, 133.52, 132.20, 132.19, 129.91, 127.48.

HRMS (TOF MS ES+) *m/z*: [M+H]<sup>+</sup> Calcd for C<sub>14</sub>H<sub>7</sub>O<sub>2</sub>Br<sub>2</sub><sup>+</sup> 364.8813; Found 364.8816.

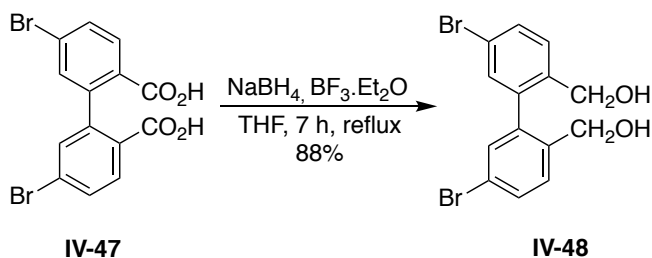


**Synthesis of IV-47**<sup>25</sup>: A mixture of **IV-46** (300 mg, 0.82 mmol), KOH powder (150 mg, 2.68 mmol) in DMI (7 mL) was stirred overnight at RT under oxygen atmosphere (O<sub>2</sub> balloon). The reaction mixture was quenched with 1M HCl (pH = 2-3) and extracted with ether. The organic layer was then washed with brine, dried over Na<sub>2</sub>SO<sub>4</sub>, concentrated *in vacuo*, and purified via column chromatography (60% EtOAc/hexane) to afford the desired product **IV-47** in 73% yield.

<sup>1</sup>H NMR (500 MHz, DMSO-*d*<sub>6</sub>)  $\delta$  12.76 (s, 2H), 7.82 (d, *J* = 8.4 Hz, 2H), 7.67 (dd, *J* = 8.4 Hz, 2.1 Hz, 2H), 7.42 (d, *J* = 2.1 Hz, 2H).

<sup>13</sup>C NMR (126 MHz, DMSO-*d*<sub>6</sub>)  $\delta$  166.79, 143.78, 132.57, 131.63, 130.45, 129.31, 124.92.

HRMS (TOF MS ES-) *m/z*: [M-H]<sup>-</sup> Calcd for C<sub>14</sub>H<sub>7</sub>O<sub>4</sub>Br<sub>2</sub><sup>-</sup> 396.8711; Found 396.8708.



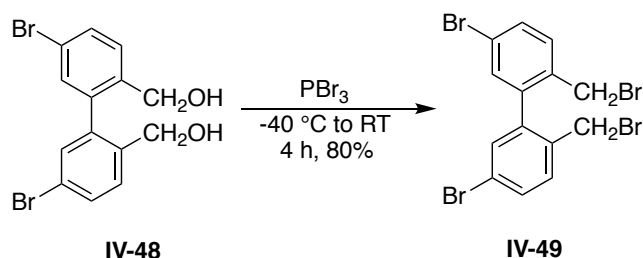
**Synthesis of IV-48**: A solution of BF<sub>3</sub>·OEt<sub>2</sub> (0.48 mL, 3.75 mmol) in dry THF (3 mL) was added slowly to a solution of NaBH<sub>4</sub> (285 mg, 7.50 mmol) and **IV-47** (100 mg, 0.25 mmol) in dry THF (5 mL) under argon atmosphere. The mixture was heated to reflux for 7 h. After cooling down to RT, the reaction was quenched with dropwise addition of H<sub>2</sub>O at 0 °C. The solvent was removed in *vacuo* and the crude mixture was re-dissolved in CH<sub>2</sub>Cl<sub>2</sub> and stirred for 0.5 h. The mixture was then transferred to a separatory funnel and the two

layers separated. The organic layer was washed with brine, dried over Na<sub>2</sub>SO<sub>4</sub>, and concentrated *in vacuo*. Purification by column chromatography (40% EtOAc/hexane) gave the desired product **IV-48** in 88% yield.

<sup>1</sup>H NMR (500 MHz, DMSO-*d*<sub>6</sub>) δ 7.65 – 7.57 (m, 2H), 7.55-7.45 (m, 2H), 7.36 – 7.24 (m, 2H), 5.28-5.10 (m, 2H), 4.20-4.02 (m, 4H).

<sup>13</sup>C NMR (126 MHz, DMSO-*d*<sub>6</sub>) δ 139.24, 138.86, 131.22, 130.74, 129.36, 119.42, 60.11.

HRMS (TOF MS ES-) *m/z*: [M+Cl]<sup>-</sup> Calcd for C<sub>14</sub>H<sub>12</sub>O<sub>2</sub>Br<sub>2</sub>Cl<sup>-</sup> 404.8893; Found 404.8882.

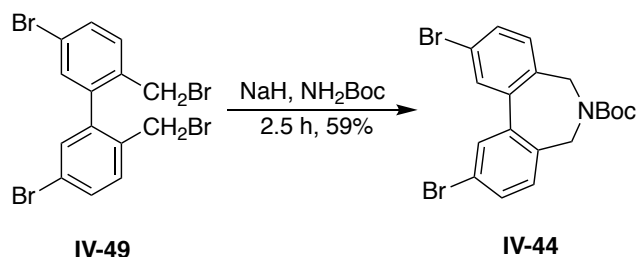


**Synthesis of IV-49:** To a flame dried round bottom flask compound **IV-48** (40 mg, 0.11 mmol) was dissolved in dry CH<sub>2</sub>Cl<sub>2</sub> (2 mL) and PBr<sub>3</sub> (0.22 mL, 1M in CH<sub>2</sub>Cl<sub>2</sub>) was added dropwise at -40 °C under argon atmosphere. The mixture was warmed to RT and stirred for 4 h before being quenched with H<sub>2</sub>O at 0 °C. The crude was extracted with CH<sub>2</sub>Cl<sub>2</sub>, dried over Na<sub>2</sub>SO<sub>4</sub>, and concentrated *in vacuo*. Purification via column chromatography (1-2% EtOAc/hexane) afforded the desired product **IV-49** in 80% yield.

<sup>1</sup>H NMR (500 MHz, Chloroform-*d*) δ 7.57 (dd, *J* = 8.3 Hz, 2.1 Hz, 2H), 7.45-7.39 (m, 4H), 4.27 (d, *J* = 10.3 Hz, 2H), 4.14 (d, *J* = 10.3 Hz, 2H).

<sup>13</sup>C NMR (126 MHz, Chloroform-*d*) δ 139.74, 134.95, 132.79, 132.30, 132.28, 122.40, 30.53.

HRMS (TOF MS AP+) m/z: [M-2HBr+H]<sup>+</sup> Calcd for C<sub>14</sub>H<sub>9</sub>Br<sub>2</sub><sup>+</sup> 334.9071; Found 334.9063.

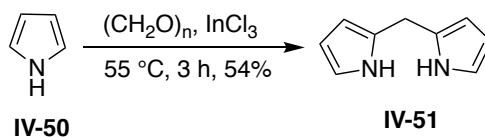


**Synthesis of IV-44:** To a flame dried round bottom flask NaH (80 mg, 2.0 mmol) was suspended in dry DMF (3 mL). To that solution was transferred a mixture of **IV-49** (200 mg, 0.40 mmol) and tert-butyl carbamate (52 mg, 0.44 mmol) in dry DMF (3 mL) dropwise over 10 mins at 0 °C. The mixture was warmed to RT and stirred for 2.5 h before being quenched with H<sub>2</sub>O at 0 °C. The crude was extracted with ethyl acetate, dried over Na<sub>2</sub>SO<sub>4</sub>, and concentrated *in vacuo*. Purification via column chromatography (2% EtOAc/hexane) afforded the desired product **IV-44** in 59% yield.

<sup>1</sup>H NMR (500 MHz, Chloroform-*d*) δ 7.63 (d, *J* = 2.0 Hz, 2H), 7.52 (dd, *J* = 8.1 Hz, 2.1 Hz, 2H), 7.34-7.20 (m, 2H), 4.17 (br, 4H), 1.51 (s, 9H).

<sup>13</sup>C NMR (126 MHz, Chloroform-*d*) δ 154.09, 141.18, 133.33, 131.70, 131.20, 130.93, 80.32, 47.44, 46.64, 28.51.

HRMS (TOF MS ES+) m/z: [M-C<sub>4</sub>H<sub>9</sub>]<sup>+</sup> Calcd for C<sub>15</sub>H<sub>10</sub>Br<sub>2</sub>NO<sub>2</sub><sup>+</sup> 393.9078; Found 393.9079.

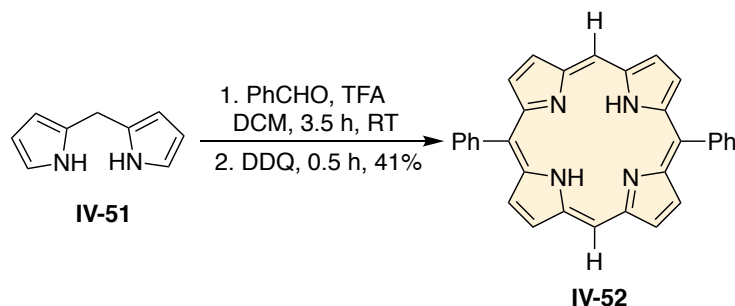


**Synthesis of IV-51:** Paraformaldehyde (350 mg, 11.66 mmol) dissolved in pyrrole (70 mL) was degassed for 15 min. The solution was heated at 55 °C for 10 min before InCl<sub>3</sub> (258 mg, 1.16 mmol) was added. The mixture was stirred at 55 °C for 3 h. After cooling to RT, powdered NaOH (1.86 g, 46.64 mmol) was added and stirred for another 1 h at RT. The mixture was then filtered, and the excess pyrrole was removed via distillation. Purification via column chromatography (10% EtOAc/hexane) gave the desired product **IV-51** in 54% yield.

<sup>1</sup>H NMR (500 MHz, Chloroform-*d*) δ 7.74 (br, 2H), 6.65-6.61 (m, 1H), 6.18-6.14 (m, 2H), 6.07-6.02 (m, 2H), 3.96 (s, 2H).

<sup>13</sup>C NMR (126 MHz, Chloroform-*d*) δ 129.09, 117.36, 108.34, 106.46, 26.36.

HRMS (TOF MS ES+) *m/z*: [M+H]<sup>+</sup> Calcd for C<sub>9</sub>H<sub>9</sub>N<sub>2</sub><sup>+</sup> 145.0766; Found 145.0778.



**Synthesis of IV-52:** **IV-51** (300 mg, 2.08 mmol) was dissolved in 400 mL of CH<sub>2</sub>Cl<sub>2</sub> and degassed for 15 mins. To this solution benzaldehyde (0.21 mL, 2.08 mmol) was added, followed by trifluoroacetic acid (0.1 mL, 1.30 mmol). The round bottom flask was rapidly wrapped with aluminum foil and the mixture was stirred for 3.5 h. To the reaction mixture was added DDQ (613 mg, 2.7 mmol) and stirred for 30 mins. Finally, Et<sub>3</sub>N (2 mL) was added to quench the reaction mixture. The mixture was run through a pad of silica and

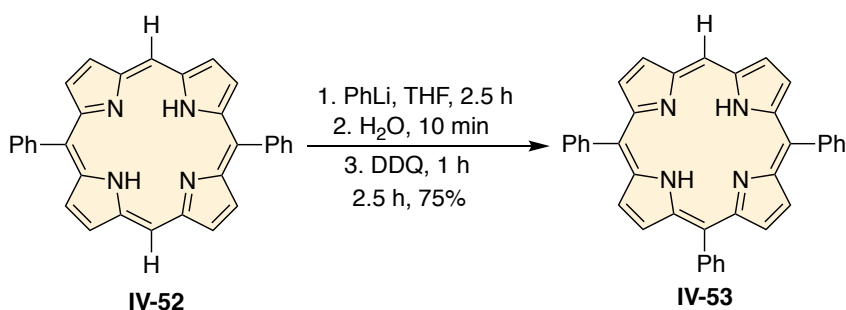


washed with CH<sub>2</sub>Cl<sub>2</sub> until black impurities start appearing. Purification via recrystallization (CH<sub>2</sub>Cl<sub>2</sub>/MeOH) gave the desired product **IV-52** in 41% yield.

<sup>1</sup>H NMR (500 MHz, Chloroform-*d*) δ 10.33 (s, 2H), 9.41 (d, *J* = 4.5 Hz, 4H), 9.09 (d, *J* = 4.5 Hz, 4H), 8.31 – 8.26 (m, 4H), 7.84-7.80 (m, 6H), -3.11 (s, 2H).

<sup>13</sup>C NMR (126 MHz, Chloroform-*d*) δ 147.31, 145.33, 141.52, 135.00, 131.76, 131.20, 127.86, 127.12, 119.24, 105.41.

HRMS (TOF MS ES+) *m/z*: [M+H]<sup>+</sup> Calcd for C<sub>32</sub>H<sub>23</sub>N<sub>4</sub><sup>+</sup> 463.1923; Found 463.1923.



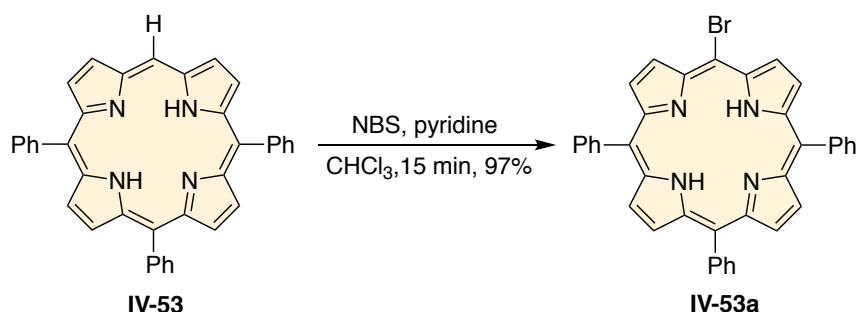
**Synthesis of IV-53**<sup>27</sup>: To a flame dried round bottom flask compound **IV-52** (462 mg, 1 mmol) was dissolved in dry THF (250 mL). To that solution was added PhLi (13 mL, 1.9 M in Bu<sub>2</sub>O) at -78 °C under argon atmosphere. The solution was stirred at that temperature for 30 min and then warmed to RT. After stirring at RT for 2.5 h, H<sub>2</sub>O (9 mL) was added to the mixture and stirred for further 30 min before DDQ (1.20 g, 5.27 mmol) was added. The mixture was stirred for 0.5 h and filtered under suction. The filtrate was concentrated *in vacuo*, dissolved in CH<sub>2</sub>Cl<sub>2</sub>, and washed with water, followed by brine. The crude was then dried over Na<sub>2</sub>SO<sub>4</sub>, concentrated *in vacuo*, re-dissolved in CH<sub>2</sub>Cl<sub>2</sub> and passed through a pad of silica, washed with CH<sub>2</sub>Cl<sub>2</sub>. The solvent was removed again and MeOH was added to allow precipitation. The precipitate was filtered, and the residue

was further purified via recrystallization (CH<sub>2</sub>Cl<sub>2</sub>/MeOH) to afford the desired compound **IV-53** in 75% yield.

<sup>1</sup>H NMR (500 MHz, Chloroform-*d*) δ 10.23 (s, 1H), 9.35 (d, *J* = 4.6 Hz, 2H), 9.03 (d, *J* = 4.6 Hz, 2H), 8.90 (ABq, 4.8 Hz, 4H), 8.27 – 8.21 (m, 6H), 7.82 – 7.73 (m, 9H), -2.99 (s, 2H).

<sup>13</sup>C NMR (126 MHz, Chloroform-*d*) δ 142.72, 141.91, 134.85, 134.65, 131.60, 131.44, 130.86, 127.86, 126.97, 126.70, 120.73, 119.78, 104.94.

HRMS (TOF MS ES+) *m/z*: [M+H]<sup>+</sup> Calcd for C<sub>38</sub>H<sub>27</sub>N<sub>4</sub><sup>+</sup> 539.2236; Found 539.2231.



**Synthesis of IV-53a:** Pyridine (89 μL, 1.1 mmol) was added to a solution of compound **IV-53** (118 mg, 0.22 mmol) in chloroform (40 mL). The solution was cooled to 0 °C and NBS (66mg, 0.37 mmol) was added. The mixture was stirred at that temperature and then quenched with acetone (3 mL). The solvent was removed in vacuo, the crude was dissolved in CH<sub>2</sub>Cl<sub>2</sub> and washed with brine solution. The organic layer was dried over Na<sub>2</sub>SO<sub>4</sub> and concentrated in vacuo to afford **IV-54** in 97% yield.

<sup>1</sup>H NMR (500 MHz, Chloroform-*d*) δ 9.68 (d, *J* = 4.8 Hz, 2H), 8.91 (d, *J* = 4.8 Hz, 2H), 8.81 (s, 4H), 8.23 – 8.17 (m, 6H), 7.83 – 7.72 (m, 9H), -2.74 (s, 2H).

$^{13}\text{C}$  NMR (126 MHz, Chloroform-*d*)  $\delta$  141.89, 141.79, 134.58, 134.51, 134.47, 127.91, 127.88, 126.79, 121.03, 120.83, 102.93.

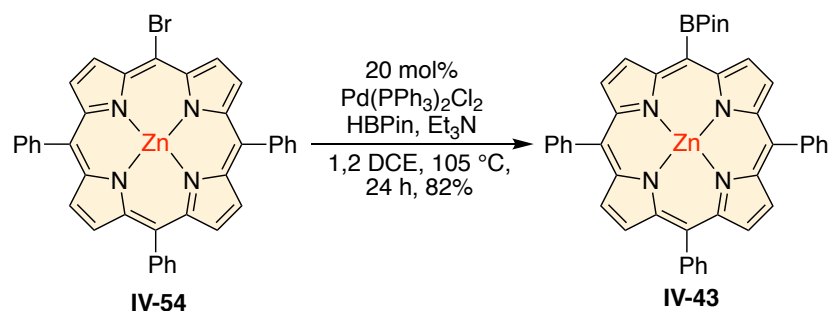
HRMS (TOF MS ES+)  $m/z$ :  $[\text{M}+\text{H}]^+$  Calcd for  $\text{C}_{38}\text{H}_{26}\text{BrN}_4^+$  617.1341; Found 617.1335.



**Synthesis of IV-54:** To a solution of **IV-54** (88 mg, 0.14 mmol) in  $\text{CHCl}_3$  (30 mL) and MeOH (10 mL) at RT was added  $\text{Zn}(\text{OAc})_2 \cdot 2\text{H}_2\text{O}$  (628 mg, 2.85 mmol) in one portion. The reaction mixture was stirred for 12 h, after which it was suction filtered, and the filtrate was concentrated in vacuo. The resulting pink solids were re-dissolved in  $\text{CH}_2\text{Cl}_2$ , washed with  $\text{H}_2\text{O}$ , brine, dried over  $\text{Na}_2\text{SO}_4$ , and concentrated in vacuo to give the title compound **IV-55** in quantitative yield.

$^1\text{H}$  NMR (500 MHz, Chloroform-*d*)  $\delta$  9.76 (d,  $J = 4.7$  Hz, 2H), 8.98 (d,  $J = 4.7$  Hz, 2H), 8.88 (s, 4H), 8.21-8.15 (m, 6H), 7.80 – 7.70 (m, 9H).

HRMS (TOF MS ES+)  $m/z$ :  $[\text{M}+\text{H}]^+$  Calcd for  $\text{C}_{38}\text{H}_{24}\text{BrN}_4\text{Zn}^+$  679.0476; Found 679.0457.

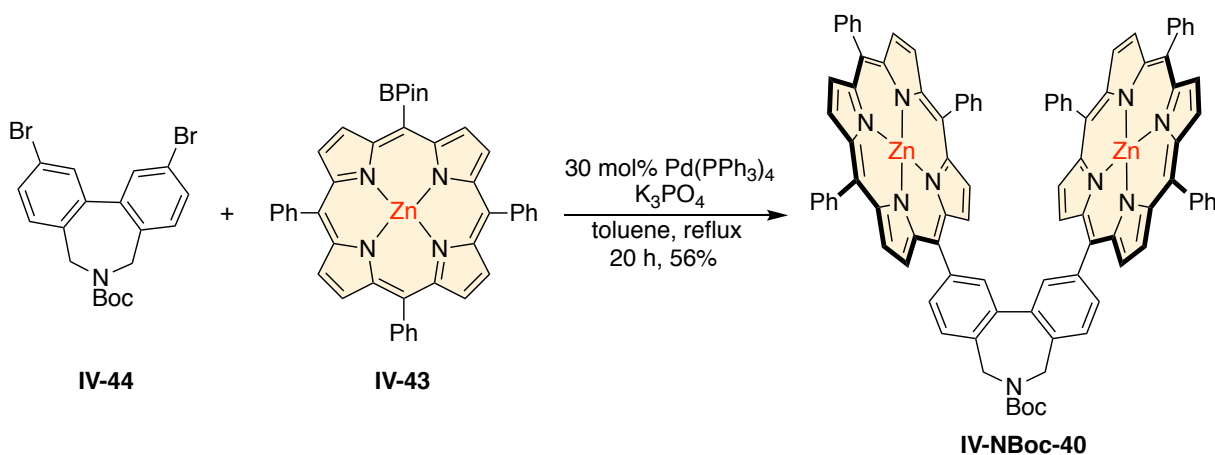


**Synthesis of IV-43**<sup>26</sup>: To a flame dried round bottom flask was added 1,2 dichloroethane (120 mL) and degassed for 30 min. To that flask **IV-54** (600 mg, 0.88 mmol), pinacolborane (4.5 mL, 30.8 mmol), triethylamine (1.6 mL, 11.44 mmol) and Pd(PPh<sub>3</sub>)<sub>2</sub>Cl<sub>2</sub> (124 mg, 0.18 mmol) were added sequentially under an argon atmosphere. The mixture was refluxed for 12 h before cooling down to RT. The solvent was then removed in vacuo and the crude was dissolved in dichloromethane, washed with H<sub>2</sub>O, and dried over Na<sub>2</sub>SO<sub>4</sub>. The crude was purified via column chromatography (8% EtOAc/hexane) to afford the desired product **IV-43** in 82% yield.

<sup>1</sup>H NMR (500 MHz, Chloroform-*d*) δ 9.95 (d, *J* = 4.7 Hz, 2H), 9.11 (d, *J* = 4.7 Hz, 2H), 8.95 (ABq, 4.7 Hz, 4H), 8.27-8.21 (m, 6H), 7.81 – 7.72 (m, 9H), 1.87 (s, 12H).

<sup>13</sup>C NMR (126 MHz, Chloroform-*d*) δ 154.47, 150.45, 150.05, 149.38, 142.91, 142.81, 134.53, 134.39, 133.04, 132.91, 132.20, 131.59, 127.58, 127.52, 126.58, 126.56, 122.67, 121.01, 85.30, 25.40.

HRMS (TOF MS ES+) *m/z*: [M+H]<sup>+</sup> Calcd for C<sub>44</sub>H<sub>36</sub>BN<sub>4</sub>O<sub>2</sub>Zn<sup>+</sup> 727.2223; Found 727.2195.



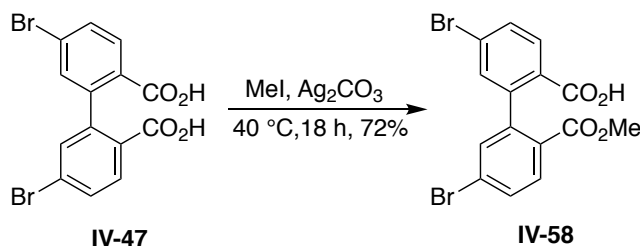
**Synthesis of IV-NBoc-40**<sup>28</sup>: K<sub>3</sub>PO<sub>4</sub> (53 mg, 0.25 mmol) was added to an oven dried round bottom flask. The flask was flame dried under vacuum and filled with argon. To the flask was then added toluene (5.4 mL), **IV-43** (65 mg, 0.089 mmol), **IV-44** (10 mg, 0.022 mmol) under argon atmosphere and the mixture was degassed for 30 min. Finally, Pd(PPh<sub>3</sub>)<sub>4</sub> (7.6 mg, 0.0066 mmol) was added to the mixture and refluxed for 20 h before cooling down to room temperature. The solvent was removed in vacuo and the crude was dissolved in CH<sub>2</sub>Cl<sub>2</sub>. The organic layer was washed with H<sub>2</sub>O, followed by brine solution, dried over Na<sub>2</sub>SO<sub>4</sub>, and concentrated in vacuo. Purification by column chromatography (12% EtOAc/hexane) gave **IV-NBoc-40** in 56% yield.

<sup>1</sup>H NMR (500 MHz, Chloroform-*d*) δ 8.96 – 8.84 (m, 12H), 8.80 (br, 4H), 8.52 (s, 2H), 8.29 (br, 2H), 8.23 – 8.11 (m, 8H), 8.00 (br, 4H), 7.95 – 7.84 (m, 2H), 7.80 – 7.62 (m, 14H), 7.54 (br, 4H), 4.89 (br, 4H), 1.69 (s, 9H).

<sup>13</sup>C NMR (126 MHz, Chloroform-*d*) δ 154.38, 150.32, 150.30, 150.26, 150.11, 143.52, 142.88, 142.77, 138.84, 134.53, 134.51, 134.45, 134.25, 134.04, 132.27, 132.12, 132.10, 131.88, 128.63, 128.02, 127.60, 127.52, 126.65, 126.59, 126.54, 121.35, 121.28, 120.18, 80.43, 48.61, 47.75, 28.73.

HRMS (TOF MS ES+)  $m/z$ :  $[M+H]^+$  Calcd for  $C_{95}H_{66}N_9O_2Zn_2^+$  1492.3922; Found 1492.3794.

#### IV-10.4. Synthesis of catalyst IV-57

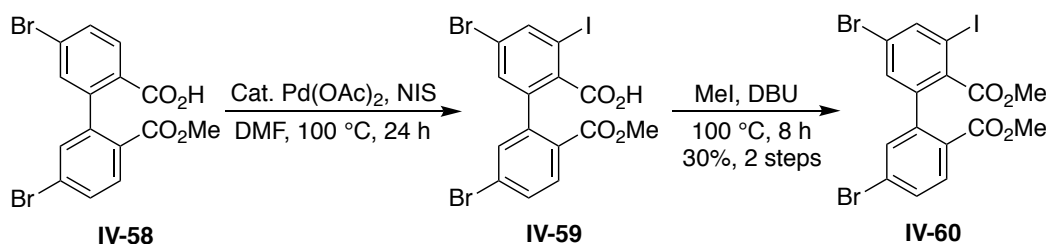


**Synthesis of IV-58**<sup>39</sup>: To a solution of **IV-47** (160 mg, 0.40 mmol) and  $Ag_2CO_3$  (55 mg, 0.20 mmol) in a sealed tube, MeI (75  $\mu$ L, 1.20 mmol) was added. The mixture was warmed to 40 °C and stirred for 18 h. After cooling to RT, the reaction was quenched with 2M HCl (12 mL). The crude mixture was then extracted with EtOAc (3x20 mL) and the combined organic layer was washed with  $H_2O$ , brine and dried over  $Na_2SO_4$ . Purification by column chromatography (30% EtOAc/hexane) resulted the final product **IV-58** in 72% yield.

$^1H$  NMR (500 MHz, Chloroform- $d$ )  $\delta$  7.94 (d,  $J$  = 8.4 Hz, 1H), 7.89 (d,  $J$  = 8.4 Hz, 1H), 7.61 (dd,  $J$  = 8.4, 2.0 Hz, 1H), 7.58 (dd,  $J$  = 8.4, 2.0 Hz, 1H), 7.35 (d,  $J$  = 2.1 Hz, 1H), 7.34 (d,  $J$  = 2.0 Hz, 1H), 3.66 (s, 3H).

$^{13}C$  NMR (126 MHz, Chloroform- $d$ )  $\delta$  168.42, 166.39, 144.02, 143.40, 133.01, 132.91, 132.02, 131.54, 130.97, 130.96, 127.84, 127.24, 127.00, 126.56, 52.21.

HRMS (TOF MS ES-)  $m/z$ :  $[M-H]^-$  Calcd for  $C_{15}H_9O_4Br_2^-$  410.8868; Found 410.8865.

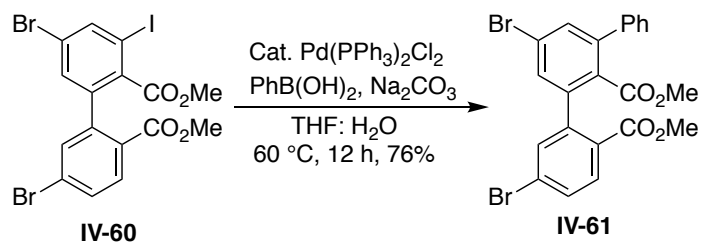


**Synthesis of IV-60<sup>40</sup>:** A mixture of **IV-58** (300 mg, 0.72 mmol), Pd(OAc)<sub>2</sub> (16 mg, 0.072 mmol) and N-iodosuccinimide (212 mg, 0.94 mmol) in DMF (3.6 mL) was stirred for 24 h at 100 °C in a sealed tube. After cooling to RT, the mixture was diluted with ethyl acetate (150 mL). The organic layer was then washed with 0.5 M HCl (4x30 mL), followed by brine, dried over Na<sub>2</sub>SO<sub>4</sub> and concentrated in vacuo. To the crude, dissolved in 3 mL dry THF was added DBU (0.26 mL, 1.75 mmol). MeI (0.44 mL, 7.2 mmol) was added and stirred at 100 °C for 8 h. The mixture was cooled to RT and quenched with 3M HCl (20 mL). The crude mixture was extracted with ethyl acetate, washed with brine, dried over Na<sub>2</sub>SO<sub>4</sub> and concentrated in vacuo. Purification by column chromatography (3% EtOAc/hexane) resulted the final product **IV-60** in 30% yield.

<sup>1</sup>H NMR (500 MHz, Chloroform-*d*) δ 8.02 (d, *J* = 1.8 Hz, 1H), 7.85 (d, *J* = 8.4 Hz, 1H), 7.60 (dd, *J* = 8.4, 2.0 Hz, 1H), 7.42 (d, *J* = 2.0 Hz, 1H), 7.40 (d, *J* = 1.8 Hz, 1H), 3.69 (s, 3H), 3.58 (s, 3H).

<sup>13</sup>C NMR (126 MHz, Chloroform-*d*) δ 167.65, 166.01, 141.09, 140.47, 140.42, 137.56, 133.63, 131.85, 131.83, 131.61, 128.67, 126.45, 123.43, 92.13, 52.47, 52.33.

HRMS (TOF MS ES+) *m/z*: [M+H]<sup>+</sup> Calcd for C<sub>16</sub>H<sub>12</sub>O<sub>4</sub>Br<sub>2</sub><sup>+</sup> 552.8147; Found 552.8149.

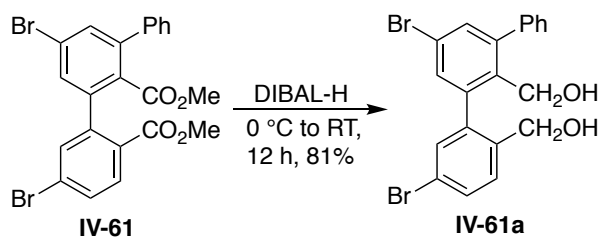


**Synthesis of IV-61:** To a solution of anhydrous THF (0.8 mL) and degassed H<sub>2</sub>O (0.2 mL) were added **IV-60** (100 mg, 0.18 mmol), PhB(OH)<sub>2</sub> (26 mg, 0.21 mmol) and Na<sub>2</sub>CO<sub>3</sub> (40 mg, 0.36) sequentially. Pd(PPh<sub>3</sub>)Cl<sub>2</sub> (12.8 mg, 0.018 mmol) was then added to the mixture and stirred at 60 °C for 12 h. After cooling to RT, H<sub>2</sub>O was added and the mixture was extracted with ethyl acetate. The organic layer was dried over Na<sub>2</sub>SO<sub>4</sub> and concentrated in vacuo. Purification by column chromatography (3% EtOAc/hexane) afforded the desired product **IV-61** in 76% yield.

<sup>1</sup>H NMR (500 MHz, Chloroform-*d*) δ 7.86 (d, *J* = 8.4 Hz, 1H), 7.59 (dd, *J* = 8.4, 2.0 Hz, 1H), 7.58 (d, *J* = 1.9 Hz, 1H), 7.49 (d, *J* = 2.0 Hz, 1H), 7.41 (d, *J* = 2.0 Hz, 1H), 7.40 – 7.34 (m, 5H), 3.68 (s, 3H), 3.27 (s, 3H).

<sup>13</sup>C NMR (126 MHz, Chloroform-*d*) δ 168.31, 166.38, 142.01, 141.48, 141.01, 139.22, 133.95, 133.75, 131.95, 131.74, 131.43, 130.91, 130.68, 130.24, 129.02, 128.47, 128.17, 128.04, 126.33, 123.20, 52.23, 51.88.

HRMS (TOF MS ES+) *m/z*: [M+H]<sup>+</sup> Calcd for C<sub>22</sub>H<sub>17</sub>O<sub>4</sub>Br<sub>2</sub><sup>+</sup> 502.9494; Found 502.9492.



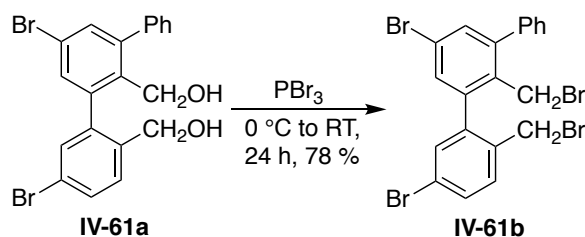


**Synthesis of IV-61a:** To a flame dried round bottom flask was added substrate **IV-61** (41 mg, 0.08 mmol) in dry CH<sub>2</sub>Cl<sub>2</sub> (0.5 mL). The solution was cooled to 0 °C and DIBAL-H (1 mL, 1M in hexane) was added dropwise under argon atmosphere. The mixture was warmed to RT and stirred for 12 h. The mixture was quenched with MeOH, poured onto sodium potassium tartrate solution and stirred for 15 mins. The crude was extracted with CH<sub>2</sub>Cl<sub>2</sub>, dried over Na<sub>2</sub>SO<sub>4</sub>, concentrated in vacuo and purified via column chromatography to afford the desired product **IV-61a** in 81% yield.

<sup>1</sup>H NMR (500 MHz, Chloroform-*d*) δ 7.56 (dd, *J* = 8.2, 2.1 Hz, 1H), 7.53 (d, *J* = 2.1 Hz, 1H), 7.50 – 7.39 (m, 6H), 7.36 (d, *J* = 2.1 Hz, 1H), 7.33 (d, *J* = 2.1 Hz, 1H), 4.40 (ABq, *J* = 11.9 Hz, 2H), 4.24 (ABq, *J* = 11.3 Hz, 2H), 3.41 (b, 1H), 2.68 (b, 1H).

<sup>13</sup>C NMR (126 MHz, Chloroform-*d*) δ 145.72, 142.11, 140.89, 139.36, 138.08, 134.57, 133.04, 132.28, 132.11, 132.03, 131.82, 131.66, 131.52, 129.27, 128.36, 127.93, 121.56, 121.44, 61.99, 58.94.

HRMS (TOF MS ES+) *m/z*: [M-H<sub>2</sub>O+H]<sup>+</sup> Calcd for C<sub>20</sub>H<sub>15</sub>OBr<sub>2</sub><sup>+</sup> 428.9490; Found 428.9472.



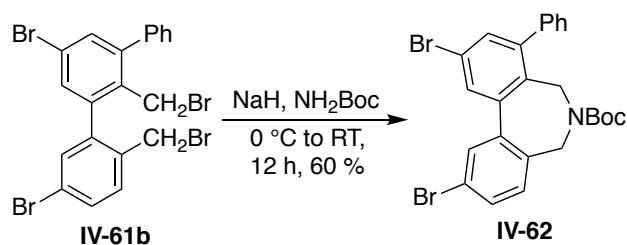
**Synthesis of IV-61b:** To a flame dried round bottom flask compound **IV-61a** (22 mg, 0.05 mmol) was dissolved in dry CH<sub>2</sub>Cl<sub>2</sub> (1 mL) and PBr<sub>3</sub> (0.1 mL, 1M in CH<sub>2</sub>Cl<sub>2</sub>) was added dropwise at 0 °C under argon atmosphere. The mixture was warmed to RT and stirred for

24 h before being quenched with H<sub>2</sub>O at 0 °C. The crude was extracted with CH<sub>2</sub>Cl<sub>2</sub>, dried over Na<sub>2</sub>SO<sub>4</sub>, and concentrated in vacuo. Purification via column chromatography (hexane) afforded the desired product **IV-61b** in 78% yield.

<sup>1</sup>H NMR (500 MHz, Chloroform-*d*) δ 7.58 (dd, *J* = 8.3, 2.1 Hz, 1H), 7.51 – 7.49 (m, 2H), 7.48 – 7.42 (m, 7H), 4.21 (ABq, *J* = 2.6 Hz, 2H), 4.19 (ABq, *J* = 10.3 Hz, 2H).

<sup>13</sup>C NMR (126 MHz, Chloroform-*d*) δ 145.45, 140.92, 140.04, 138.80, 134.89, 133.70, 132.90, 132.46, 132.28, 132.26, 132.08, 128.88, 128.43, 128.14, 122.29, 122.14, 30.91, 29.41.

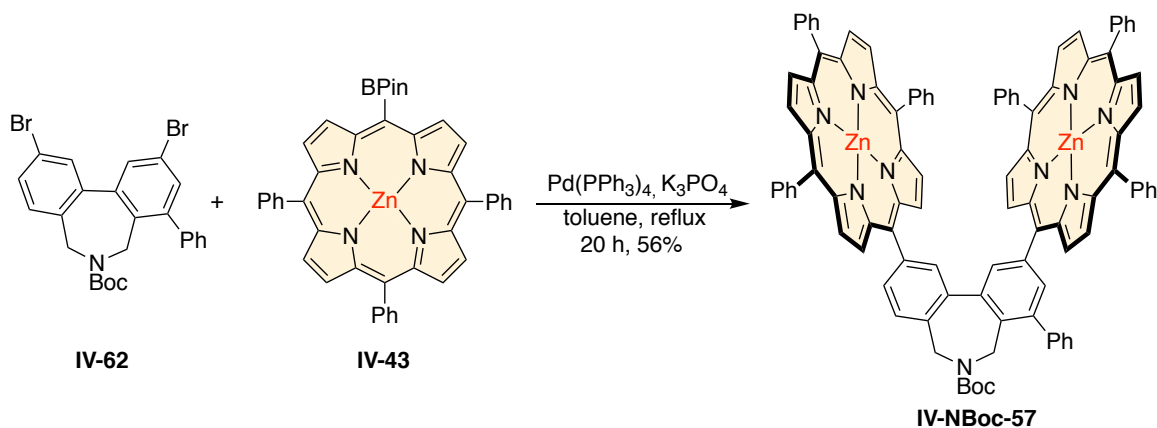
HRMS (TOF MS AP+) *m/z*: [M-2HBr+H]<sup>+</sup> Calcd for C<sub>20</sub>H<sub>13</sub>Br<sub>2</sub><sup>+</sup> 410.9384; Found 410.9365.



**Synthesis of IV-62:** To a flame dried round bottom flask NaH (12 mg, 0.30 mmol) was suspended in dry DMF (0.3 mL). To that solution was transferred a mixture of **IV-61b** (24 mg, 0.042 mmol) and tert-butyl carbamate (6.3 mg, 0.054 mmol) in dry DMF (0.3 mL) dropwise over 10 min at 0 °C. The mixture was warmed to RT and stirred 12 h before being quenched with H<sub>2</sub>O at 0 °C. The crude was extracted with ethyl acetate, dried over Na<sub>2</sub>SO<sub>4</sub>, and concentrated in vacuo. Purification via column chromatography (2% EtOAc/hexane) afforded the desired product **IV-62** in 60% yield.

$^1\text{H}$  NMR (500 MHz, Chloroform-*d*)  $\delta$  7.75 (d,  $J$  = 2.0 Hz, 1H), 7.67 (d,  $J$  = 2.0 Hz, 1H), 7.64 (d,  $J$  = 2.0 Hz, 1H), 7.60 (dd,  $J$  = 8.0, 2.0 Hz, 1H), 7.54 – 7.46 (m, 4H), 7.46 – 7.40 (m, 1H), 7.35 (d,  $J$  = 8.0 Hz, 1H), 4.45 (s, 2H), 4.19 (s, 2H), 1.57 (s, 9H).

$^{13}\text{C}$  NMR (126 MHz, Chloroform-*d*)  $\delta$  153.51, 144.87, 142.47, 141.46, 139.45, 133.19, 132.98, 131.91, 131.48, 130.79, 130.52, 130.09, 129.32, 128.48, 127.81, 122.40, 121.81, 80.04, 46.25, 43.61, 28.17.



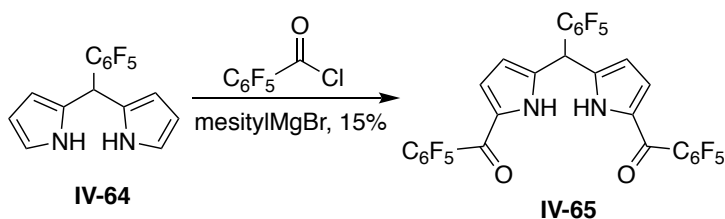
**Synthesis of IV-NBoc-57**<sup>28</sup>:  $\text{K}_3\text{PO}_4$  (53 mg, 0.25 mmol) was added to an oven dried round bottom flask. The flask was flame dried under vacuum and filled with argon. To the flask was then added toluene (5.4 mL), **IV-43** (65 mg, 0.089 mmol), **IV-62** (11.6 mg, 0.022 mmol) under argon atmosphere and the mixture was degassed for 30 min. Finally,  $\text{Pd(PPh}_3)_4$  (7.6 mg, 0.066 mmol) was added to the mixture and refluxed for 20 h before cooling down to room temperature. The solvent was removed in vacuo and the crude was dissolved in  $\text{CH}_2\text{Cl}_2$ . The organic layer was washed with  $\text{H}_2\text{O}$ , followed by brine solution, dried over  $\text{Na}_2\text{SO}_4$ , and concentrated in vacuo. Purification by column chromatography (15% EtOAc/hexane) gave **IV-NBoc-40** in 72% yield.

$^1\text{H}$  NMR (500 MHz, Chloroform-*d*)  $\delta$  8.87 (br, 16H), 8.57 (br, 1H), 8.57 (br, 1H), 8.31 (br, 2H), 8.21 – 8.06 (m, 9H), 7.96 (d,  $J = 7.6$  Hz, 2H), 7.88 (br, 1H), 7.80 – 7.59 (m, 17H), 7.56 – 7.48 (m, 3H), 7.56 – 7.48 (m, 2H), 5.54 (br, 4H), 1.52 (s, 9H).

$^{13}\text{C}$  NMR (126 MHz, Chloroform-*d*)  $\delta$  153.76, 150.19, 150.16, 150.15, 150.13, 150.01, 143.34, 142.72, 142.61, 141.13, 140.97, 140.07, 139.07, 136.03, 134.37, 134.31, 134.14, 133.82, 133.53, 132.19, 132.13, 131.98, 131.96, 131.79, 130.98, 129.97, 128.46, 128.25, 127.48, 127.39, 126.52, 126.45, 121.25, 121.22, 121.16, 120.12, 119.86, 80.05, 47.32, 44.50, 28.28.

HRMS (TOF MS ES+)  $m/z$ :  $[\text{M}+2\text{H}]^{2+}$  Calcd for  $\text{C}_{101}\text{H}_{71}\text{N}_9\text{O}_2\text{Zn}_2^{2+}$  784.7157; Found 784.7111.

#### IV-10.5. Synthesis of catalyst IV-70

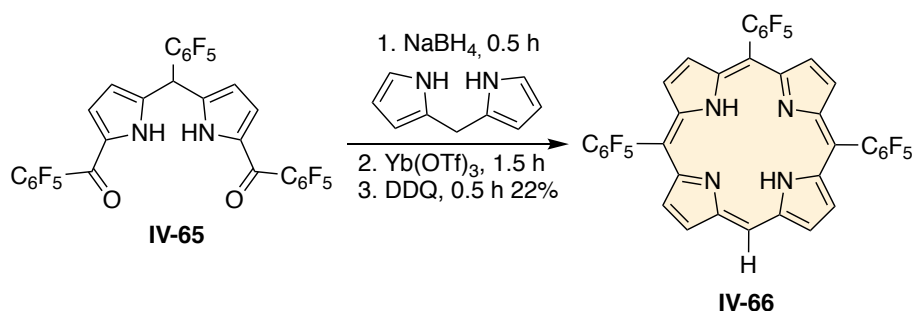


**Synthesis of IV-65<sup>41</sup>:** To a flame-dried round bottom flask substrate **IV-64** (906 mg, 2.90 mmol) was added to toluene (5.8 mL) under argon atmosphere, and stirred for 10 min. The solution was then cooled to 0 °C, after which mesitylMgBr (1 M in THF, 12.2 mL, 12.2 mmol) was added dropwise over 15 min, and stirred for a further 30 min at 0 °C. Following this, 2,3,4,5,6- pentafluorobenzoyl chloride (0.85 mL, 5.89 mmol) was added dropwise, and the reaction was maintained at 0 °C for another 1 h. The mixture was then poured onto 100 mL of cold sat. aq. NH<sub>4</sub>Cl solution and extracted with EtOAc (100 mL). The organic layer was washed with brine, dried over Na<sub>2</sub>SO<sub>4</sub>, and finally concentrated in vacuo. Purification via column chromatography (10% EtOAc/hexane) resulted the final product **IV-65** in 15% yield.

<sup>1</sup>H NMR (500 MHz, DMSO-*d*<sub>6</sub>) δ 12.72 (br, 2H), 6.90-6.85 (m, 2H), 6.05 (s, 1H), 6.03-6.00 (m, 2H).

<sup>19</sup>F NMR (470 MHz, DMSO-*d*<sub>6</sub>) δ -140.84– -140.99 (m, 2F), -142.43 – -142.60 (m, 4F), -152.86 (t, *J* = 22.2 Hz, 2F), -155.73 (t, *J* = 22.4 Hz, 1F), -160.71 – -160.94 (m, 4F), -162.2 – -162.38 (m, 2F).

HRMS (TOF MS ES+) *m/z*: [M+H]<sup>+</sup> Calcd for C<sub>29</sub>H<sub>10</sub>N<sub>2</sub>O<sub>2</sub>F<sub>15</sub><sup>+</sup> 701.0346; Found 701.0339.

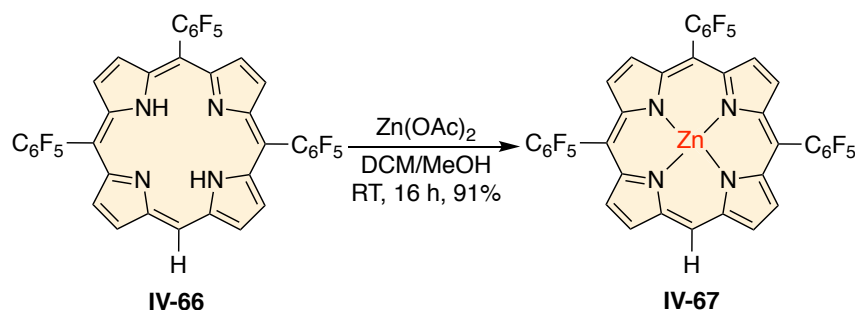


**Synthesis of IV-66<sup>41</sup>:** To a solution of **IV-65** (200 mg, 0.286 mmol), THF (8.6 mL) and MeOH (2.9 mL) at RT was added NaBH4 (540.2 mg, 14.3 mmol) portion wise over 10 min. Following the addition, the reaction mixture was stirred for 20 min, after which it was poured into a separating funnel consisting of sat. aq. NH4Cl (60 mL) and ethyl acetate (60 mL). The layers were separated, and the organic layer was washed with H2O (60 mL), brine (60 mL), dried (Na2SO4), and transferred to a 250 mL round bottom flask before being concentrated in vacuo. The flask containing the crude material was purged with a stream of argon for 5 min after which CH2Cl2 (114 mL) and **IV-51** (41.8 mg, 0.286 mmol) were added sequentially. The mixture was then heated to 34 °C and Yb(OTf)3 (234.2 mg, 0.38 mmol) added in one portion. The mixture was stirred for 1 h 30 min at 34 °C after which it was cooled to RT and DDQ (194.8 mg, 0.858 mmol) was added. Following an additional 30 min stirring, Et3N (0.26 mL, 1.85 mmol) was added dropwise to the reaction. The reaction mixture was filtered through a pad of SiO2 eluting with CH2Cl2 and the solvent was removed in vacuo. Purification by column chromatography (20% CH2Cl2/hexane) afforded the title compound **IV-66** in 22% yield.

<sup>1</sup>H NMR (500 MHz, Chloroform-*d*)  $\delta$  10.39 (s, 1H), 9.48 (d, *J* = 4.7 Hz, 2H), 8.98 (d, *J* = 4.6 Hz, 2H), 8.96 – 8.90 (m, 4H), -3.13 (br, 2H).

$^{19}\text{F}$  NMR (470 MHz, Chloroform-*d*)  $\delta$  -136.46 – -136.64 (m, 6F), -151.70 (t,  $J$  = 20.8 Hz, 3F), -161.47 – -161.70 (m, 6F).

HRMS (TOF MS ES+)  $m/z$ :  $[\text{M}+\text{H}]^+$  Calcd for  $\text{C}_{38}\text{H}_{12}\text{N}_4\text{F}_{15}^+$  809.0822; Found 809.0811.



**Synthesis of IV-67<sup>41</sup>:** To a solution of **IV-66** (409 mg, 0.51 mmol) in  $\text{CHCl}_3$  (90 mL) and MeOH (30 mL) at RT was added  $\text{Zn(OAc)}_2 \cdot 2\text{H}_2\text{O}$  (2.78 g, 12.8 mmol) in one portion. The reaction mixture was stirred for 16 h, after which it was suction filtered, and the filtrate was concentrated in vacuo. The resulting pink solids were re-dissolved in  $\text{CH}_2\text{Cl}_2$  (300 mL), washed with  $\text{H}_2\text{O}$ , brine (500 mL), dried ( $\text{Na}_2\text{SO}_4$ ), and concentrated in vacuo. Purification by column chromatography (Hexane: $\text{CH}_2\text{Cl}_2$ , 1:1) gave the title compound **IV-67** in 91% yield.

$^1\text{H}$  NMR (500 MHz, Chloroform-*d*)  $\delta$  10.42 (s, 1H), 9.54 (d,  $J$  = 4.5 Hz, 2H), 9.06 (d,  $J$  = 4.5 Hz, 2H), 9.04 – 8.97 (m, 4H).

$^{19}\text{F}$  NMR (470 MHz, Chloroform-*d*)  $\delta$  -136.67 - 137.20 (m, 6F), -152.05 – -153.14 (m, 6F), -161.68 - 162.24 (m, 6F).

HRMS (TOF MS ES+)  $m/z$ :  $[\text{M}+\text{H}]^+$  Calcd for  $\text{C}_{38}\text{H}_{10}\text{F}_{15}\text{N}_4\text{Zn}^+$  870.9957; Found 870.9920.



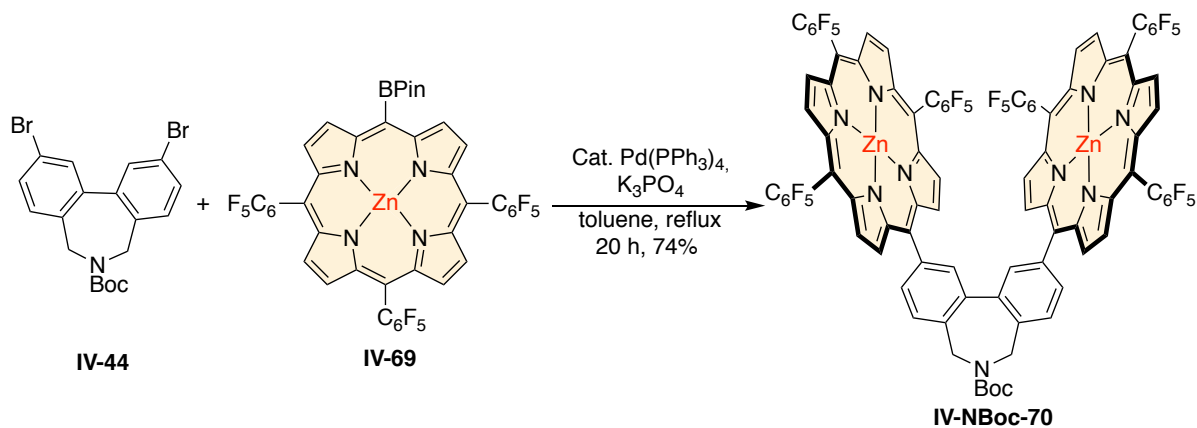


**Synthesis of IV-69**<sup>26</sup>: To a flame dried round bottom flask was added 1,2 dichloroethane (41 mL) and degassed for 30 min. To that flask **IV-68** (390 mg, 0.41 mmol), pinacolborane (2.1 mL, 14.35 mmol), triethylamine (0.74 mL, 5.3 mmol) and Pd(PPh<sub>3</sub>)<sub>2</sub>Cl<sub>2</sub> (43 mg, 0.06 mmol) were added sequentially under an argon atmosphere. The mixture was refluxed for 12 h before cooling down to RT. The solvent was then removed in vacuo and the crude was dissolved in dichloromethane, washed with H<sub>2</sub>O, and dried over Na<sub>2</sub>SO<sub>4</sub>. The crude was purified via column chromatography to afford the desired product **IV-69** in 56% yield.

<sup>1</sup>H NMR (500 MHz, Chloroform-*d*)  $\delta$  10.02 (d, *J* = 4.7 Hz, 2H), 9.02 (d, *J* = 4.7 Hz, 2H), 8.96-8.93 (m, 4H), 1.87 (s, 6H).

<sup>19</sup>F NMR (470 MHz, Chloroform-*d*)  $\delta$  -136.66 – -137.20 (m, 6F), -152.46 – -152.90 (m, 3F), -162.00 – -162.42 (m, 6F).

HRMS (TOF MS ES+) *m/z*: [M]<sup>+</sup> Calcd for C<sub>44</sub>H<sub>20</sub>BF<sub>15</sub>N<sub>4</sub>O<sub>2</sub>Zn<sup>+</sup> 996.0731; Found 997.0729.



**Synthesis of IV-NBoc-70**<sup>28</sup>: K<sub>3</sub>PO<sub>4</sub> (80 mg, 0.38 mmol) was added to an oven dried round bottom flask. The flask was flame dried under vacuum and filled with argon. To the flux was then added toluene (7.8 mL), **IV-69** (119 mg, 0.14 mmol), **IV-44** (15 mg, 0.034

mmol) under argon atmosphere and the mixture was degassed for 30 min. Finally,  $\text{Pd}(\text{PPh}_3)_4$  (12 mg, 0.01 mmol) was added to the mixture and refluxed for 20 h before cooling down to room temperature. The solvent was removed in vacuo and the crude was dissolved in  $\text{CH}_2\text{Cl}_2$ . The organic layer was washed with  $\text{H}_2\text{O}$ , followed by brine solution, dried over  $\text{Na}_2\text{SO}_4$ , and concentrated in vacuo. Purification by column chromatography (15% EtOAc/hexane) gave **IV-NBoc-70** in 74% yield.

$^1\text{H}$  NMR (500 MHz, Chloroform-*d*)  $\delta$  9.04 (d,  $J = 4.6$  Hz, 4H), 8.93 – 8.85 (m, 8H), 8.76 (br, 4H), 8.48 (s, 2H), 8.26 (d,  $J = 6.3$  Hz, 2H), 7.86 (br, 2H), 4.84 (br, 2H), 4.60 (br, 2H), 1.57 (s, 9H).

$^{19}\text{F}$  NMR (470 MHz, Chloroform-*d*)  $\delta$  -136.52 – -137.59 (m, 12F), -152.18 – -152.33 (m,  $J = 22.4$ , 6F), -161.50 – -162.73 (m, 12F).

#### **IV-10.6. General procedure for the deprotection of the Boc group under basic condition<sup>42</sup>**

To a vigorously stirred solution of **IV-NBoc-40** (30 mg, 0.02 mmol) and 2,6 lutidine (58  $\mu\text{L}$ , 0.5 mmol) in  $\text{CH}_2\text{Cl}_2$  at 0 °C was added trimethylsilyl triflate (54  $\mu\text{L}$ , 0.3 mmol) dropwise under argon atmosphere. After 15 min, the ice bath was removed, and the mixture was stirred at room temperature for 3.5 h. The reaction mixture was placed in an ice-bath again and quenched with saturated  $\text{NH}_4\text{Cl}_{\text{aq}}$  (0.5 mL) and stirred for 15 min at room temperature. Subsequently the mixture was extracted with  $\text{CH}_2\text{Cl}_2$ , dried over  $\text{Na}_2\text{SO}_4$ , and concentrated in vacuo. To the crude mixture was added acetonitrile and the solid was filtered. The residue was washed with several portions of acetonitrile to remove excess 2,6-lutidine and dried under vacuum to afford the desired product **IV-40** in 84%

yield. The product was used directly to the conjugate addition reaction without any further purification.

Catalyst **IV-56** and **IV-70** were synthesized similarly from **IV-NBoc-56** and **IV-NBoc-70** respectively.

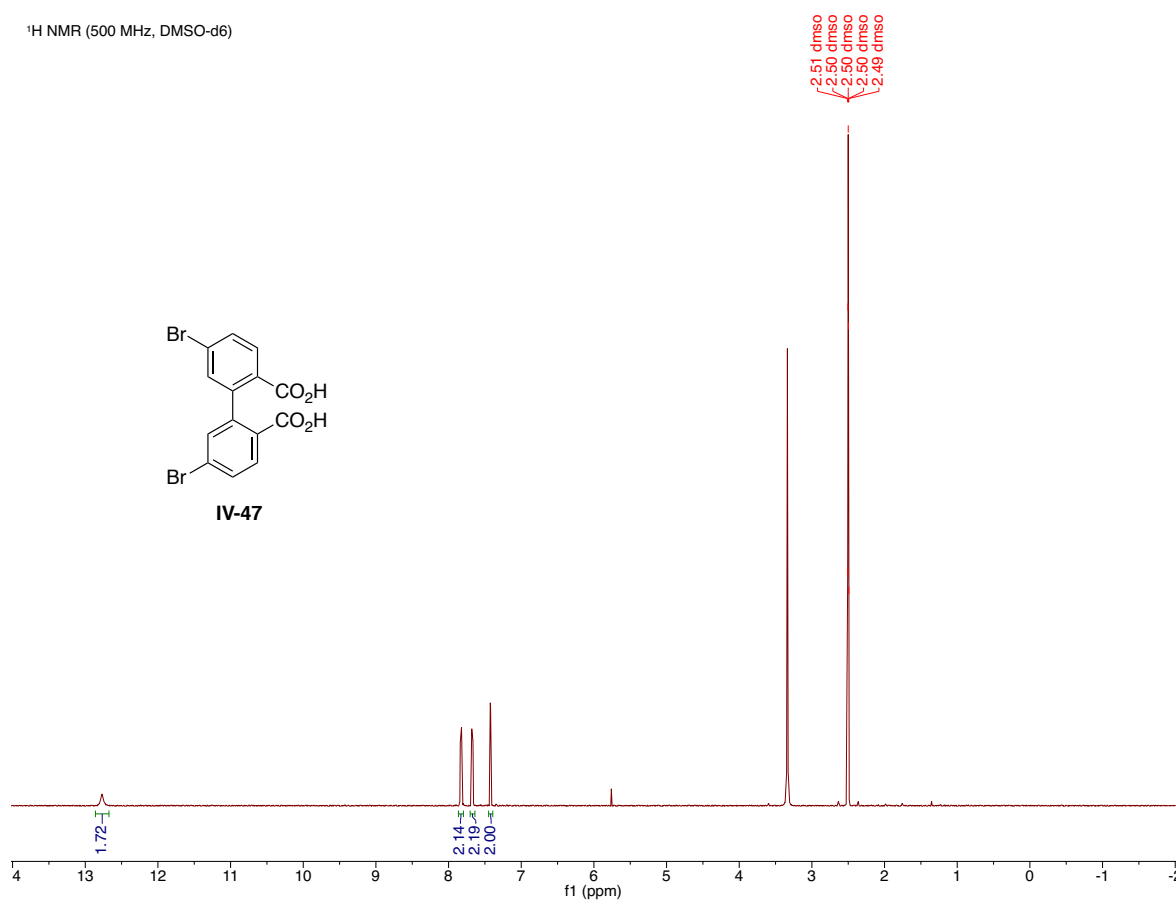
#### **IV-10.7. General procedure for the *syn*-selective asymmetric Michael addition reaction catalyzed by programmable racemic catalyst**

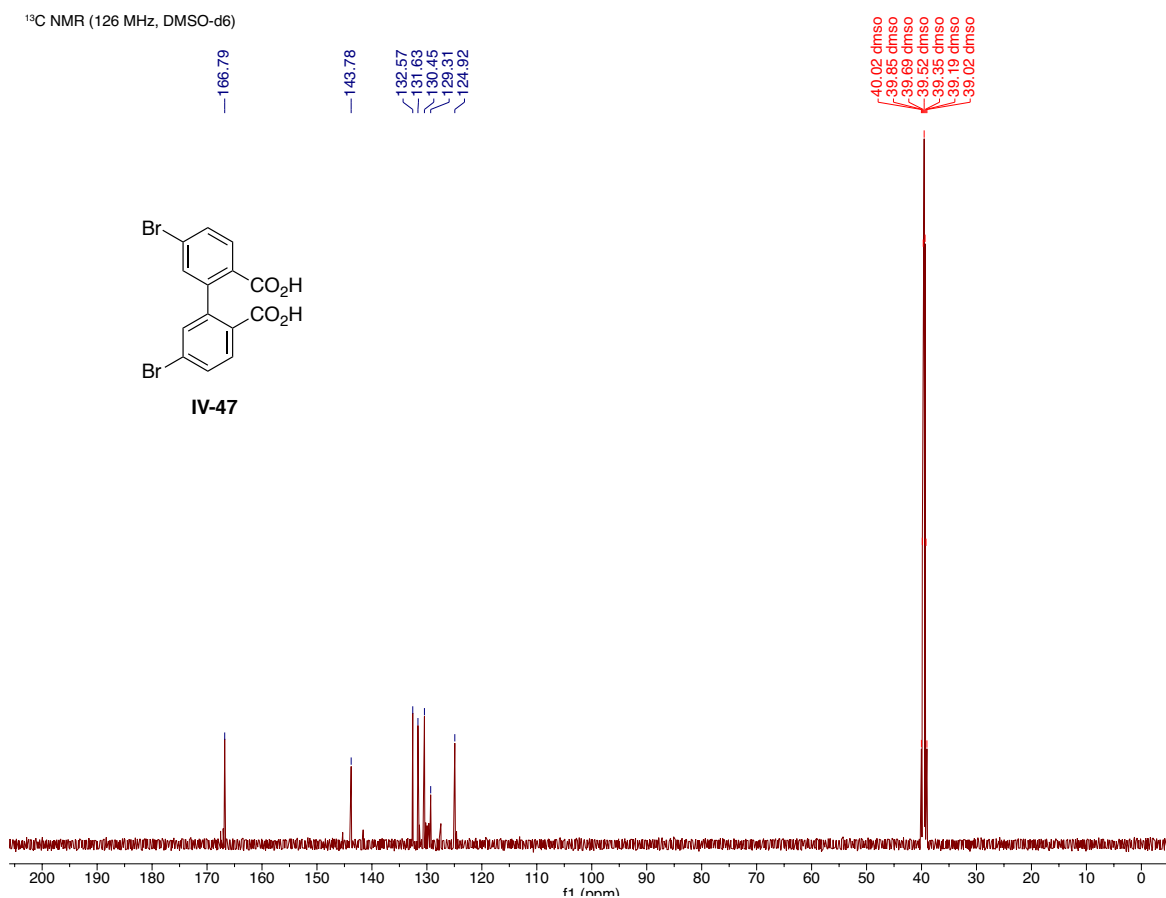
To a solution of amine catalyst **IV-40** (3.5 mg, 0.0025 mmol) in 1-bromo-3-chlorobenzene (0.2 mL) in a small vial was added **III-*R<sub>P</sub>*-19** (1.2 mg, 0.0025 mmol) and stirred for 20 min. To the mixture was added aldehyde **IV-36** (7.2  $\mu$ L, 0.10 mmol) and electrophile **IV-37** (9.5 mg, 0.05 mmol) at room temperature. The reaction mixture was then stirred for 48 h. All volatiles were subsequently removed in vacuo and the crude mixture was dissolved in CH<sub>2</sub>Cl<sub>2</sub> (1 mL) and benzyl 2-(triphenylphosphoranylidene)acetate (64 mg, 0.15 mmol) was added. The olefination reaction was allowed to proceed until complete consumption of the conjugate addition adduct. After solvent removal, the crude was passed through a plug of silica gel and washed with 20% EtOAc/hexane mixture (400 mL). After removing the solvent, the crude was purified via column chromatography (6% EtOAc/Hexane) on silica gel to afford the corresponding product **IV-*ent*-39** as an inseparable diastereomeric mixture. The spectral data matched the reported in the literature.

HPLC analysis for **IV-*ent*-39**: Chiralpak IA, 98:2 hexane/*i*-PrOH, flow rate = 0.42 mL/min,  $\lambda$  = 240 nm, retention time = 104.4 min (major), 1132.4 min (minor).

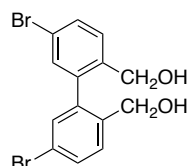
## IV-10.8. NMR spectra:

<sup>1</sup>H NMR (500 MHz, DMSO-d<sub>6</sub>)

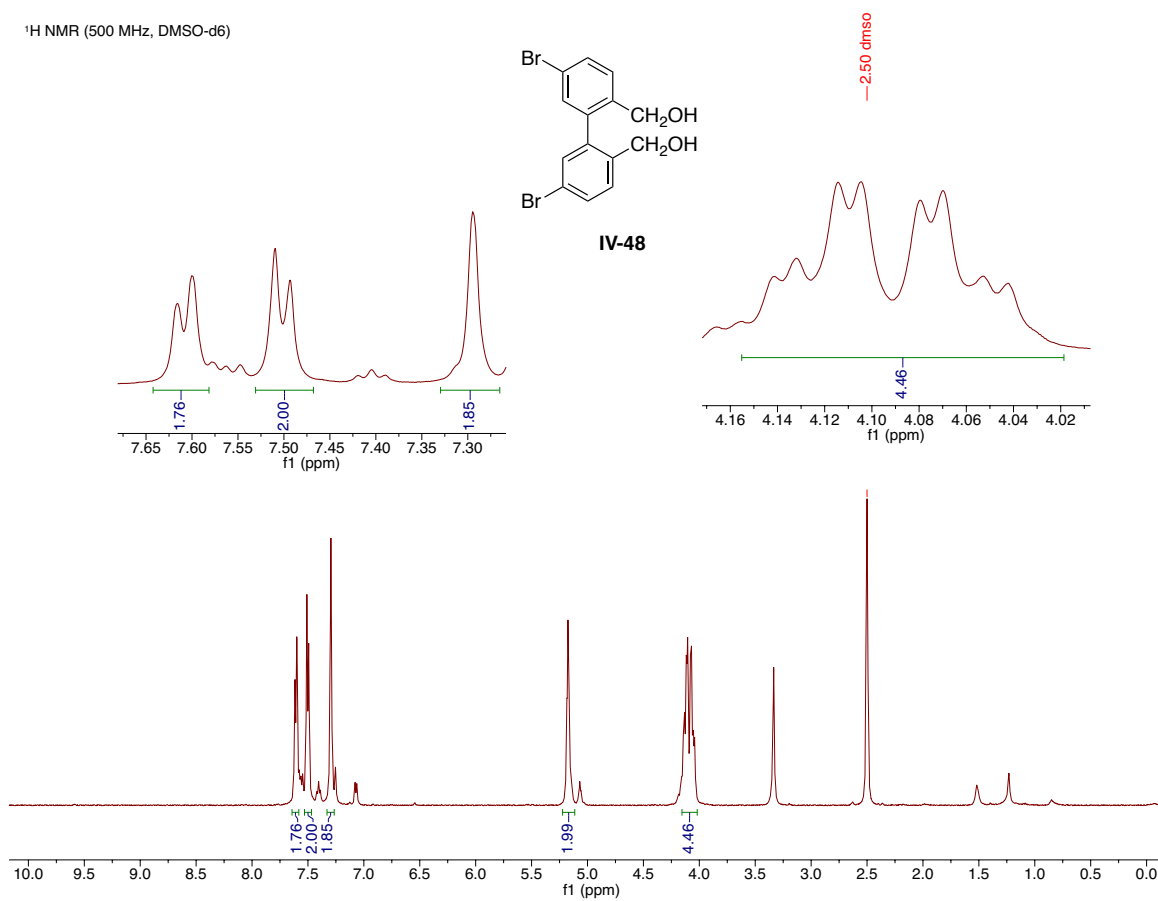




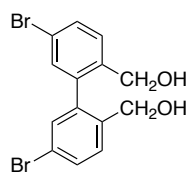
<sup>1</sup>H NMR (500 MHz, DMSO-d<sub>6</sub>)



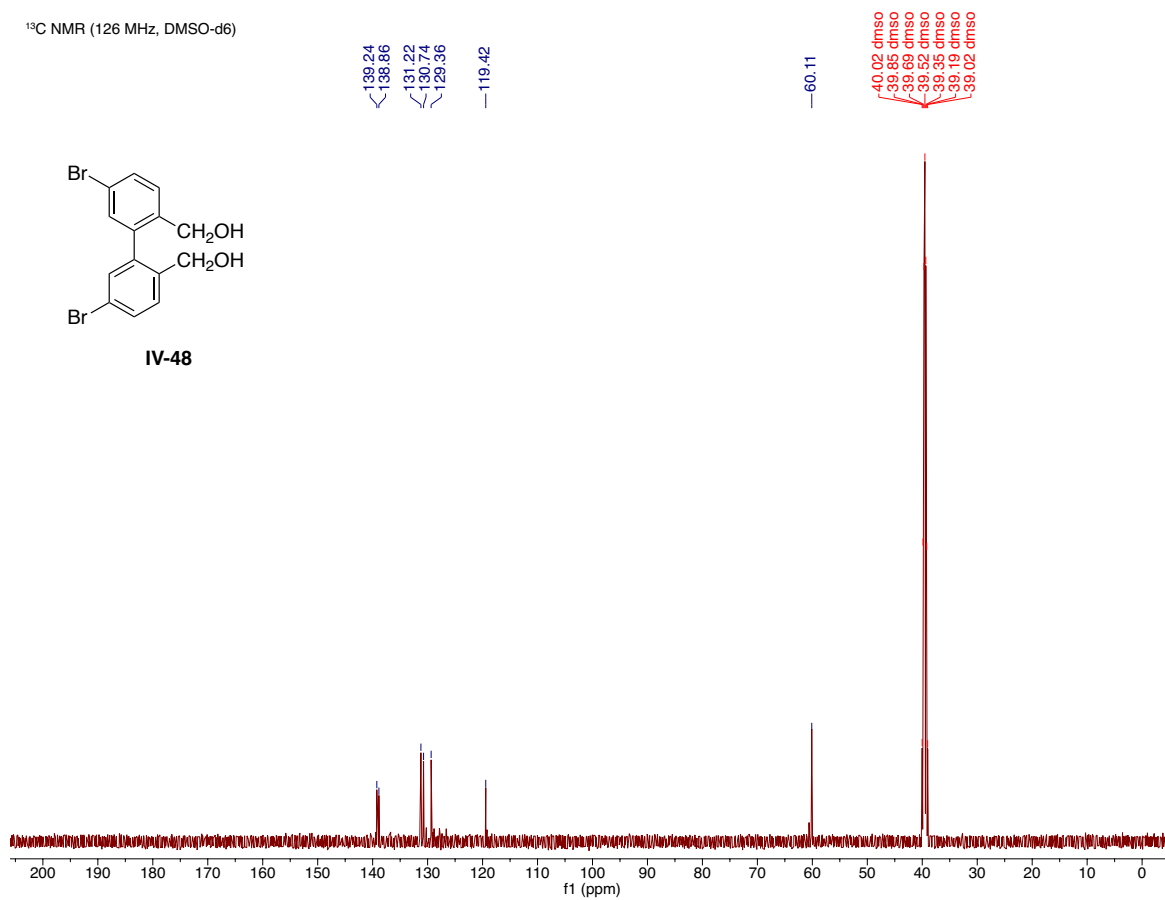
IV-48



<sup>13</sup>C NMR (126 MHz, DMSO-d<sub>6</sub>)

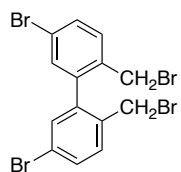


IV-48

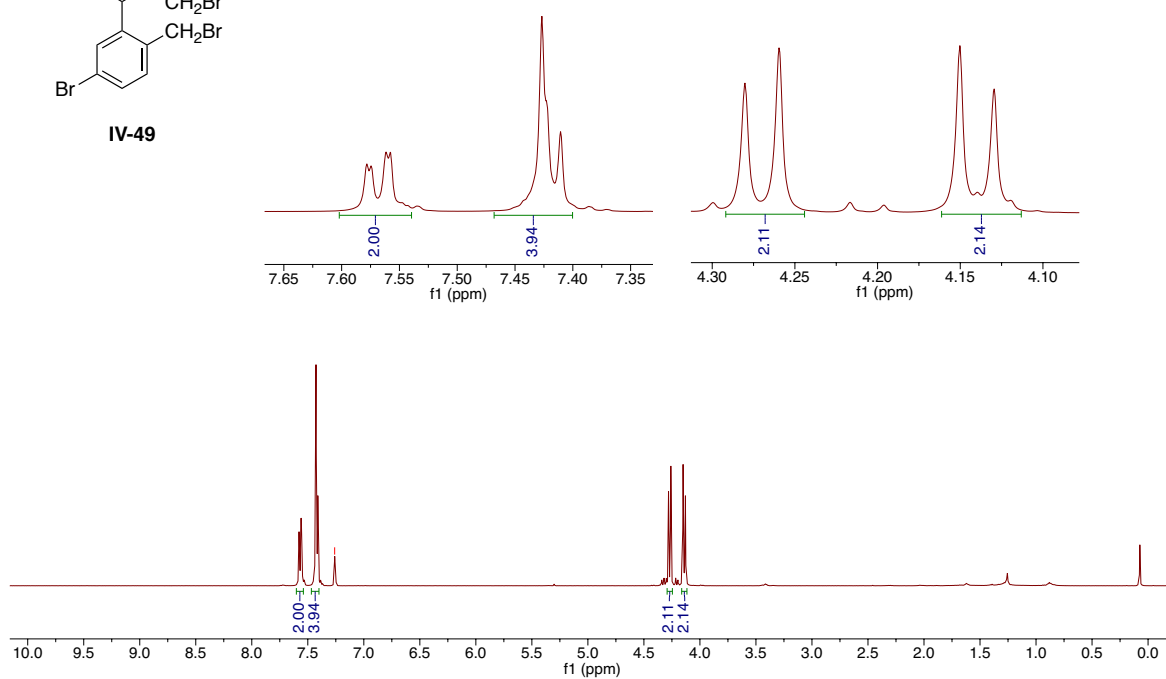


<sup>1</sup>H NMR (500 MHz, CDCl<sub>3</sub>)

—7.26 cdd3

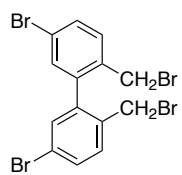


IV-49

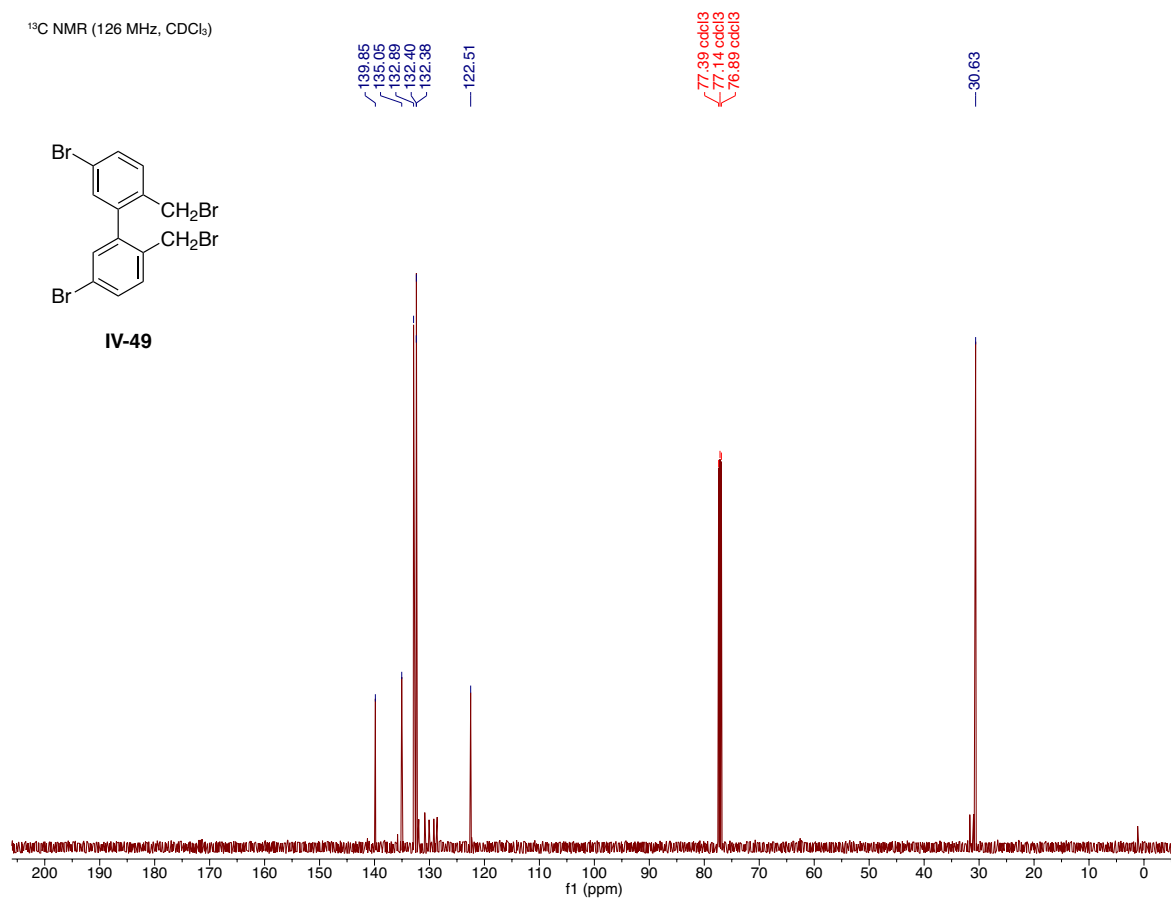




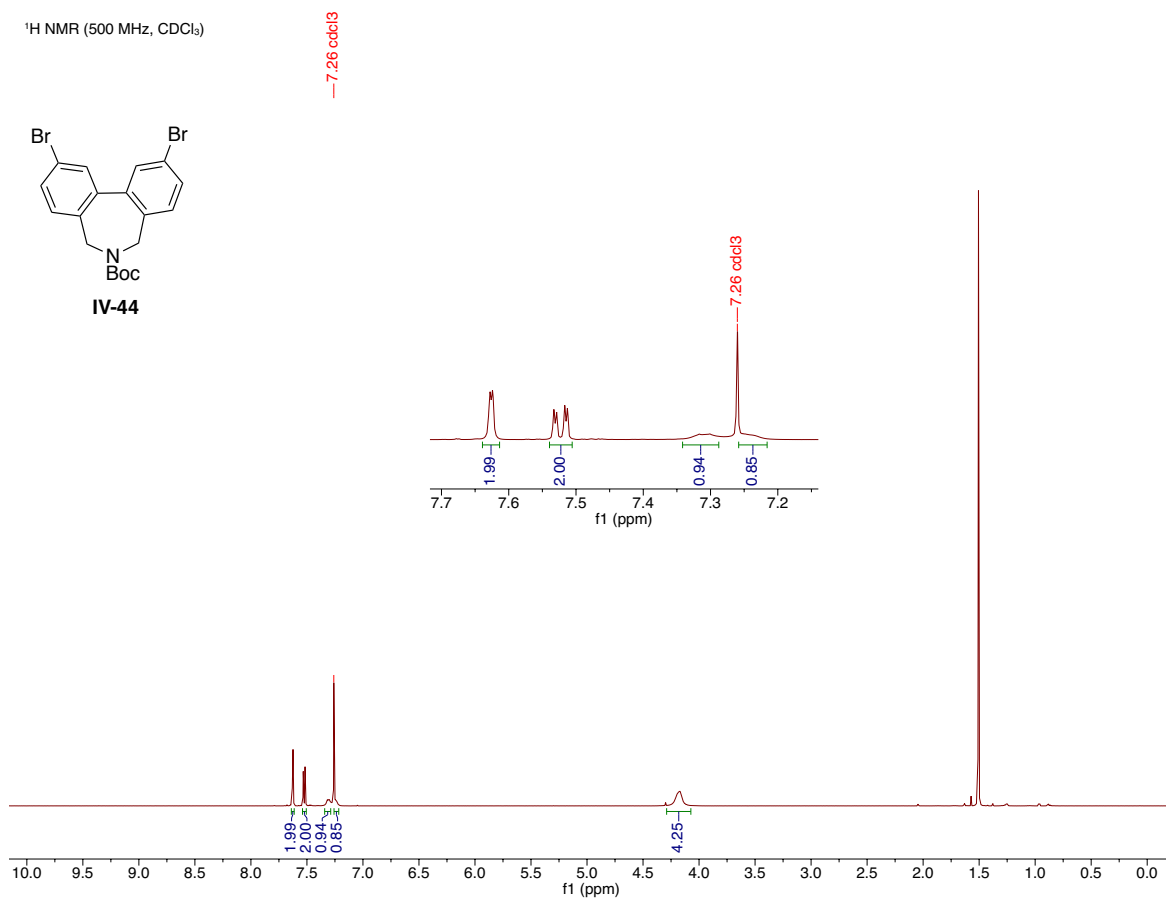
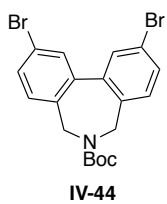
<sup>13</sup>C NMR (126 MHz, CDCl<sub>3</sub>)



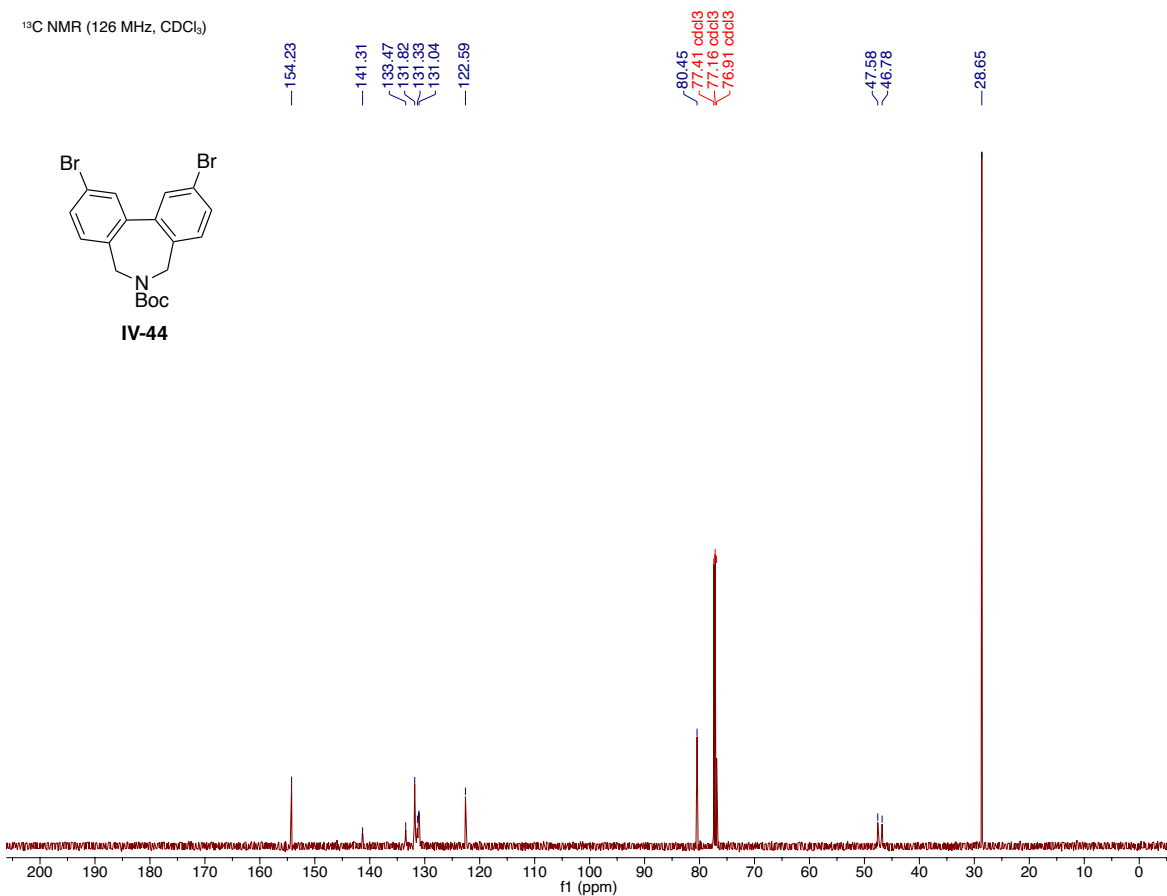
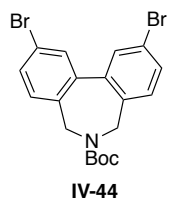
IV-49



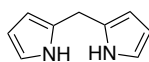
<sup>1</sup>H NMR (500 MHz, CDCl<sub>3</sub>)



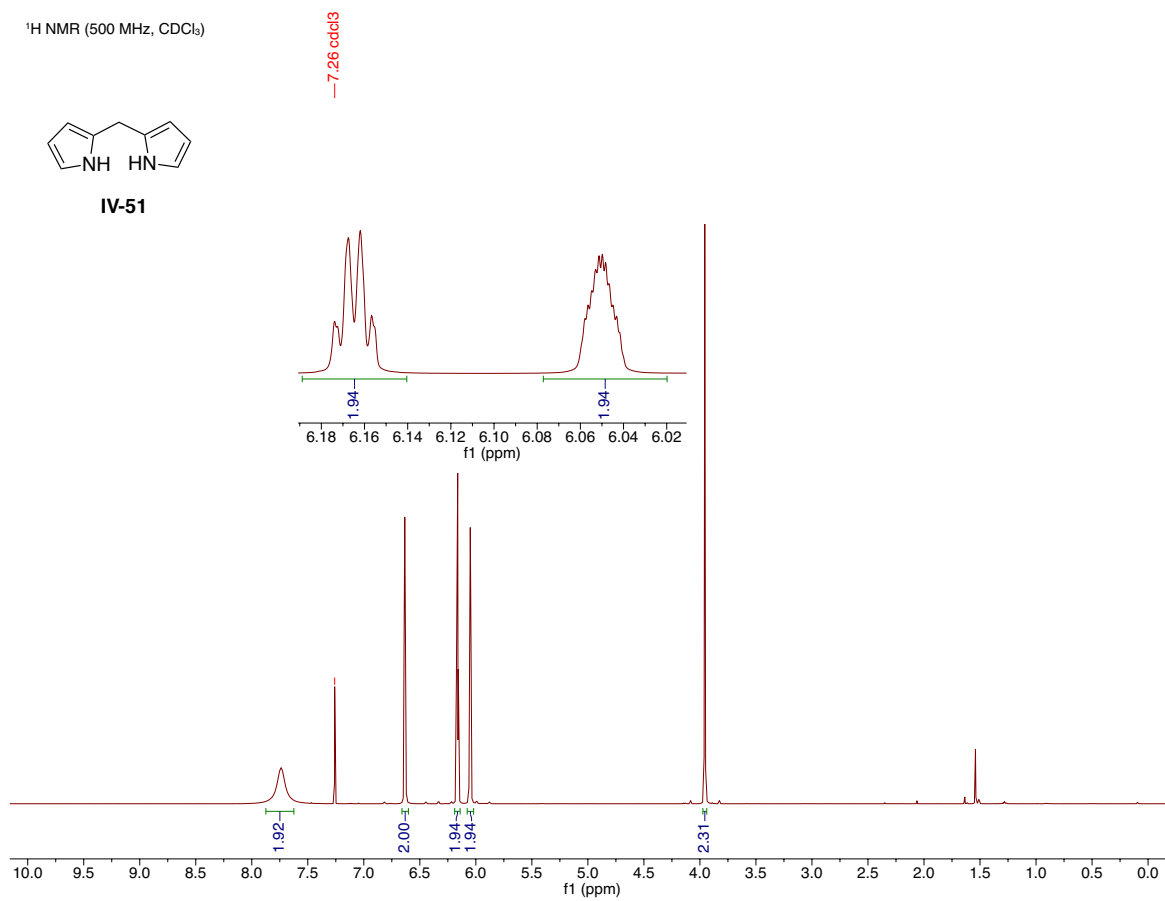
<sup>13</sup>C NMR (126 MHz, CDCl<sub>3</sub>)



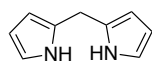
<sup>1</sup>H NMR (500 MHz, CDCl<sub>3</sub>)



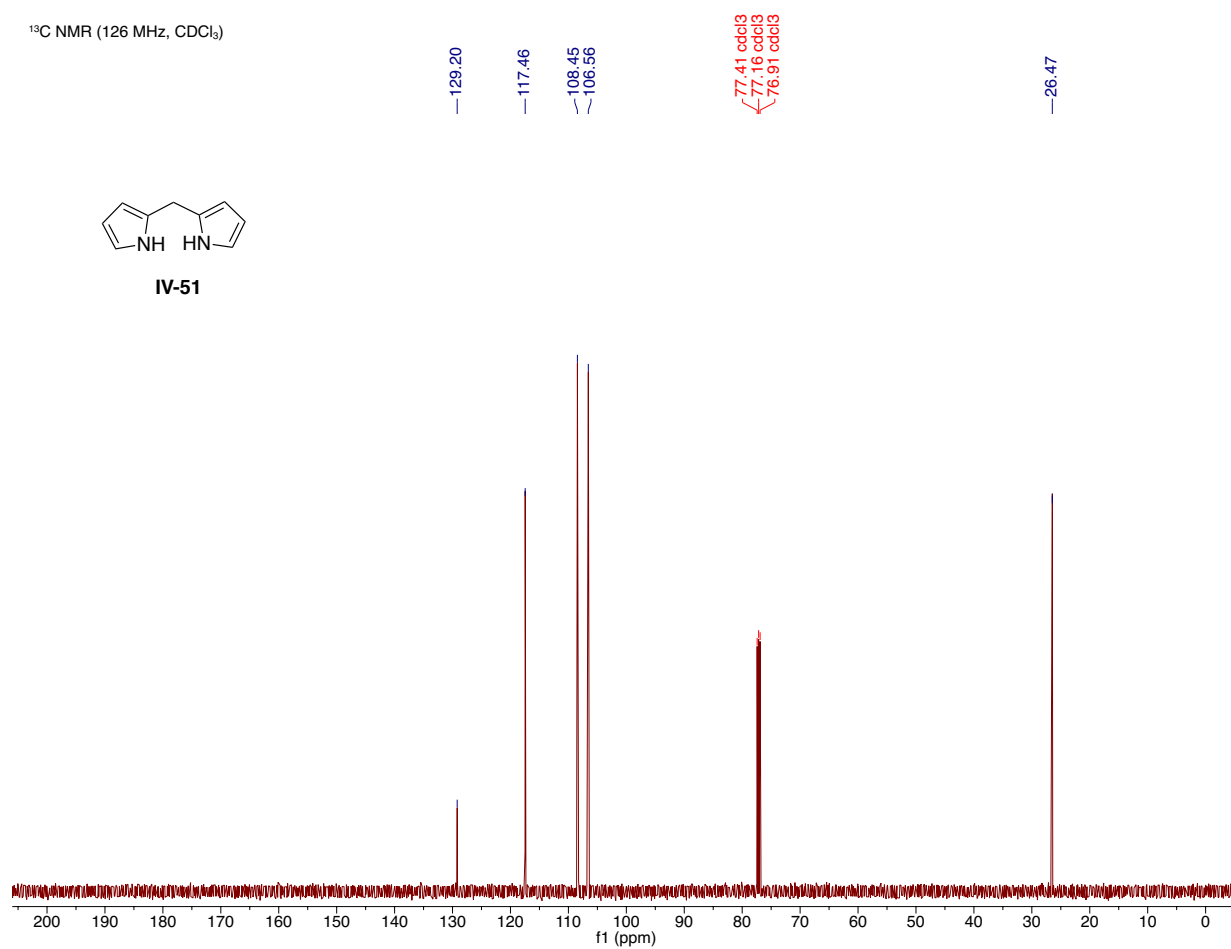
IV-51

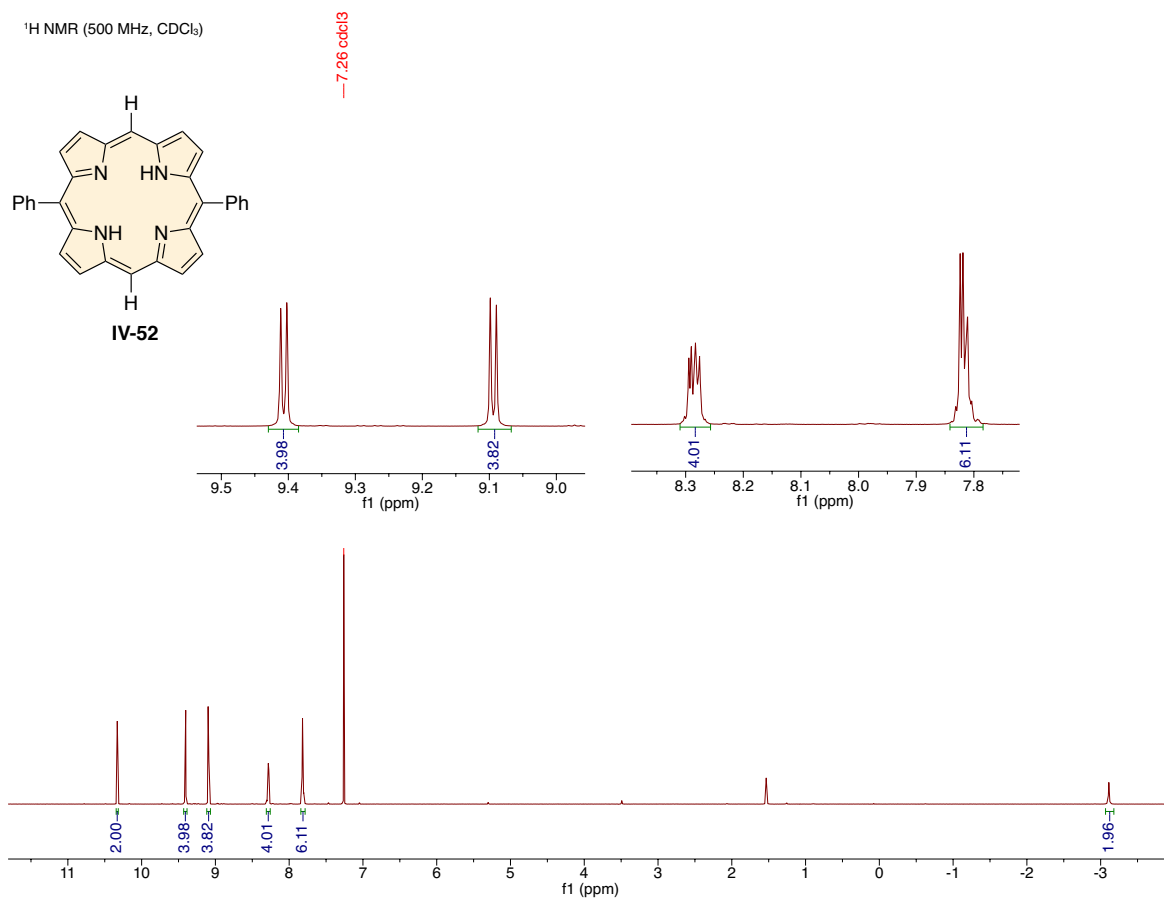


<sup>13</sup>C NMR (126 MHz, CDCl<sub>3</sub>)



IV-51





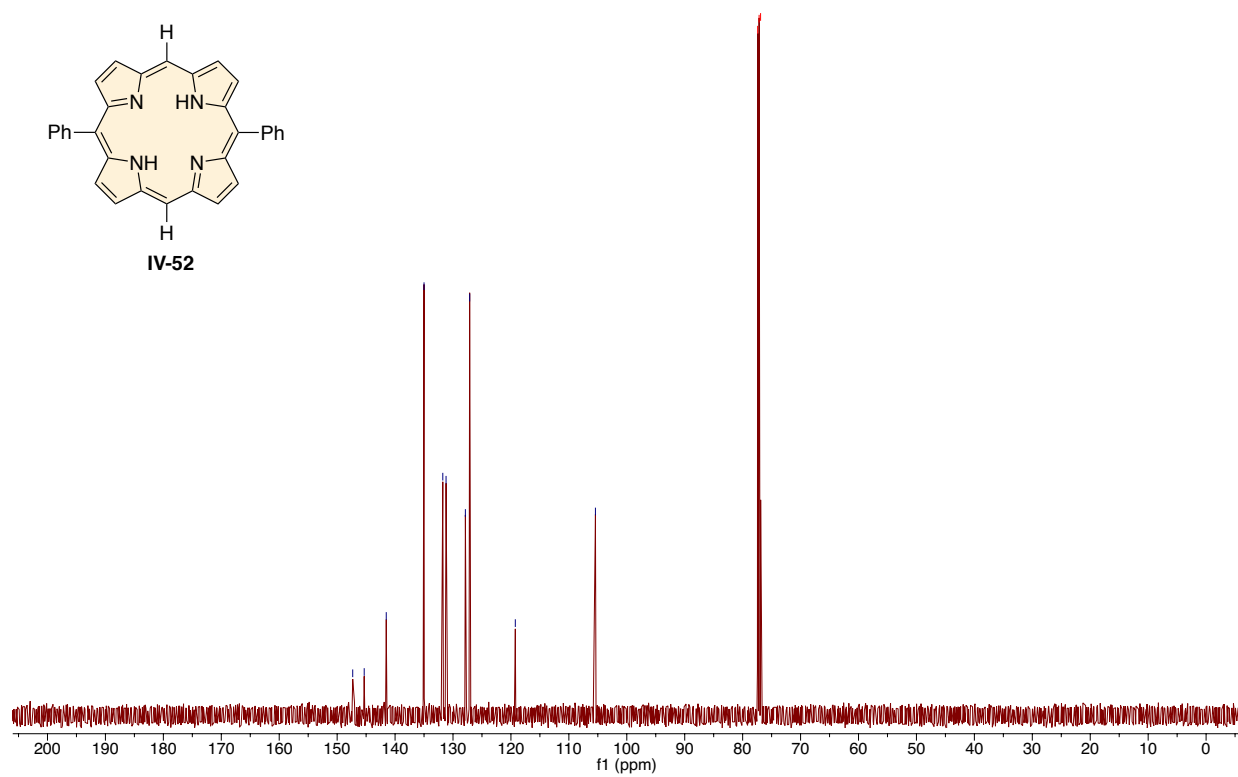
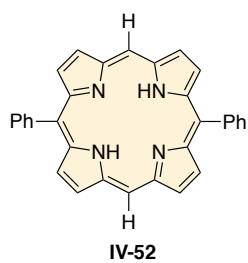
<sup>13</sup>C NMR (126 MHz, CDCl<sub>3</sub>)

147.31  
145.33  
141.52  
135.00  
131.76  
131.20  
127.86  
127.12

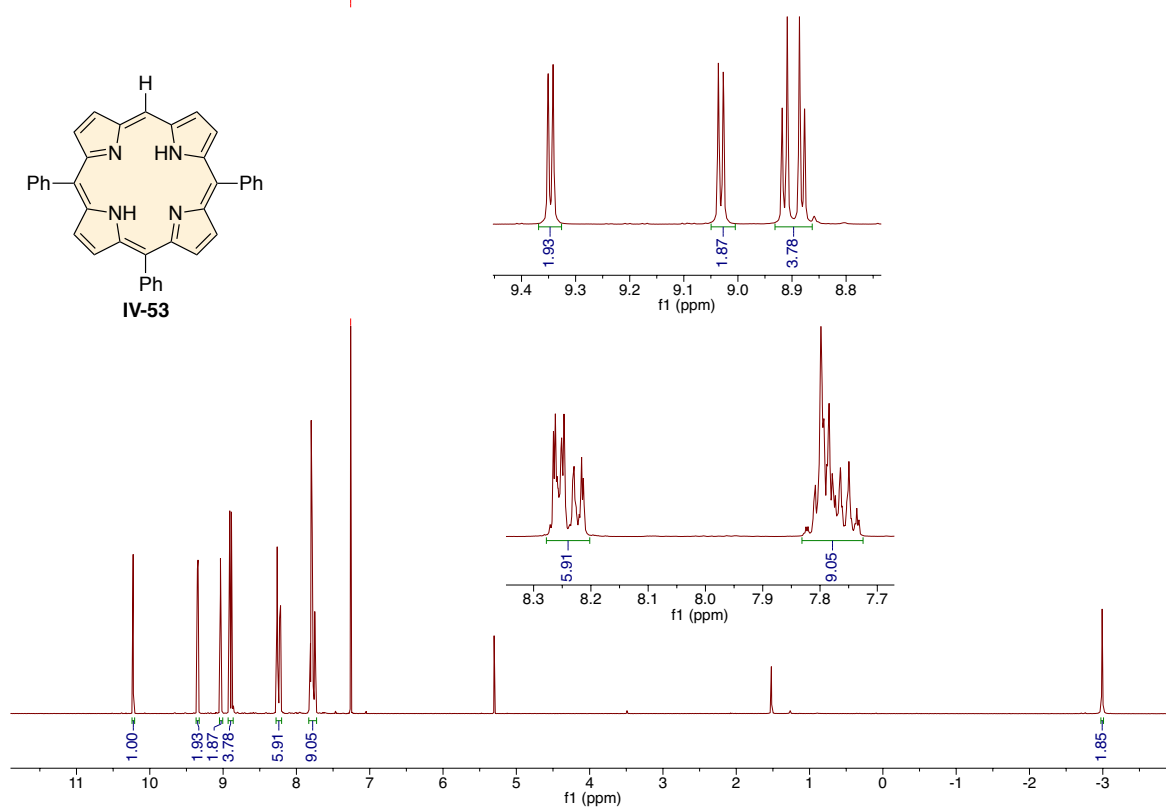
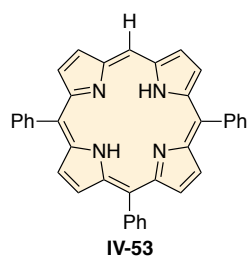
119.24

105.41

77.41 cdcl3  
77.16 cdcl3  
76.91 cdcl3



— 7.26 cdcl<sub>3</sub>



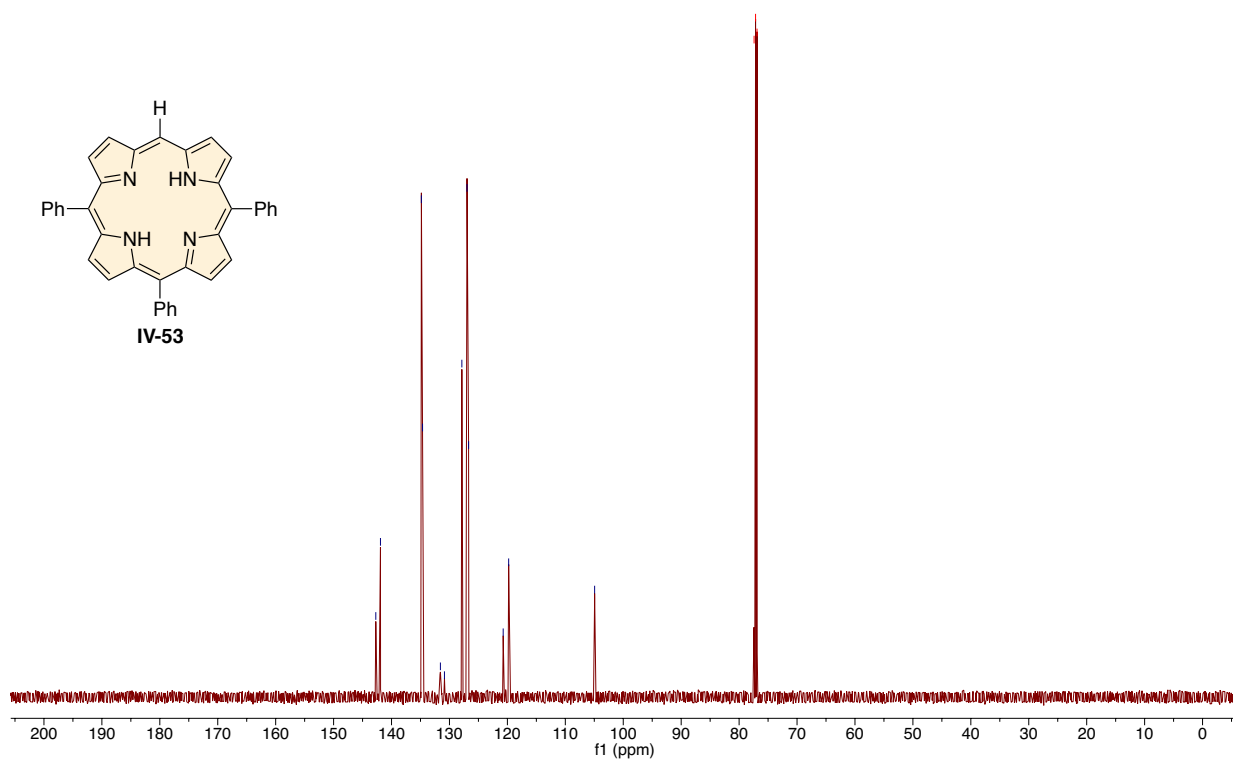
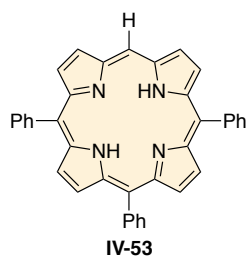


<sup>13</sup>C NMR (126 MHz, CDCl<sub>3</sub>)

142.72  
141.91  
134.85  
134.65  
131.56  
130.86  
127.86  
126.97  
126.70  
120.73  
119.78

104.94

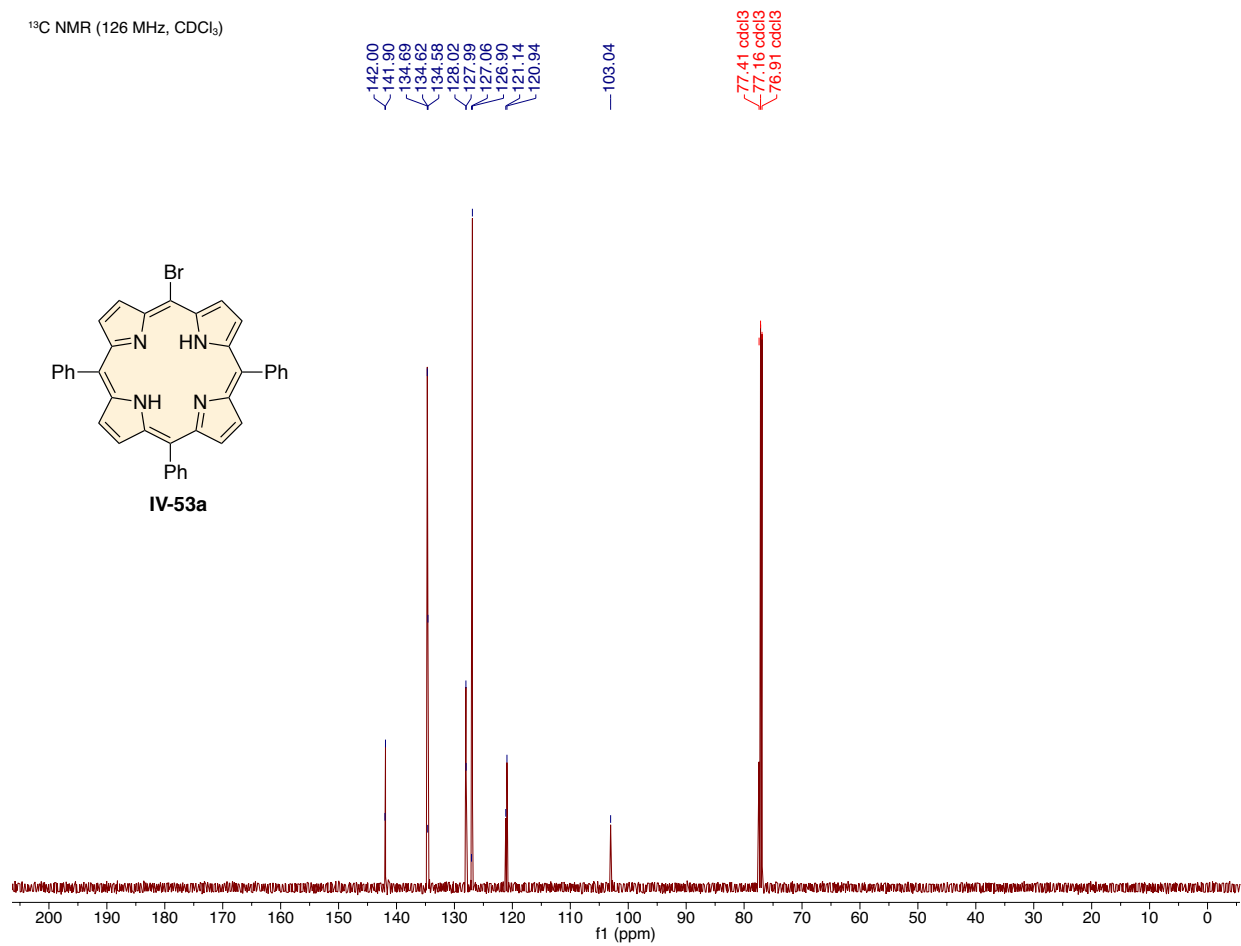
77.41 cdcl3  
77.16 cdcl3  
76.91 cdcl3



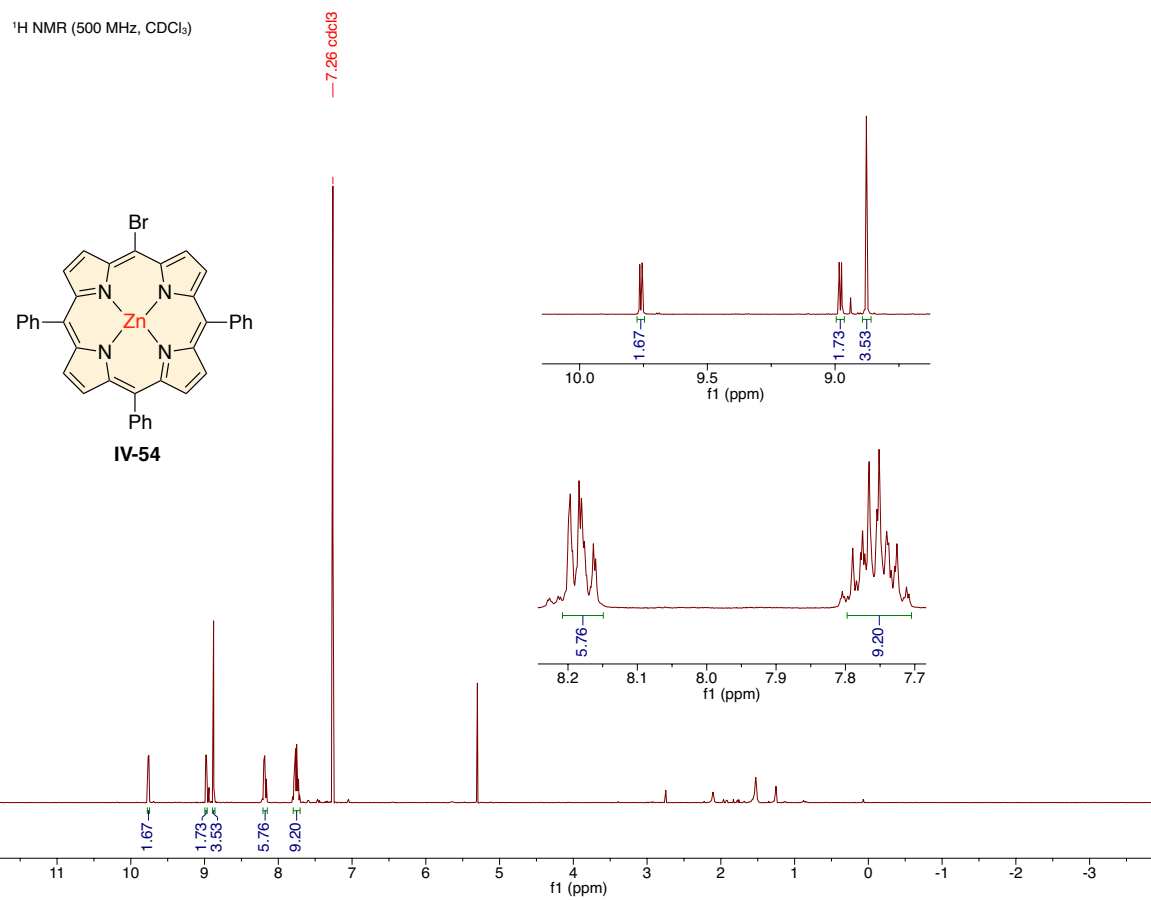
—7.26 cdcl<sub>3</sub>



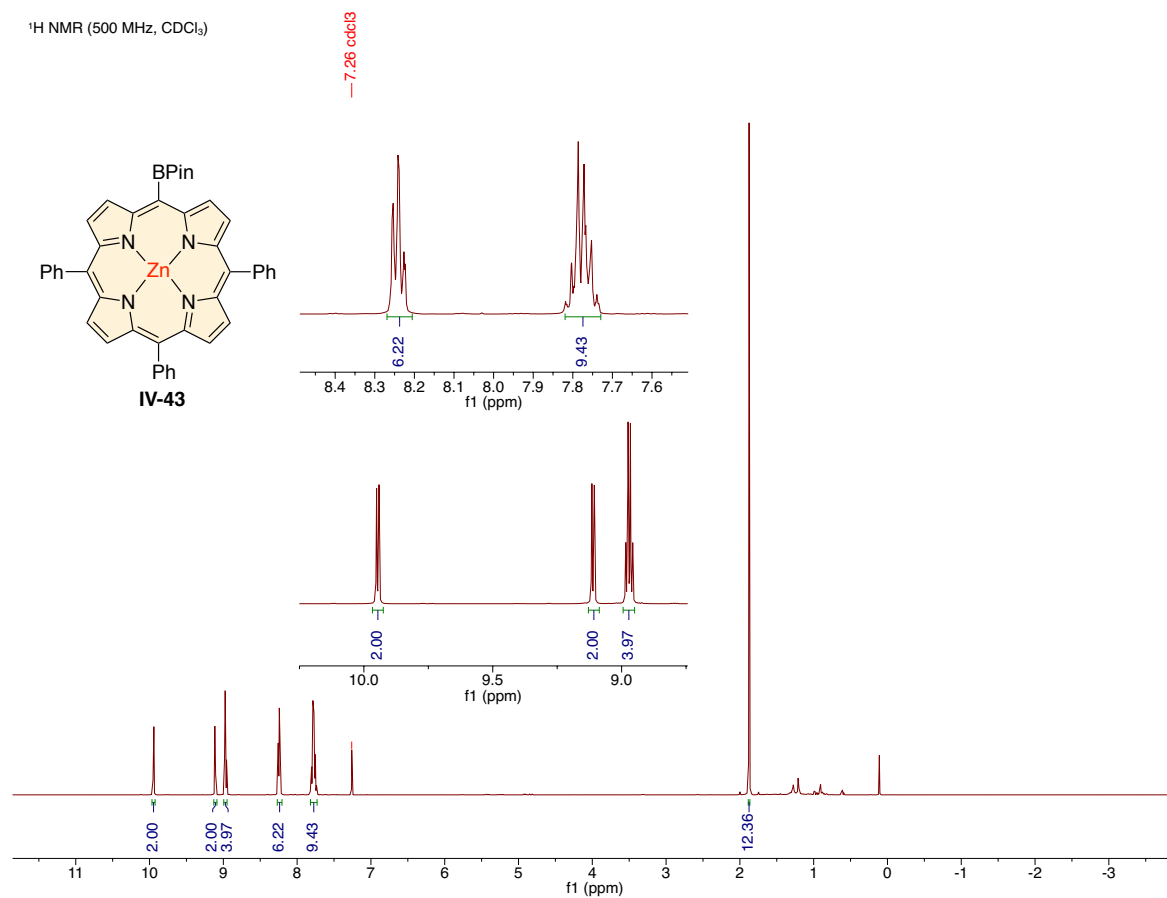
<sup>13</sup>C NMR (126 MHz, CDCl<sub>3</sub>)



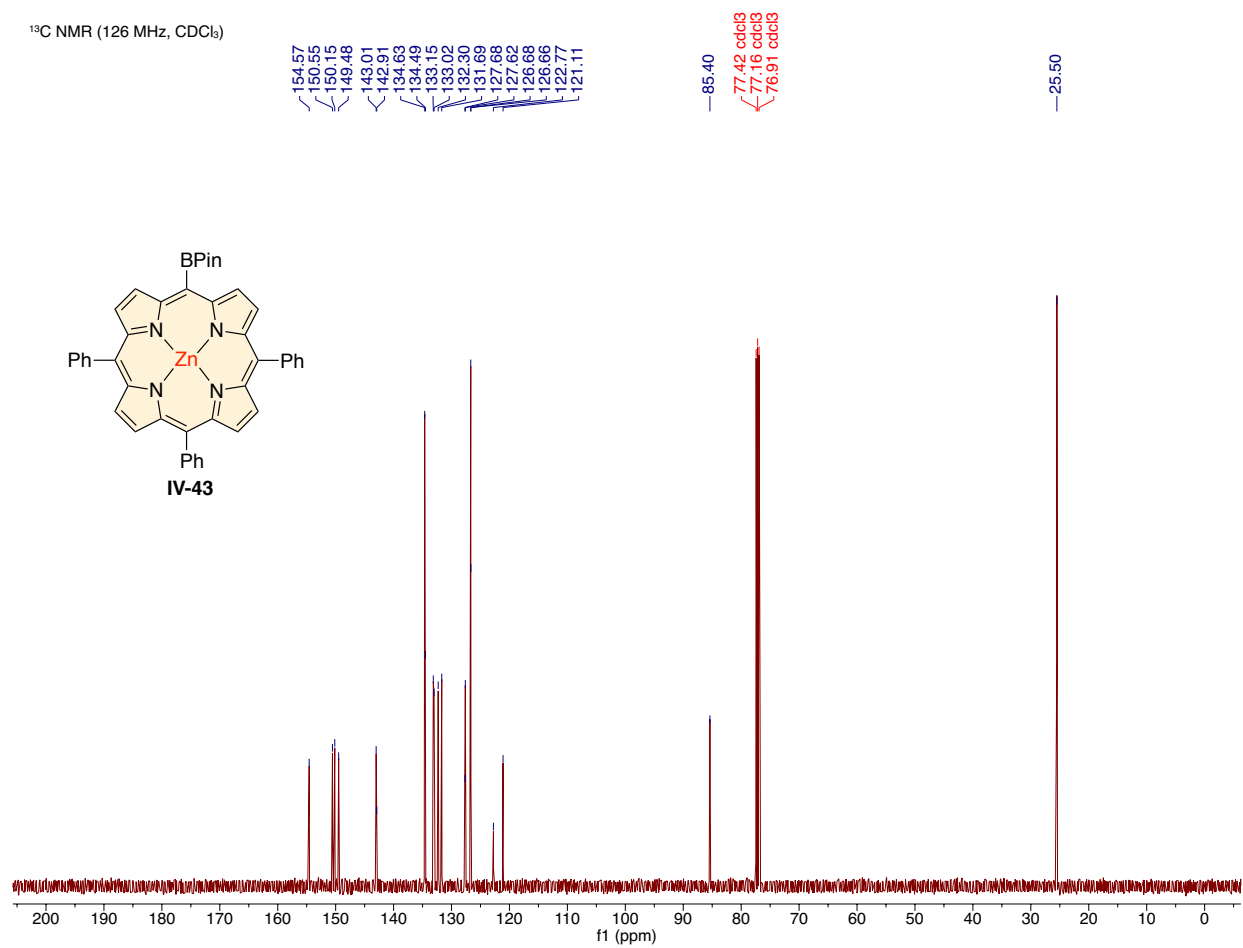
<sup>1</sup>H NMR (500 MHz, CDCl<sub>3</sub>)



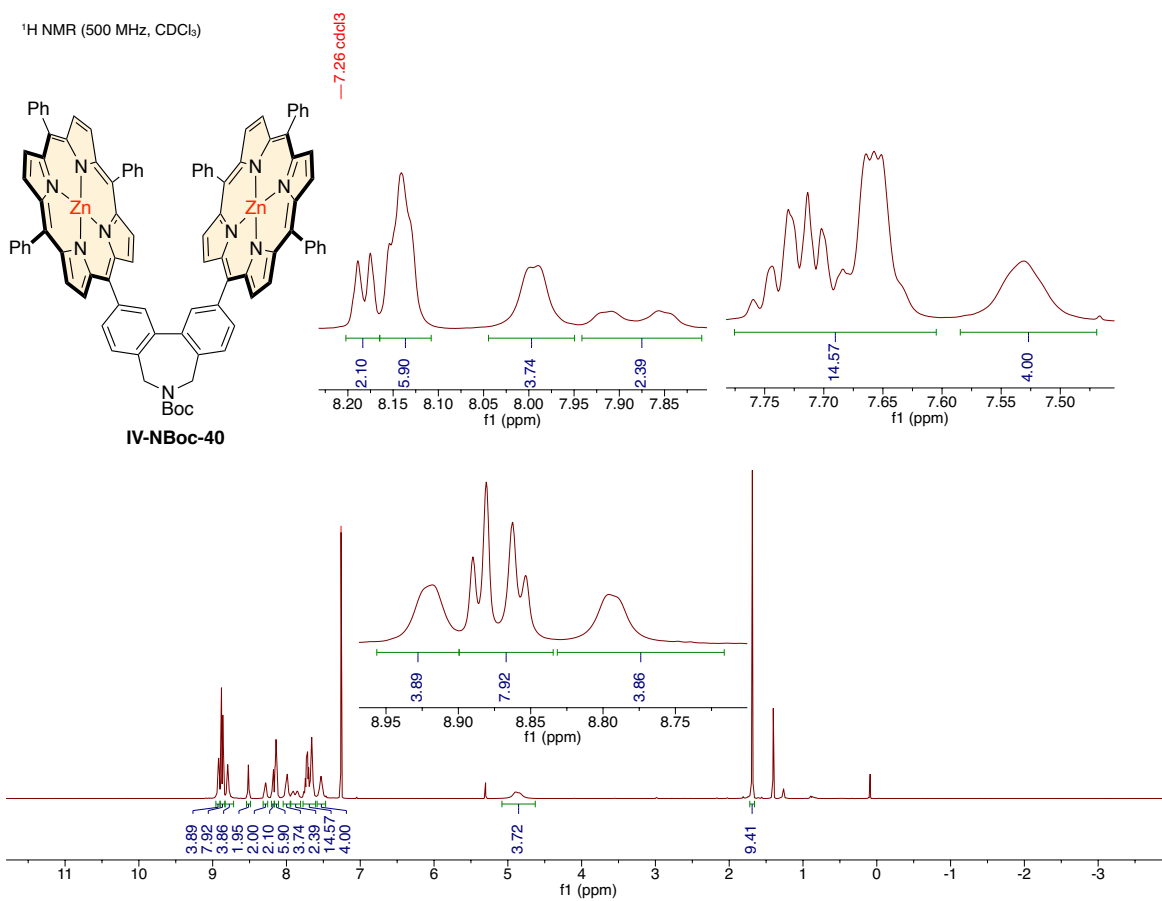
<sup>1</sup>H NMR (500 MHz, CDCl<sub>3</sub>)



<sup>13</sup>C NMR (126 MHz, CDCl<sub>3</sub>)



<sup>1</sup>H NMR (500 MHz, CDCl<sub>3</sub>)

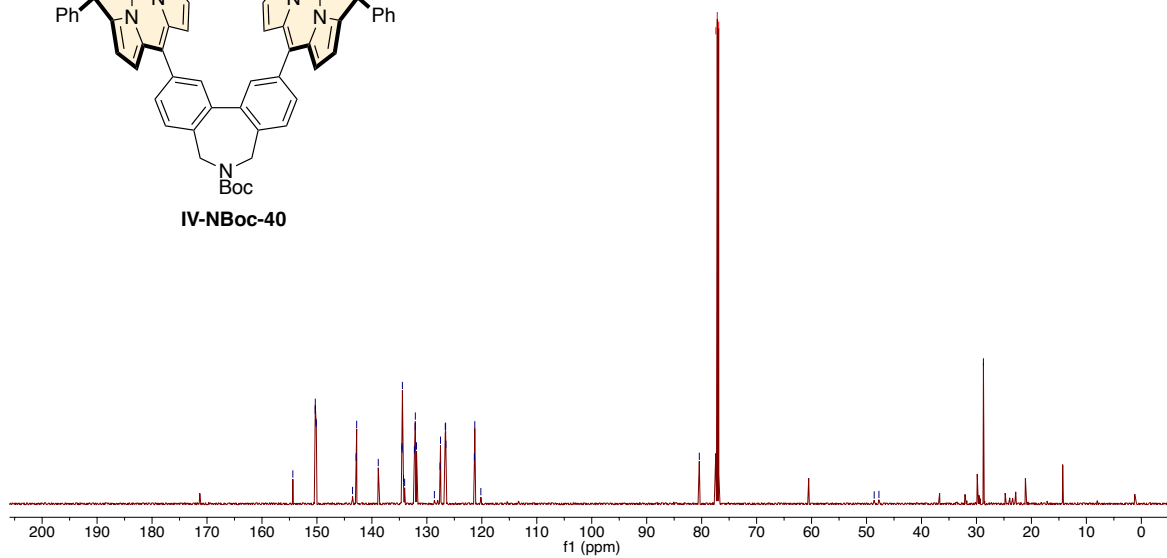
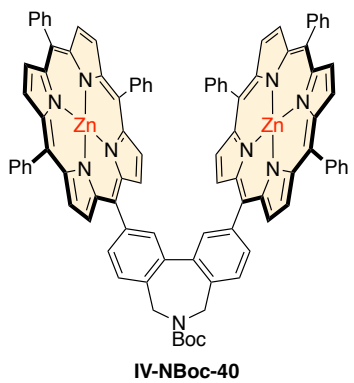


$^{13}\text{C}$  NMR (126 MHz,  $\text{CDCl}_3$ )

154.38  
150.32  
150.30  
150.26  
150.11  
143.52  
142.88  
142.77  
138.84  
134.53  
134.51  
134.45  
134.25  
134.04  
132.27  
132.12  
132.10  
131.98  
128.88  
127.60  
127.52  
126.65  
126.59  
126.54  
121.35  
121.28  
120.18  
80.43  
77.41  $\text{CDCl}_3$   
77.16  $\text{CDCl}_3$   
76.91  $\text{CDCl}_3$

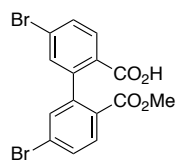
48.61  
47.75

28.73

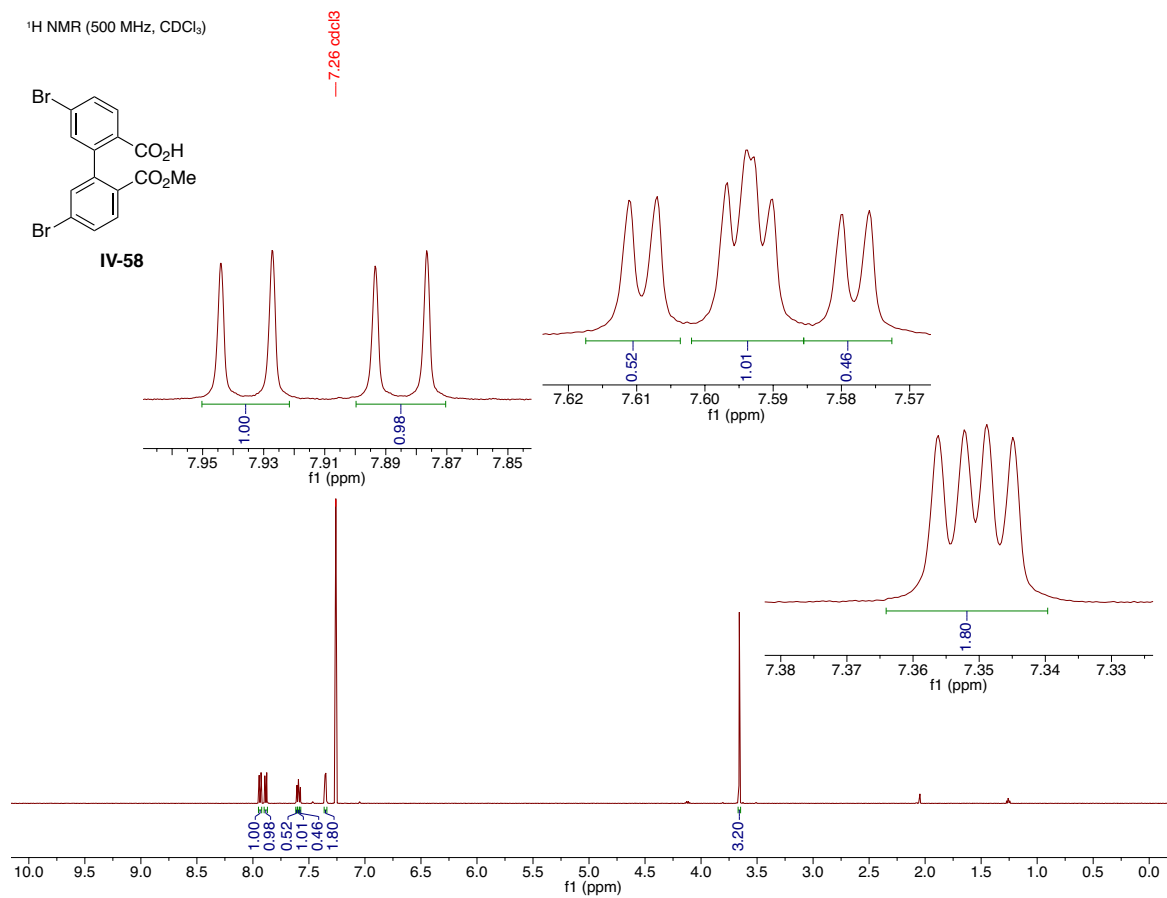


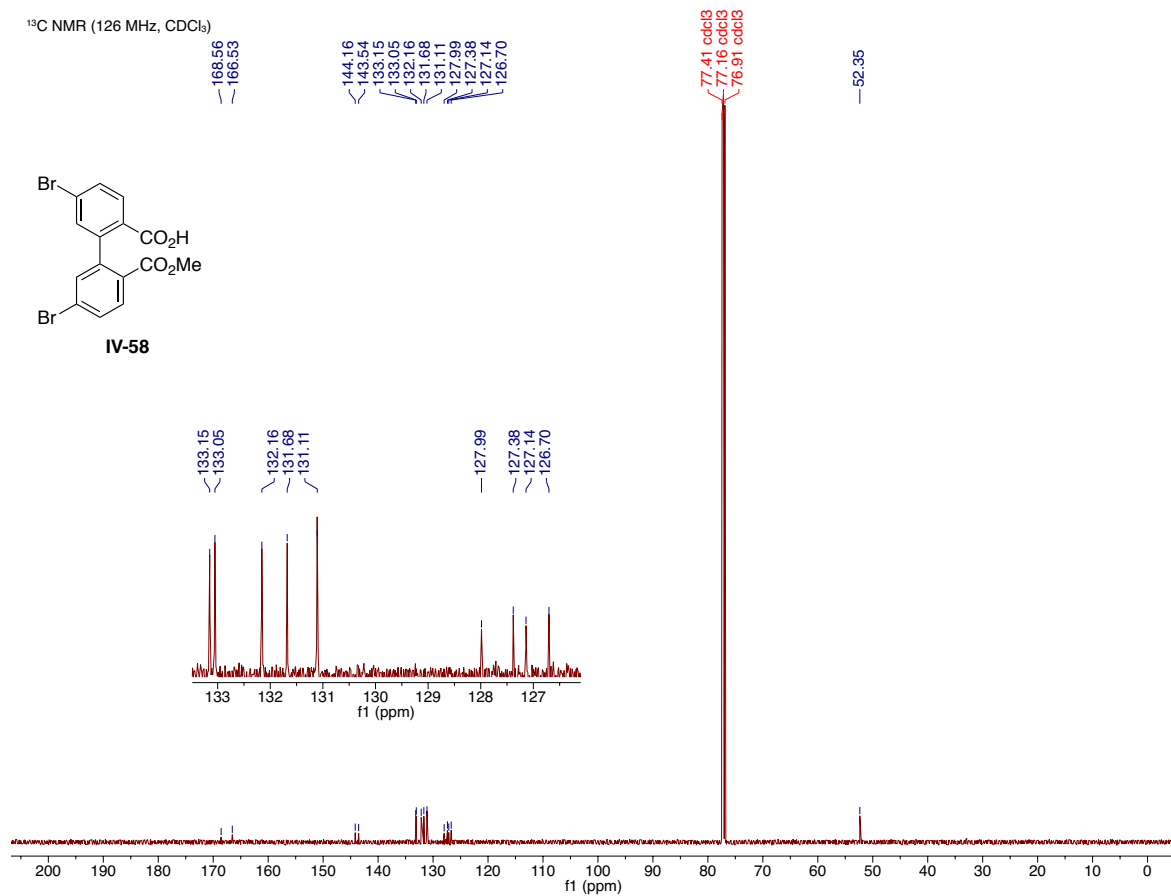


<sup>1</sup>H NMR (500 MHz, CDCl<sub>3</sub>)

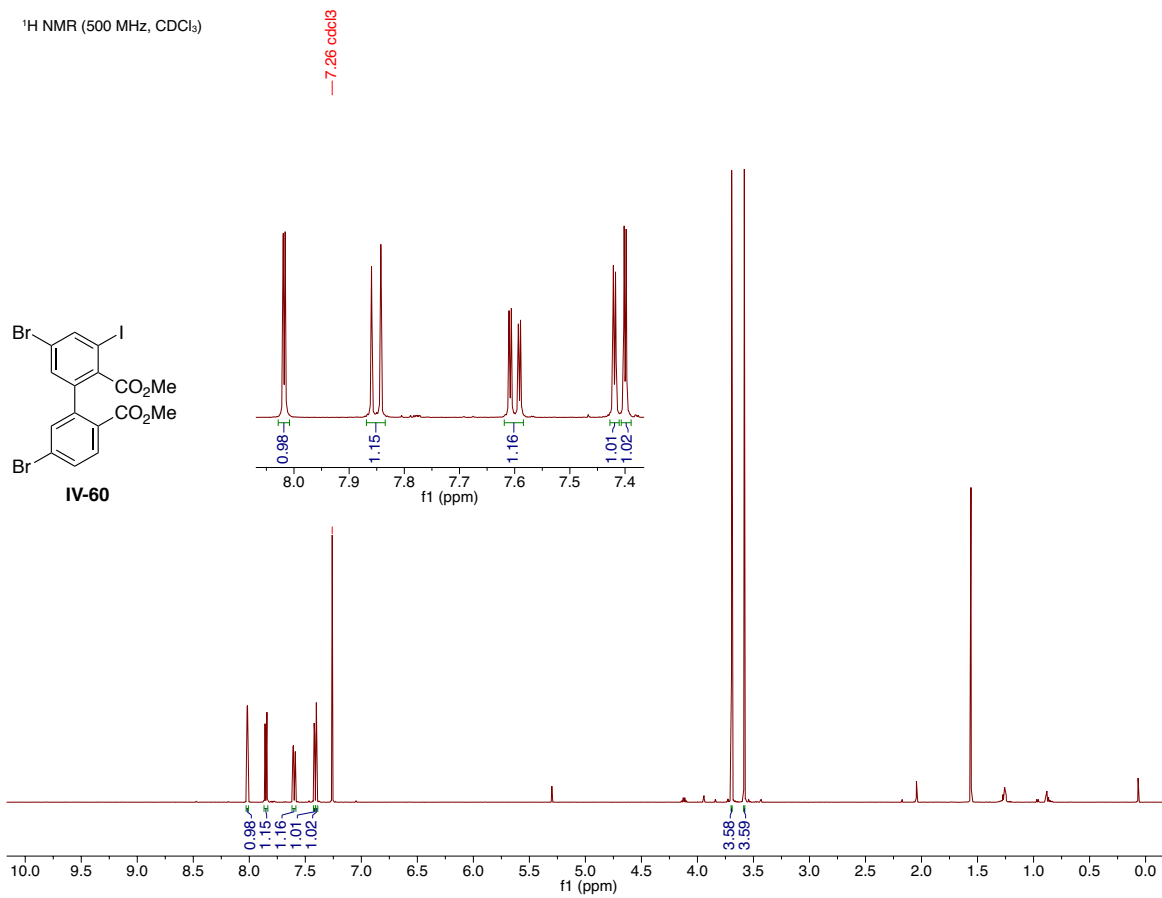


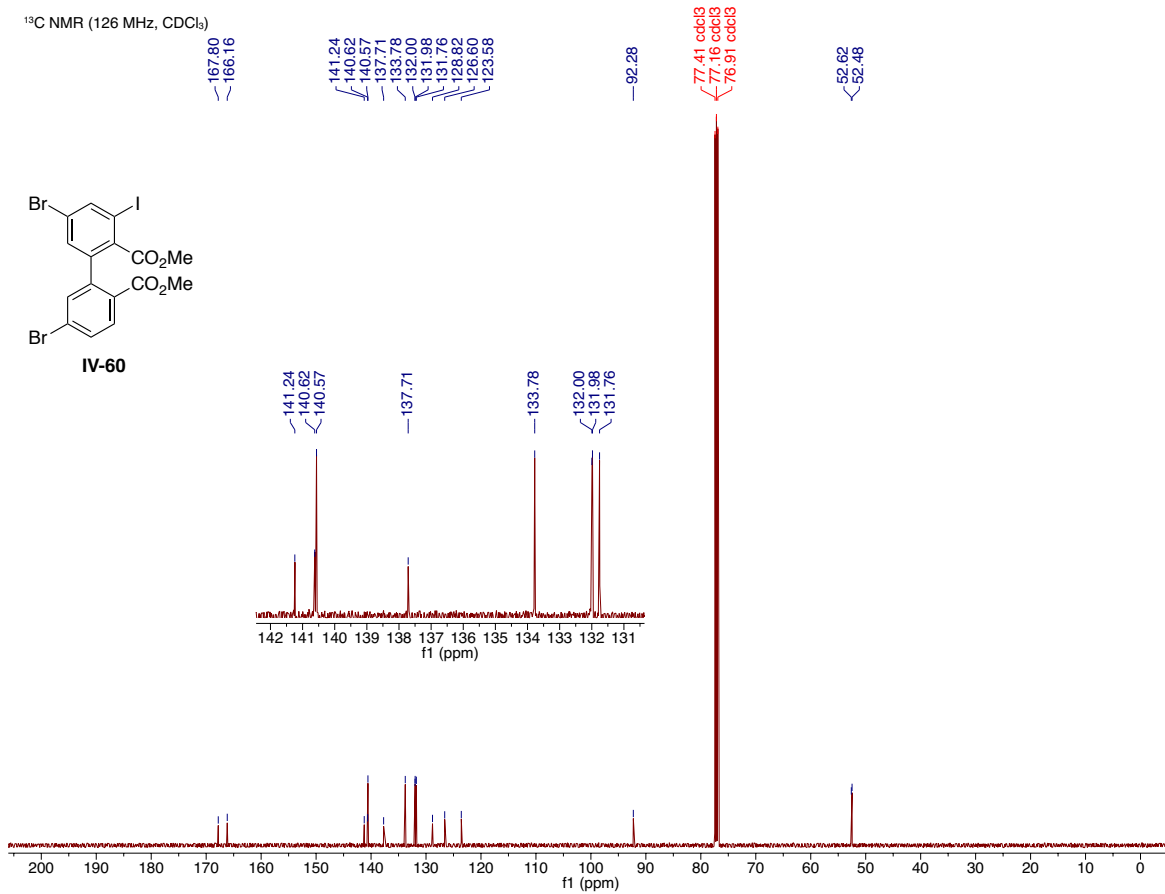
IV-58



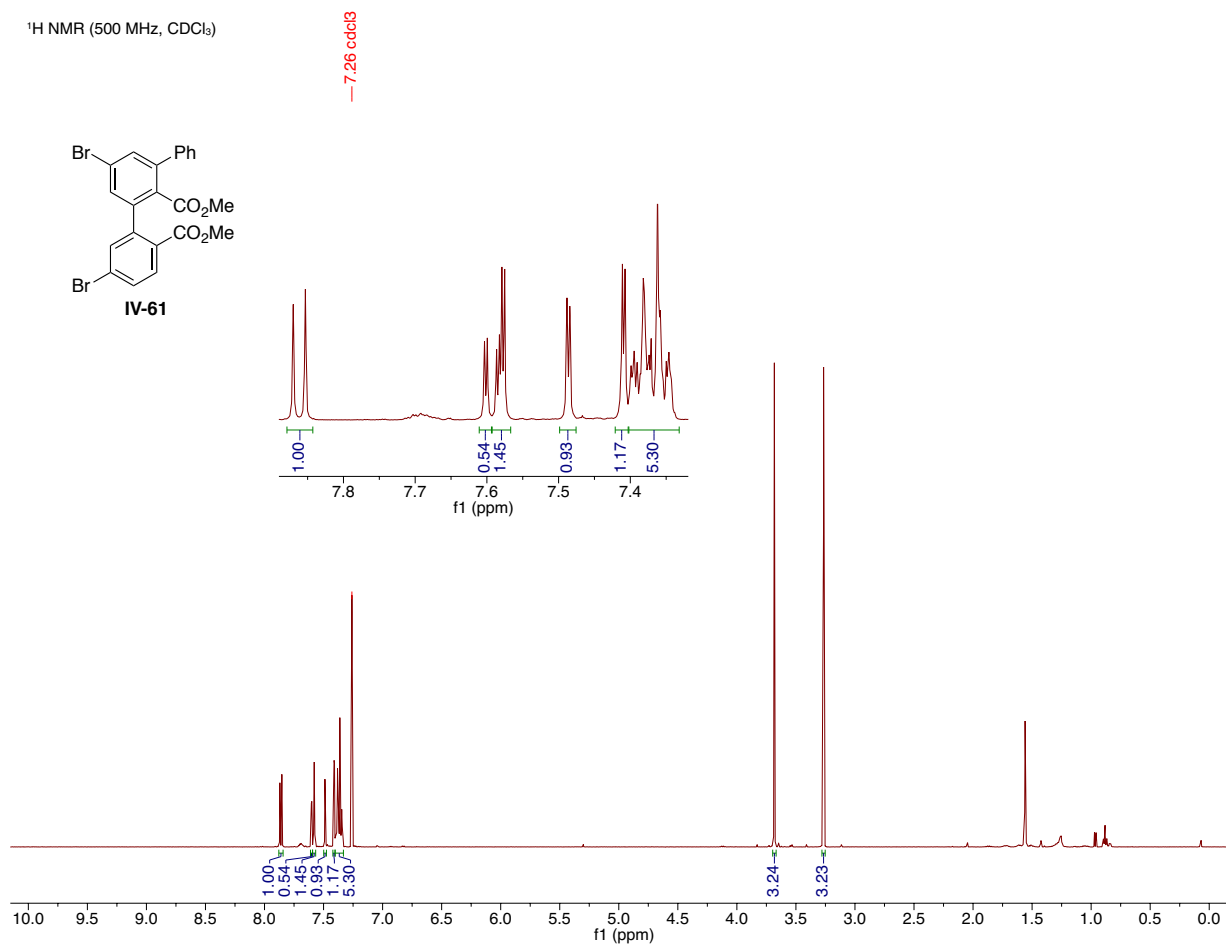
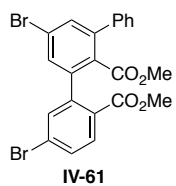


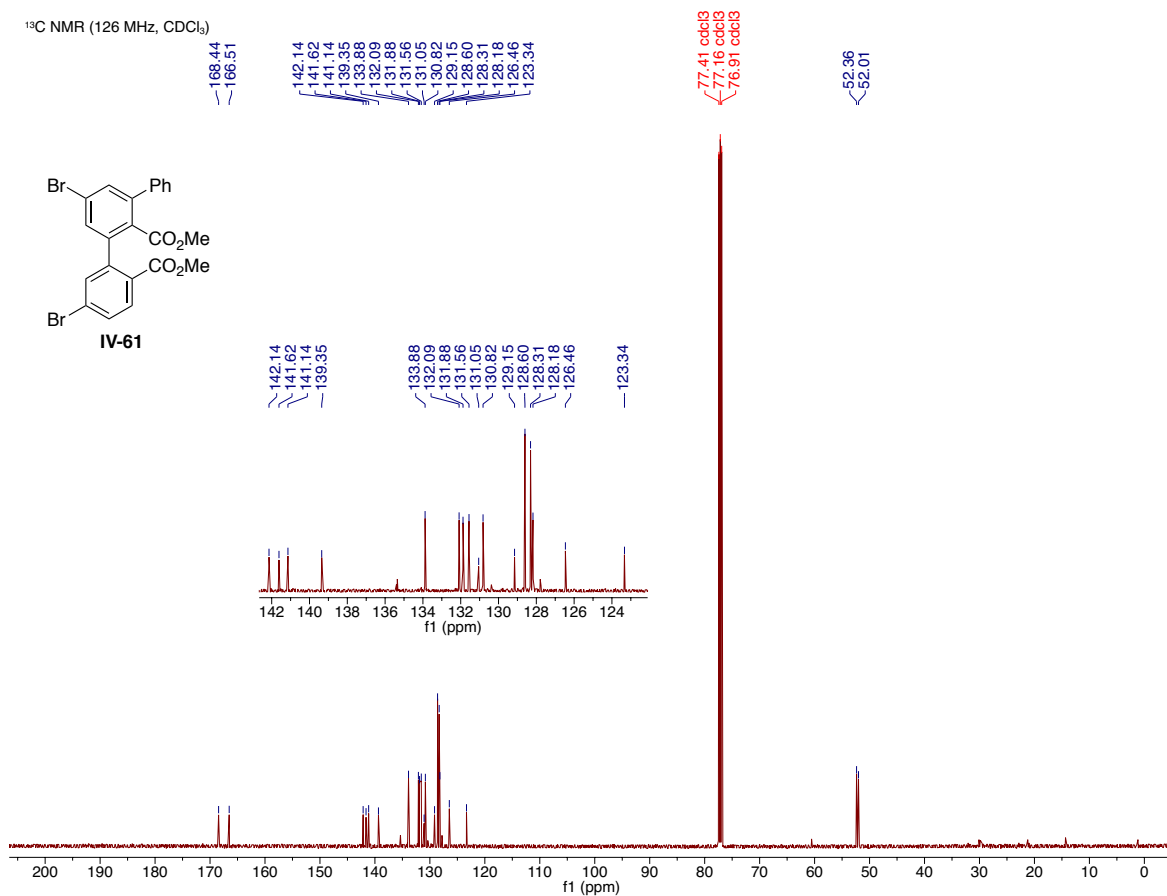
<sup>1</sup>H NMR (500 MHz, CDCl<sub>3</sub>)



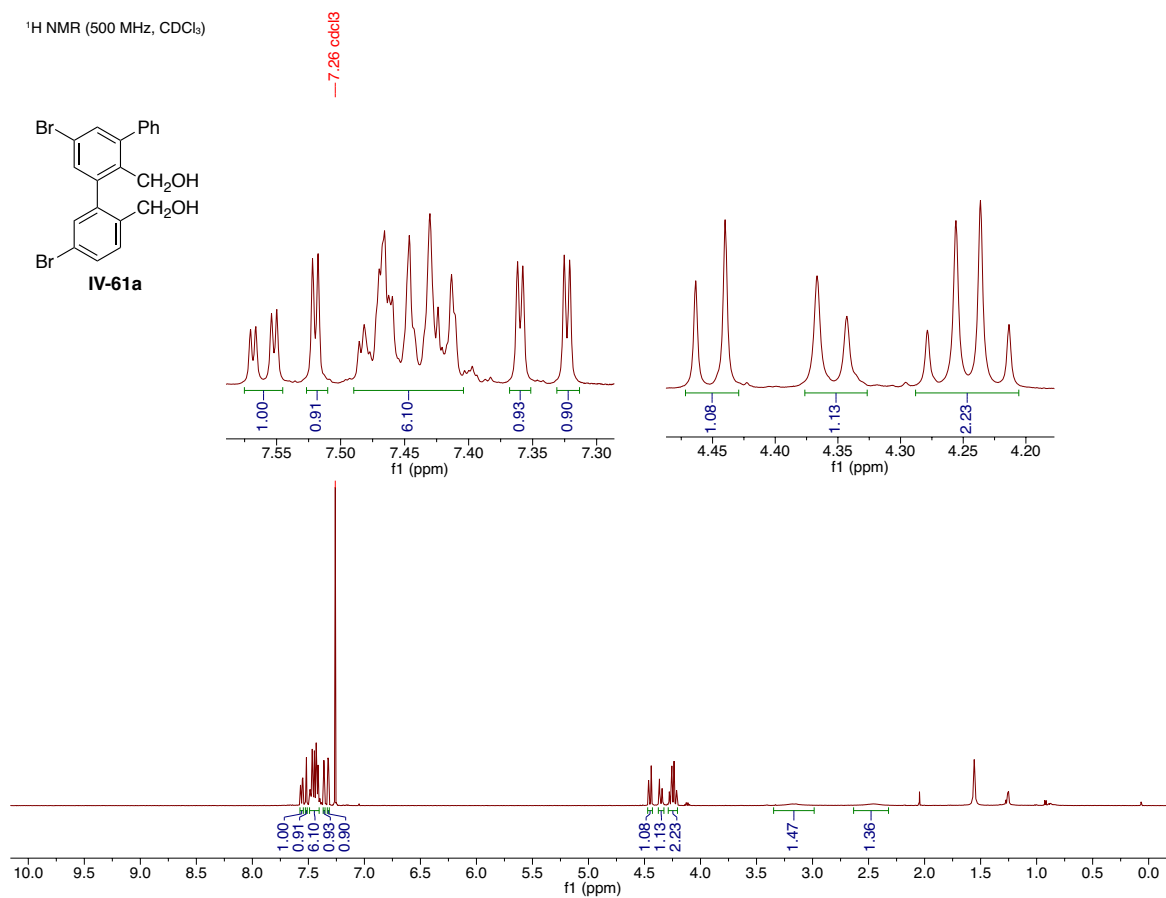
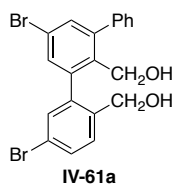


<sup>1</sup>H NMR (500 MHz, CDCl<sub>3</sub>)

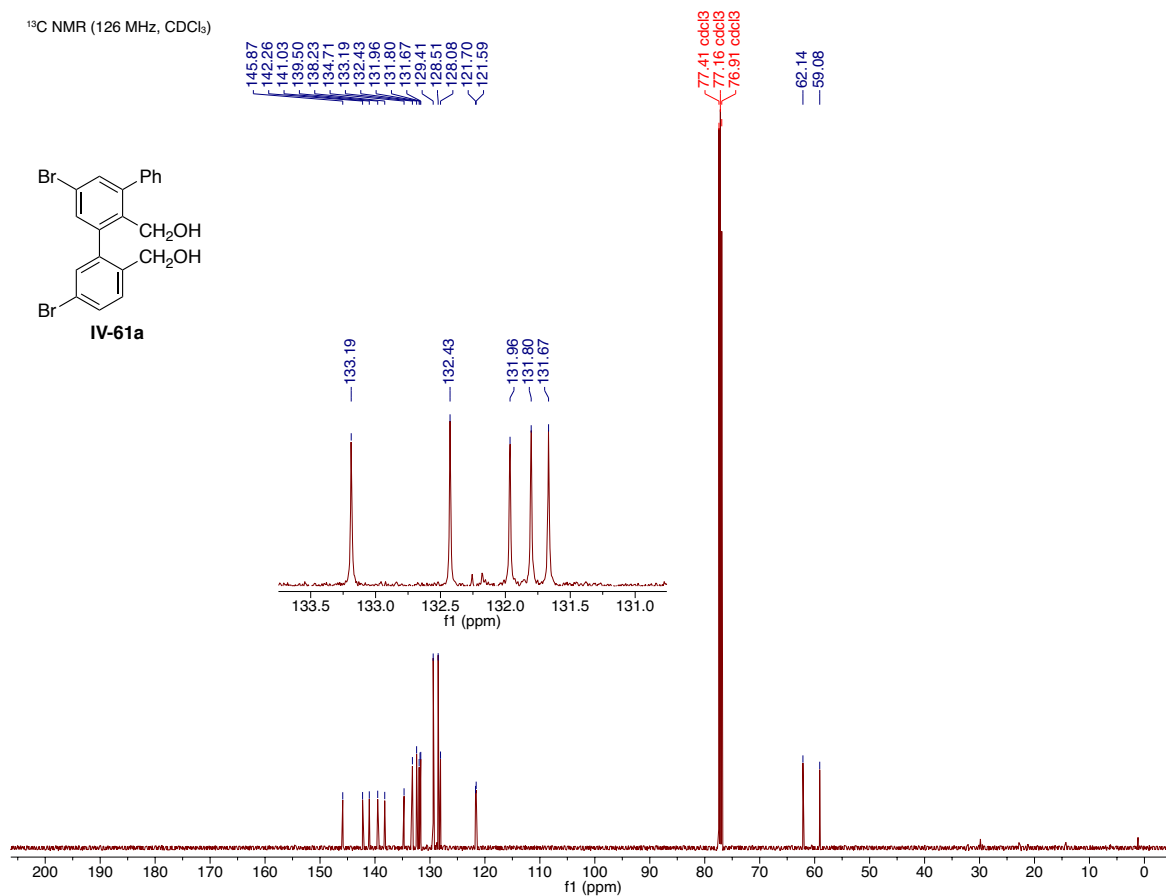
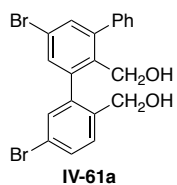




<sup>1</sup>H NMR (500 MHz, CDCl<sub>3</sub>)

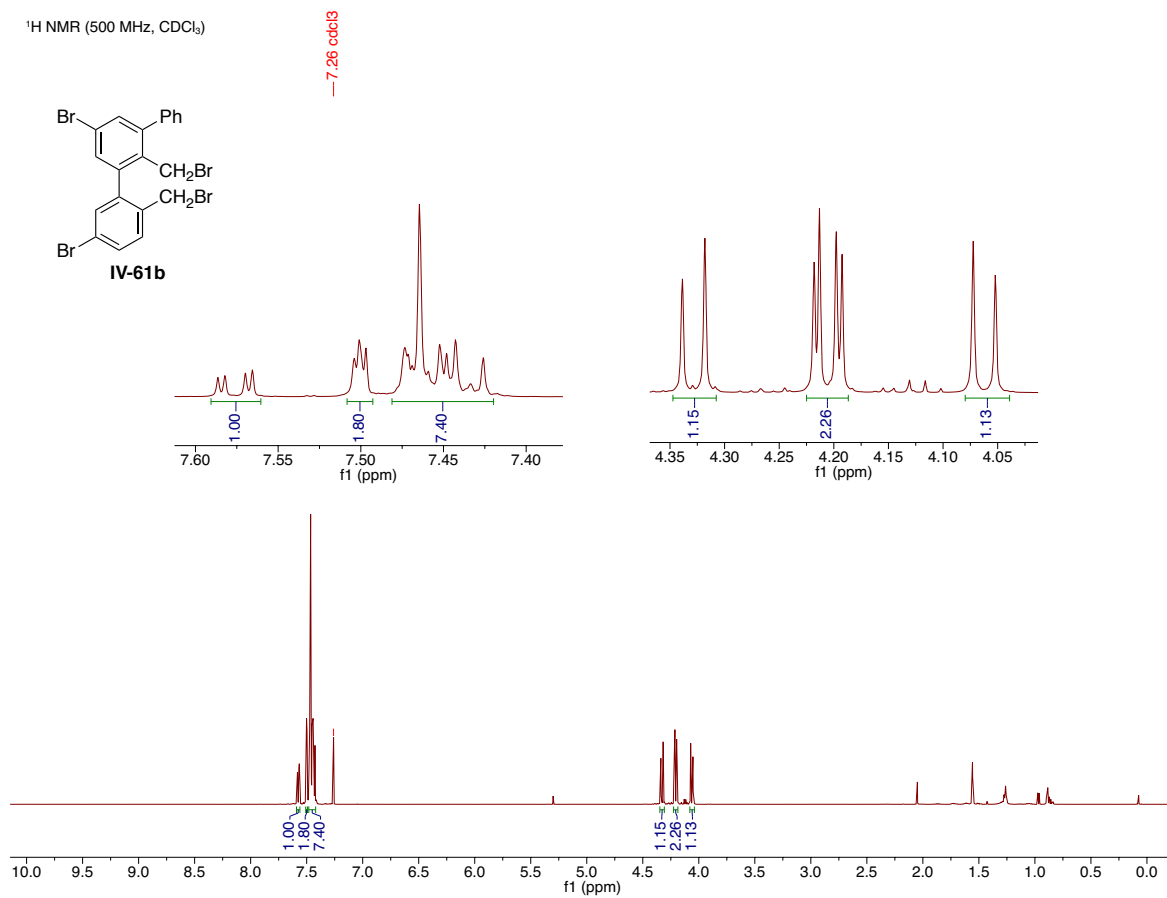
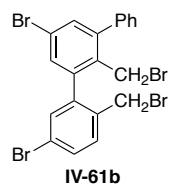


<sup>13</sup>C NMR (126 MHz, CDCl<sub>3</sub>)

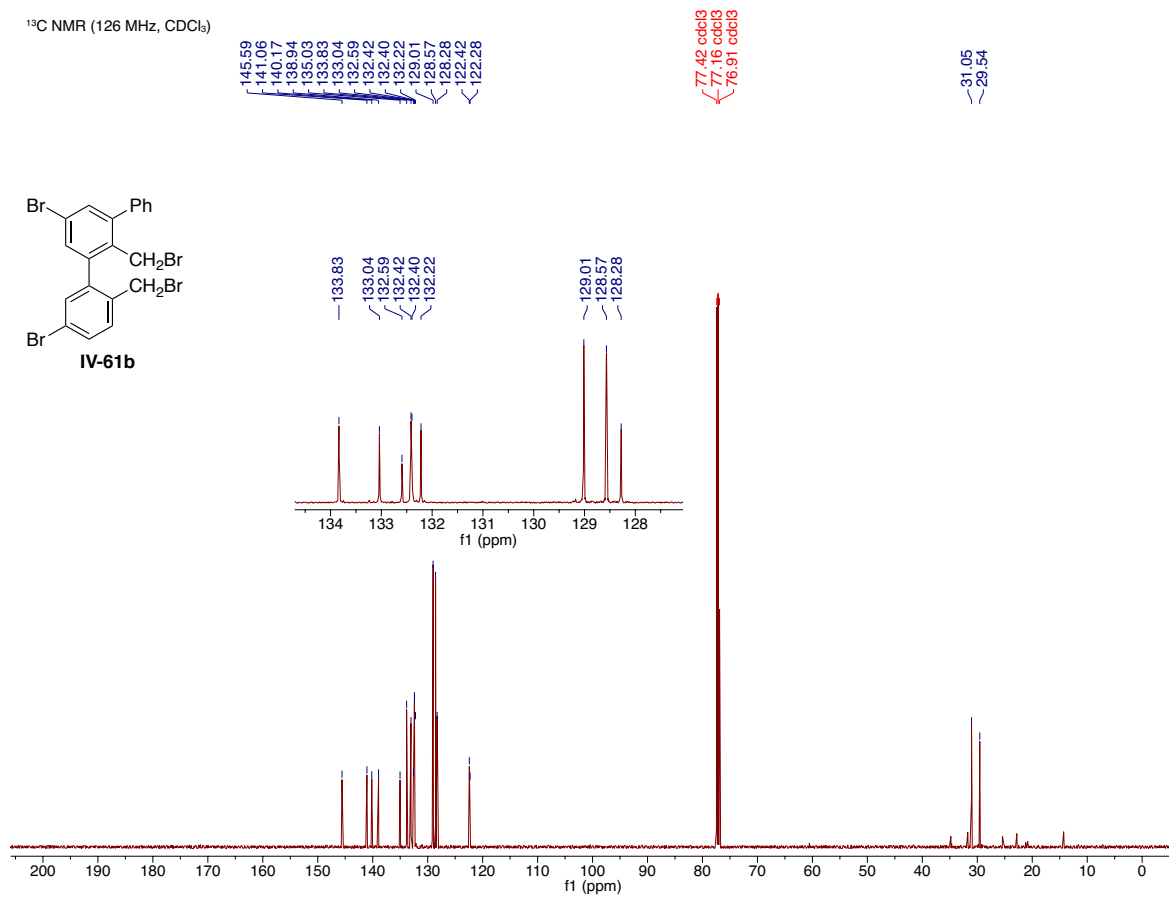
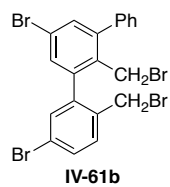




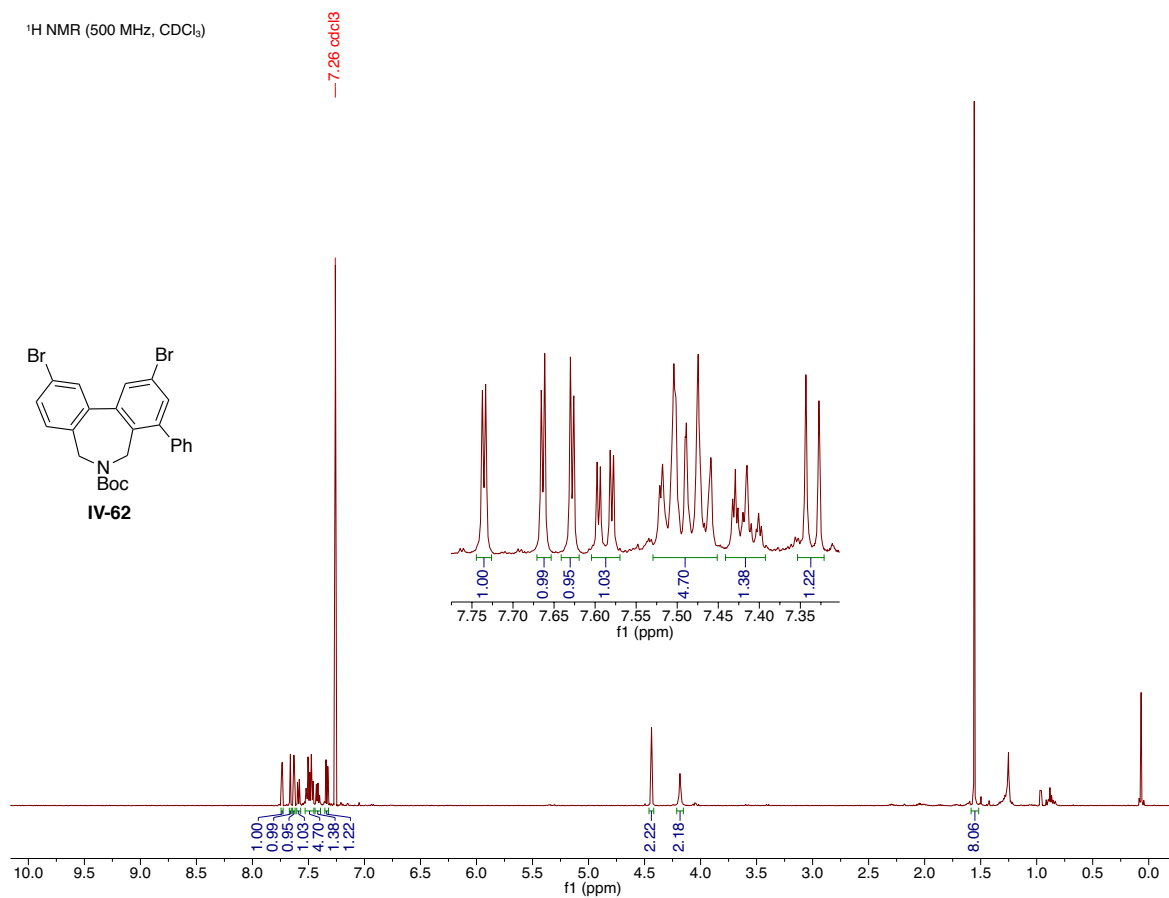
<sup>1</sup>H NMR (500 MHz, CDCl<sub>3</sub>)



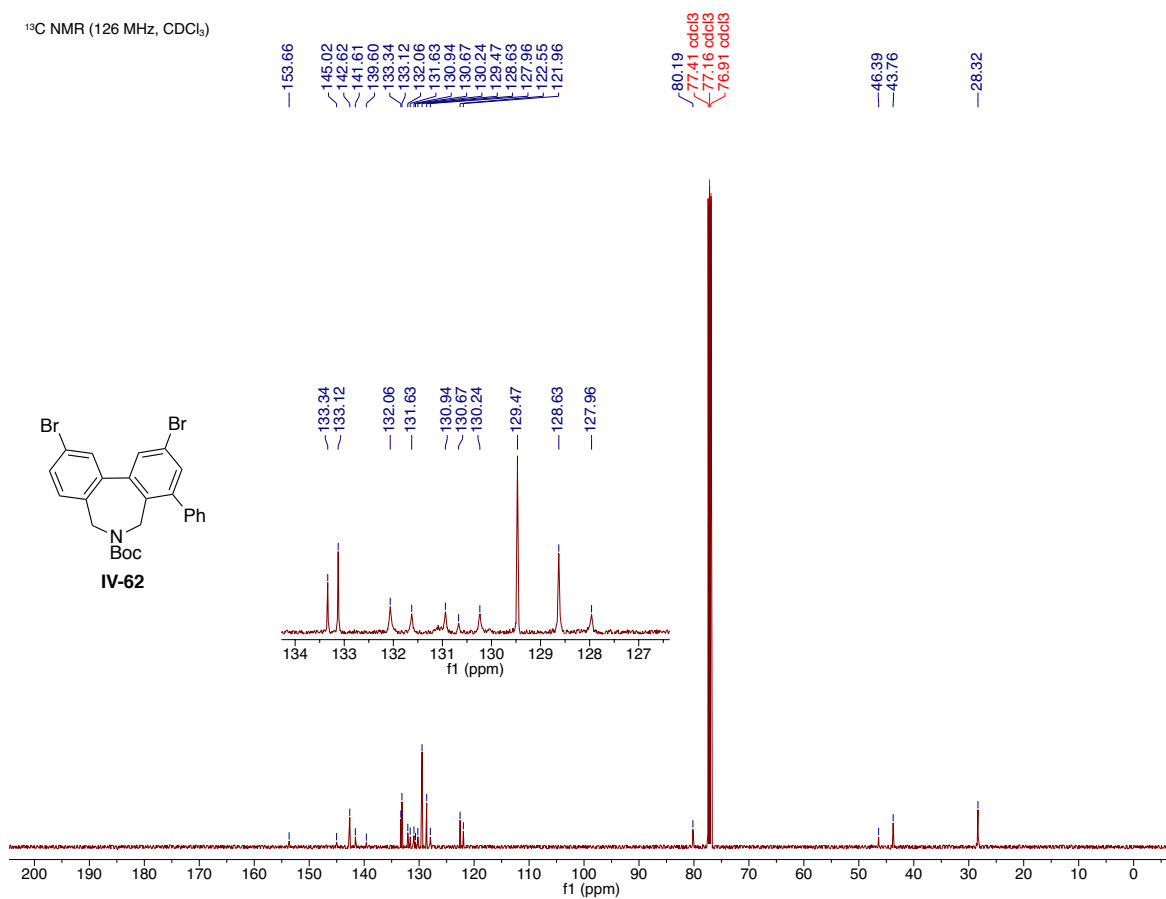
<sup>13</sup>C NMR (126 MHz, CDCl<sub>3</sub>)



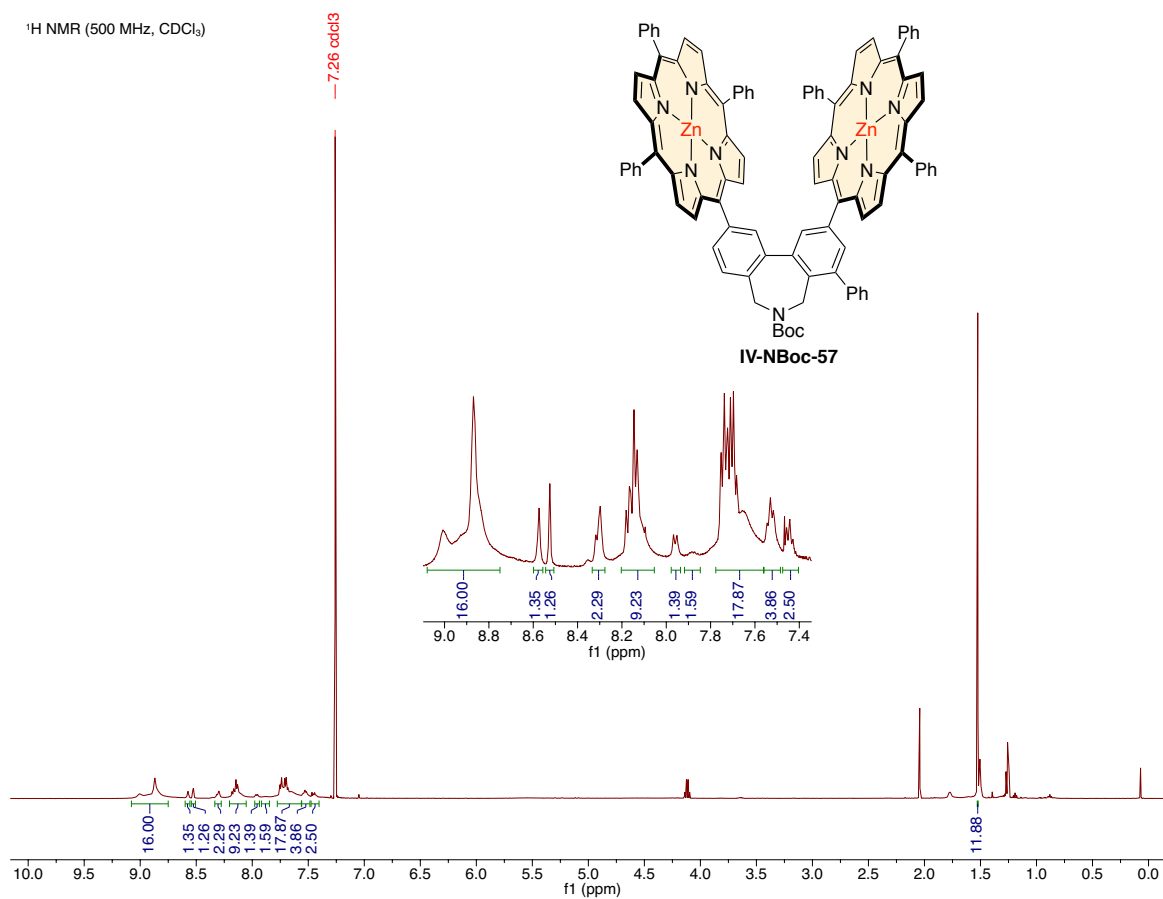
<sup>1</sup>H NMR (500 MHz, CDCl<sub>3</sub>)

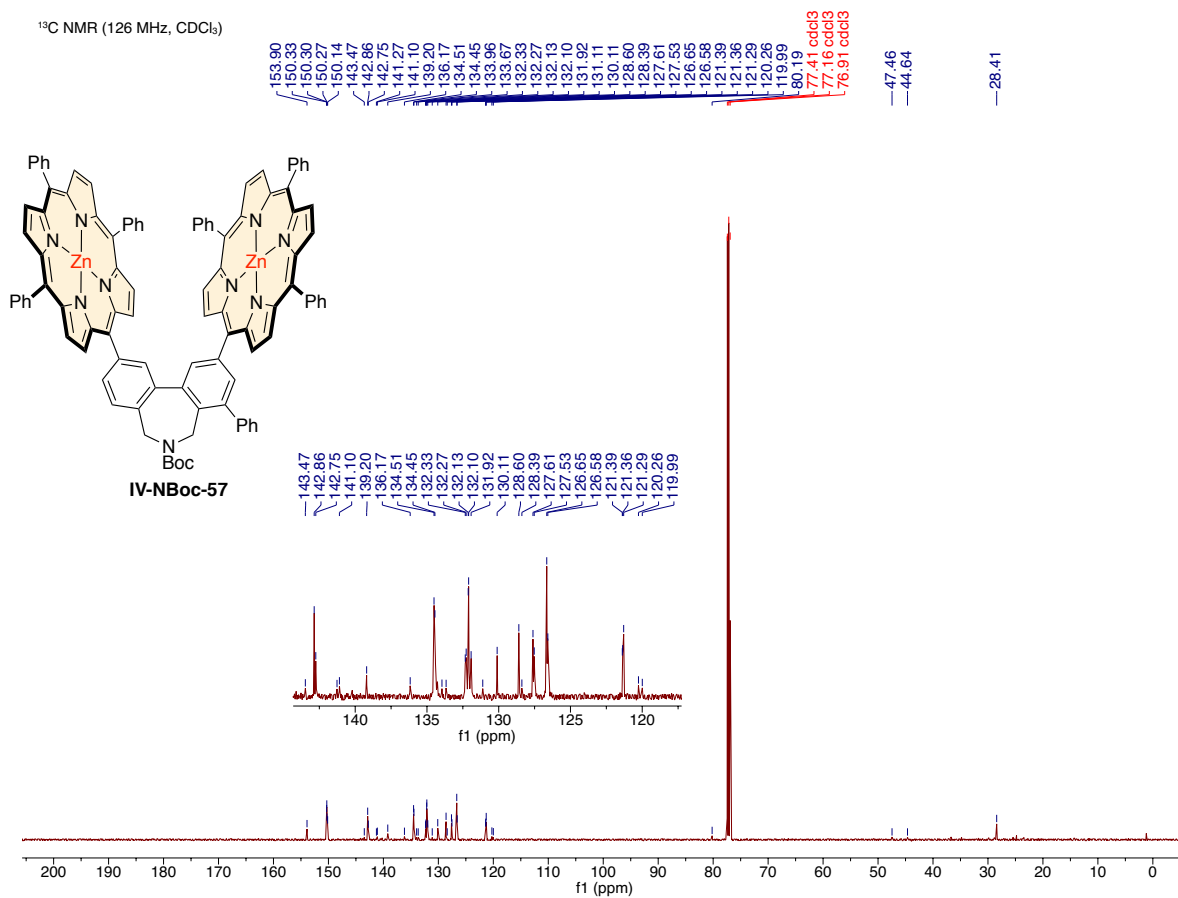


<sup>13</sup>C NMR (126 MHz, CDCl<sub>3</sub>)

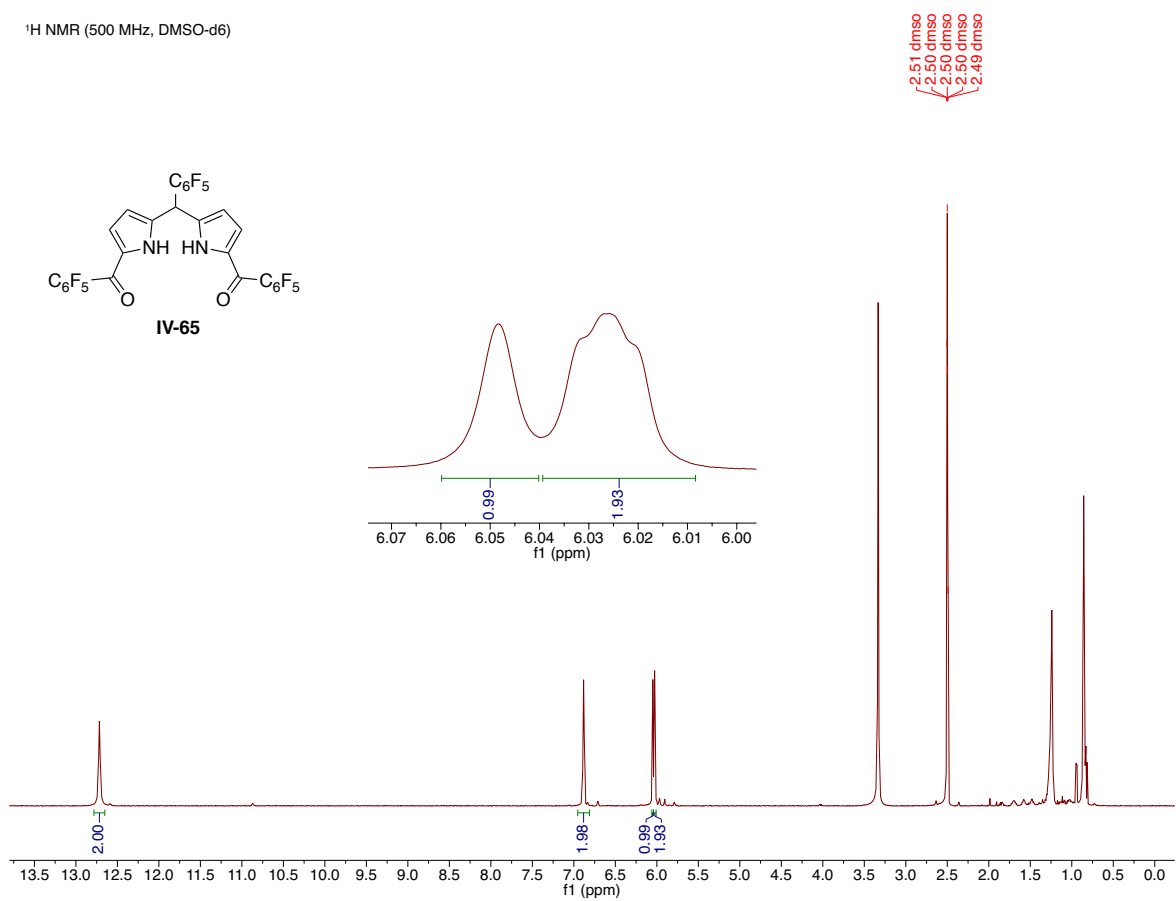


<sup>1</sup>H NMR (500 MHz, CDCl<sub>3</sub>)

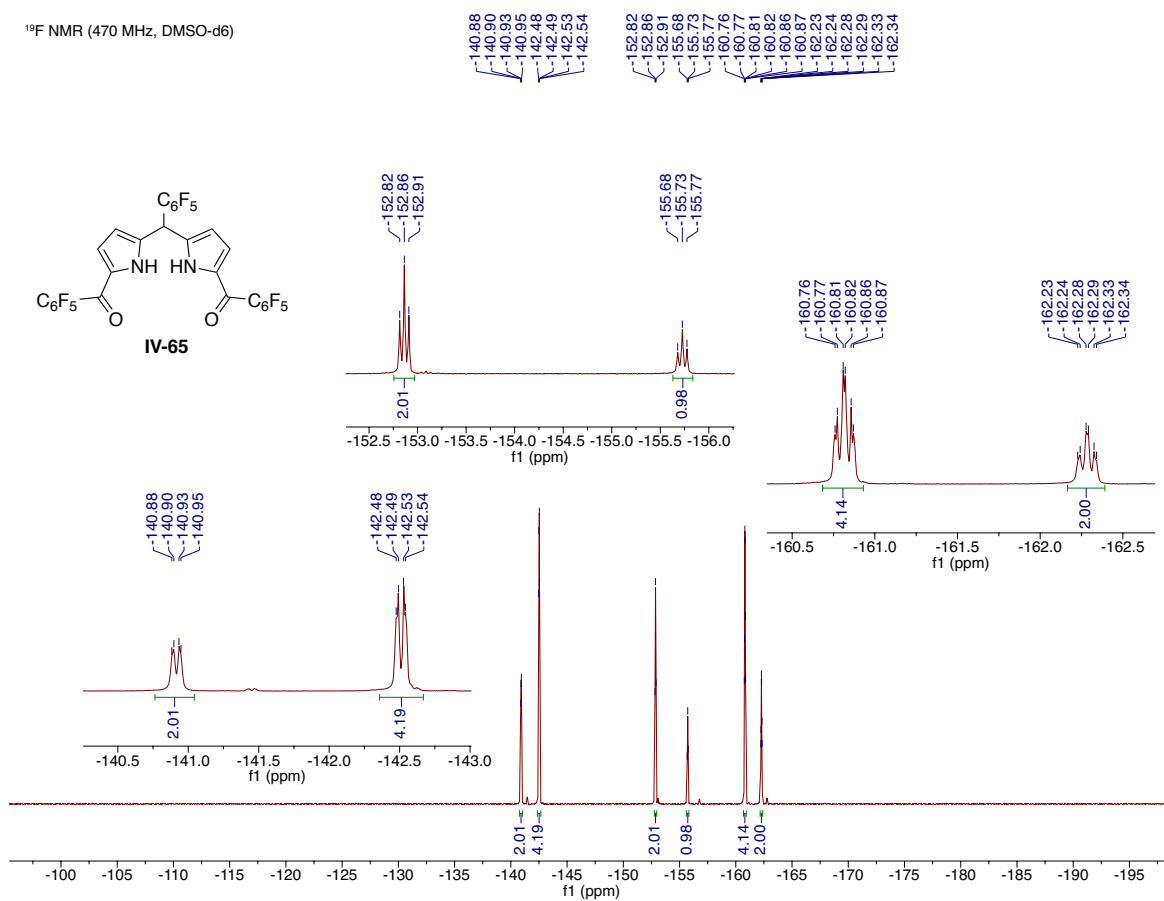




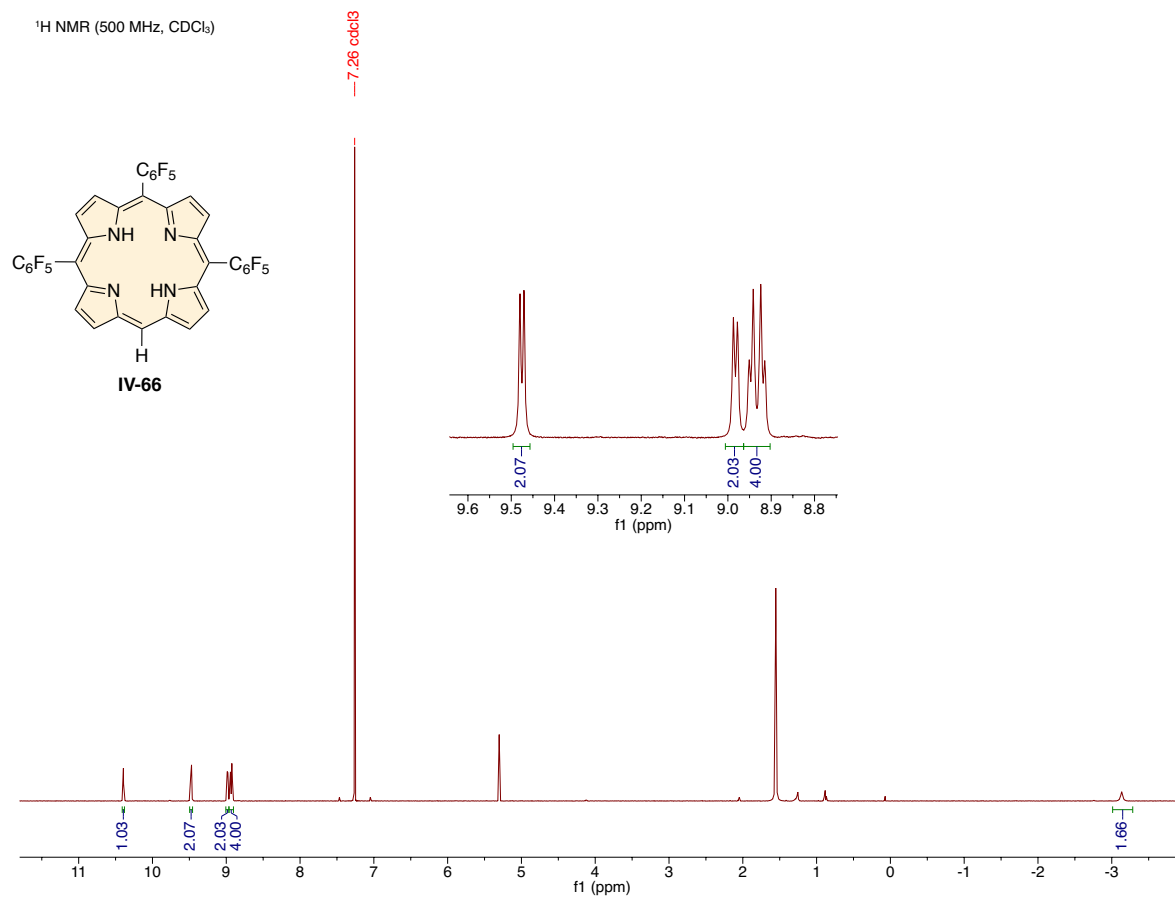
<sup>1</sup>H NMR (500 MHz, DMSO-d<sub>6</sub>)

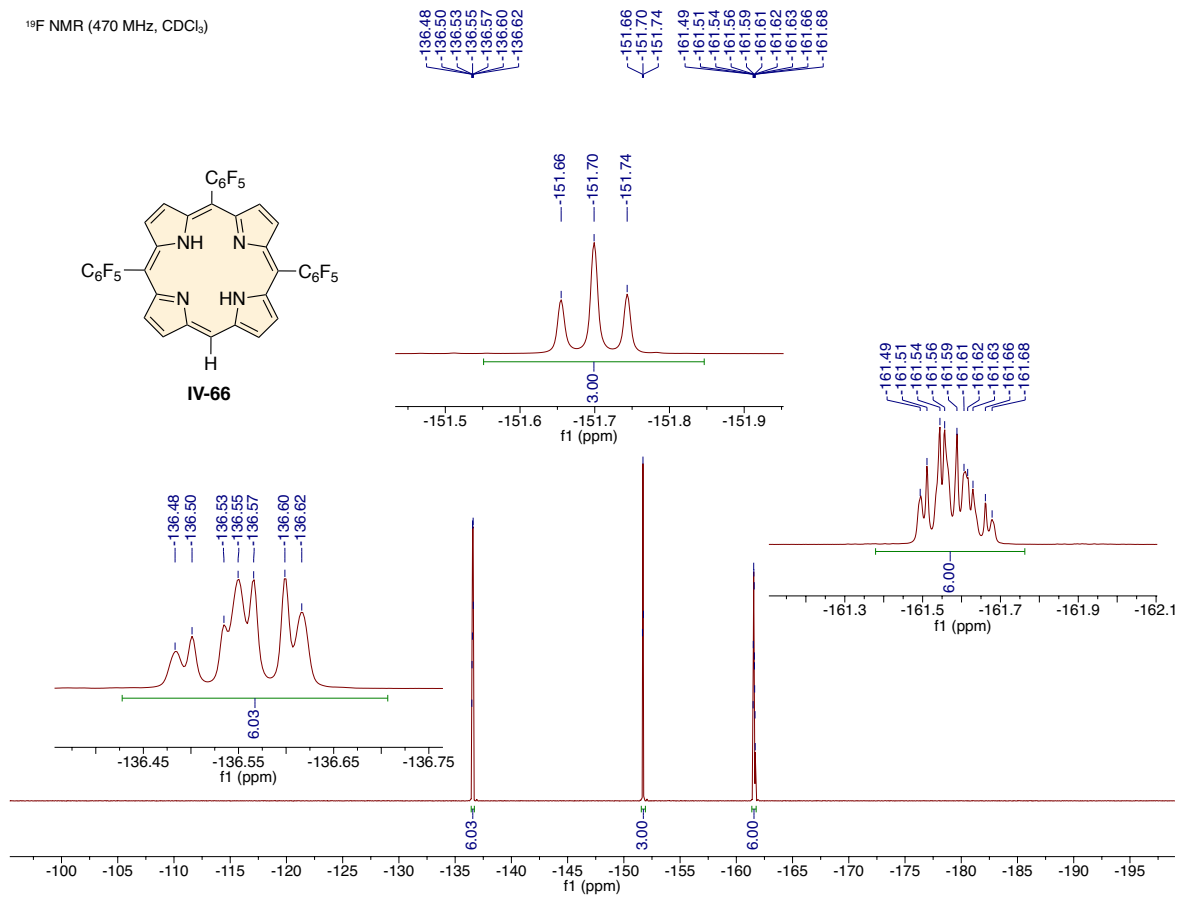


<sup>19</sup>F NMR (470 MHz, DMSO-d<sub>6</sub>)



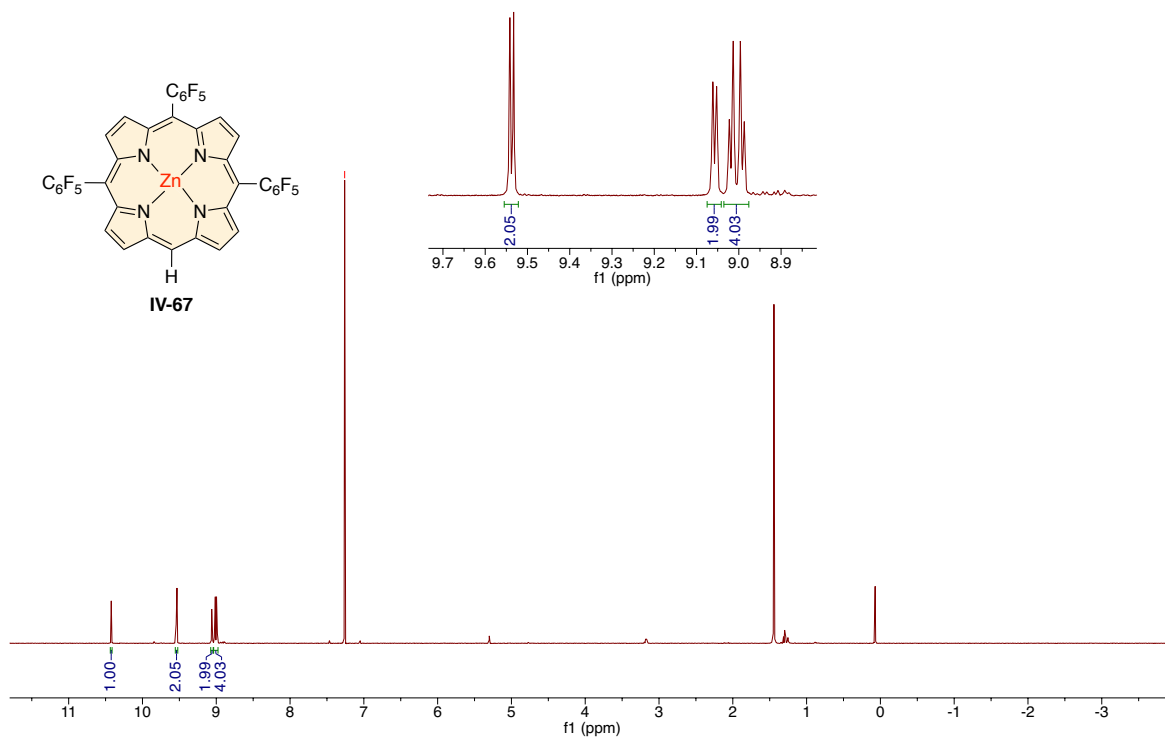


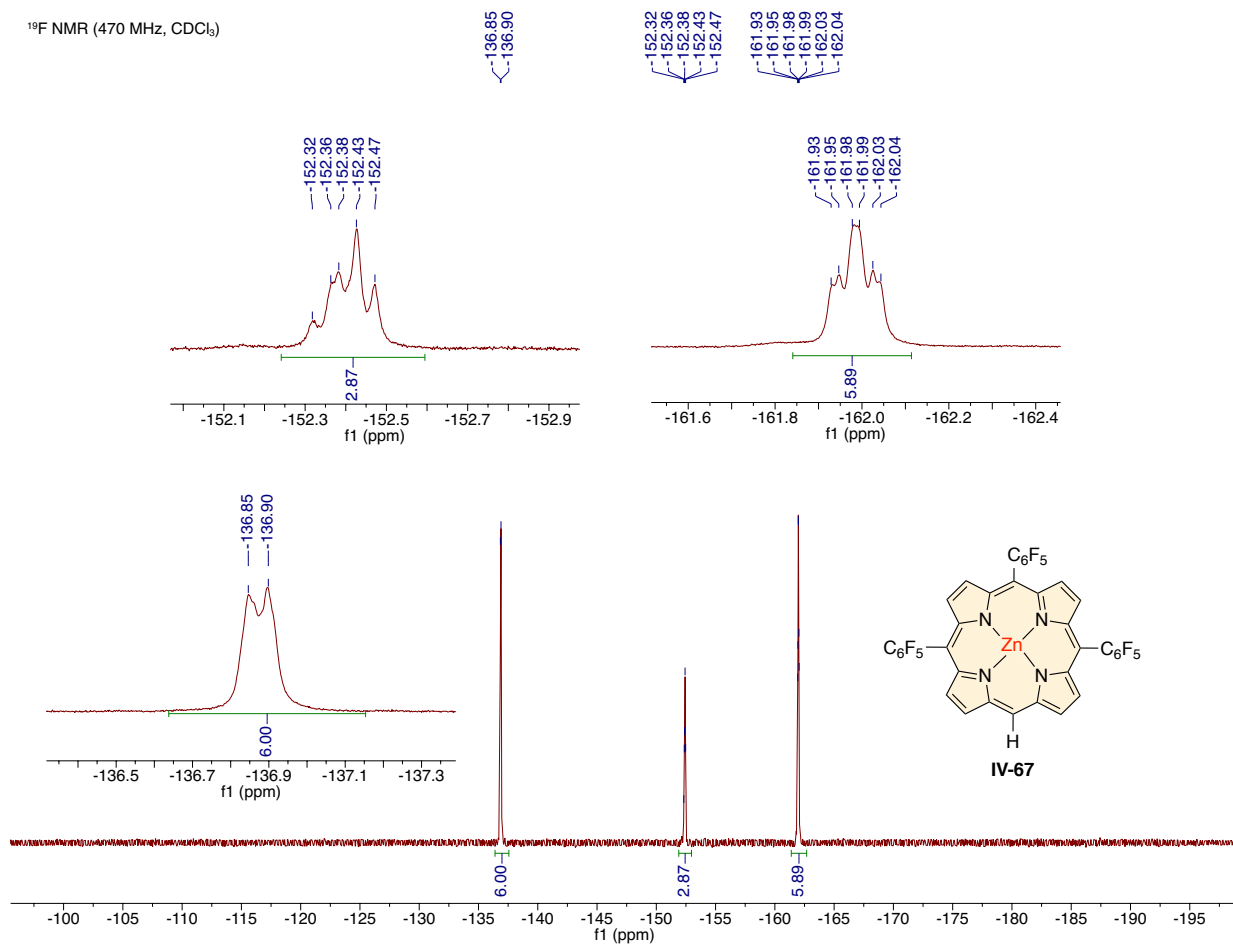




<sup>1</sup>H NMR (500 MHz, CDCl<sub>3</sub>)

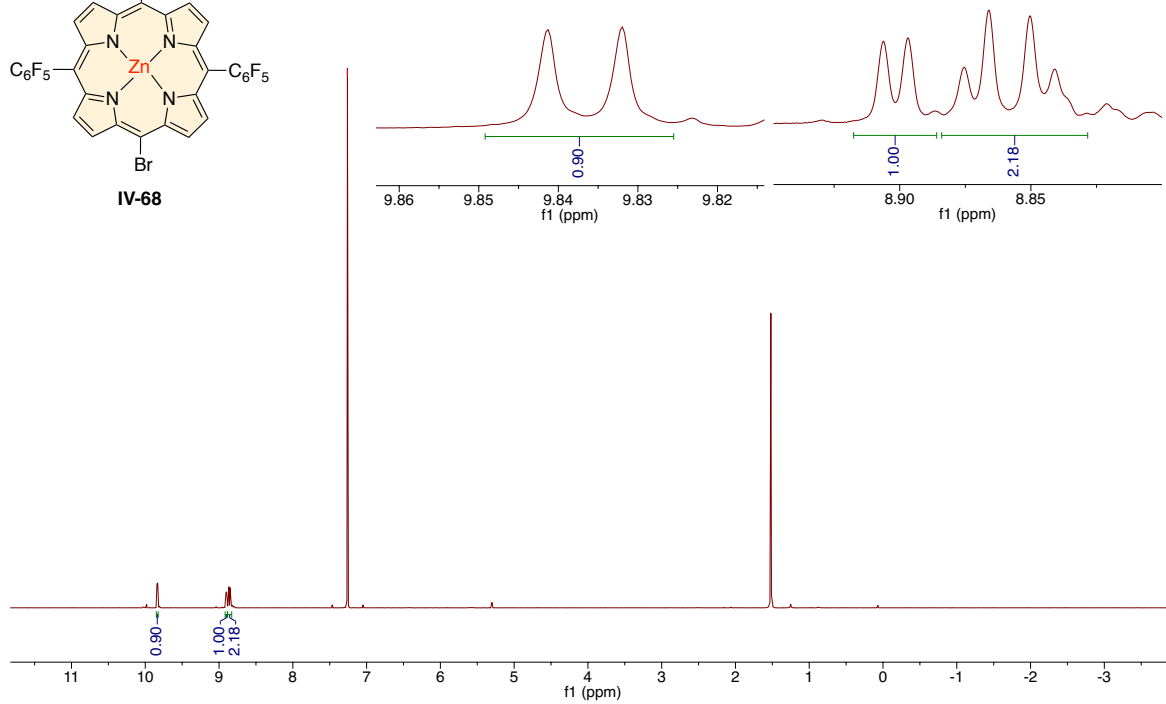
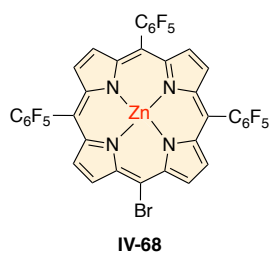
— 7.26 odd3





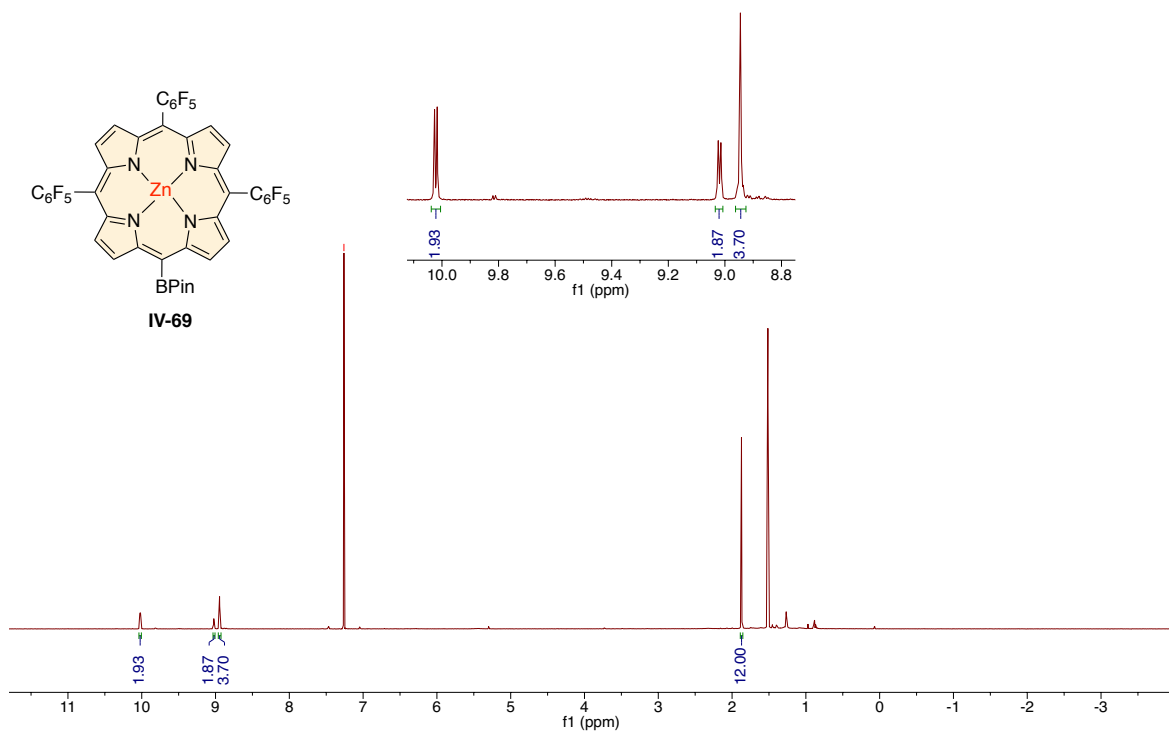
<sup>1</sup>H NMR (500 MHz, CDCl<sub>3</sub>)

—7.26 cdcl<sub>3</sub>

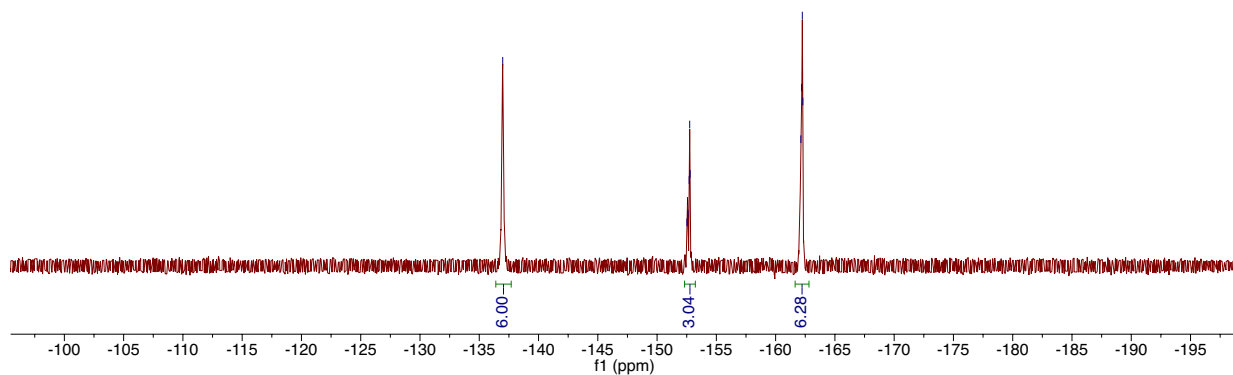
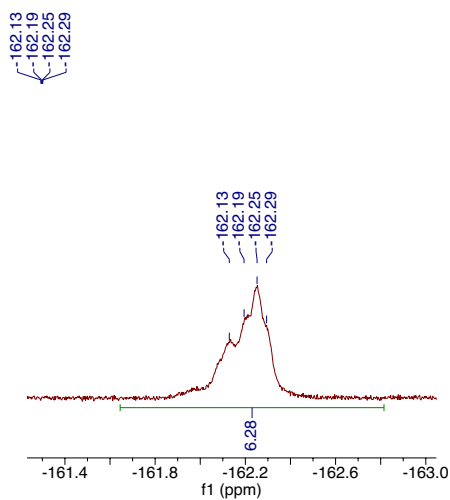
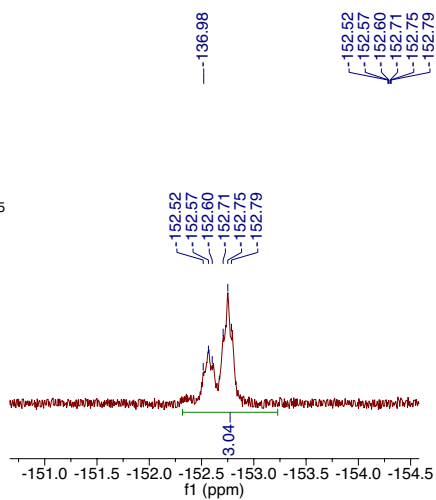
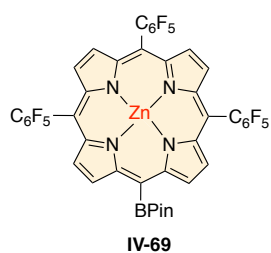


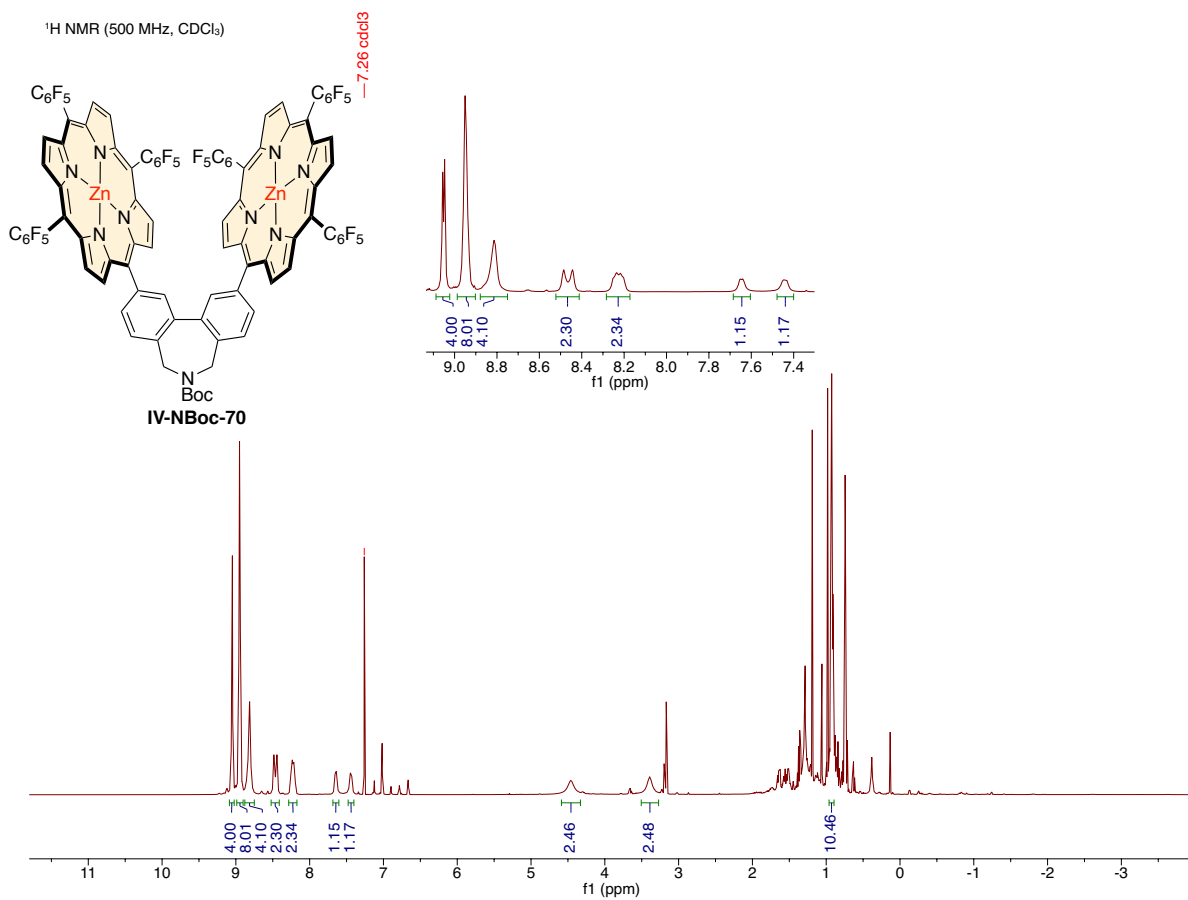
<sup>1</sup>H NMR (500 MHz, CDCl<sub>3</sub>)

— 7.26 cdc13

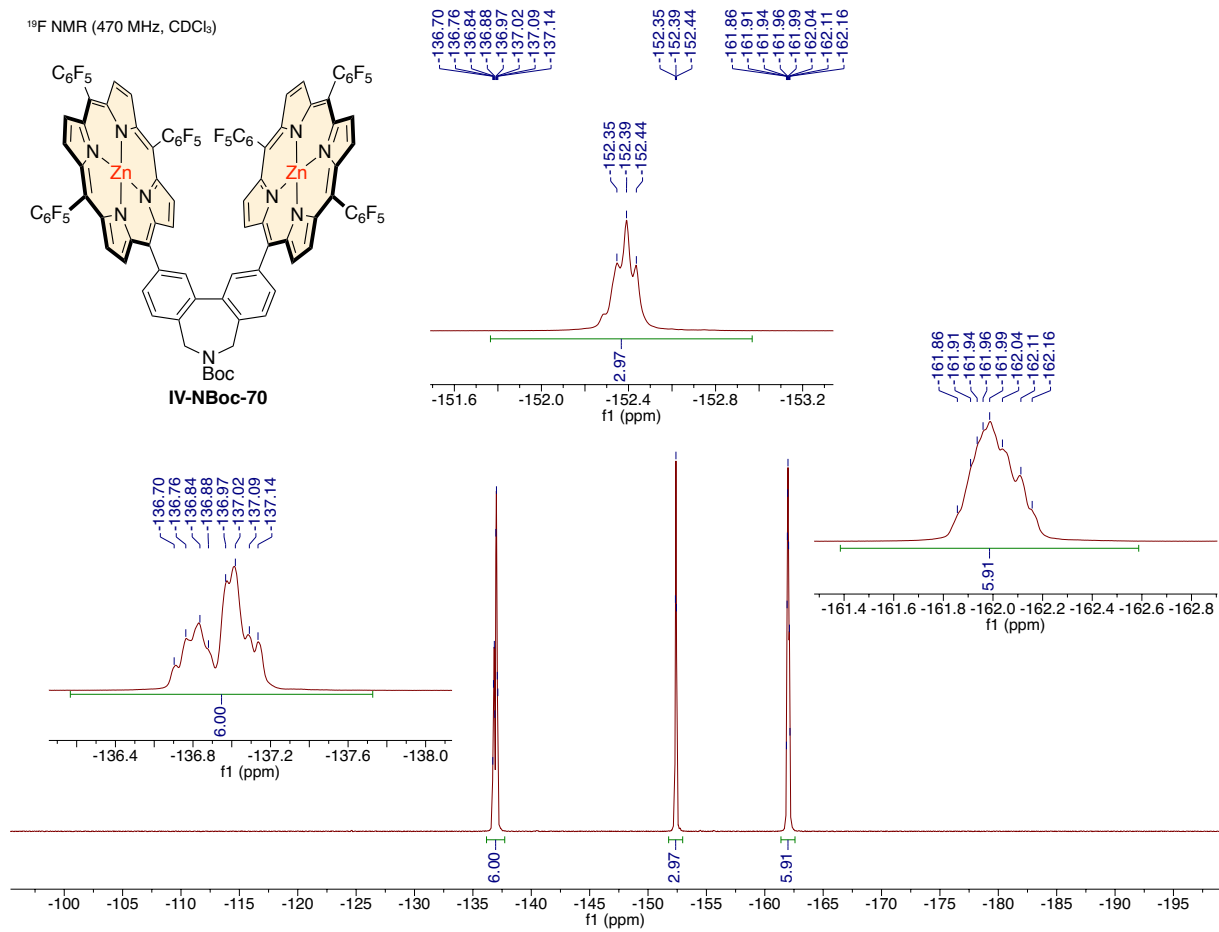


$^{19}\text{F}$  NMR (470 MHz,  $\text{CDCl}_3$ )

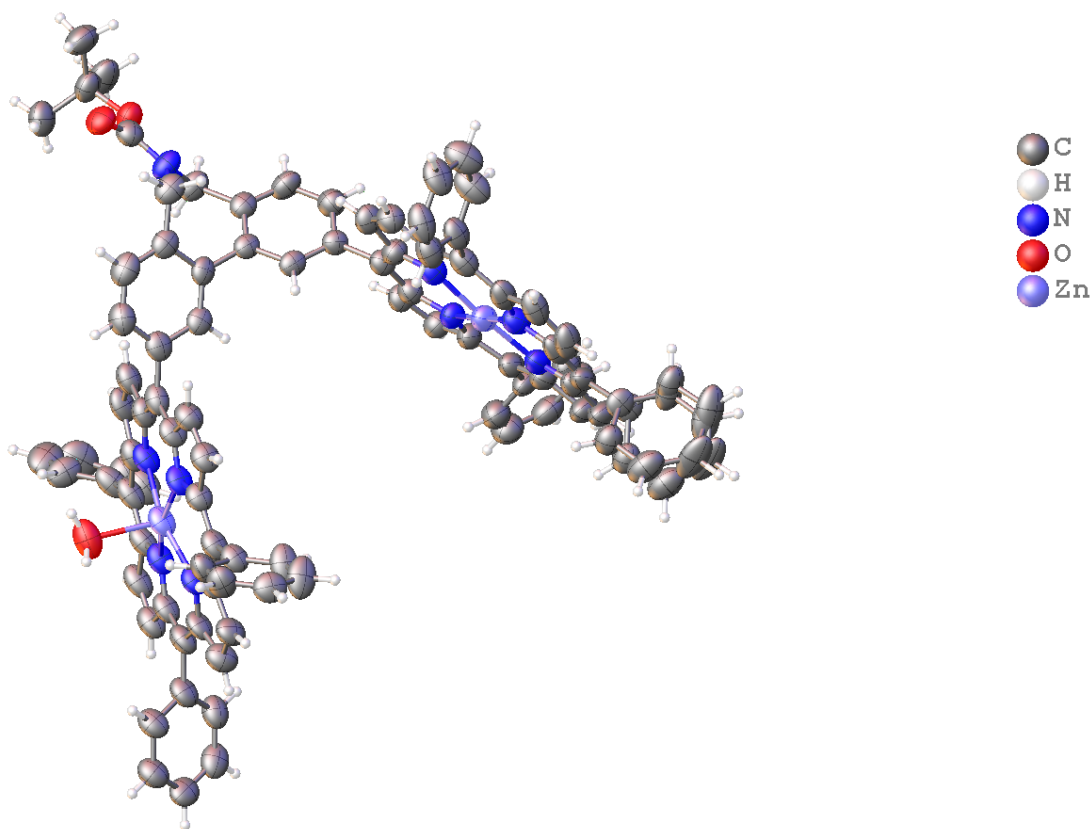








#### IV-10.9. Crystal structure of IV-NBoc-40



**Experimental.** Single red needle crystals of **IV-NBoc-40** used as received. A suitable crystal with dimensions  $0.20 \times 0.07 \times 0.04 \text{ mm}^3$  was selected and mounted on a nylon loop with paratone oil on a XtaLAB Synergy, Dualflex, HyPix diffractometer. The crystal was kept at a steady  $T = 100.00(10) \text{ K}$  during data collection. The structure was solved with the ShelXS solution program using direct methods and by using Olex2 as the graphical interface. The model was refined with ShelXL 2018/3 using full matrix least squares minimisation on  $F^2$ .

**Crystal Data.**  $\text{C}_{95}\text{H}_{67}\text{N}_9\text{O}_3\text{Zn}_2$ ,  $M_r = 1513.31$ , monoclinic,  $P2_1/n$  (No. 14),  $a = 19.0993(4) \text{ \AA}$ ,  $b = 12.9001(3) \text{ \AA}$ ,  $c = 31.9564(8) \text{ \AA}$ ,  $\beta = 93.374(2)^\circ$ ,  $\alpha = \gamma = 90^\circ$ ,  $V = 7859.9(3) \text{ \AA}^3$ ,  $T = 100.00(10) \text{ K}$ ,  $Z = 4$ ,  $Z' = 1$ ,  $\mu(\text{Cu K}\alpha) = 1.203$ , 25242 reflections measured, 9015 unique ( $R_{\text{int}} = 0.0363$ ) which were used in all calculations. The final  $wR_2$  was 0.2016 (all data) and  $R_1$  was 0.0675 ( $I \geq 2 \sigma(I)$ ).

<b>Compound</b>	<b>IV-NBoc-40</b>
Formula	C <sub>95</sub> H <sub>67</sub> N <sub>9</sub> O <sub>3</sub> Zn <sub>2</sub>
$D_{calc.}/\text{g cm}^{-3}$	1.279
$\mu/\text{mm}^{-1}$	1.203
Formula Weight	1513.31
Color	red
Shape	needle
Size/mm <sup>3</sup>	0.20×0.07×0.04
$T/\text{K}$	100.00(10)
Crystal System	monoclinic
Space Group	$P2_1/n$
$a/\text{\AA}$	19.0993(4)
$b/\text{\AA}$	12.9001(3)
$c/\text{\AA}$	31.9564(8)
$\alpha/^\circ$	90
$\beta/^\circ$	93.374(2)
$\gamma/^\circ$	90
$V/\text{\AA}^3$	7859.9(3)
$Z$	4
$Z'$	1
Wavelength/ $\text{\AA}$	1.54184
Radiation type	Cu K $_{\alpha}$

$\theta_{min}^{\circ}$	2.629
$\theta_{max}^{\circ}$	59.997
Measured	25242
Refl's.	
Indep't Refl's	9015
Refl's $I \geq 2 \sigma(I)$	6829
$R_{int}$	0.0363
Parameters	980
Restraints	0
Largest Peak	0.996
Deepest Hole	-0.572
GooF	1.060
$wR_2$ (all data)	0.2016
$wR_2$	0.1776
$R_1$ (all data)	0.0893
$R_1$	0.0675

A red needle-shaped crystal with dimensions  $0.20 \times 0.07 \times 0.04 \text{ mm}^3$  was mounted on a nylon loop with paratone oil. Data were collected using a XtaLAB Synergy, Dualflex, HyPix diffractometer equipped with an Oxford Cryosystems low-temperature device, operating at  $T = 100.00(10) \text{ K}$ .

Data were measured using  $\omega$  scans of  $0.5^\circ$  per frame for 45.0/180.0 s using  $\text{Cu K}\alpha$  radiation (micro-focus sealed X-ray tube, 50 kV, 1 mA). The total number of runs and images was based on the strategy calculation from the program CrysAlisPro. The achieved resolution was  $\theta = 59.997$ .

Cell parameters were retrieved using the CrysAlisPro software and refined using CrysAlisPro on 8374 reflections, 33 % of the observed reflections. Data reduction was performed using the CrysAlisPro software which corrects for Lorentz polarization. The final completeness is 77.20 out to 59.997 in  $\theta$  CrysAlisPro 1.171.40.84a. Numerical absorption correction based on gaussian integration over a multifaceted crystal model Empirical absorption correction using spherical harmonics, implemented in SCALE3 ABSPACK scaling algorithm.

The structure was solved in the space group  $P2_1/n$  (# 14) by using direct methods using the ShelXS structure solution program. The structure was refined by Least Squares using version 2018/2 of XL incorporated in Olex2. All non-hydrogen atoms were refined anisotropically. Hydrogen atom positions were calculated geometrically and refined using the riding model, except for the hydrogen atom on the non-carbon atom(s) which were found by difference Fourier methods and refined isotropically when data permits.

There is a single molecule in the asymmetric unit, which is represented by the reported sum formula. In other words: Z is 4 and Z' is 1.

## REFERENCES

1. Erbas-Cakmak, S.; Leigh, D. A.; McTernan, C. T.; Nussbaumer, A. L., *Chem. Rev.* **2015**, *115*, 10081-10206.
2. Blanco, V.; Leigh, D. A.; Marcos, V., *Chem. Soc. Rev.* **2015**, *44*, 5341-5370.
3. Gostl, R.; Senf, A.; Hecht, S., *Chem. Soc. Rev.* **2014**, *43*, 1982-1996.
4. Leigh, D. A.; Marcos, V.; Wilson, M. R., *ACS Catal.* **2014**, *4*, 4490-4497.
5. Stoll, R. S.; Hecht, S., *Angew. Chem. Int. Ed. Engl.* **2010**, *49*, 5054-5075.
6. Escorihuela, J.; Burguete, M. I.; Luis, S. V., *Chem. Soc. Rev.* **2013**, *42*, 5595-5617.
7. Bartok, M., *Chem. Rev.* **2010**, *110*, 1663-1705.
8. Romanazzi, G.; Degennaro, L.; Mastroilli, P.; Luisi, R., *ACS Catal.* **2017**, *7*, 4100-4114.
9. Wang, J.; Feringa, B. L., *Science* **2011**, *331*, 1429-1432.
10. Pollard, M. M.; Meetsma, A.; Feringa, B. L., *Org. Biomol. Chem.* **2008**, *6*, 507-512.
11. Storch, G.; Trapp, O., *Angew. Chem. Int. Ed. Engl.* **2015**, *54*, 3580-3586.
12. Mortezaei, S.; Catarineu, N. R.; Canary, J. W., *J. Am. Chem. Soc.* **2012**, *134*, 8054-8057.
13. Zahn, S.; Canary, J. W., *Science* **2000**, *288*, 1404-1407.
14. Nagata, Y.; Nishikawa, T.; Suginome, M., *J. Am. Chem. Soc.* **2014**, *136*, 15901-15904.
15. Aikawa, K.; Mikami, K., *Chem. Commun.* **2012**, *48*, 11050-11069.
16. Punniyamurthy, T.; Mayr, M.; Dorofeev, A. S.; Bataille, C. J.; Gosiewska, S.; Nguyen, B.; Cowley, A. R.; Brown, J. M., *Chem. Commun.* **2008**, 5092-5094.
17. Maier, F.; Trapp, O., *Angew. Chem. Int. Ed. Engl.* **2014**, *53*, 8756-8760.
18. Storch, G.; Trapp, O., *Chirality* **2018**, *30*, 1150-1160.
19. Yamamoto, T.; Murakami, R.; Komatsu, S.; Suginome, M., *J. Am. Chem. Soc.* **2018**, *140*, 3867-3870.



20. Chakraborty, D.; Gholami, H.; Sarkar, A.; Joyce, L. A.; Jackson, J. E.; Borhan, B., *Chem. Sci.* **2021**, *12*, 1750-1755.
21. Gholami, H.; Anyika, M.; Zhang, J.; Vasileiou, C.; Borhan, B., *Chem. Eur. J.* **2016**, *22*, 9235-9239.
22. Anyika, M.; Gholami, H.; Ashtekar, K. D.; Acho, R.; Borhan, B., *J. Am. Chem. Soc.* **2014**, *136*, 550-553.
23. Gholami, H.; Zhang, J.; Anyika, M.; Borhan, B., *Org. Lett.* **2017**, *19*, 1722-1725.
24. Kan, S. B. J.; Maruyama, H.; Akakura, M.; Kano, T.; Maruoka, K., *Angew. Chem. Int. Ed. Engl.* **2017**, *56*, 9487-9491.
25. Wang, X.; Chen, R. X.; Wei, Z. F.; Zhang, C. Y.; Tu, H. Y.; Zhang, A. D., *J. Org. Chem.* **2016**, *81*, 238-249.
26. Hyslop, A. G.; Kellett, M. A.; Iovine, P. M.; Therien, M. J., *J. Am. Chem. Soc.* **1998**, *120*, 12676-12677.
27. Takanami, T.; Hayashi, M.; Chijimatsu, H.; Inoue, W.; Suda, K., *Org. Lett.* **2005**, *7*, 3937-3940.
28. Chng, L. L.; Chang, C. J.; Nocera, D. G., *J. Org. Chem.* **2003**, *68*, 4075-4078.
29. Matano, Y.; Matsumoto, K.; Terasaka, Y.; Hotta, H.; Araki, Y.; Ito, O.; Shiro, M.; Sasamori, T.; Tokito, N.; Imahori, H., *Chem. Eur. J.* **2007**, *13*, 891-901.
30. Fang, Y.; Jiang, X.; Kadish, K. M.; Nefedov, S. E.; Kirakosyan, G. A.; Enakieva, Y. Y.; Gorbunova, Y. G.; Tsivadze, A. Y.; Stern, C.; Bessmertnykh-Lemeune, A.; Guillard, R., *Inorg. Chem.* **2019**, *58*, 4665-4678.
31. Officer, D. L.; Lodato, F.; Jolley, K. W., *Inorg. Chem.* **2007**, *46*, 4781-4783.
32. Li, X.; Tanasova, M.; Vasileiou, C.; Borhan, B., *J. Am. Chem. Soc.* **2008**, *130*, 1885-1893.
33. Olsson, S.; Dahlstrand, C.; Gogoll, A., *Dalton Trans.* **2018**, *47*, 11572-11585.
34. Proni, G.; Pescitelli, G.; Huang, X.; Nakanishi, K.; Berova, N., *J. Am. Chem. Soc.* **2003**, *125*, 12914-12927.
35. Kepp, K. P., *Inorg. Chem.* **2016**, *55*, 9461-9470.
36. Saha, B.; Ikbal, S. A.; Rath, S. P., *Inorg. Chem.* **2020**, *59*, 7795-7809.

37. Kharel, S.; Bhuvanesh, N.; Gladysz, J. A.; Blumel, J., *Inorganica Chim. Acta* **2019**, *490*, 215-219.
38. Francke, R.; Little, R. D., *J. Am. Chem. Soc.* **2014**, *136*, 427-435.
39. Furuta, T.; Nikaido, M.; Yamamoto, J.; Kuribayashi, T.; Kawabata, T., *Synthesis* **2013**, *45*, 1312-1318.
40. Caspers, L. D.; Finkbeiner, P.; Nachtsheim, B. J., *Chem. Eur. J.* **2017**, *23*, 2748-2752.
41. Frost, J. R.; Huber, S. M.; Breitenlechner, S.; Bannwarth, C.; Bach, T., *Angew. Chem. Int. Ed. Engl.* **2015**, *54*, 691-695.
42. Bastiaans, H. M. M.; vanderBaan, J. L.; Ottenheijm, H. C. J., *J. Org. Chem.* **1997**, *62*, 3880-3889.